Developments in Petroleum Science, 42

casing design theory and practice

S.S. RAHMAN
Center for Petroleum Engineering, University of New South Wales, Sydney, Australia

and

G.V. CHILINGARIAN
School of Engineering, University of Southern California, Los Angeles, California, USA

1995
ELSEVIER
Amsterdam – Lausanne – New York – Oxford – Shannon – Tokyo

ELSEVIER SCIENCE B.V.
Sara Burgerhartstraat 25
P.O. Box 211, 1000 AE Amsterdam, The Netherlands

ISBN: 0-444-81743-3

This book is printed on acid-free paper.

Printed in The Netherlands

Chapter 1

FUNDAMENTAL ASPECTS OF CASING DESIGN

1.1 PURPOSE OF CASING

At a certain stage during the drilling of oil and gas wells, it becomes necessary to line the walls of a borehole with steel pipe which is called casing. Casing serves numerous purposes during the drilling and production history of oil and gas wells, these include:

1. Keeping the hole open by preventing the weak formations from collapsing, i.e., caving of the hole.

2. Serving as a high strength flow conduit to surface for both drilling and production fluids.

3. Protecting the freshwater-bearing formations from contamination by drilling and production fluids.

4. Providing a suitable support for wellhead equipment and blowout preventers for controlling subsurface pressure, and for the installation of tubing and subsurface equipment.

5. Providing safe passage for running wireline equipment.

6. Allowing isolated communication with selectively perforated formation(s) of interest.

1.2 TYPES OF CASING

When drilling wells, hostile environments, such as high-pressured zones, weak and fractured formations, unconsolidated formations and sloughing shales, are often encountered. Consequently, wells are drilled and cased in several steps to seal off these troublesome zones and to allow drilling to the total depth. Different casing sizes are required for different depths, the five general casings used to complete a well are: conductor pipe, surface casing, intermediate casing, production casing and liner. As shown in Fig. 1.1, these pipes are run to different depths and one or two of them may be omitted depending on the drilling conditions; they may also be run as liners or in combination with liners. In offshore platform operations, it is also necessary to run a cassion pipe.

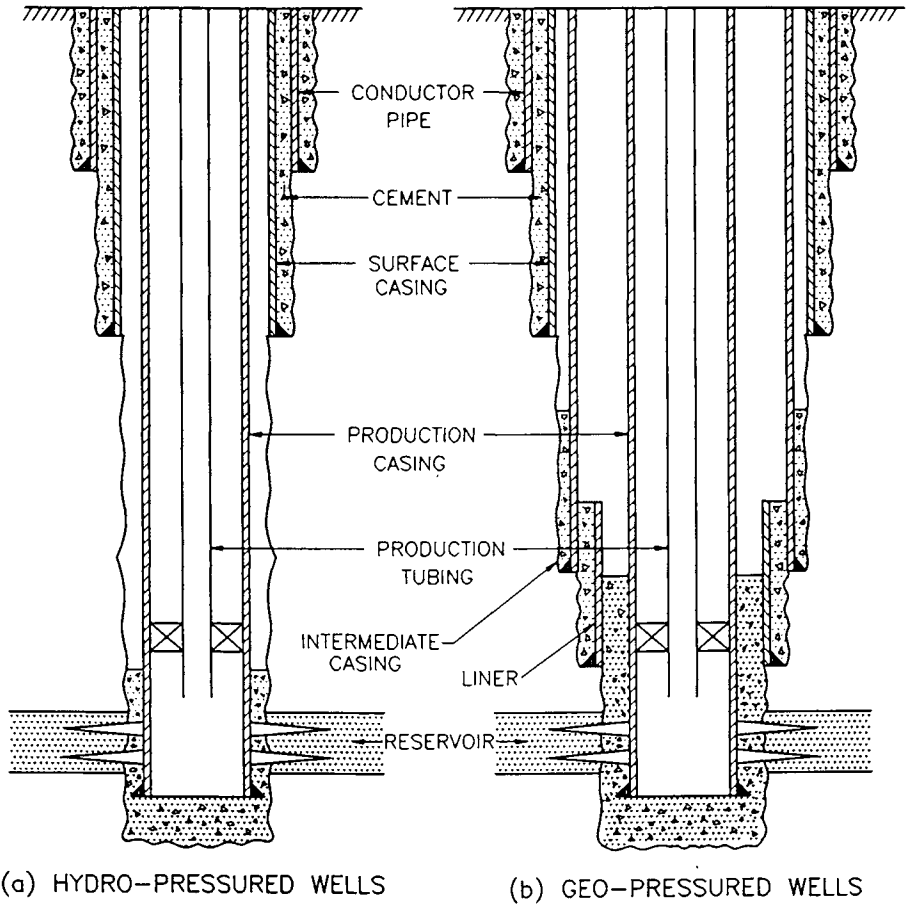

Fig. 1.1: Typical casing program showing different casing sizes and their setting depths.

1.2.1 Cassion Pipe

On an offshore platform, a cassion pipe, usually 26 to 42 in. in outside diameter (OD), is driven into the sea bed to prevent washouts of near-surface unconsolidated formations and to ensure the stability of the ground surface upon which the rig is seated. It also serves as a flow conduit for drilling fluid to the surface. The cassion pipe is tied back to the conductor or surface casing and usually does not carry any load.

1.2.2 Conductor Pipe

The outermost casing string is the conductor pipe. The main purpose of this casing is to hold back the unconsolidated surface formations and prevent them from falling into the hole. The conductor pipe is cemented back to the surface and it is either used to support subsequent casings and wellhead equipment or the pipe is cut off at the surface after setting the surface casing. Where shallow water or gas flow is expected, the conductor pipe is fitted with a diverter system above the flowline outlet. This device permits the diversion of drilling fluid or gas flow away from the rig in the event of a surface blowout. The conductor pipe is not shut-in in the event of fluid or gas flow, because it is not set in deep enough to provide any holding force.

The conductor pipe, which varies in length from 40 to 500 ft onshore and up to 1,000 ft offshore, is 7 to 20 in. in diameter. Generally, a 16-in. pipe is used in shallow wells and a 20-in. in deep wells. On offshore platforms, conductor pipe is usually 20 in. in diameter and is cemented across its entire length.

1.2.3 Surface Casing

The principal functions of the surface casing string are to: hold back unconsolidated shallow formations that can slough into the hole and cause problems, isolate the freshwater-bearing formations and prevent their contamination by fluids from deeper formations and to serve as a base on which to set the blowout preventers. It is generally set in competent rocks, such as hard limestone or dolomite, so that it can hold any pressure that may be encountered between the surface casing seat and the next casing seat.

Setting depths of the surface casing vary from a few hundred feet to as much as 5,000 ft. Sizes of the surface casing vary from 7 to 16 in. in diameter, with $10\frac{3}{4}$ in. and $13\frac{3}{8}$ in. being the most common sizes. On land, surface casing is usually cemented to the surface. For offshore wells, the cement column is frequently limited to the kickoff point.

1.2.4 Intermediate Casing

Intermediate or protective casing is set at a depth between the surface and production casings. The main reason for setting intermediate casing is to case off the formations that prevent the well from being drilled to the total depth. Troublesome zones encountered include those with abnormal formation pressures, lost circulation, unstable shales and salt sections. When abnormal formation pressures are present in a deep section of the well, intermediate casing is set to protect formations below the surface casing from the pressures created by the drilling fluid specific weight required to balance the abnormal pore pressure. Similarly, when normal pore pressures are found below sections having abnormal pore pressure, an additional intermediate casing may be set to allow for the use of more economical, lower specific weight, drilling fluids in the subsequent sections. After a troublesome lost circulation, unstable shale or salt section is penetrated, intermediate casing is required to prevent well problems while drilling below these sections.

Intermediate casing varies in length from 7,000 ft to as much as 15,000 ft and from 7 in. to $11\frac{3}{4}$ in. in outside diameter. It is commonly cemented up to 1,000 ft from the casing shoe and hung onto the surface casing. Longer cement columns are sometimes necessary to prevent casing buckling.

1.2.5 Production Casing

Production casing is set through the prospective productive zones except in the case of open-hole completions. It is usually designed to hold the maximal shut-in pressure of the producing formations and may be designed to withstand stimulating pressures during completion and workover operations. It also provides protection for the environment in the event of failure of the tubing string during production operations and allows for the production tubing to be repaired and replaced.

Production casing varies from $4\frac{1}{2}$ in. to $9\frac{5}{8}$ in. in diameter, and is cemented far enough above the producing formations to provide additional support for subsurface equipment and to prevent casing buckling.

1.2.6 Liners

Liners are the pipes that do not usually reach the surface, but are suspended from the bottom of the next largest casing string. Usually, they are set to seal off troublesome sections of the well or through the producing zones for economic reasons. Basic liner assemblies currently in use are shown in Fig. 1.2, these

include: drilling liner, production liner, tie-back liner, scab liner, and scab tie-back liner (Brown - Hughes Co., 1984).

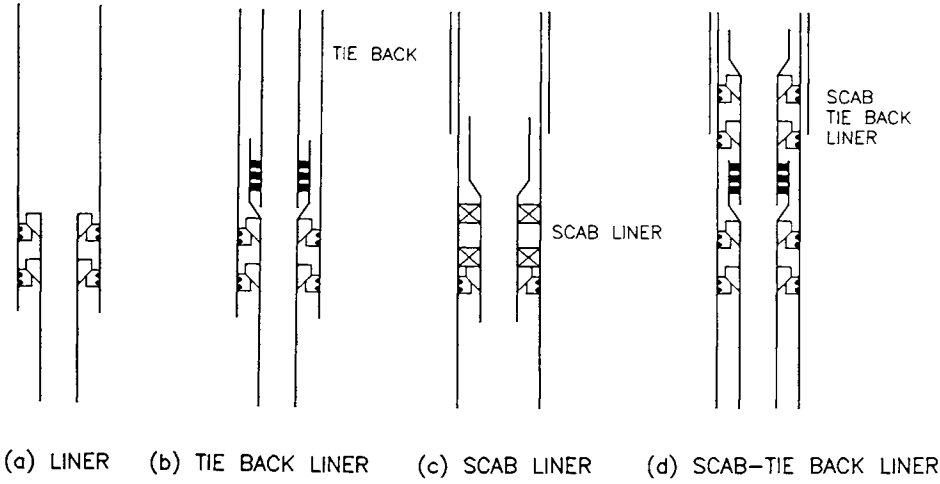

Fig. 1.2: Basic liner system. (After Brown - Hughes Co., 1984.)

Drilling liner: Drilling liner is a section of casing that is suspended from the existing casing (surface or intermediate casing). In most cases, it extends downward into the openhole and overlaps the existing casing by 200 to 400 ft. It is used to isolate abnormal formation pressure, lost circulation zones, heaving shales and salt sections, and to permit drilling below these zones without having well problems.

Production liner: Production liner is run instead of full casing to provide isolation across the production or injection zones. In this case, intermediate casing or drilling liner becomes part of the completion string.

Tie-back liner: Tie-back liner is a section of casing extending upwards from the top of the existing liner to the surface. This pipe is connected to the top of the liner (Fig. 1.2(b)) with a specially designed connector. Production liner with tie-back liner assembly is most advantageous when exploratory drilling below the productive interval is planned. It also gives rise to low hanging-weights in the upper part of the well.

Scab liner: Scab liner is a section of casing used to repair existing damaged casing. It may be cemented or sealed with packers at the top and bottom (Fig. 1.2(c)).

Scab tie-back liner: This is a section of casing extending upwards from the existing liner, but which does not reach the surface and is normally cemented in place. Scab tie-back liners are commonly used with cemented heavy-wall casing to isolate salt sections in deeper portions of the well.

The major advantages of liners are that the reduced length and smaller diameter of the casing results in a more economical casing design than would otherwise be possible and they reduce the necessary suspending capacity of the drilling rig. However, possible leaks across the liner hanger and the difficulty in obtaining a good primary cement job due to the narrow annulus must be taken into consideration in a combination string with an intermediate casing and a liner.

1.3 PIPE BODY MANUFACTURING

All oilwell tubulars including casing have to meet the requirements of the API (American Petroleum Institute) Specification 5CT (1992), formerly Specifications 5A, 5AC, 5AQ and 5AX. Two basic processes are used to manufacture casing: seamless and continuous electric weld.

1.3.1 Seamless Pipe

Seamless pipe is a wrought steel pipe manufactured by a seamless process. A large percentage of tubulars and high quality pipes are manufactured in this way. In the seamless process, a billet is pierced by a mandrel and the pierced tube is subsequently rolled and re-rolled until the finished diameters are obtained (Fig. 1.3). The process may involve a plug mill or mandrel mill rolling. In a plug mill, a heated billet is introduced into the mill, where it is held by two rollers that rotate and advance the billet into the piercer. In a mandrel mill, the billet is held by two obliquely oriented rotating rollers and pierced by a central plug. Next, it passes to the elongator where the desired length of the pipe is obtained. In the plug mills the thickness of the tube is reduced by central plugs with two single grooved rollers.

In mandrel mills, sizing mills similar in design to the plug mills are used to produce a more uniform thickness of pipe. Finally, reelers similar in design to the piercing mills are used to burnish the pipe surfaces and to produce the final pipe dimensions and roundness.

1.3.2 Welded Pipe

In the continuous electric process, pipe with one longitudinal seam is produced by electric flash or electric resistance welding without adding extraneous metal. In the electric flash welding process, pipes are formed from a sheet with the desired dimensions and welded by simultaneously flashing and pressing the two ends. In the electric resistance process, pipes are manufactured from a coiled

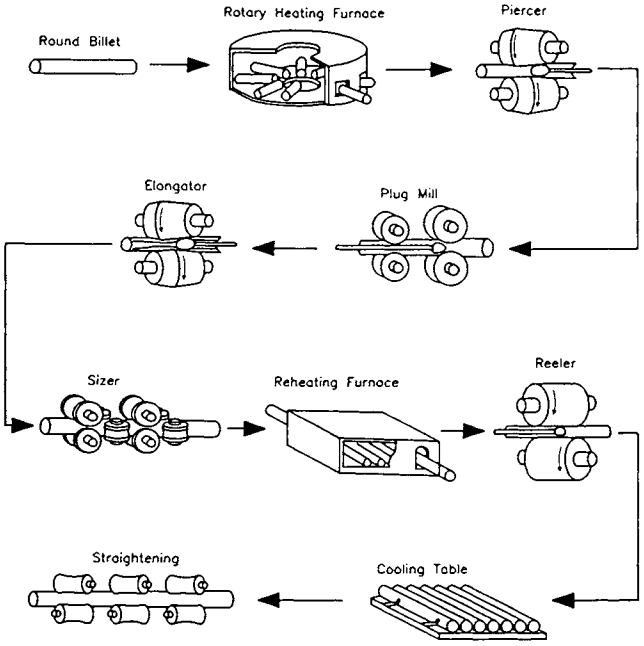

Fig. 1.3: Plug Mill Rolling Process for Kawasaki's 7-16$\frac{3}{8}$ in. pipe. (Courtesy of Kawasaki Steel Corporation.)

sheet which is fed into the machine, formed and welded by electric arc (Fig. 1.4). Pipe leaving the machine is cut to the desired length. In both the electric flash and electric arc welding processes, the casing is passed through dies that deform it sufficiently to exceed the elastic limit, a process which raises the elastic limit in the direction stressed and reduces it somewhat in the perpendicular direction: Bauchinger effect. Casing is also cold-worked during manufacturing to increase its collapse resistance.

1.3.3 Pipe Treatment

Careful control of the treatment process results in tension and burst properties equivalent to 95,000 psi circumferential yield.

Strength can be imparted to tubular goods in several ways. Insofar as most steels are relatively mild (0.30 % carbon), small amounts of manganese are added to them and the material is merely normalized. When higher-strength materials are required, they are normalized and tempered. Additional physical strength may be obtained by quenching and tempering (QT) a mild or low-strength steel. This QT process improves fracture toughness, reduces the metal's sensitivity to notches,

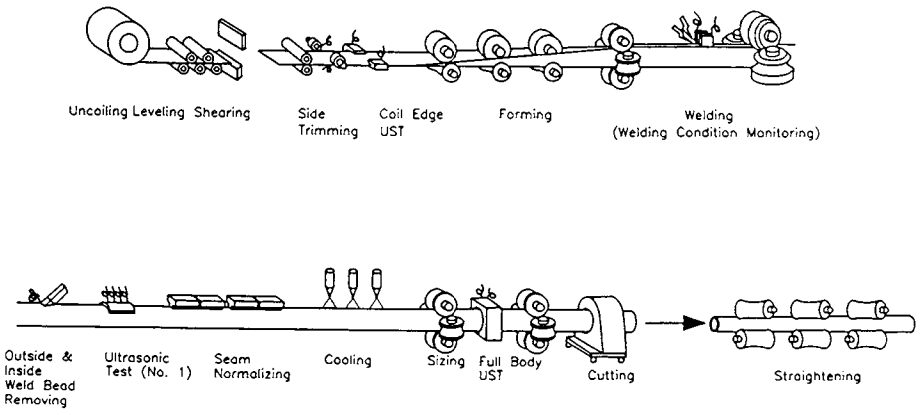

Fig. 1.4: Nippon's Electric Welding Method of manufacturing casing. (Courtesy of Nippon Steel Corporation.)

lowers the brittle fracture temperature and decreases the cost of manufacturing. Thus, many of the tubulars manufactured today are made by the low cost QT process, which has replaced many of the alloy steel (normalized and tempered) processes.

Similarly, some products, which are known as 'warm worked', may be strengthened or changed in size at a temperature below the critical temperature. This may also change the physical properties just as cold-working does.

1.3.4 Dimensions and Weight of Casing and Steel Grades

All specifications of casing include outside diameter, wall thickness, drift diameter, weight and steel grade. In recent years the API has developed standard specifications for casing, which have been accepted internationally by the petroleum industry.

1.3.5 Diameters and Wall Thickness

As discussed previously, casing diameters range from $4\frac{1}{2}$ to 24 in. so they can be used in different sections (depths) of the well. The following tolerances, from API Spec. 5CT (1992), apply to the outside diameter (OD) of the casing immediately behind the upset for a distance of approximately 5 inches:

Casing manufacturers generally try to prevent the pipe from being undersized to ensure adequate thread run-out when machining a connection. As a result, most

Table 1.1: API manufacturing tolerances for casing outside diameter. (After API Spec. 5CT, 1992.)

Outside diameter (in.)	Tolerances (in.)	
$1.05 - 3\frac{1}{2}$	$+\frac{3}{32}$	$-\frac{1}{32}$
$4 - 5$	$+\frac{7}{64}$	-0.75% OD
$5\frac{1}{2} - 8\frac{5}{8}$	$+\frac{1}{8}$	-0.75% OD
$\geq 9\frac{5}{8}$	$+\frac{5}{32}$	-0.75% OD

casing pipes are found to be within $\pm 0.75\%$ of the tolerance and are slightly oversized.

Inside diameter (ID) is specified in terms of wall thickness and drift diameter. The maximal inside diameter is, therefore, controlled by the combined tolerances for the outside diameter and the wall thickness. The minimal permissible pipe wall thickness is 87.5 % of the nominal wall thickness, which in turn has a tolerance of -12.5 %.

The minimal inside diameter is controlled by the specified drift diameter. The drift diameter refers to the diameter of a cylindrical drift mandrel, Table 1.2, that can pass freely through the casing with a reasonable exerted force equivalent to the weight of the mandrel being used for the test (API Spec. 5CT, 1992). A bit of a size smaller than the drift diameter will pass through the pipe.

Table 1.2: API recommended dimensions for drift mandrels. (After API Spec. 5CT, 1992.)

Casing and liner (in.)	Length (in.)	Diameter (ID) (in.)
$\leq 8\frac{5}{8}$	6	ID $-\frac{1}{8}$
$9\frac{5}{8} - 13\frac{3}{8}$	12	ID $-\frac{5}{32}$
≥ 16	12	ID $-\frac{3}{16}$

The difference between the inside diameter and the drift diameter can be explained by considering a 7-in., 20 lb/ft casing, with a wall thickness, t, of 0.272-in.

$$\begin{aligned} \text{Inside diameter} &= \text{OD} - 2t \\ &= 7 - 0.544 \\ &= 6.456 \text{ in.} \end{aligned}$$

$$\begin{aligned} \text{Drift diameter} &= \text{ID} - \tfrac{1}{8} \\ &= 6.456 - 0.125 \\ &= 6.331 \text{ in.} \end{aligned}$$

Drift testing is usually carried out before the casing leaves the mill and immediately before running it into the well. Casing is tested throughout its entire length.

1.3.6 Joint Length

The lengths of pipe sections are specified by API RP 5B1 (1988), in three major ranges: R1, R2 and R3, as shown in Table 1.3.

Table 1.3: API standard lengths of casing. (After API RP 5B1, 1988.)

Range	Length (ft)	Average length (ft)
1	16 - 25	22
2	25 - 34	31
3	over 34	42

Generally, casing is run in R3 lengths to reduce the number of connections in the string, a factor that minimizes both rig time and the likelihood of joint failure in the string during the life of the well (joint failure is discussed in more detail on page 18). R3 is also easy to handle on most rigs because it has a single joint.

1.3.7 Makeup Loss

When lengths of casing are joined together to form a string or section, the overall length of the string is less than the sum of the individual joints. The reason that the completed string is less than the sum of the parts is the makeup loss at the couplings.

It is clear from Fig. 1.5 that the makeup loss per joint for a string made up to the powertight position is:

$$L_l = \frac{L_c}{2} - J$$

where:

l_j = length of pipe.
l_{jc} = length of the casing with coupling.
L_c = length of the coupling.

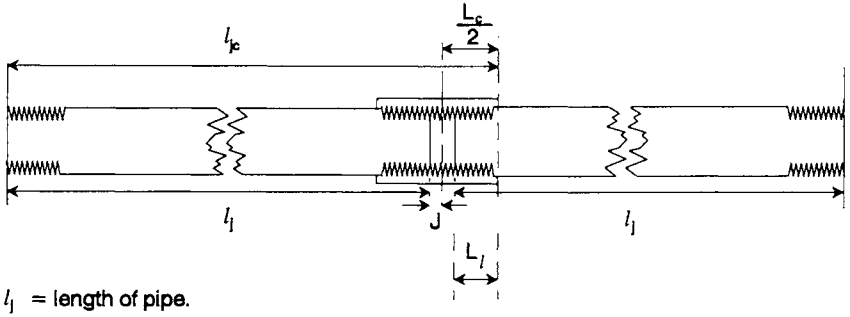

l_j = length of pipe.

l_{jc} = length of casing with coupling.

J = distance between end of casing in power tight position and the center of the coupling.

L_l = makeup loss.

L_c = length of the coupling.

Fig. 1.5: Makeup loss per joint of casing.

J = distance between the casing end in the power tight position and the coupling center.

L_l = makeup loss.

EXAMPLE 1-1[a]:

Calculate the makeup loss per joint for a $9\frac{5}{8}$-in., N-80, 47 lb/ft casing with short threads and couplings. Also calculate the loss in a 10,000-ft well (ignore tension effects) and the additional length of madeup string required to reach true vertical depth (TVD). Express the answer in general terms of l_{jc}, the average length of the casing in feet of the tallied (measured) casing and then calculate the necessary makeup lengths for $l_{jc} = 21$, 30 and 40 - assumed average lengths of R1, R2 and R3 casing available.

Solution:

For a casing complete with couplings, the length l_{jc} is the distance measured from the uncoupled end of the pipe to the outer face of the coupling at the opposite end, with the coupling made-up power-tight (API Spec. 5CT).

From Table 1.4, $L_c = 7\frac{3}{4}$ in. and $J = 0.500$-in. Thus,

$$\begin{aligned} L_l &= \frac{L_c}{2} - J \\ &= 3.875 - 0.500 \\ &= 3.375 \text{ in.} \end{aligned}$$

[a]Based on Example. 2.1, Craft et al. (1962).

Table 1.4: Round-thread casing dimensions for long threads and couplings.

D in.	t in.	$J^{\dagger}$ in.	$L_c^{\ddagger}$ in.
4.5	All	0.5	7
5	All	0.5	7.75
5.5	All	0.5	8
6.625	All	0.5	8.75
7	All	0.5	9
7.625	All	0.5	9.25
8.625	All	0.5	10
9.625	All	0.5	10.5

† STD 5B ‡ Spec 5CT

The number of joints in 1,000 ft of tallied casing is $1{,}000/l_{jc}$ and, therefore, the makeup loss in 1,000 ft is:

$$\begin{aligned} \text{Makeup loss per 1,000 ft} &= 3.375 \times 1{,}000/l_{jc} \\ &= 3.375/l_{jc} \text{ in.} \\ &= 3.375/(12l_{jc}) \text{ ft} \end{aligned}$$

As tension effects are ignored this is the makeup loss in *any* 1,000-ft section.

If L_T is defined as the total casing required to make 1,000 ft of made-up, power-tight string, then:

$$\text{makeup loss} = \frac{L_T}{1{,}000}\left(\frac{3.375}{12l_{jc}}\right) \text{ ft}$$

$$1{,}000 = L_T - L_T\left(\frac{3.375}{12l_{jc}}\right) \text{ ft}$$

$$\Rightarrow L_T = \left(\frac{1{,}000l_{jc}}{l_{jc} - 0.28125}\right) \text{ ft}$$

Finally, using the general form of the above equation in L_T, Table 1.5 can be produced to give the makeup loss in a 10,000-ft string.

1.3.8 Pipe Weight

According to the API Bul. 5C3 (1989), pipe weight is defined as nominal weight, plain end weight, and threaded and coupled weight. Pipe weight is usually ex-

Table 1.5: Example 1: makeup loss in 10,000 ft strings for different API casing lengths.

R	L (ft)	L_T (ft)	makeup Loss (ft)
1	21	10.135.75	135.75
2	30	10.094.63	94.63
3	40	10.070.81	70.81

pressed in lb/ft. The API tolerances for weight are: +6.5 % and -3.5 % (API Spec. 5CT, 1992).

Nominal weight is the weight of the casing based on the theoretical weight per foot for a 20-ft length of threaded and coupled casing joint. Thus, the nominal weight, W_n in lb/ft, is expressed as:

$$W_n = 10.68\,(d_o - t)\,t + 0.0722\,d_o^2 \tag{1.1}$$

where:

W_n = nominal weight per unit length, lb/ft.
d_o = outside diameter, in.
t = wall thickness, in.

The nominal weight is not the exact weight of the pipe, but rather it is used for the purpose of identification of casing types.

The plain end weight is based on the weight of the casing joint excluding the threads and couplings. The plain end weight, W_{pe}, in lb/ft, is expressed as:

$$W_{pe} = 10.68\,(d_o - t) \text{ lb/ft} \tag{1.2}$$

Threaded and coupled weight, on the other hand, is the average weight of the pipe joint including the threads at both ends and coupling at one end when in the power tight position. Threaded and coupled weight, W_{tc}, is expressed as:

$$W_{tc} = \frac{1}{20}\{\,(W_{pe}\,[20 - (L_c + 2J)/24] + \text{Weight of coupling} - \text{Weight removed in threading two pipe ends}\,\} \tag{1.3}$$

where:

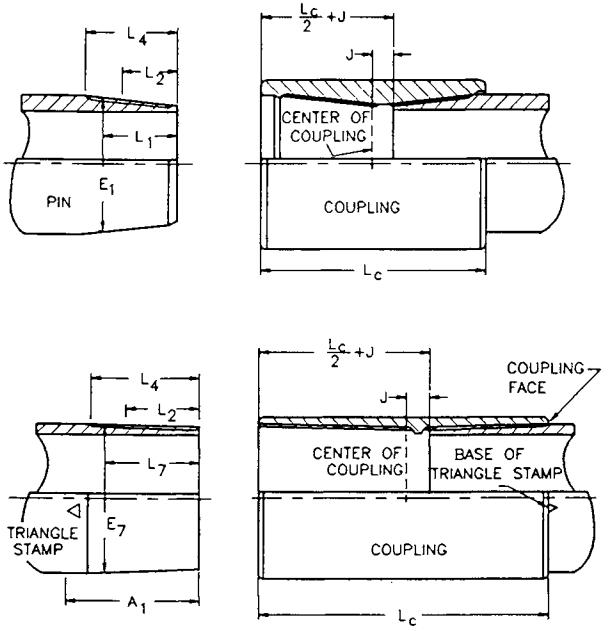

L_1	PIPE END TO HAND TIGHT PLANE	E_1	PITCH DIAMETER AT HAND TIGHT PLANE
L_2	MINIMUM LENGTH, FULL CRESTED THREAD	E_7	PITCH DIAMETER AT L7 DISTANCE
L_4	THREADED LENGTH	J	END OF POWER TIGHT PIN TO CENTER OF COUPLING
L_7	TOTAL LENGTH, PIN TIP TO VANISH POINT LENGTH, PERFECT THREADS	L_c	LENGTH OF COUPLING

Fig. 1.6: Basic axial dimensions of casing couplings: API Round threads (top). API Buttress threads (bottom).

W_{tc} = threaded and coupled weight, lb/ft.
L_c = coupling length, in.
J = distance between the end of the pipe and center of the coupling in the power tight position, in.

The axial dimensions for both API Round and API Buttress couplings are shown in Fig. 1.6.

1.3.9 Steel Grade

The steel grade of the casing relates to the tensile strength of the steel from which the casing is made. The steel grade is expressed as a code number which consists of a letter and a number, such as N-80. The letter is arbitrarily selected

to provide a unique designation for each grade of casing. The number designates the minimal yield strength of the steel in thousands of psi. Strengths of API steel grades are given in Table 1.6.

Hardness of the steel pipe is a critical property especially when used in H_2S (sour) environments. The L-grade pipe has the same yield strength as the N-grade, but the N-grade pipe may exceed 22 Rockwell hardness and is, therefore, not suitable for H_2S service. For sour service, the L-grade pipe with a hardness of 22 or less, or the C-grade pipe can be used.

Many non-API grades of pipes are available and widely used in the drilling industry. The strengths of some commonly used non-API grades are presented in Table 1.7. These steel grades are used for special applications that require very high tensile strength, special collapse resistance or other properties that make steel more resistant to H_2S.

Table 1.6: Strengths of API steel grades. (API Spec. 5CT, 1992.)

API Grade	Yield Strength (psi) Minimum	Yield Strength (psi) Maximum	Minimum Ultimate Tensile Strength (psi)	Minimum Elongation * (%)
H-40	40,000	80,000	60,000	29.5
J-55	55,000	80,000	75,000	24.0
K-55	55,000	80,000	95,000	19.5
L-80	80,000	95,000	95,000	19.5
N-80	80,000	110,000	100,000	18.5
C-90	90,000	105,000	100,000	18.5
C-95	95,000	110,000	105,000	18.0
T-95	95,000	110,000	105,000	18.0
P-110	110,000	140,000	125,000	15.0
Q-125	125,000	150,000	135,000	14.0

* Elongation in 2 inches, minimum per cent for a test specimen with an area ≥ 0.75 in^2.

1.4 CASING COUPLINGS AND THREAD ELEMENTS

A coupling is a short piece of pipe used to connect the two ends, pin and box, of the casing. Casing couplings are designed to sustain high tensile load while

Table 1.7: Strengths of non-API steel grades.

Non-API Grade	Manufacturer	Yield Strength (psi) Minimum	Maximum	Minimal Ultimate Tensile Strength (psi)	Minimal* Elongation (%)
S-80	Lone Star Steel	75.000 **	-	75.000	20.0
		55.000 †	-		
Mod. N-80	Mannesmann	80.000	95.000	100.000	24.0
C-90 ‡	Mannesmann	90.000	105.000	120.000	26.0
SS-95	Lone Star Steel	95.000 **	-	95.000	18.0
		75.000 †	-		
S00-95	Mannesmann	95.000	110.000	110.000	20.0
S-95	Lone Star Steel	95,000 **	-	110.000	16.0
		92,000 †	-		
S00-125	Mannesmann	125.000	150.000	135.000	18.0
S00-140	Mannesmann	140.000	165.000	150.000	17.0
V-150	U.S. Steel	150.000	180.000	160.000	14.0
S00-155	Mannesmann	155.000	180.000	165.000	20.0

* Test specimen with area greater than 0.75 sq in.
** Circumferential.
† Longitudinal
‡ Maximal ultimate tensile strength of 120.000 psi.

at the same time providing pressure containment from both net internal and external pressures. Their ability to resist tension and contain pressure depends primarily on the type of threads cut on the coupling and at the pipe ends. With the exception of a growing number of proprietary couplings, the configurations and specifications of the couplings are standardized by API (API RP 5B1, 1988).

1.4.1 Basic Design Features

In general, casing couplings are specified by the types of threads cut on the pipe ends and coupling. The principal design features of threads are: form, taper, height, lead and pitch diameter (Fig. 1.7).

Form: Design of thread form is the most obvious way to improve the load bearing capacity of a casing connection. The two most common thread

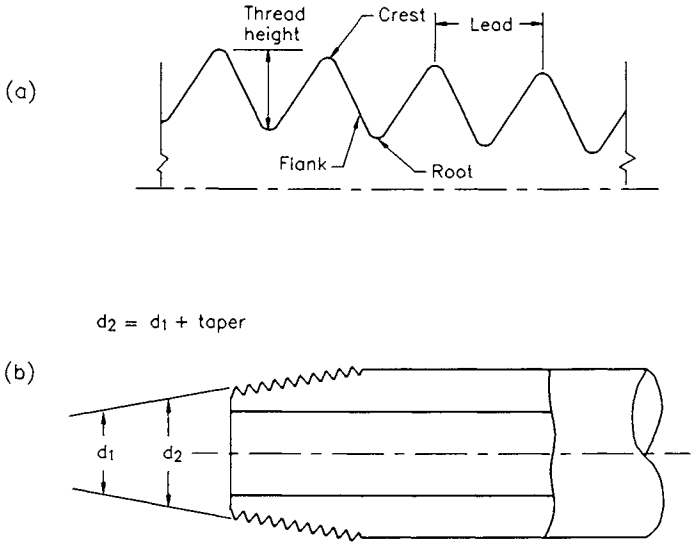

Fig. 1.7: Basic elements of a thread. The thread taper is the change in diameter per unit distance moved along the thread axis. Thus, the change in diameter, $d_2 - d_1$, per unit distance moved along the thread axis, is equal to the taper per unit on diameter. Refer to Figs. 9 and 10 for further clarification.

forms are: squared and V-shape. The API uses round and buttress threads which are special forms of squared and V-shape threads.

Taper: Taper is defined as the change in diameter of a thread expressed in inches per foot of thread length. A steep taper with a short connection provides for rapid makeup. The steeper the taper, however, the more likely it is to have a jumpout failure, and the shorter the thread length, the more likely it is to experience thread shear failure.

Height: Thread height is defined as the distance between the crest and the root of a thread measured normal to the axis of the thread. As the thread height of a particular thread shape increases, the likelihood of jumpout failure decreases; however, the critical material thickness under the last engaged thread decreases.

Lead: Lead is defined as the distance from one point on the thread to the corresponding point on the adjacent thread and is measured parallel to the thread axis.

Pitch Diameter: Pitch diameter is defined as the diameter of an imaginary cone that bisects each thread midway between its crest and root.

Threaded casing connections are often rated according to their joint efficiency and sealing characteristics. Joint efficiency is defined as the tensile strength of the joint divided by the tensile strength of the pipe. Generally, failure of the joint is recognized as jumpout, fracture, or thread shear.

Jumpout: In a jumpout, the pin and box separate with little or no damage to the thread element. In a compression failure, the pin progresses further into the box.

Fracture: Fracturing occurs when the pin threaded section separates from the pipe body or there is an axial splitting of the coupling. Generally this occurs at the last engaged thread.

Thread Shear: Thread shear refers to the stripping off of threads from the pin and/or box.

Generally speaking, shear failure of most threads under axial load does not occur. In most cases, failure of V-shape threads is caused by jumpout or occasionally, by fracture of the pipe in the last engaged threads. Square threads provide a high strength connection and failure is usually caused by fracture in the pipe near the last engaged thread. Many proprietary connections use a modified buttress thread and some use a negative flank angle to increase the joint strength.

In addition to its function of supporting tension and other loads, a joint must also prevent the leakage of the fluids or gases which the pipe must contain or exclude. Consequently, the interface pressure between the mating threads in a joint must be sufficiently large to obtain proper mating and sealing. This is accomplished by thread interference, metal to metal seal, resilient ring or combination seals.

Thread Interference: Sealing between the threads is achieved by having the thread members tapered and applying a makeup torque sufficient to wedge the pin and box together and cause interference between the thread elements. Gaps between the roots and crests and between the flanks of the mating surfaces, which are required to allow for machining tolerance, are plugged by a thread compound. The reliability of these joints is, therefore, related to the makeup torque and the gravity of the thread compound. Excessive makeup or insufficient makeup can both be harmful to the sealing properties of joints. The need for excessive makeup torque to generate high pressure often causes yielding of the joint.

Metal-to-Metal Seal: There are two types of metal-to-metal seal: radial and shoulder. Radial is usually used as the primary seal and the shoulder as the backup seal. A radial seal generally occurs between flanks and between the crests and roots as a result of: pressure due to thread interference created by

makeup torque, pressure due to the radial component of the stress created by internal pressure and pressure due to the torque created by the negative flank angle (Fig. 1.8). Shoulder sealing occurs as a result of pressure from thread interference, which is directly related to the torque imparted during the joint makeup. Low makeup torque may provide insufficient bearing pressure, whereas high makeup torque can plastically deform the sealing surface (Fig. 1.8(c)).

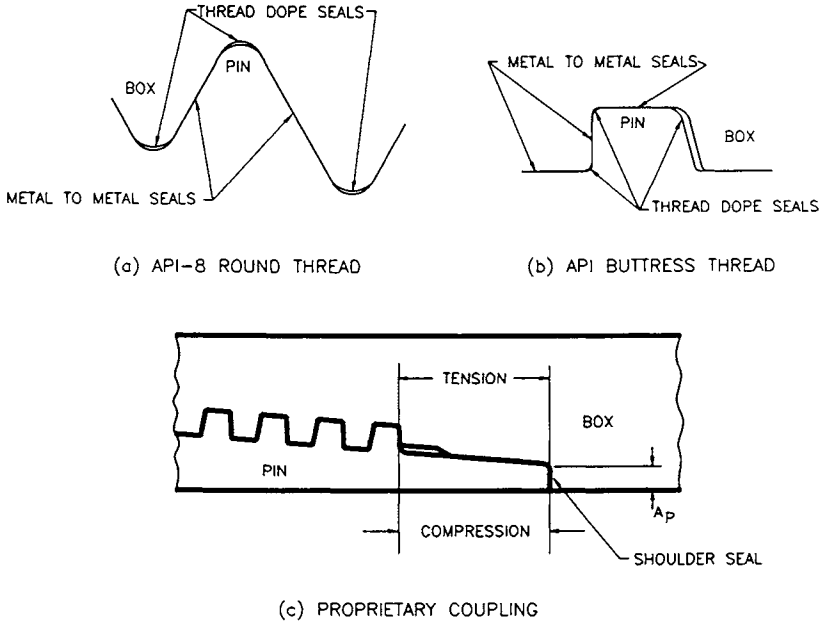

Fig. 1.8: Metal-to-metal seal: (a) API 8-Round thread, (b) API Buttress thread, (c) proprietary coupling. (After Rawlins, 1984.)

Resilient Rings: Resilient rings are used to provide additional means of plugging the gaps between the roots and crests. Use of these rings can upgrade the standard connections by providing sealing above the safe rating that could be applied to connections without the rings. Their use, however, reduces the strength of the joint and increases the hoop (circumferential) stress.

Combination Seal: A combination of two or more techniques can be used to increase the sealing reliability. The interdependence of these seals, however, can result in a less effective overall seal. For example, the high thread interference needed to seal high pressure will decrease the bearing pressure of the metal-to-metal seal. Similarly, the galling effect resulting from the use of a resilient ring may make the metal-to-metal seal ineffective (Fig. 1.9).

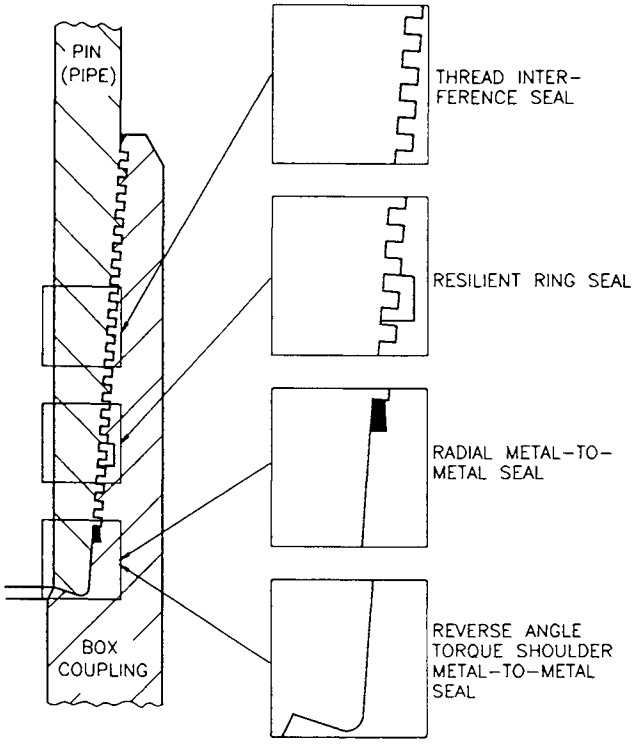

Fig. 1.9: Combination seals. (After Biegler, 1984.)

1.4.2 API Couplings

The API provides specifications for three types of casing couplings: round thread, buttress thread and extreme-line coupling.

API Round Thread Coupling

Eight API Round threads with a taper of $\frac{3}{4}$ in./ft are cut per inch on diameter for all pipe sizes. The API Round thread has a V-shape with an included angle of 60° (Fig. 1.10), and thus the thread roots and crests are truncated with a radius. When the crest of one thread is mated against the root of another, there exists a clearance of approximately 0.003-in. which provides a leak path. In practice, a special thread compound is used when making up two joints to prevent leakage. Pressure created by the flank interface due to the makeup torque provides an additional seal. This pressure must be greater than the pressure to be contained.

API Round thread couplings are of two types: short thread coupling (STC) and long thread coupling (LTC). Both STC and LTC threads are weaker than the pipe body and are internally threaded. The LTC is capable of transmitting a higher axial load than the STC.

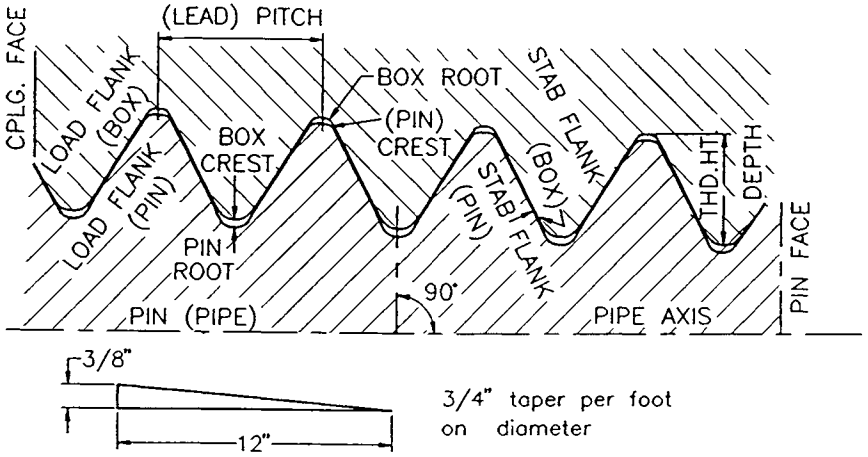

Fig. 1.10: Round thread casing configuration. (After API RP 5B1, 1988.)

API Buttress Thread Coupling

A cross-section of a API Buttress coupling is presented in Fig. 1.11. Five threads are cut in one inch on the pipe diameter and the thread taper is $\frac{3}{4}$ in./ft for casing sizes up to $7\frac{5}{8}$ in. and 1 in./ft for sizes 16 in. or larger. Long coupling, square shape and thread run-out allow the API Buttress coupling to transmit higher axial load than API Round thread. The API Buttress couplings, however, depend on similar types of seal to the API Round threads. Special thread compounds are used to fill the clearance between the flanks and other meeting parts of the threads. Seals are also provided by pressure at the flanks, roots and crests during the making of a connection. In this case, tension has little effect on sealing, whereas compression load could separate the pressure flanks causing a spiral clearance between the pressure flanks and thereby permitting a leak. Frequent changes in load from tension to neutral to compression causes leaks in steam injection wells equipped with API Buttress couplings.

A modified buttress thread profile is cut on a taper in some proprietary connections to provide additional sealing. For example, in a Vallourec VAM casing coupling, the thread crest and roots are flat and parallel to the cone. Flanks are 3° and 10° to the vertical of the pipe axis, as shown in Fig. 1.12, and 5 threads per inch are on the axis of the pipe. Double metal-to-metal seals are provided at the pin end by incorporating a reverse shoulder at the internal shoulder (Fig. 1.12), which is resistant to high torque and allows non-turbulent flow of fluid.

Metal-to-metal seals, at the internal shoulder of VAM coupling, are affected most by the change in tension and compression in the pipe. When the makeup torque is applied, the internal shoulder is locked into the coupling, thereby creating tension in the box and compression in the pin. If tensile load is applied to the connection, the box will be elongated further and the compression in the pin will

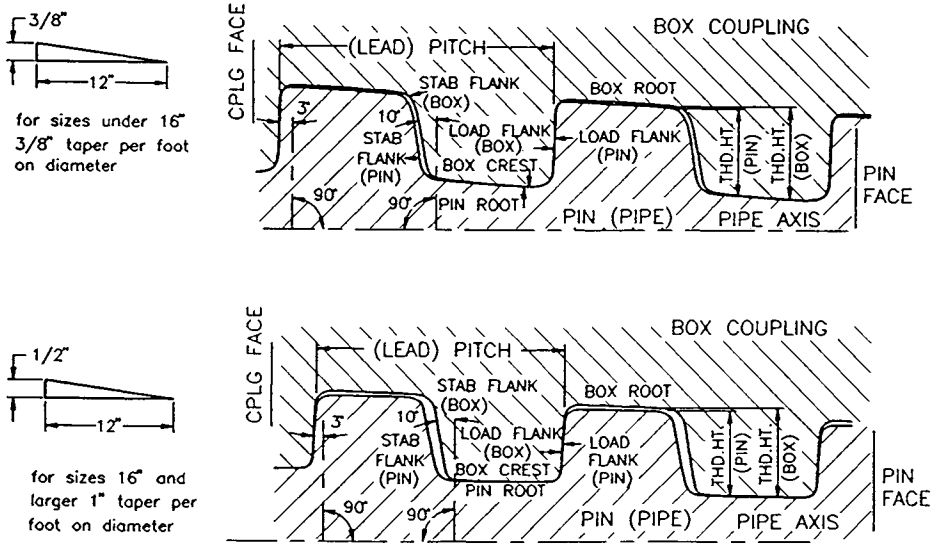

Fig. 1.11: (a) API Buttress thread configuration for $13\frac{3}{8}$ in. outside diameter and smaller casing; (b) API Buttress thread configuration for 16 in. outside diameter and larger casing. (After API RP 5B1, 1988.)

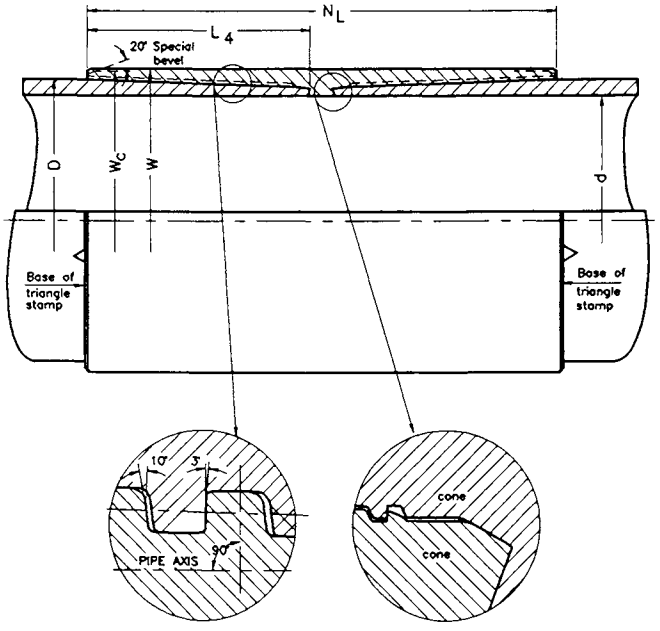

Fig. 1.12: Vallourec VAM casing coupling. (After Rabia, 1987; courtesy of Graham & Trotman)

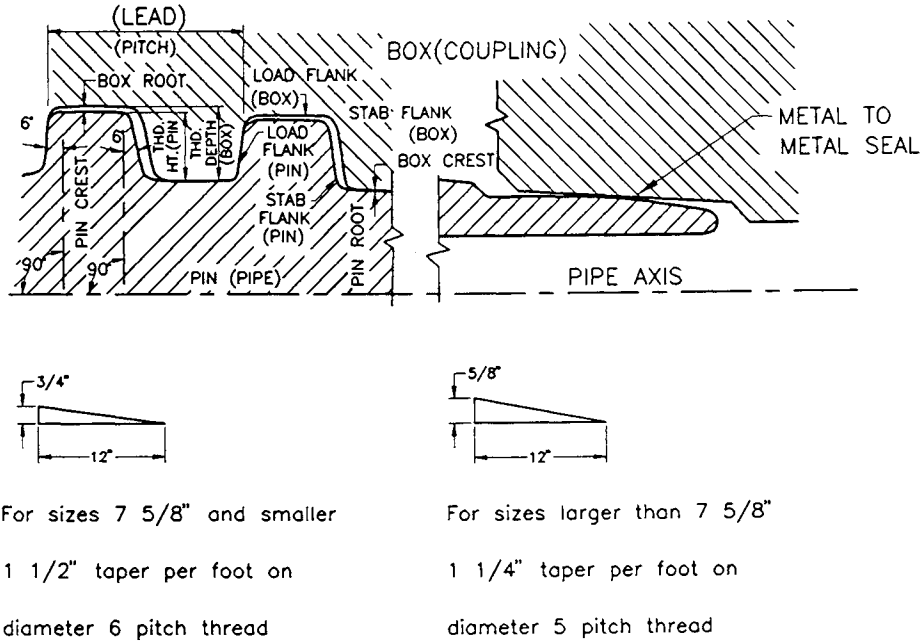

Fig. 1.13: API Extreme-line casing thread configuration. (After API RP 5B1, 1988.)

be reduced due to the added load. Should the tensile load exceed the critical value, the shoulders may separate.

API Extreme-line Thread Coupling

API Extreme-line coupling differs from API Round thread and API Buttress thread couplings in that it is an integral joint, i.e., the box is machined into the pipe wall. With integral connectors, casing is made internally and externally upset to compensate for the loss of wall thickness due to threading. The thread profile is trapezodial and additional metal-to-metal seal is provided at the pin end and external shoulder. As a result, API Extreme-line couplings do not require any sealing compound, although the compound is still necessary for lubrication. The metal-to-metal seal at the external shoulder of the pin is affected in the same way as VAM coupling when axial load is applied.

In an API Extreme-line coupling, 6 threads per inch are cut on pipe sizes of 5 in. to $7\frac{5}{8}$ in. with $1\frac{1}{2}$ in./ft of taper and 5 threads per inch are cut on pipe sizes of $8\frac{5}{8}$ in. to $10\frac{3}{8}$ in. with $1\frac{1}{4}$ in./ft of taper. Figure 1.13 shows different design features of API Extreme-line coupling.

1.4.3 Proprietry Couplings

In recent years, many proprietary couplings with premium design features have been developed to meet special drilling and production requirements. Some of these features are listed below.

Flush Joints: Flush joints are used to provide maximal annular clearance in order to avoid tight spots and to improve the cement bond.

Smooth Bores: Smooth bores through connectors are necessary to avoid turbulent flow of fluid.

Fast Makeup Threads: Fast makeup threads are designed to facilitate fast makeup and reduce the tendency to cross-thread.

Metal-to-Metal Seals: Multiple metal-to-metal seals are designed to provide improved joint strength and pressure containment.

Multiple Shoulders: Use of multiple shoulders can provide improved sealing characteristics with adequate torque and compressive strength.

Special Tooth Form: Special tooth form, e.g., a squarer shape with negative flank angle provide improved joint strength and sealing characteristics.

Resilient Rings: If resilient rings are correctly designed, they can serve as secondary pressure seals in corrosive and high-temperature environments.

1.5 REFERENCES

Adams, N.J., 1985. *Drilling Engineering - A Complete Well Planning Approach.* Penn Well Books, Tulsa, OK, pp. 357–366, 385.

API Bul. 5C3, 5th Edition, July 1989. *Bulletin on Formulas and Calculations for Casing, Tubing, Drill Pipe and Line Pipe Properties.* API Production Department.

API Specification STD 5B, 13th Edition, May 31, 1988. *Specification for Threading, Gaging, and Thread Inspection of Casing, Tubing, and Line Pipe Threads.* API Production Department.

API RP 5B1, 3rd Edition, June 1988. *Recommended Practice for Gaging and Inspection of Casing, Tubing and Pipe Line Threads.* API Production Department.

API Specification 5CT, 3rd Edition, Nov. 1, 1992. *Specification for Casing and Tubing.* API Production Department.

Biegler, K.K., 1984. *Conclusions Based on Laboratory Tests of Tubing and Casing Connections.* SPE Paper No. 13067, Presented at 59th Annu. Techn. Conf. and Exhib., Houston, TX, Sept. 16–19.

Bourgoyne A.T., Jr., Chenevert, M.E., Millheim, K.K. and Young, F.S., Jr., 1985. *Applied Drilling Engineering.* SPE Textbook Series, Vol. 2, Richardson, TX, USA, pp. 300–306.

Brown-Hughes Co., 1984. *Technical Catalogue.*

Buzarde, L.E., Jr., Kastro, R.L., Bell, W.T. and Priester C.L., 1972. *Production Operations, Course 1.* SPE, pp. 132–172.

Craft, B.C., Holden, W.R. and Graves, E.D., Jr., 1962. *Well Design: Drilling and Production.* Prentice-Hall, Inc., Englewood Cliffs, NJ, USA, pp. 108–109.

Rabia, H., 1987. *Fundamentals of Casing Design.* Graham & Trotman, London, UK, pp. 1–23.

Rawlins, M., 1984. How loading affects tubular thread shoulder seals. *Petrol. Engr. Internat.*, 56: 43–52.

Chapter 2

PERFORMANCE PROPERTIES OF CASING UNDER LOAD CONDITIONS

Casing is subjected to different loads during landing, cementing, drilling, and production operations. The most important loads which it must withstand are: tensile, burst and collapse loads. Accordingly, tensile, burst and collapse strengths of casing are defined by the API as minimal performance properties (API Bul. 5C2, 1987; API Bul. 5C3, 1989). There are other loads, however, that may be of equal or greater importance and are often limiting factors in the selection of casing grades. These loads include: wear, corrosion, vibration and pounding by drillpipe, the effects of gun perforating and erosion. In this chapter, the sources and characteristics of the loads which are important to the casing design and the formulas to compute them are discussed.

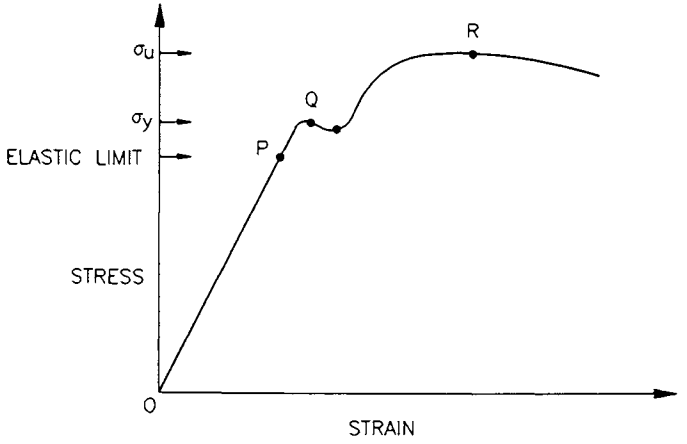

Fig. 2.1: Elastoplastic material behavior with transition range.

2.1 TENSION

Under axial tension, pipe body may suffer three possible deformations: elastic, elasto-plastic or plastic, as illustrated in Fig. 2.1. The straight portion of the curve OP represents elastic deformation. Within the elastic range the metallurgical properties of the steel in the pipe body suffer no permanent damage and it regains its original form if the load is withdrawn. Beyond the elastic limit (point P), the pipe body suffers a permanent deformation which often results in the loss of strength. Points Q and R on the curve are defined respectively as the yield strength (σ_y) and minimal ultimate strength (σ_u) of the material. Axial tensile load on the casing string, therefore, should not exceed the yield strength of the material during running, drilling, and production operations.

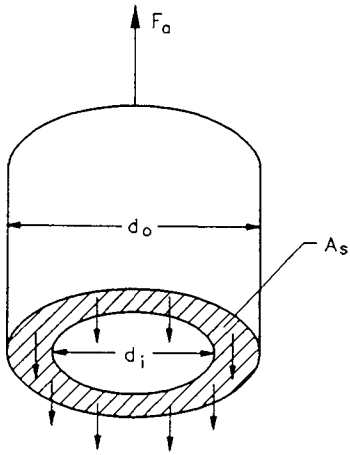

Fig. 2.2: Free body diagram of tension and reaction forces.

The strength of the casing string is expressed as pipe body yield strength and joint strength. Pipe body yield strength is the minimal force required to cause permanent deformation of the pipe. This force can be computed from the free body diagram shown in Fig. 2.2. Axial force, F_a, acts to pull apart the pipe of cross-sectional area of A_s.

Thus,

$$F_a = \sigma_y A_s \tag{2.1}$$

or

$$F_a = \frac{\pi}{4} \sigma_y (d_o^2 - d_i^2) \tag{2.2}$$

where:

σ_y = minimal yield strength, psi.
d_o = nominal outside diameter of the pipe, in.
d_i = inside diameter of the pipe, in.

EXAMPLE 2-1:

Calculate the pipe-body yield strength for $9\frac{5}{8}$ in., N-80 casing, with a nominal weight of 47 lb/ft and a nominal wall thickness of 0.472-in.

Solution:

The minimum yield strength for N-80 steel:

$$\sigma_y = 80,000 \text{ psi}$$

The internal diameter, d_i:

$$\begin{aligned} d_i &= 9.625 - 2(0.472) \\ &= 8.681 \text{ in.} \end{aligned}$$

Thus, the cross-sectional area, A_s, is:

$$\begin{aligned} A_s &= \frac{\pi}{4}(9.625^2 - 8.681^2) \\ &= 13.57 \text{ in.}^2 \end{aligned}$$

Therefore, from Eq. 2.1:

$$\begin{aligned} F_a &= A_s \sigma_y \\ &= 13.57 \times 80,000 \\ &= 1.086 \times 10^3 \text{ lbf} \end{aligned}$$

Minimal yield strength is defined as the axial force required to produce a total elongation of 0.5 % of the gauge length of the specimen. For grades P-105 and P-110 the total elongation of gauge length is 0.6 %.

Joint strength is the minimal tensile force required to cause the joint to fail. Formulas used to compute the joint strength are based partly on theoretical considerations and partly on empirical observation.

For API Round thread, joint strength is defined as the smaller of minimal joint fracture force and minimal joint pullout force. Calculation of these forces proceeds as follows:

Tensional force for fracture, F_{aj} (lbf):

$$F_{aj} = 0.95\, A_{jp} \sigma_{up} \tag{2.3}$$

Tensional force for joint pullout:

$$F_{aj} = 0.95\, A_{jp} L_{et} \left[\frac{0.74\, d_o^{-0.59}\, \sigma_{up}}{0.5\, L_{et} + 0.14\, d_o} + \frac{\sigma_y}{L_{et} + 0.14\, d_o} \right] \tag{2.4}$$

where:

A_{jp} = area under last perfect thread, in.^{2}
L_{et} = length of engaged thread, in.
σ_{up} = minimum ultimate yield strength of the pipe, psi.

Area A_{jp} is expressed as:

$$A_{jp} = \frac{\pi}{4} [(d_o - 0.1425)^2 - d_i^2] \tag{2.5}$$

Coupling Fracture Strength:

$$F_{aj} = 0.95\, A_{jp} \sigma_{uc} \tag{2.6}$$

A_{jc} = area under last perfect thread, in.^{2}
= $\pi\, [d_{co}^2 - d_{root}^2]/4$
d_{co} = outside diameter of the coupling, in.
d_{root} = diameter at the root of the coupling thread of the pipe in the powertight position rounded to the nearest 0.001 in. for API Round thread casing and tubing, in.
σ_{uc} = minimum ultimate yield strength of the coupling, psi.

EXAMPLE 2-2:

For API Round thread calculate: (i) tensional force for fracture, (ii) tensional force for joint pullout. Use the same size and grade casing as in Example 2-1. Additional information from manufacturer's specifications: $L_{et} = 4.041$ in. (long thread), $\sigma_u = 100{,}000$ psi (Table 1.1).

Solution:

From Eq. 2.5, the cross-sectional area under the last perfect thread, A_{jp}, is:

$$A_{jp} = \frac{\pi}{4}[(9.625 - 0.1425)^2 - 8.681^2]$$
$$= 11.434 \text{ sq. in.}$$

(i) From Eq. 2.3 one can calculate fracture force as:

$$F_{aj} = 0.95 \times 11.434 \times 10^5$$
$$= 1{,}086 \times 10^3 \text{ lbf}$$

(ii) Similarly Eq. 2.4 yields the force for the joint pullout:

$$F_{aj} = 10.8623 \times 4.041 \left[\frac{0.74 \times (9.625)^{-0.59} \times 10^5}{0.5\,(4.041) + 0.14(9.625)} + \frac{80.000}{4.041 + 0.14\,(9.625)}\right]$$
$$= 905 \times 10^3 \text{ lbf}$$

From the above analysis the limiting factor is the joint pullout, so for API Round thread (long), N-80, $9\frac{5}{8}$ in. casing, the joint strength is: $F_{aj} = 905 \times 10^3$ lbf.

Similarly, formulas used to calculate the minimal pipe-thread strength and minimal coupling thread strength for API Buttress connections can be expressed by the following equations:

Tensional force for pipe thread failure:

$$F_{aj} = 0.95\, A_{sp}\, \sigma_u \left[1.008 - 0.0396\,(1.083 - \frac{\sigma_y}{\sigma_u})\, d_o\right] \tag{2.7}$$

Tensional force for coupling thread failure:

$$F_{aj} = 0.95\, A_{sc}\, \sigma_u \tag{2.8}$$

where:

A_{sp} = A_s = area of steel in pipe body, in.^{2}
A_{sc} = area of steel in coupling, in.^{2}

A_{sc} is expressed as:

$$A_{sc} = \frac{\pi}{4}\,(d_{co}^2 - d_{root}^2) \tag{2.9}$$

where:

d_{co} = outside diameter of coupling, in.
d_{root} = diameter at the root of the coupling thread of the pipe in the powertight position rounded to the nearest 0.001 in. for API Buttress thread casing, in.

EXAMPLE 2-3:

For N-80, $9\frac{5}{8}$ in. API Buttress thread connections calculate: (i) pipe thread strength, (ii) coupling (regular) thread strength, (iii) coupling 'special clearance' thread strength. Use the data from Example 2-2 plus the additional manufacturer's data: $d_{co} = 10.625$ in. (regular), $d_{co} = 10.125$ in. (special clearance), $d_{root} = 9.4517$ in. Assume that $\sigma_{up} = \sigma_{uc}$

Solution:

First it is necessary to calculate the cross-sectional area of the pipe body, A_{sp}, and the couplings, A_{sc}. One obtains:

$$\begin{aligned} A_{sp} &= \frac{\pi}{4}(9.625^2 - 8.681^2) \\ &= 13.572 \text{ sq. in.} \end{aligned}$$

and from Eq. 2.9,

$$\begin{aligned} A_{sc} &= \frac{\pi}{4}(10.625^2 - 8.681^2) \\ &= 18.5 \text{ sq. in. (regular)} \end{aligned}$$

$$\begin{aligned} A_{sc} &= \frac{\pi}{4}(10.125^2 - 8.681^2) \\ &= 10.35 \text{ sq. in. (special clearance)} \end{aligned}$$

By simple substitution of the above into the respective equations:

(i) Eq. 2.7,

$$\begin{aligned} F_{aj} &= 0.95 \times 13.572 \times \left(1.008 - 0.0396\left(1.083 - \frac{80,000}{10^5}\right) \times 9.625\right) \\ &= 1,161 \times 10^3 \text{ lbf} \end{aligned}$$

(ii) Eq. 2.9,

$$\begin{aligned} F_{aj} &= 0.95 \times 18.5 \times 10^5 \\ &= 1,757 \times 10^3 \text{ lbf (regular)} \end{aligned}$$

(iii) Eq. 2.9,

$$\begin{aligned} F_{aj} &= 0.95 \times 10.35 \times 10^5 \\ &= 983 \times 10^3 \text{ lbf (special clearance)} \end{aligned}$$

Once again it is the minimum performance characteristic of the casing which appears in the design tables. Thus, for N-80, $9\frac{5}{8}$ in., API Buttress thread, the joint strengths are:

For regular couplings, $F_{aj} = 1161 \times 10^3$ lbf and for special clearance couplings, $F_{aj} = 983 \times 10^3$ lbf.

For API Extreme-line casing, joint strength is defined as the force required to cause failure of the pipe, box, or pin. The minimal value is determined by the minimal steel cross-sectional area of the box, pin, or pipe body. Formulas used to compute the tensile force for each case are:

Tensional force for pipe failure:

$$F_{aj} = \frac{\pi \sigma_u}{4} (d_o^2 - d_i^2) \tag{2.10}$$

Tensional force for box failure:

$$F_{aj} = \frac{\pi \sigma_u}{4} (d_{jo}^2 - d_{box}^2) \tag{2.11}$$

where:

d_{jo} = external diameter of the joint, in.
d_{box} = internal diameter of the box under the last perfect thread, in.

Tensional force for pin failure:

$$F_{aj} = \frac{\pi \sigma_u}{4} (d_{pin}^2 - d_{ji}^2) \tag{2.12}$$

where:

d_{ji} = internal diameter of the joint, in.
d_{pin} = external diameter of the pin under the last perfect thread, in.

Details of the formulas used to compute joint strength are presented in API Bul. 5C2 (1987) and API Bul. 5C3 (1989).

Axial tension results primarily from the weight of the casing string suspended below the casing hanger or below the joint of interest. Other tensional loads can arise due to bending, drag, shock load, and pressure testing of casing string. The sum of these forces is the total tensile force on the string.

2.1.1 Suspended Weight

The weight of pipe in air is computed by multiplying its nominal weight, W_n (lb/ft), by the total length of the pipe. However, when the pipe is immersed in drilling fluid, its weight is reduced due to buoyancy force which is equal to the weight of the drilling fluid displaced by the pipe body (Archimedes' Principle). Buoyancy force acts on the entire pipe and reduces the suspended weight of the pipe. It is, therefore, important to account for the buoyancy force in calculating the weight of the pipe. Thus, the effective or buoyant weight of pipe, F_a, can be expressed as follows:

$$F_a = F_{air} - F_{bu} \tag{2.13}$$

where:

F_{air} = weight of the string in air, lbf.
F_{bu} = buoyancy force, lbf.
F_a = resultant axial force. lbf.

The above equation can be rewritten as:

$$\begin{aligned} F_a &= lA_s\gamma_s - lA_s\gamma_m \\ &= lA_s(\gamma_s - \gamma_m) \\ &= lA_s\gamma_s\left(1 - \frac{\gamma_m}{\gamma_s}\right) \\ &= F_{air}\left(1 - \frac{\gamma_m}{\gamma_s}\right) \end{aligned} \tag{2.14}$$

or

$$F_a = F_{air}\, BF \tag{2.15}$$

where:

BF = $\left(1 - \frac{\gamma_m}{\gamma_s}\right)$
γ_s = specific weight[a] of steel, 65.4 lb/gal.
γ_m = specific weight of drilling fluid, lb/gal.
BF = buoyancy factor

The buoyancy of the casing string is the same in any position. However, when it is vertical the entire force is concentrated at the lower end, whereas in the horizontal position it is distributed evenly over the length. At positions between horizontal and vertical, the force is a mix of concentrated and distributed.

It could be argued that buoyancy is a distributed force even in the vertical case and, therefore, reduces the weight of each increment of the pipe by the weight of the fluid displaced by that increment. However, this argument is incorrect.

Static fluids can only exert a force in a direction normal to a surface. For a vertical pipe, the only area that a fluid pressure could push upwards is the cross-section at the bottom. Thus, the buoyancy force must be concentrated at the bottom face of the pipe.

[a]The relationship between specific weight γ in lb/gal (ppg) and pressure (weight) gradient, G_p , in lbf/in.^{2}ft (psi/ft), is $G_p = 0.052 \times \gamma$.

Equation 2.15 is valid only when the casing is immersed in drilling fluid, i.e., the fluid specific weight inside and outside the string is the same. During cementing operations the drilling fluid inside the casing is progressively displaced by higher specific weight cement, thereby reducing the buoyancy factor and increasing the casing hanging weight. As the cementing operation progresses, the cement flows up the outside of the casing continuing to displace the lower specific weight drilling fluid. As the cement moves up the outside of the casing the buoyancy force increases resulting in a lowering of the hanging weight.

Similarly, casing is exposed to high specific weight drilling fluid from the inside when drilling deeper sections of the well. As a result of this, the buoyancy force increases and the effective casing weight decreases. The buoyancy force under these conditions can be expressed (Lubinski, 1951) as:

$$\begin{aligned} &\text{Buoyant weight per unit length} \\ &= \text{downward forces - upward forces} \\ &= (W_n + G_{p_i} A_i) - G_{p_o} A_o \end{aligned} \tag{2.16}$$

where:

G_{p_i} = pressure gradient of the fluid inside the casing, psi/ft.
G_{p_o} = pressure gradient of the fluid in the annulus, psi/ft.
A_i = area corresponding to the casing ID, in.^{2}
A_o = area corresponding to the casing OD, in.^{2}

EXAMPLE 2-4:

Consider a 6,000-ft section of N-80, 47 lb/ft, $9\frac{5}{8}$ in. casing under the following conditions across its entire length: (i) suspended in air, (ii) immersed in 9.8 lb/gal mud, (iii) 12 lb/gal cement inside and 9.8 lb/gal mud outside, (iv) 9.8 lb/gal mud inside and 12 lb/gal cement outside.

Solution:

(i) The weight in air, F_{air}, is given by:

$$\begin{aligned} F_{air} &= W_n\, l = 47 \times 6{,}000 \\ &= 282{,}000 \text{ lbf} \end{aligned}$$

(ii) The effective weight is given by Eq. 2.15. Thus, by calculating the buoyancy factor, BF, from Eq. 2.16:

$$\begin{aligned} BF &= \left(1 - \frac{9.8}{65.4}\right) \\ &= 0.85 \end{aligned}$$

one obtains:

$$F_a = 282{,}000 \times 0.85 = 239{,}807 \text{ lbf}$$

(iii) The buoyant weight, F_a, is given by Eq. 2.17. First, calculating the cross-sectional areas of the casing:

$$A_i = \frac{\pi(8.681)^2}{4} = 27.272 \text{ sq in.}$$

$$A_o = \frac{\pi(9.625)^2}{4} = 30.238 \text{ sq in.}$$

Then:

$$\begin{aligned} F_a &= \{(47 + [12 \times 0.052]\,27.272) - 30.238\,(9.8 \times 0.052)\}\,6.000 \\ &= 291{,}650 \text{ lbf} \end{aligned}$$

(iv) As in (iii) above:

$$\begin{aligned} F_a &= \{(47 + [9.8 \times 0.052]\,27.2722) - 30.238(12 \times 0.052)\}6{,}000 \\ &= 252{,}180 \text{ lbf} \end{aligned}$$

Note in particular that the maximum effective weight of the string is not F_{air}, the weight in air, but rather the condition given in part (iii) when the casing is filled with cement and surrounded by low specific weight mud, i.e., $F_a > F_{air}$ when $G_{p_i} A_i > G_{p_o} A_o$

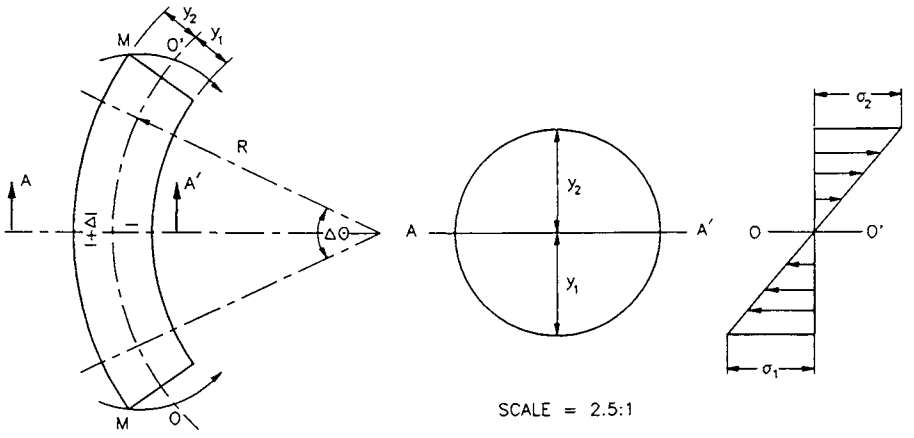

Fig. 2.3: Pure bending of a circular beam. NOTE: $y_1 = y_2 = d_o/2$ of the beam.

2.1.2 Bending Force

Casing is subjected to bending forces when run in deviated wells. As a result of bending, the upper surface of the pipe stretches and is in tension, whereas

the lower surface shortens and is in compression. Stress distribution across a cylindrical pipe body under bending force is illustrated in Fig. 2.3. Between the stretched and compressed surfaces, there exists a neutral plane OO′ in which the longitudinal deformation is zero. Thus, the deformation at the outer portion of the pipe, $\Delta\varepsilon_2$, can be expressed as follows:

$$\Delta\varepsilon_2 = \frac{(l+\Delta l)-l}{l} \tag{2.17}$$

$$= \frac{\Delta l}{l} \tag{2.18}$$

where:

$$\Delta l = (R+y_2)\,\Delta\Theta - R\,\Delta\Theta = y_2\,\Delta\Theta \tag{2.19}$$

$= $ axial deformation.

l = section of the pipe length.

R = radius of curvature.

Θ = angle subtended by the pipe section.

$\Delta\Theta$ = angular deformation.

y_2 = axial deformation above OO′ plane.

If the pipe remains elastic after bending, then the equation for longitudinal strain can be expressed as:

$$\frac{\Delta l}{l} = \frac{\Delta\sigma_2}{E} \tag{2.20}$$

or

$$\Delta\sigma_2 = E\,\frac{y_2}{R} \tag{2.21}$$

where:

E = modulus of elasticity, 30×10^6 psi.

$\Delta\sigma_2$ = incremental bending stress.

Combining Eqs. 2.19 and 2.21, and converting into field units by expressing Θ in radians per 100 ft of pipe, y_2 in inches and A_s in square inches, one obtains the equation for bending force, F_b:

$$F_b = A_s\Delta\sigma_2$$

$$= A_sE \cdot \frac{y_2}{12} \cdot \frac{\Theta}{100} \cdot \frac{\pi}{180} \tag{2.22}$$

Considering $y_1 = y_2 = d_o/2$ and the nominal weight of the pipe, W_n, to be equal to $3.46\,A_s$[b], then Eq. 2.22 can be simplified to:

$$F_b = 2.10 \times 10^{-6}\, W_n\, E d_o\, \Theta \tag{2.23}$$

or

$$F_b = 63\, d_o W_n\, \Theta \tag{2.24}$$

where:

d_o	=	nominal diameter of the pipe, in.
A_s	=	pipe cross-sectional area, in.^{2}
Θ	=	degrees (°) per 100 feet ('dogleg severity').
W_n	=	nominal weight of pipe, lb/ft.

EXAMPLE 2-5:

Calculate the axial load due to bending in the string in Example 2-4 given that the maximum 'dogleg severity', Θ, is 3°/100 ft.

Solution:

Applying Eq. 2.24 one obtains:

$$\begin{aligned} F_b &= 63 \times 9.625 \times 47 \times 3 \\ &= 85{,}500\ \text{lbf} \end{aligned}$$

Equation 2.24, recommended by Bowers (1955), Greenip (1978), and Rabia (1987), is widely used to determine axial load due to pipe bending. The equation should, however, only be used in circumstances where the pipe is in continuous contact with the borehole.

In practice, the casing cannot be in continuous contact with the borehole because the borehole is always irregularly shaped and the casing is often run in the hole with protectors and centralizers. If the pipe is supported at two points, due to the hole irregularities or the use of centralizers, the radius of curvature of the pipe is not constant. In this case, the maximal axial stress is significantly greater than that predicted by Eq. 2.24.

If a pipe section of length l_j, supported at points P and Q subtends an angle θ at the center of curvature (Fig. 2.4), which does not exceed its elastic limit,

[b]For most casing sizes, the cross-sectional area is related to nominal weight per foot, with negligible error (Goins et al., 1965, 1966), through the relation: A = W_n/3.46 in.^{2}.

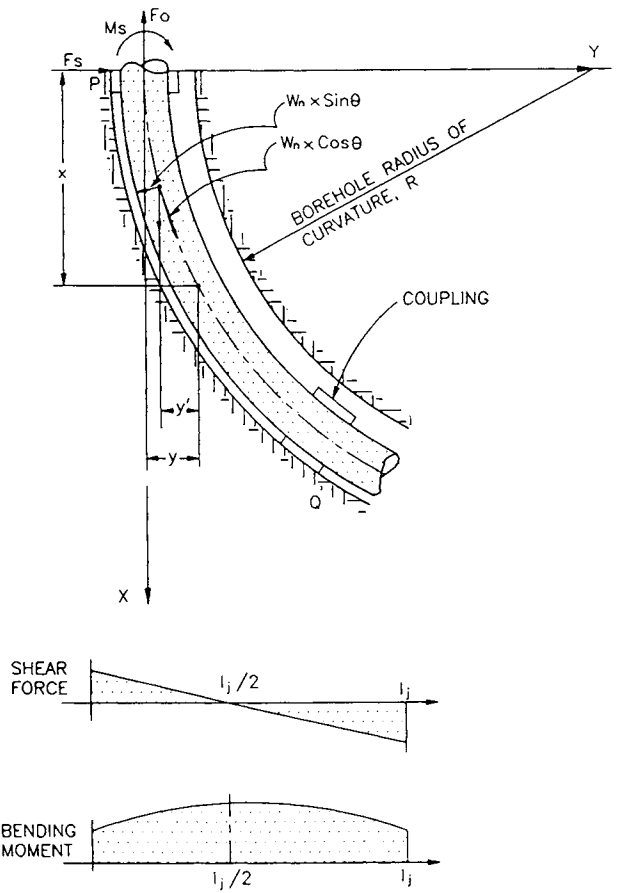

Fig. 2.4: Bending of casing supported at casing collars.

classical deflection theory can be applied to determine the resultant axial stress (Lubinski, 1961). In this case the radius of curvature of the pipe is given by:

$$\frac{1}{R} = \frac{M}{EI} \tag{2.25}$$

where:

I = moment of inertia, in.^{4}
M = bending moment, ft-lbf

For a circular pipe, I is expressed as:

$$I = \frac{\pi}{64}(d_o^4 - d_i^4) \tag{2.26}$$

where:

d_o = outside diameter of the pipe, in.
d_i = inside diameter of the pipe, in.

If the curvature of the bent section is small then the radius of curvature can be given by:

$$\frac{1}{R} = \frac{d^2y}{dx^2} \tag{2.27}$$

Combining Eqs. 2.25 and 2.27 one obtains:

$$\frac{d^2y}{dx^2} = \frac{M}{EI} \tag{2.28}$$

From Fig. 2.4, the bending moment M_x at any distance x (where $x < l_j$, the joint length) is given by:

$$M_x = M_s + F_a y + F_w x - W_n \frac{x^2}{2} \sin\theta - W_n x y' \cos\theta \cdot \tag{2.29}$$

where:

F_a = axial force, lbf.
F_w = force exerted by the borehole wall at the couplings, lbf.
M_s = bending moment at O, ft-lbf.
y and y' = refer to Fig 2.4.

The last two terms of Eq. 2.29 are small and for simplicity they are neglected. Similarly, the axial tension, F_a, is considered to be constant throughout the pipe. Thus, substituting Eqs. 2.21 and 2.28 into Eq. 2.29 and simplifying, one obtains the classical differential equation for a beam column (Timoshenko et al., 1961):

$$\frac{d^2y}{dx^2} - \frac{F_a y}{EI} = \frac{2\,\Delta\sigma_2}{Ed_o} + \frac{F_w x}{EI} \tag{2.30}$$

where $\Delta\sigma_2$ is a maximum, $\Delta\sigma_{max}$, at $y_2 = d_o/2$.

Maximal bending force is obtained by integrating Eq. 2.30. Defining υ^2 as:

$$\psi^2 = \frac{F_a}{EI} \tag{2.31}$$

one obtains the integral solution:

$$y = \frac{1}{\psi^2}\left[\frac{2\,\Delta\sigma_{max}}{Ed_o}\right](\cosh\psi x - 1) + \frac{F_w}{\upsilon^3 EI}\,[\sinh\upsilon x - \upsilon x] \tag{2.32}$$

The boundary conditions for the system are:

1. As there is no pipe-to-wall contact, the load on the pipe is considered to be symmetric and, therefore, the shear force at the middle of the joint is zero. Hence,

$$\left(\frac{d^3y}{dx^3}\right)_{x=l_j/2} = 0 \tag{2.33}$$

where:

l_j = length of a joint of casing.

2. It follows from Eq. 2.33 above, that the midpoint of the joint must be parallel to the borehole and, therefore, that the slope of the pipe is:

$$\left(\frac{dy}{dx}\right)_{x=l_j/2} = \frac{l}{2} \cdot \frac{1}{R} \tag{2.34}$$

Applying the boundary conditions to Eq. 2.32 yields the following expression for the radius of curvature:

$$\frac{1}{R} = \frac{2\,\Delta\sigma_{max}}{E d_o} \frac{\tanh(\psi l_j/2)}{(\psi l_j/2)} \tag{2.35}$$

Rearranging the equation in terms of $\Delta\sigma_{max}$, and expressing R in terms of dogleg severity, Θ, one obtains:

$$\Delta\sigma_{max} = \frac{E d_o \Theta}{2\,l_j} \frac{\psi l_j}{2} \frac{1}{\tanh(\psi l_j/2)} \tag{2.36}$$

Similarly the bending force, F_b, is given by:

$$F_b = A_s\,\Delta\sigma_{max} \tag{2.37}$$

$$= \frac{A_s\,E d_o \Theta}{2 l_j} \frac{\psi l_j}{2} \frac{1}{\tanh(\psi l_j/2)} \tag{2.38}$$

Solving for maximal stress and expressing the equation in field units:

$$F_b = 63\,W_n\,d_o \Theta \frac{6\,\psi l_j}{\tanh(6\,\psi l_j)} \tag{2.39}$$

Equation 2.39 was suggested by several authors: Mitchel (1990) and Bourgoyne et al. (1986); and it is being used in rating the tensional joint strength of couplings

subjected to bending. Using this equation the following formulas were developed by the API (API Bul. 5C3, 1989) to estimate the joint strength of API Round thread coupling.

The joint strength of API Round casing with combined bending and internal pressure is calculated on a total load basis.

Full fracture strength:

$$F_{au} = 0.95 A_{jp} \sigma_{up} \tag{2.40}$$

Jumpout and reduced fracture strength:

$$F_{aj} = 0.95 A_{jp} L_{et} \left[\frac{0.74 d_o^{-0.59} \sigma_{up}}{0.5 L_{et} + 0.14 d_o} + \frac{(1 + 0.5z)\sigma_y}{L_{et} + 0.14 d_o} \right] \tag{2.41}$$

Bending load failure strength:

When $F_{ab}/A_{jp} \geq \sigma_{up}$, the joint strength is given by:

$$F_{ab} = 0.95\, A_{jp} \left\{ \sigma_{up} - \left[\frac{140.5\, \Theta d_o}{(\sigma_{up} - \sigma_y)^{0.8}} \right]^5 \right\} \tag{2.42}$$

When $F_{ab}/A_{jp} < \sigma_{up}$, the joint strength is given by:

$$F_{ab} = 0.95\, A_{jp} \left(\frac{\sigma_{up} - \sigma_y}{0.644} + \sigma_y - 218.15\, \Theta d_o \right) \tag{2.43}$$

where:

A_{jp} = cross-sectional area of pipe wall under the last perfect thread, in.^{2}

$$= \frac{\pi}{4} \left[(d_o - 0.1425)^2 - (d_o - 2t)^2 \right] \tag{2.44}$$

F_{ab} = total tensile failure load with bending Θ, lbf.

Total load = External load + sealing head load

= External load + $p_i A_i$

p_i = internal pressure, psi.

A_i = internal area, in.^{2}

$$= \frac{\pi}{4}(d_o - 2t)^2$$

F_{au} = total tensile load at fracture, lbf.

z = ratio of internal pressure stress to yield strength

$$= \frac{p_i d_o}{2\sigma_y t}$$

F_{aj} = minimum joint strength, lbf.

EXAMPLE 2-6:

For a 40-ft length of $9\frac{5}{8}$ in., 47 lb/ft, N-80 casing with API long, round thread couplings subjected to a 300,000 lbf axial tension force in a section of hole with a 'dogleg severity' of 3°/100 ft calculate the maximal axial stress assuming: (i) uniform contact with the borehole, (ii) contact only at the couplings. In addition, compute the joint strength of the casing.

Solution:

From Examples 2-1 and 2-2 the nominal values for pipe body yield strength, $1,086 \times 10^3$ lbf, and nominal joint strength, 905×10^3 lbf, were calculated.

The cross-sectional area of the pipe is given by:

$$A_s = \frac{\pi}{4}(9.625^2 - 8.681^2) = 13.5725 \text{ sq. in.}$$

Without bending, the axial stress is given by:

$$\sigma_a = \frac{300,000}{13.572} = 22,104 \text{ psi}$$

The additional stress due to bending is:

(i) From Eq. 2.24, which assumes that the pipe is in uniform contact with the borehole:

$$\Delta\sigma_2 = \frac{F_b}{A_s} = \frac{63 \times 9.625 \times 47 \times 3}{13.5725} = 6,400 \text{ psi}$$

Thus, the total stress in the pipe is:

$$\sigma_a + \Delta\sigma_2 = 22,104 + 6,400 = 28,504 \text{ psi}$$

a 29 % increase in stress due to bending.

(ii) From Eq. 2.39, which assumes that contact between the casing and the borehole is limited to the couplings. First from Eq. 2.26:

$$I = \frac{\pi}{64}(9.625^4 - 8.681^4) = 142.51 \text{ in.}^4$$

Similarly, from Eq. 2.31:

$$\begin{aligned} \psi &= \sqrt{\frac{F_a}{EI}} = \sqrt{\frac{300,000}{30 \times 10^6 \times 142.51}} \\ &= 8.377 \times 10^{-3} \text{ in.}^{-1} \end{aligned}$$

Thus,

$$\begin{aligned}\Delta\sigma_{max} &= \frac{F_b}{A_s} \\ &= \left(\frac{64 \times 9.625 \times 47 \times 3}{13.5725}\right)\left(\frac{6 \times (8.377 \times 10^{-3}) \times 40}{\tanh(6 \times 8.377 \times 10^{-3} \times 40)}\right) \\ &= 13,337 \text{ psi}\end{aligned}$$

Thus, the total stress in the pipe is:

$$\sigma_a + \Delta\sigma_{max} = 22,104 + 13,337 = 35,441 \text{ psi}$$

A 60 % increase in stress due to bending. Note that in the second case the additional stress due to bending is more than double that calculated assuming uniform contact with the borehole.

In this example both methods produce maximal axial stresses well below the 80,000 psi minimal yield stress of N-80 grade casing.

(iii) The minimal ultimate yield strength of N-80 grade casing is σ_{up} = 100,000 psi, so using Eq. 2.42 one obtains the value for joint strength:

$$\begin{aligned}\frac{F_{ab}}{A_{jp}} &= 0.95 \times \left(100,000 - \left(\frac{140.5 \times 3 \times 9.625}{(100,000 - 80,000)^{0.8}}\right)^5\right) \\ &= 94,993 \text{ psi}\end{aligned}$$

Inasmuch as $F_{ab}/A_{jp} > 80,000$, the above value for joint strength is valid and there is no need to apply Eq. 2.43.

Similarly, the cross-sectional area of pipe wall under the last perfect thread, A_{jp}, is:

$$\begin{aligned}A_{jp} &= \frac{\pi}{4}\{(9.625 - 0.1425)^2 - (9.625 - 2(0.472))^2\} \\ &= 11.434 \text{ sq. in.}\end{aligned}$$

and the calculated joint strength is:

$$F_{ab} = 94,993 \times 11.434 = 1,086,150 \text{ lbf}$$

This value is above the nominal joint strength value of 905 $\times$ 10^3 lbf given in the tables and so the nominal table value must instead be based on joint pull-out strength. Thus, under the given conditions joint strength is determined by the minimal pull-out force.

2.1.3 Shock Load

When casing is being run into the hole it is subjected to acceleration loading by setting of the slips and the application of hoisting brakes. Unlike the suspended weight of the pipe and the bending force, the accelerating or shock load acts on a certain part of the pipe for only a short period of time. However, the combined effects of shock load, suspended weight and bending force can lead to parting of the pipe. The effect of shock load on drillpipe was first recognized by Vreeland (1961) and a systematic procedure for determining the shock load during the running of casing strings in the hole was later presented by Rabia (1987).

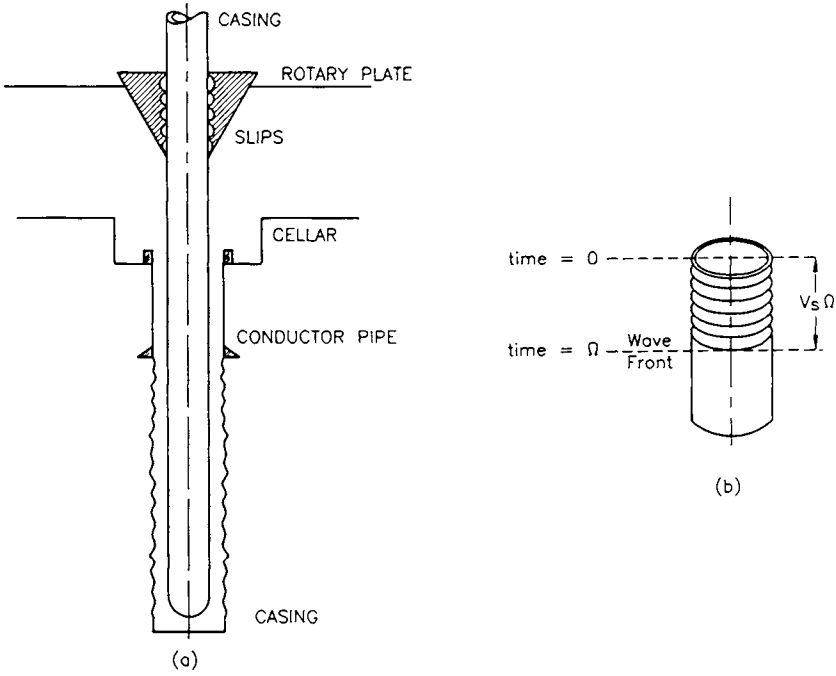

Fig. 2.5: Effect of shock load on pipe body. (After Vreeland, 1961.)

When, during the running of casing, the string is stopped suddenly in the slips, a compressive stress wave is generated in the pipe body near the slips (Fig. 2.5), which travels downwards from the slip area towards the casing shoe. On reaching the unrestrained shoe, the compressive stress-wave is reflected upwards towards the surface as a tensile stress-wave. Arriving back at the surface, the reflected tensile stress-wave encounters the fixed end held in the slips whereupon it is reflected back downwards towards the casing shoe as a tensile stress-wave. At the free end (shoe), the two opposite stress waves cancel each other, whereas at the fixed end (slips) the two tensile stress-waves, one moving upwards and the other moving downwards and of opposite sign, combine to produce a stress equal

to twice the tensile stress (Coates, 1970).

Consider that the casing string is moving downwards at a speed of V_p when its downward motion is arrested by the setting of the slips. The particles in the pipe body continue to move at a velocity V_p, thereby inducing a stress wave to propagate downwards from the slips at a velocity V_s. After a time Ω has elapsed, the wave will have travelled a distance $V_s\Omega$. During the same time, the particles in the pipe body travel a distance $V_p\Omega$.

Applying the Law of Conservation of Momentum, the change in momentum of the pipe element, $V_s\Omega$, can be given by:

$$\begin{aligned} mV_p &= \text{Impulsive force} \times \text{time} \\ &= (\sigma_s A_s)\,\Omega \end{aligned} \tag{2.45}$$

where:

m = mass of the pipe section $V_s\Omega$, i.e., $V_s\Omega\, A_s\, \gamma_s/g$, lb.
V_s = velocity of the stress wave, ft/s.
= characteristic wave velocity for steel is 17,028 ft/s.
V_p = velocity of particles in pipe, ft/s.
σ_s = compressive stress resulting from the action of the slips, psi.

Rewriting Eq. 2.45:

$$\left(\frac{V_s\Omega\, A_s\, \gamma_s}{g}\right) V_p = \sigma_s\, A_s\Omega \tag{2.46}$$

which after cancelling yields:

$$\sigma_s = \frac{\gamma_s\, V_p\, V_s}{g} \tag{2.47}$$

Net stress is twice the stress induced by the slip action and, therefore, the total shock load can be expressed by:

$$F_s = (2\,\sigma_s)\, A_s \tag{2.48}$$

or

$$F_s = \frac{2\,\gamma_s\, V_p\, V_s\, A_s}{g} \tag{2.49}$$

Expressing Eq. 2.49 in field units yields:

$$F_s = 3,200\, W_n \tag{2.50}$$

where:

F_s = shock load, lbf.
V_s = 17,028 ft/s.
V_p = 3.04 ft/s for 40 ft of casing.
γ_s = 489.5 lb/ft^3.
g = 32.174 ft/s./s.
A_s = $W_n/3.46$ in^2 (W_n in lb/ft).

The peak running speed is about twice the average running speed because initially the casing is at rest; so Rabia (1987) suggested using a factor of two in Eq. 2.49.

EXAMPLE 2-7:

Consider sections of N-80, 47 lb/ft casing being run into the borehole at an average rate of 9 seconds per 40 ft. Calculate the total shock load if the casing is moving at its peak velocity when the slips are set.

Solution:

Equation 2.50 is based on the premise that V_p is 3.04 ft/s, i.e., 13s per 40 ft. In this example the rate is 9s per 40 ft, thus:

$$F_{s_1} = 3,200 \times 47 \times \left(\frac{13}{9}\right) = 217,250 \text{ lbf}$$

Alternatively using Eq. 2.49:

$$\begin{aligned} F_{s_2} &= \left(\frac{2 \times 489.5}{32.17}\right) \times \left(\frac{40}{9}\right) \times 17028 \times \left(\frac{47}{3.46}\right) \times \left(\frac{1}{144}\right) \\ &= 217,250 \text{ lbf} \end{aligned}$$

From Rabia (1987), recall that the peak running speed is twice the average, so the shock load is:

$$F_{s_{peak}} = 2 \times 217,250 = 434,500 \text{ lbf}$$

2.1.4 Drag Force

Casing strings are usually reciprocated or rotated during landing and cementing operations, which results in an additional axial load due to the mechanical friction between the pipe and borehole. This force is described as drag force, F_d, and is expressed as:

$$F_d = -f_b |F_n| \tag{2.51}$$

where:

f_b = borehole friction factor.
$|F_n|$ = absolute value of the normal force.

Thus, the magnitude of the drag force depends on the friction factor and the normal force resulting from the weight of the pipe. Due to the complex geometry of deviated wells, the drag force is a major contributor to the total axial load. It is, however, extremely difficult to predict the borehole friction factor because it depends on a large number of factors, the most important of which include: hole geometry, surface configuration of casing, drilling fluid and filter cake properties, and borehole irregularities.

As a result of field experience and laboratory test results, several methods for calculating friction factor have been proposed. In a recent study, Maidla (1987) proposed the following analytical model for the friction factor:

$$f_b = \frac{F_h - F_{bu_v} \pm F_{vd}}{\int_0^\ell W_d(l, f_b)\, dl} \tag{2.52}$$

where:

F_h = hook load, lbf.
F_{bu_v} = vertically projected component of buoyant weight, lbf.
F_{vd} = hydrodynamic viscous drag force, lbf.
$W_d(l, f_b)$ = unit drag or rate of change of drag, lb/ft.
l = length of casing, ft
ℓ = measured depth, ft.

The above equation was used extensively by Maidla (1987) under field conditions and the values of friction factors reported varied between 0.3 and 0.6. Drag force in a vertical well is relatively low, so methods for estimating friction factor and related drag force are discussed under Casing Design for Special Applications on page 177.

2.1.5 Pressure Testing

Pressure testing is routinely carried out after the casing is run and cemented. A pressure test of 60 % of the burst rating of the weakest grade of casing in the string is often used (Rabia, 1987). During testing an additional tensile stress is exerted on the casing due to the internal pressure. The minimum tension safety factor should again be 1.8 for the top joint of each grade.

2.2 BURST PRESSURE

Burst pressure originates from the column of drilling fluid and acts on the inside wall of the pipe. Casing is also subjected to kick-imposed burst pressure if a kick occurs during drilling operations.

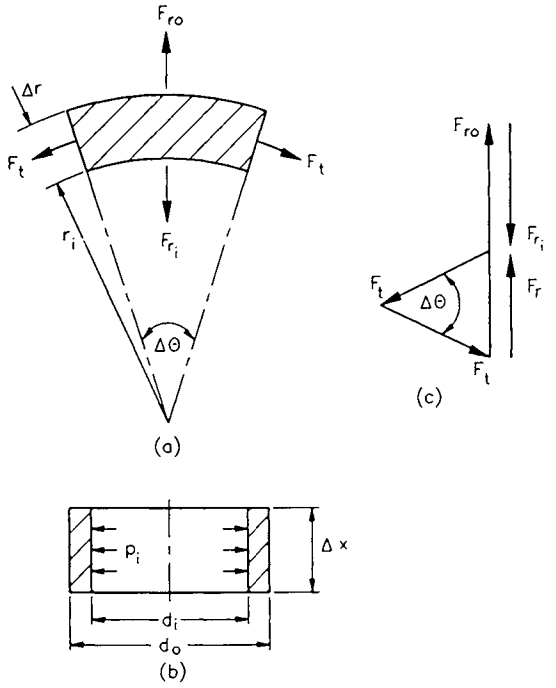

Fig. 2.6: Free body diagram of the pipe body under internal pressure.

The free-body diagram for burst pressure acting on a cylinder is presented in Fig. 2.6. If a ring element subtends an angle $\Delta\theta$ at any radius r while under a constant axial load, then the radial and tangential forces on the ring element are given by:

radial force: $F_r = p_i \Delta x\, r_i \Delta\theta$
tangential force: $2F_t = 2\sigma_t \Delta x \Delta r_i$

where:

σ_t = tangential stress due to internal pressure, psi.
p_i = internal pressure, psi.
r_i = internal radius of casing, in.

From the equilibrium condition of the small element one obtains:

$$p_i \Delta x\, r_i \Delta\theta = 2\sigma_t \sin \frac{\Delta\theta}{2} \Delta x \Delta r \tag{2.53}$$

For small $\Delta\theta$, $\sin(\Delta\theta/2) \approx \Delta\theta/2$, and Eq. 2.53 reduces to:

$$p_i = \sigma_t \frac{\Delta r}{r_i} \tag{2.54}$$

For a thin-walled cylinder with a high nominal diameter to thickness ratio and σ_t equal to σ_y, the yield strength of the pipe material, Eq. 2.54 can be expressed as follows:

$$p_b = 2\sigma_y \frac{1}{(d_o/t)} \tag{2.55}$$

where:

d_o = outside diameter of the cylinder, in.
t = cylinder wall thickness, in.
p_b = burst pressure rating of the material, psi.

Equation 2.55 is identical to Barlow's formula for thick-walled pipe which is derived using the membrane theory for symmetrical containers. If the wall thickness is assumed to be very small compared to the other dimensions of the pipe the axial stress can be considered to be zero. In this case the tangential and radial forces are the principal forces along the principal planes.

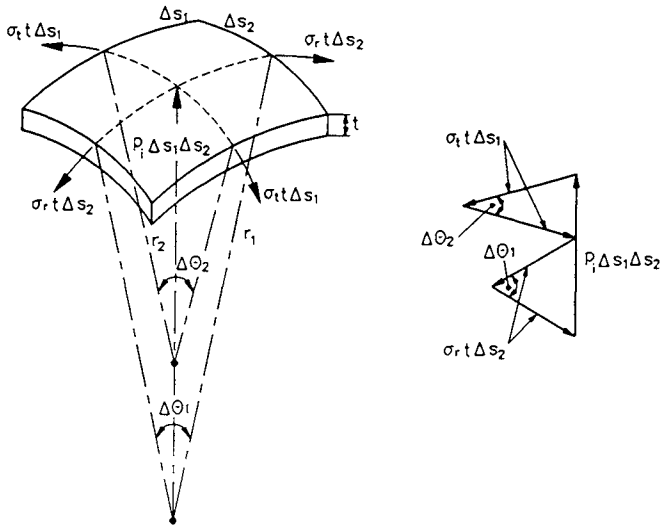

Fig. 2.7: Free body diagram of a rectangular shell element under internal pressure.

A small element ($\Delta s_1 \times \Delta s_2$) of a container, which is subjected to a burst pressure of p_i, is included between the radii r_1 and r_2. $\Delta\theta_1$ and $\Delta\theta_2$ denote the angles be-

tween the radii r_1 and r_2, respectively. Figure 2.7 presents the free-body diagram of the element used to derive Barlow's formula. From the equilibrium conditions of the element one obtains (assuming $\sin(\Delta\theta/2) \approx \Delta\theta/2$:

$$-2\,\sigma_r\,t\,\Delta s_2\,\frac{\Delta\theta_1}{2} - 2\sigma_t\,t\,\Delta s_1\,\frac{\Delta\theta_2}{2} + p_i\,\Delta s_1\,\Delta s_2 = 0 \tag{2.56}$$

If $\Delta s_1 = r_1\Delta\theta_1$, and $\Delta s_2 = r_2\Delta\theta_2$, then Eq. 2.56 becomes:

$$\frac{\sigma_r}{r_1} + \frac{\sigma_t}{r_2} = \frac{p_i}{t} \tag{2.57}$$

If a cylindrical pipe of radius r is subjected to an uniform internal pressure p_i and r_1 tends to infinity, then the equation of thick-walled pipe is:

$$\sigma_t = \frac{p_i r}{t} \tag{2.58}$$

Expressing the equation in terms of nominal diameter, d_o, and yield strength of the pipe body, σ_y, one obtains Barlow's formula:

$$p_i = \frac{2\,\sigma_y}{(d_o/t)} \tag{2.59}$$

The API burst pressure rating is based on Barlow's formula. The factor of 0.875 assumes a minimal wall thickness and arises from the 12.5 % manufacturer's tolerance allowed by the API in the nominal wall thickness. Thus, the burst pressure rating is given by:

$$p_{br} = 0.875\,\frac{2\,\sigma_y}{(d_o/t)} \tag{2.60}$$

where:

p_{br} = burst pressure rating as defined by the API.

EXAMPLE 2-8:

Calculate the burst pressure rating of N-80, 47 lb/ft, $9\frac{5}{8}$ in. casing.

Solution:

From Eq. 2.60:

$$p_{br} = 0.875 \times \left(2 \times 80{,}000 \times \left(\frac{0.472}{9.625}\right)\right) = 6{,}875\,\text{psi}$$

This figure represents the minimal internal pressure at which permanent deformation could occur provided that the pipe is not subjected to external pressure or axial loading.

2.3 COLLAPSE PRESSURE

Primary collapse loads are generated by the hydrostatic head of the fluid column outside the casing string. These fluids are usually drilling fluids and, sometimes, cement slurry. Casing is also subjected to severe collapse pressure when drilling through troublesome formations such as: plastic clays and salts .

Strength of the casing under external pressure depends, in general, on a number of factors. Those considered most important when determining the critical collapse strength are: length, diameter, wall thickness of the casing and the physical properties of the casing material (yield point, elastic limit, Poisson's ratio, etc.).

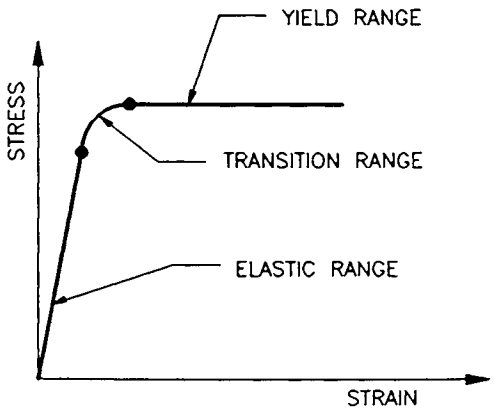

Fig. 2.8: Elastoplastic material behavior with transition range for steel casing under collapse pressure.

Casing specimens manufactured out of steel with elastic ideal-plastic material behavior can fail in three possible ways when subjected to overload due to external pressure: elastic, plastic, and by exceeding the ultimate tensile strength of material (Fig. 2.8).

Casing having a low d_o/t ratio and low strength, reaches the critical collapse value as soon as the material begins to yield under the action of external pressure. Specimens exhibit ideally-plastic collapse behavior and the failure due to external pressure occurs in the so-called 'yield range'.

In contrast to low d_o/t and low strength failure in the yield range, casing with high d_o/t ratio and high strength, collapses below the yield strength of the material. The ability of these pipes to withstand external pressure is limited by the failure by collapse rather than buckling, of long, thin struts while in compression. In this case, failure is caused by purely elastic deformation of the casing and results

in out-of-roundness of the pipe. The collapse behavior is known as failure in the elastic range.

A systematic procedure for determining the different collapse strengths is given in the following sections.

2.3.1 Elastic Collapse

The general form of elastic collapse behavior was first presented by Bresse (1859) and by Bryan (1888) (Krug, 1982). The equation for elastic collapse in thin-walled and long casing specimens is a function of d_o/t and material constants: Young's modulus and Poisson's ratio.

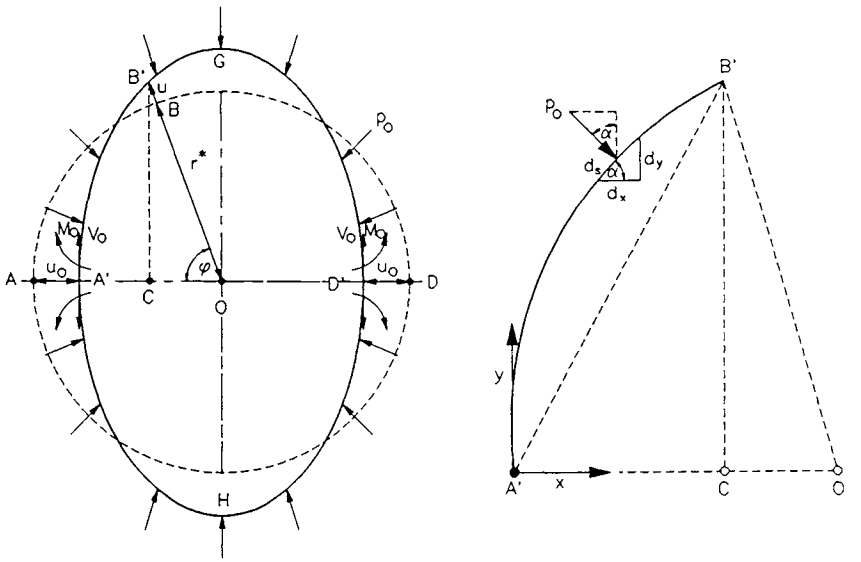

Fig. 2.9: Buckling tendency of thin-walled casing under external pressure.

Casing may be considered as an ideal, uniformly compressed ring with some slight deformation from the circular form at equilibrium. Thus, the critical value of the uniform pressure is the value which is necessary to keep the ring in equilibrium in the assumed slightly deformed shape. The ring with slightly deformed shape is presented in Fig. 2.9. The dotted line indicates the initial circular shape of the ring, whereas the full line represents the slightly deformed ring. It is also assumed that AD and GH are the axes of symmetry of the buckled ring. The longitudinal compressive force and the bending moment acting at each end of cross-section $A' - D'$ are represented by V_o and M_o (respectively). p_o is the

uniform normal pressure per unit length of the center-line of the ring and u_o is the radial displacement at A' and D'. The bending moment is considered to be negative when it produces a decrease in the initial curvature of the circle at A.

Denoting r^* as the initial radius of the ring and u as the radial deformation at B', the equation of the curvature at any point on the arc $A'B'$ can be expressed by (Timoshenko et al., 1961):

$$A'B'(\phi) = \frac{r^2 + 2(r')^2 - r \cdot r''}{(r^2 + (r')^2)^{3/2}} \tag{2.61}$$

where: $r = r(\phi) = r^* + u(\phi)$ (2.62)

Substituting Eq. 2.62 in Eq. 2.61 and neglecting the small quantities of higher order like u^2, $u'u$, etc., one obtains:

$$A'B'(\phi) = \frac{1}{r^*} - \frac{u}{(r^*)^2} - \frac{u''}{(r^*)^2} \tag{2.63}$$

Similarly, the equation of the curvature at any point on the arc AB is given as:

$$AB(\phi) = \frac{1}{r^*} \tag{2.64}$$

The equation for the bending moment due to the deformation is given by:

$$-A'B' + AB = \frac{M}{EI} \tag{2.65}$$

where:

M = bending moment due to deformation, ft-lbf.
I = moment of inertia of the pipe, in.^{4}

Now, substituting Eqs. 2.63 and 2.64 in Eq. 2.65, one obtains the differential equation for the deflected arc $A'B'$:

$$\frac{d^2u}{d\phi^2} + u = \frac{M(r^*)^2}{EI} \tag{2.66}$$

The vertical component of force, V_o, due to pressure p_o, can be expressed as:

$$V_o = p_o \overline{A'O} \tag{2.67}$$
$$= p_o [r^* - (-u_o)]$$
$$= p_o (r^* + u_o) \tag{2.68}$$

and the bending moment at B' of the deflected ring is:

$$M = M_o + V_o \overline{A'C} - M_{p_o} \tag{2.69}$$

where:

M_{p_o} = bending moment (per unit length) due to the external pressure p_o at any section of ring.
M_o = bending moment about O.

From Fig. 2.9(b), the vertical and horizontal components of force p_o are given by:

$$V = \int p_o \, ds \, \cos\alpha \tag{2.70}$$

$$H = \int p_o \, ds \, \sin\alpha \tag{2.71}$$

Referring to Fig. 2.9 (b), the bending moment due to pressure p_o, i.e., M_{p_o}, at any point on the arc $A'B'$ can be expressed as:

$$\begin{aligned} M_{p_o} &= \int p_o \, ds \, \cos\alpha \, (\overline{A'C} - x) + \int p_o \, ds \sin\alpha \, (\overline{B'C} - y) \\ &= \int_{x=0}^{\overline{A'C}} p_o \, (\overline{A'C} - x) \, dx + \int_{y=0}^{\overline{B'C}} p_o \, (\overline{B'C} - y) \, dy \\ &= \frac{p_o}{2} \, (\overline{A'B'})^2 \end{aligned} \tag{2.72}$$

Substituting Eqs. 2.67 and 2.72 in Eq. 2.69 and applying the laws of cosines one obtains:

$$M = M_o - \frac{p_o}{2} \, (\overline{OB'}^2 - \overline{A'O}^2) \tag{2.73}$$

However, substituting $\overline{OB'} = r^* + u$, and $\overline{A'O} = r^* - u_o$ into Eq. 2.73 and then neglecting the squares of small quantities u and u_o, the bending moment becomes:

$$M = M_o - p_o \, r^* \, (u_o - u) \tag{2.74}$$

Finally, substituting Eq. 2.74 into Eq. 2.66, the final expression of the differential equation for the deflected ring becomes:

$$u''(\phi) + \left(1 + \frac{(r^*)^3 p_o}{EI} \right) u(\phi) = \frac{p_o (r^*)^3 u_o + (r^*)^2 M_o}{EI} \tag{2.75}$$

The critical value of the uniform pressure is obtained by integrating Eq. 2.75. Thus, using the notation:

$$\Psi^2 = 1 + \frac{(r^*)^3 p_o}{EI} \tag{2.76}$$

one obtains the general solution:

$$u(\phi) = C_1 \cos \Psi o + C_2 \sin \Psi o + \frac{p_o (r^*)^3 u_o + (r^*)^2 M_o}{EI + (r^*)^3 p_o} \tag{2.77}$$

If one now considers the boundary conditions at the cross-section $A'B'$ of the buckled ring, the two extreme values of o (0 and $\pi/2$), are obtained when $u'(0) = 0$ and $u'(\pi/2) = 0$, respectively. From the first condition it follows that $C_2 = 0$ and from the second, that:

$$C_1 \Psi \sin \Psi \pi/2 = 0 \tag{2.78}$$

Inasmuch as $C_1 \neq 0$, it follows that $\sin \Psi \times \pi/2 = 0$. Thus, the equation for eigen values is:

$$\Psi \pi/2 = n \pi$$

which yields:

$$\Psi = 2n \quad (n = 1, 2, 3...) \tag{2.79}$$

For $n = 1$, the smallest value of Ψ and, consequently, the smallest value of p_o for which the buckled ring remains at steady state, are obtained. Substituting $\Psi = 2$ into Eq. 2.76, one obtains the general expression for critical pressure p_{cr}:

$$p_{cr} = \frac{3EI}{(r^*)^3} \tag{2.80}$$

Defining the ring as having unit width and thickness t, I can be written as:

$$I = \frac{t^3 1}{12} \tag{2.81}$$

Substituting Eq. 2.81 into Eq. 2.80 and replacing r^* with $d_o/2$, the equation for critical pressure becomes:

$$p_{cr} = 2E \left(\frac{t}{d_o}\right)^3 \tag{2.82}$$

The expression for critical pressure for a buckled ring can also be used in determining the buckling strength of a long circular tube, $t \ll$ pipe length l, exposed to uniform external pressure. To obtain the collapse pressure (elastic range), p_{ce}, it is important to introduce the restrained Poisson's number (ν). The equation of deformation according to the theory of elasticity is given by:

$$\varepsilon_x = \frac{1}{E}(\sigma_x - \nu\,\sigma_y) \tag{2.83}$$

$$\varepsilon_y = \frac{1}{E}(\sigma_y - \nu\,\sigma_x) \tag{2.84}$$

Provided that the resulting radial stress is sufficiently large to compensate for the radial deformation then:

$$\sigma_y = \nu\,\sigma_x \tag{2.85}$$

and the axial deformation is given by:

$$\varepsilon_x = \frac{\sigma_x}{E}(1 - \nu^2) = \frac{\sigma_x}{E'} \tag{2.86}$$

where:

$$E' = \frac{E}{1 - \nu^2} \tag{2.87}$$

Substituting $E/(1 - \nu^2)$ for the modulus of elasticity in Eq. 2.82 and expressing diameter to thickness ratio as d_o/t, the Bresse (1859) equation for calculating the collapse strength of tubular goods in the elastic range is:

$$p_{ce} = \frac{2\,E}{1 - \nu^2}\,\frac{1}{(d_o/t)^3} \tag{2.88}$$

where:

p_{ce} = collapse resistance in elastic range (Bresse).

EXAMPLE 2-9:

Using a value of $\nu = 0.3$, find the collapse strength of N-80, 47 lb/ft, $9\frac{5}{8}$ in. casing in the elastic range.

Solution:

From Eq. 2.88:

$$p_{ce} = \left(\frac{2 \times (30 \times 10^6)}{1 - (0.3)^2} \times \left(\frac{0.472}{9.625} \right)^3 \right) = 7,776 \text{ psi}$$

2.3.2 Ideally Plastic Collapse

In the case of pipes exhibiting ideally plastic material behavior, the material at the inner surface of the pipe body begins to yield to the tangential stress induced by the external pressure at a critical value of pressure computed using the Lamé formula (Grassie, 1965).

Previously, it was assumed that the wall thickness of the thin-walled cylinder was small in comparison to the mean radius and, therefore, the stress could be assumed to be uniform over the material. However, with the thick-walled cylinder (low d_o/t ratio), the stress distribution is no longer uniform over the thickness of the pipe material.

If it is assumed that both the cross-section of the cylinder and the load are symmetrical with the longitudinal axis, the radial, tangential, and axial stresses are the principal stresses and, similarly, their corresponding planes are the principal planes.

An annular ring element of radius r, subtending an angle $\Delta\theta$ at the center of a cylinder, is presented in Fig. 2.10. σ_r, σ_t and σ_a represent radial, tangential, and axial stresses (respectively), acting on the ring element at any radius r, and $(F_r + \Delta F_r)$ is the radial force at a radius $(r + \Delta r)$. Thus, the radial and tangential forces can be expressed as follows:

1. Radial force:

$$\Delta F_r = -\sigma_r \, r \, \Delta\theta \, \Delta z \tag{2.89}$$

$$\Delta F_{r+\Delta r} = (\sigma_r + \Delta\sigma_r)(r + \Delta r) \, \Delta\theta \, \Delta z \tag{2.90}$$

2. Tangential force:

$$2 \, \Delta F_t = 2 \sigma_t \sin \frac{\Delta\theta}{2} \, \Delta r \, \Delta z \tag{2.91}$$

For small angles of $\Delta\theta$, $\sin(\Delta\theta/2) \approx \Delta\theta/2$. Thus:

$$2 \, F_t = \sigma_t \, \Delta\theta \, \Delta r \, \Delta z \tag{2.92}$$

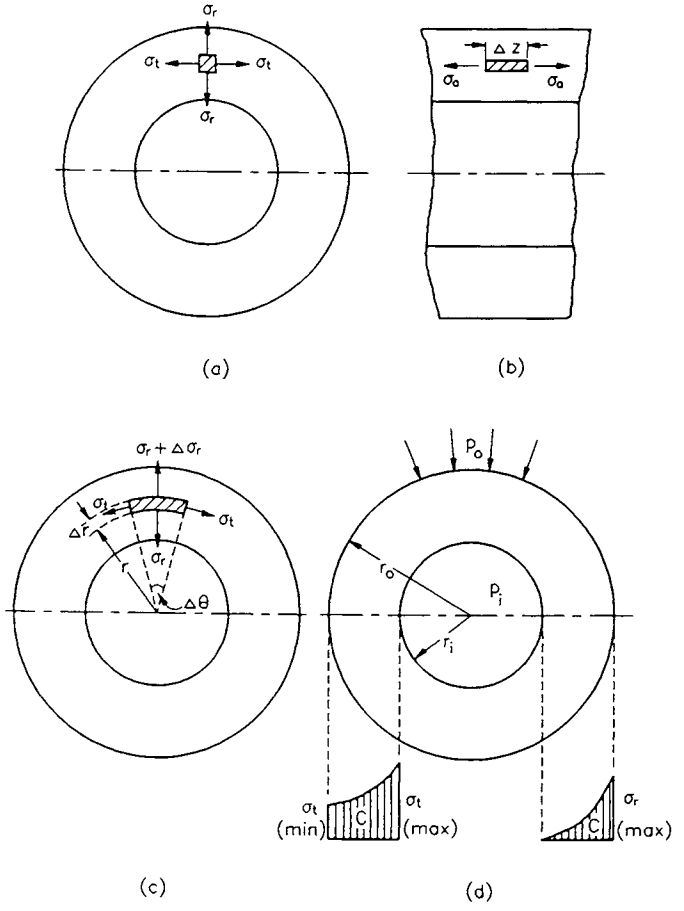

Fig. 2.10: Stresses in thick-walled casing under external pressure.

From the equilibrium conditions of the small element:

$$\Delta F_{r+\Delta r} - \Delta F_r = \sigma_t \, \Delta\theta \, \Delta r \, \Delta z \tag{2.93}$$

Substituting Eqs. 2.89 and 2.90 into 2.93 and neglecting the product of small quantities one obtains:

$$r \, \Delta\sigma_r = (\sigma_t - \sigma_r) \, \Delta r$$

or

$$\frac{r}{\Delta r} \, \Delta\sigma_r = \sigma_t - \sigma_r \tag{2.94}$$

In differential form, the above equation can be expressed as:

$$\frac{r\,d\sigma_r}{dr} = \sigma_t - \sigma_r \tag{2.95}$$

If u is the radial displacement, the strain equations due to the principal stresses σ_r, σ_t and σ_a (all assumed positive if tensile) can be expressed as:

$$\varepsilon_r = \frac{u\,(r + \Delta r) - ur}{\Delta r} = \frac{du}{dr} = \frac{1}{E}\left[\sigma_r - \nu\,(\sigma_t + \sigma_a)\right] \tag{2.96}$$

$$\varepsilon_t = \frac{2\,\pi\,(r + u) - 2\pi r}{2\pi r} = \frac{u}{r} = \frac{1}{E}\left[\sigma_t - \nu\,(\sigma_a + \sigma_r)\right] \tag{2.97}$$

$$\varepsilon_a = \frac{1}{E}\left[\sigma_a - \nu\,(\sigma_r + \sigma_t)\right] \tag{2.98}$$

For a long cylinder, the axial strain due to the symmetrical loading condition can be considered constant and thus:

$$\frac{d\varepsilon_a}{dr} = 0 = \frac{d\sigma_a}{dr} - \nu\left(\frac{d\sigma_r}{dr} + \frac{d\sigma_t}{dr}\right) \tag{2.99}$$

or

$$\frac{d\sigma_a}{dr} = \nu\left(\frac{d\sigma_r}{dr} + \frac{d\sigma_t}{dr}\right) \tag{2.100}$$

Differentiating Eq. 2.97 with respect to r, equating the result with Eq. 2.96, and substituting Eq. 2.100 for $d\sigma_a/dr$ gives:

$$\sigma_r - \sigma_t = r\left[(1 - \nu)\frac{d\sigma_t}{dr} - \nu\frac{d\sigma_r}{dr}\right] \tag{2.101}$$

Substituting Eq. 2.95 in Eq. 2.101, the following equation is obtained:

$$\begin{aligned} r\,(1 - \nu)\frac{d\sigma_t}{dr} - r\,\nu\frac{d\sigma_r}{dr} + r\frac{d\sigma_r}{dr} &= 0 \\ r\,(1 - \nu)\left(\frac{d\sigma_t}{dr} + \frac{d\sigma_r}{dr}\right) &= 0 \\ r\,(1 - \nu)\frac{d}{dr}(\sigma_t + \sigma_r) &= 0 \end{aligned} \tag{2.102}$$

However, as $r(1-\nu) \neq 0$ it follows that:

$$\sigma_t + \sigma_r = \text{ constant, which for convenience is called } 2K_1 \tag{2.103}$$

Substituting Eq. 2.95 into Eq. 2.103:

$$\frac{r\,d\sigma_r}{dr} = 2\,K_1 - 2\,\sigma_r \tag{2.104}$$

Equating to K_1 and multiplying both sides by r one obtains:

$$r^2\,\frac{d\sigma_r}{dr} + 2\,\sigma_r\,r = 2\,K_1 r \tag{2.105}$$

or

$$\frac{d}{dr}\,(r^2\sigma_r) = 2\,K_1 r \tag{2.106}$$

Finally, integrating both sides, the Lamé equations are obtained for radial and tangential stresses at any radius r:

$$\sigma_r = K_1 + \frac{K_2}{r^2} \tag{2.107}$$

and, therefore, from Eq. 2.103:

$$\sigma_t = K_1 - \frac{K_2}{r^2} \tag{2.108}$$

The values of the constants K_1 and K_2 are determined by the terminal conditions.

If p_o is an external pressure and r_i and r_o are the internal and external radii of the cylinder, respectively, then from inspection of Fig. 2.10 one obtains:

$$-p_o = K_1 + \frac{K_2}{r_o^2} \tag{2.109}$$

$$0 = K_1 + \frac{K_2}{r_i^2} \tag{2.110}$$

Combining Eqs. 2.109 and 2.110 and solving for K_1 and K_2 yields:

$$K_1 = +p_o\left(\frac{r_o^2}{r_i^2 - r_o^2}\right) \tag{2.111}$$

$$K_2 = -p_o\left(\frac{r_o^2\,r_i^2}{r_i^2 - r_o^2}\right) \tag{2.112}$$

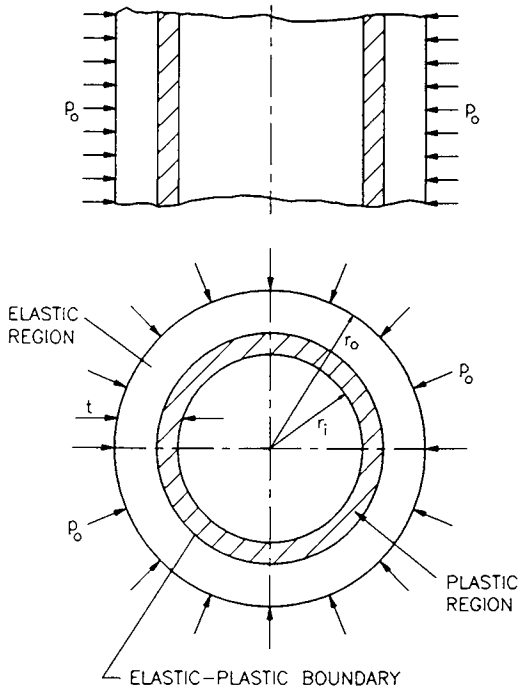

Fig. 2.11: Elastic and plastic material zones in thick-walled casing under external pressure.

Substituting Eqs. 2.111 and 2.112 into Eq. 2.108, the tangential and radial stresses due to the external pressure p_o are respectively:

$$\sigma_t = -\frac{p_o r_o^2}{r_o^2 - r_i^2}\left[1 + \frac{r_i^2}{r^2}\right] \tag{2.113}$$

$$\sigma_r = -\frac{p_o r_o^2}{r_o^2 - r_i^2}\left[1 - \frac{r_i^2}{r^2}\right] \tag{2.114}$$

The maximal tangential stress, $\sigma_{t_{max}}$, occurs at the internal surface of the pipe where $r = r_i$:

$$\sigma_{t_{max}} = -p_o\left[\frac{2r_o^2}{r_o^2 - r_i^2}\right] \tag{2.115}$$

Thus, the critical collapse pressure, p_{cy_1}, at which the internal surface of the casing begins to yield is equal to:

$$p_{cy_1} = \frac{\sigma_{0.2}\,(r_o^2 - r_i^2)}{2\,r_o^2} \tag{2.116}$$

where:

$\sigma_{0.2}{}^{c}$ = tensile stress required to produce a total elongation of 0.2 % in the gauge length of the test specimen.

p_{cy_1} = critical collapse pressure for onset of internal yield in ideally plastic material (Lamé).

The critical collapse pressure can be rewritten in terms of the ratio of nominal diameter, d_o, to wall thickness, t, by replacing r_i and r_o with $[(d_o/2) - t]$ and $(d_o/2)$, respectively:

$$p_{cy_1} = 2\,\sigma_{0.2}\,\frac{(d_o/t) - 1}{(d_o/t)^2} \tag{2.117}$$

In Eq. 2.117, the point at which the tangential stress, induced at the inner surface of the pipe body by the external pressure, reaches the yield point is considered to be a load limit. The onset of plastic deformation of the material at the inner surface of the specimen, however, does not imply that the casing has already failed rather that a plastic-elastic boundary forms (MacGregor et al., 1948) which with increasing load, shifts from the inner surface of the cylinder toward the outer surface (Fig. 2.11). Thus, the pipe body is subdivided into an interior (plastically deformed zone) and an exterior (elastic zone).

The onset of localized yield is not the only possible indication that the critical value of external pressure has been reached. The collapse strength can also be defined as that point at which the average stress over the casing wall reaches the value of the yield limit as given by Barlow's formula:

$$p_{cy_2} = \frac{2\,\sigma_{0.2}}{(d_o/t)} \tag{2.118}$$

where:

p_{cy_2} = critical collapse pressure for onset of internal yield in casing (Barlow).

Both the Lamé and Barlow formulas are used to calculate the collapse strength of the oilfield tubular goods.

---

[c]A natural yield limit is usually absent for higher steel grades; the 0.2 % permanent strain limit is usually employed as yield strength.

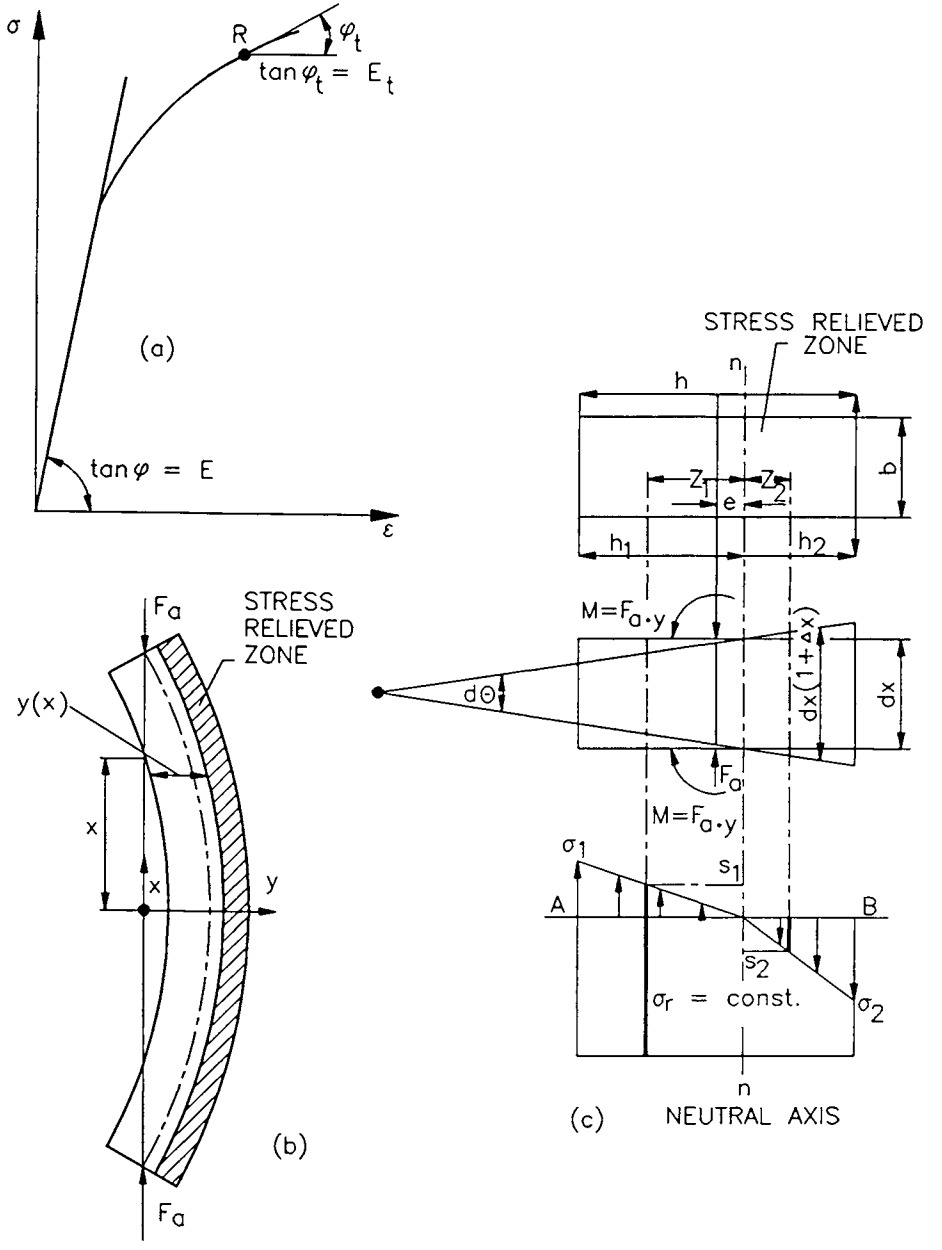

Fig. 2.12: Buckling of long struts and the related modulus of elasticity.

2.3.3 Collapse Behavior in the Elastoplastic Transition Range

The collapse behavior of casing specimens, which fail in the elastoplastic transition range, represents a problem of instability, as does elastic collapse behavior. The prediction of critical external pressure, however, can no longer be based on Young's modulus because the bending stiffness now depends on the local slope of the stress-versus-strain curve (Heise and Esztergar, 1970). Young's modulus, E, is, therefore, replaced by the tangent modulus, E_t (see Fig. 2.12(a)) in Eq. 2.88. Thus, the equation for transition collapse, p_{ct_t}, is:

$$p_{ct_t} = \frac{2\,E_t}{1-\nu}\,\frac{1}{(d_o/t)^3} \tag{2.119}$$

where:

p_{ct_t} = critical external pressure for collapse in transition range based on E_t, tangent modulus.

Calculation of collapse pressure using Eq. 2.119 yields values which are lower than experimentally derived results. Heise and Esztergar (1970) introduced the concept of a 'reduced modulus' which results in higher calculated collapse values.

The reduced modulus, E_r, is based on the theory of buckling according to Engesser and Von Karman (Szabo, 1977).

The following assumptions are made in the development of the theory (Bleich, 1952):

1. The displacements are very small in comparison to the cross-sectional dimensions of the pipe.
2. Plane cross-sections remain plane and normal to the center-line after bending.
3. The relationship between stress and strain in any longitudinal fiber is given by the stress-strain diagram, Fig. 2.12(a).
4. The plane of bending is a plane of symmetry of the pipe section.

Consider that the section in Fig. 2.12(b) is compressed by an axial load, F_a, such that $\sigma = F_a/A$ exceeds the limit of proportionality. Upon further increase in F_a, the pipe reaches a condition of unstable equilibrium at which point it is deflected slightly. In every cross-section there will be an axis $n-n$ (Fig. 2.12(c)) perpendicular to the plane of bending in which the cross-sectional stress prior to

bending, σ, remains unchanged. On one side of the $n-n$ plane, the longitudinal compressive stresses will be increased by bending at a rate proportional to $d\sigma/d\varepsilon = E_t$, whereas on the other side of $n-n$, there will be a reduction in the longitudinal stresses due to the superimposed bending stresses associated with strain reversal.

In the case of the stress reduction, Hooke's Law, $\sigma = E\,\varepsilon_x$, is applicable because the reversal only relieves the elastic portion of the strain. In the stress diagram, Fig. 2.12(c), the concave (stress relief) side is bounded by NA and the convex (stress increase) side by NB.

Referring again to Fig. 2.12(c), equilibrium between the internal stresses and the external load, F_a, requires that:

$$\int_0^{h_1} s_1 dA - \int_0^{h_2} s_2 dA = 0 \tag{2.120}$$

and,

$$\int_0^{h_1} s_1(z_1 - e)dA - \int_0^{h_2} s_2(z_2 + e)dA \;=\; F_a y \;=\; M$$

The deflection y is taken with respect to the centroid axis as illustrated in Fig. 2.12(b). From Fig. 2.12(c) one can infer:

$$s_1 = \frac{\sigma_1}{h_1} z_1 \;\text{ and }\; s_2 = \frac{\sigma_2}{h_2} z_2$$

Similarly:

$$\Delta dx = h_2 d\theta = \frac{\sigma_2 dx}{E}$$

Thus, it follows that:

$$\frac{d\theta}{dx} = \frac{\sigma_2}{E h_2} = \frac{\sigma_1}{E_t h_1} \tag{2.121}$$

For small deformations:

$$\frac{d\theta}{dx} = \frac{d^2 y}{dx^2} \tag{2.122}$$

Thus, combining Eq. 2.122 with Eq. 2.122 yields:

$$\sigma_2 = E h_2 \frac{d^2 y}{dx^2} \;\text{ and }\; \sigma_1 = E h_1 \frac{d^2 y}{dx^2}$$

Substituting the above expressions for σ_1 and σ_2 into Eq. 2.120 yields:

$$E_t \frac{d^2y}{dx^2} \int_0^{h_1} z_1 dA - E \frac{d^2y}{dx^2} \int_0^{h_2} z_2 dA = 0$$

or

$$E_t S_1 - E S_2 = 0 \tag{2.123}$$

where:

S_1 and S_2 = statical moments of the cross-sectional areas to the left and right of the axis $n - n$, respectively.

In order to represent the pipe section as a rectangular cross-section, pipe wall thickness, t, is considered as height, h, and the unit length, 1, as base (Refer to Fig 2-12(c)). Using this notation, Eq. 2.123 reduces to:

$$E\, h_1^2 = E_t\, h_2^2 \tag{2.124}$$

As shown in Fig 2-12(c), $h = h_1 + h_2$. Thus, the changes in cross-sectional areas $(h_1 \times 1)$ and $(h_2 \times 1)$ from the neutral axis are given by:

$$h_1 = \frac{h\sqrt{E_t}}{\sqrt{E} + \sqrt{E_t}} \tag{2.125}$$

and

$$h_2 = \frac{h\sqrt{E}}{\sqrt{E} + \sqrt{E_t}} \tag{2.126}$$

The moment of inertia of the deformed sections can be given as:

$$I_1 = \frac{bh_1^3}{3}, \quad I_2 = \frac{bh_2^3}{3} \text{ and } I = \frac{bh^3}{12}$$

Combining Eqs. 2.125 and 2.126 and substituting for the moment of inertia, one can define an additional parameter, E_r (reduced modulus):

$$E_r = \frac{4E \cdot E_t}{(\sqrt{E} + \sqrt{E_t})^2} \tag{2.127}$$

Hence, the collapse pressure for elasto-plastic transition range can be determined by means of the equation:

$$p_{ct_r} = \frac{2E_r}{1-\nu^2}\frac{1}{(d_o/t)^3} \tag{2.128}$$

where:

p_{ct_r} = critical external pressure for collapse in transition range based on E_r, reduced modulus.

The average tangential stress is obtained using the following equation:

$$\overline{\sigma}_{t_{E_r}} = \frac{E_r}{1-\nu^2}\frac{1}{(d_o/t)^2} \tag{2.129}$$

where:

$\overline{\sigma}_{t_{E_r}}$ = average tangential stress for a particular value of E_r.

In contrast to Young's modulus, E_r, is not a constant, but depends on the particular value of the stress. Exact knowledge of the stress-strain behavior of the material is, therefore, necessary for the determination of the collapse pressure and the calculation must be performed by means of an iterative procedure.

Sturm (1941) proposed using the tangential modulus as the effective modulus in order for the results to be conservative and to simplify the calculations in determining the collapse pressure. His general equation for collapse strength, for which the stresses exceed the limit of proportionality, is given by:

$$p_c^* = K^* E_t (t/d_o)^3 \tag{2.130}$$

where:

p_c^* = collapse pressure for stresses above the elastic limit (Sturm, 1941).

K^* denotes the collapse coefficient, which becomes equal to:

$$K^* = \frac{2}{(1-\nu^2)} \tag{2.131}$$

for infinitely long casing steel specimens.

The stress-strain relationship is presented in Fig. 2.13. The curve of tangential modulus has been approximated by a single straight line, resulting in three distinct cases:

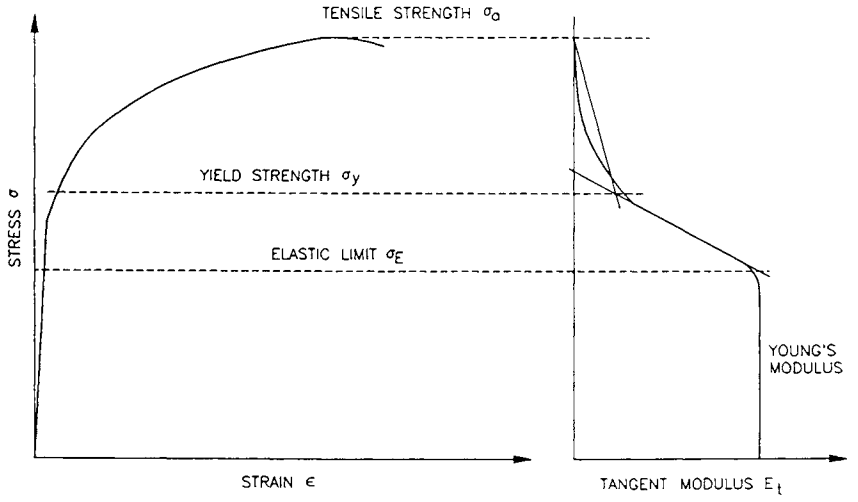

Fig. 2.13: Relationship between stress, strain and the tangent modulus . (After Krug, 1982; courtesy of ITE-TU Clausthal.)

1. If the average nominal stress, $\overline{\sigma}_n$, lies between the limit of elasticity, σ_E, and the yield limit, σ_y, the following equation applies:

$$E_t = E \left\{ 1 - (1 - \xi) \frac{\overline{\sigma}_n - \sigma_E}{\sigma_y - \sigma_E} \right\} \tag{2.132}$$

   The parameter ξ denotes the ratio of Young's modulus to the tangent modulus at the yield point, σ_y.

2. If the average nominal stress, $\overline{\sigma}_n$, lies between the yield point, σ_y, and the tensile stress, σ_a, the equation becomes:

$$E_t = \xi \, E \left\{ 1 - \frac{\overline{\sigma}_n - \sigma_y}{\sigma_a - \sigma_y} \right\} \tag{2.133}$$

3. If the average nominal stress lies below the limit of proportionality, σ_p, whereas the maximal total stress, σ_{max}, lies above the limit of elasticity because of eccentricity, the experimentally determined formula applies:

$$E_t = E \left\{ 1 - \frac{1}{4} \left(\frac{\sigma_{max} - \sigma_E}{\sigma_a - \overline{\sigma}_n} \right)^2 \right\} \tag{2.134}$$

For the calculation of the collapse pressure in the elastoplastic transition range according to the methods described, accurate knowledge of stress–strain relationships for each material is required. Furthermore, the equations do not take into

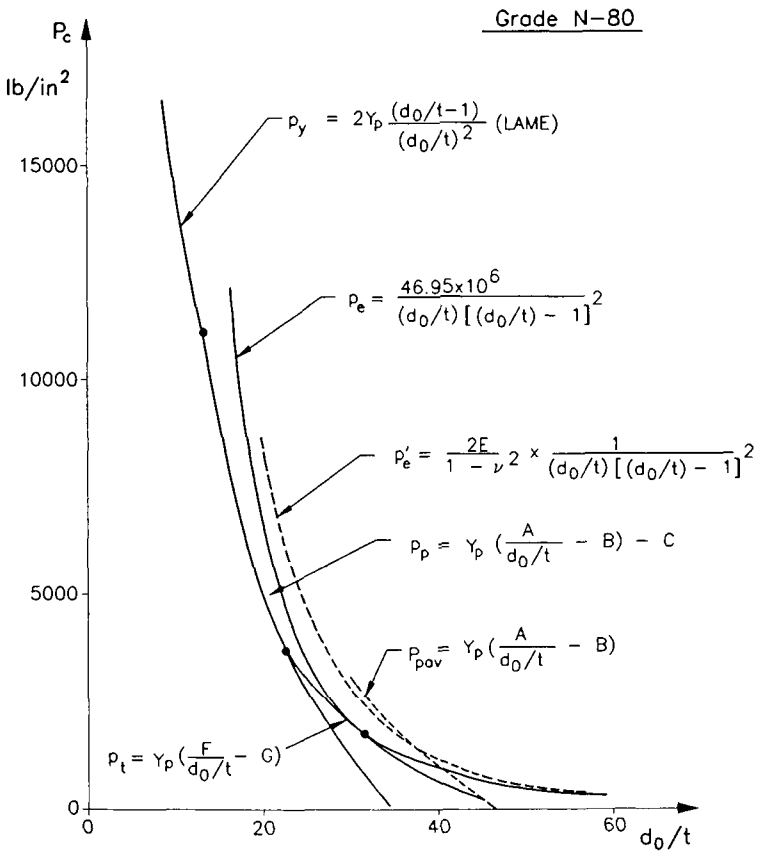

Fig. 2.14: Critical collapse pressure according to API.

account the fact that Poisson's ratio for steel varies from $\nu = 0.3$ in the elastic range to $\nu = 0.5$ in the plastic range. Moreover, imperfections may occur in the pipe body, which can influence the collapse strength. For these reasons, it appears both sensible and expedient to describe the collapse behavior by simple empirical formulas from the start. In practice, these simplifications are made for oilfield tubular goods because their standardized dimensions lie, for the most part, in this range (Krug, 1982).

2.3.4 Critical Collapse Strength for Oilfield Tubular Goods

Critical collapse resistance of casing is calculated in accordance with the API equations given in the API Bul. 5C3 (1989). The equations are those adopted at the 1968 Standardization Conference and reported in Circular PS-1360 dated September 1968. For standard casings, the collapse values can be taken from

the appropriate tables of API Bul. 5C2 (1987). In a 1977 report, Clinedinst proposed new collapse formulas, which provide better agreement with the test results obtained by Krug (1982). In this section, limitations and scope of API collapse formulas and the formulas developed by other investigators are reviewed.

2.3.5 API Collapse Formula

The collapse strength for the yield range (yield strength collapse) is calculated using the Lamé equation. In this equation, critical external pressure is defined with reference to a state at which the tangential stress reaches the value of yield strength at the internal surface for the casing subjected to the maximal stress. Although the results reported by Krug (1982) have shown that the real values of collapse pressure are in fact higher, the onset of yield in the casing material is considered to be the decisive factor. Nevertheless, no further correction factor has been introduced into the following formulas to take into account the geometrical deviations from the nominal data:

$$p_y = 2\,Y_p\,\frac{(d_o/t) - 1}{(d_o/t)^2} \tag{2.135}$$

where:

Y_p = yield strength as defined by the API, lbf/in.^{2}

For determining the elastic collapse strength, p'_e, an equation proposed by Clinedinst (1939) is utilized:

$$p'_e = \frac{2\,E}{1 - \nu^2}\,\frac{1}{(d_o/t)\,\{(d_o/t) - 1\}^2} \tag{2.136}$$

Though the formula for p'_e is very similar to the Bresse equation (Eq. 2.88) it results in higher calculated collapse values, especially for smaller d_o/t ratios. Test results presented by Krug (1982) show that the equation for p'_e provides a good approximation only for the upper scatter range of the results. The ultimate formula has been specified by introducing a correction factor which decreases the value of the external pressure to 71.25% of the theoretical value. For values of Young's modulus, $E = 30 \times 10^6$ lbf/in.^{2}, and Poisson's ratio, $\nu = 0.3$, the numerical equation is:

$$p_e = \frac{46.95 \times 10^6}{(d_o/t)\,[(d_o/t) - 1]^2} \tag{2.137}$$

The equation for plastic transition zone (plastic range) has been derived empirically from the results of almost 2,500 collapse tests on casing specimens of grades

Table 2.1: API minimal collapse resistance formulas. (After API Bul. 5C3, 1989.)

$$Y_{pa} = \sigma_y \left\{ \left[1 - 0.75 \left(\frac{\sigma_a}{\sigma_y} \right)^2 \right]^{0.5} - 0.5 \left(\frac{\sigma_a}{\sigma_y} \right) \right\}$$

$= $ yield strength of axial stress equivalent grade, psi

$= \sigma_y$ for $\sigma_a = 0$

Failure model	Applicable d_o/t range
1. Elastic $p_e = \dfrac{46.95 \times 10^6}{d_o/t\,(d_o/t - 1)^2}$	$\dfrac{d_o}{t} \geq \dfrac{2 + B/A}{3\,B/A}$
2. Transition $p_t = \left(\dfrac{F}{d_o/t} - G \right) Y_{pa}$	$\dfrac{Y_{pa}\,(A - F)}{C + Y_{pa}\,(B - G)} \leq \dfrac{d_o}{t} \leq \dfrac{2 + B/A}{3\,B/A}$
3. Plastic $p_p = Y_{pa} \left(\dfrac{A}{d_o/t} - B \right) - C$	$\dfrac{[(A-2)^2 + 8\,(B + C/Y_{pa})]^{1/2} + (A - 2)}{2\,(B + C/Y_{pa})} \leq \dfrac{d_o}{t} \leq \dfrac{Y_{pa}\,(A - F)}{C + Y_{pa}\,(B - G)}$
4. Yield $p_y = 2\,Y_{pa} \dfrac{(d_o/t) - 1}{(d_o/t)^2}$	$\dfrac{d_o}{t} \leq \left[\dfrac{[(A-2)^2 + 8\,(B + C/Y_{pa})]^{1/2} + (A - 2)}{2\,(B + C/Y_{pa})} \right]$

where:

$$A = 2.8762 + 0.10679 \times 10^{-5}\,Y_{pa} + 0.21301 \times 10^{-10}\,Y_{pa}^2 - 0.53132 \times 10^{-16}\,Y_{pa}^3$$

$$B = 0.026233 + 0.50609 \times 10^{-6}\,Y_{pa}$$

$$C = -465.93 + 0.030867\,Y_{pa} - 0.10483 \times 10^{-7}\,Y_{pa}^2 + 0.36989 \times 10^{-13}\,Y_{pa}^3$$

$$F = \frac{\left[46.95 \times 10^6 \left(\dfrac{3\,B/A}{2 + B/A} \right)^3 \right]}{\left[Y_{pa} \left(\dfrac{3\,B/A}{2 + B/A} - B/A \right) \left(1 - \dfrac{3\,B/A}{2 + B/A} \right)^2 \right]}$$

$$G = (F \times B)/A$$

Table 2.2: Empirical parameters used for collapse pressure calculation - for zero axial load, i.e., $\sigma_a = 0$. (After API Bul. 5C3, 1989.)

	Empirical Coefficients				
	Plastic Collapse			Transition Collapse	
Steel Grade*	A	B	C	F	G
H-40	2.950	0.0465	754	2.063	0.0325
- 50	2.976	0.0515	1.056	2.003	0.0347
J, K-55	2.991	0.0541	1.206	1.989	0.0360
-60	3.005	0.0566	1.356	1.983	0.0373
-70	3.037	0.0617	1.656	1.984	0.0403
C-75 and E	3.054	0.0642	1.806	1.990	0.0418
L, N-80	3.071	0.0667	1.955	1.998	0.0434
-90	3.106	0.0718	2.254	2.017	0.0466
C, T-95 and X	3.124	0.0743	2.404	2.029	0.0482
-100	3.143	0.0768	2.553	2.040	0.0499
P-105 and G	3.162	0.0794	2.702	2.053	0.0515
P-110	3.181	0.0819	2.852	2.066	0.0532
-120	3.219	0.0870	3.151	2.092	0.0565
Q-125	3.239	0.0895	3.301	2.106	0.0582
-130	3.258	0.0920	3.451	2.119	0.0599
S-135	3.278	0.0946	3.601	2.133	0.0615
-140	3.297	0.0971	3.751	2.146	0.0632
-150	3.336	0.1021	4.053	2.174	0.0666
-155	3.356	0.1047	4.204	2.188	0.0683
-160	3.375	0.1072	4.356	2.202	0.0700
-170	0.412	0.1123	4.660	2.231	0.0734
-180	3.449	0.1173	4.966	2.261	0.0769

* Grades indicated without letter designation are not API grades but are grades in use or grades being considered for use and are shown for information purposes.

K-55, N-80 and P-110. The formula for average collapse strength, $p_{p_{av}}$, has been determined by means of regression analysis:

$$p_{p_{av}} = Y_p \left[\frac{A}{d_o/t} - B \right] \tag{2.138}$$

The parameters A and B are dependent on the respective yield point. In order to take into account the effect of tolerance limits, a constant pressure C has subsequently been calculated for each steel grade. Thus, minimum plastic collapse is obtained by subtracting the factor C from the average collapse strength, $p_{p_{av}}$:

$$p_{p_{min}} = Y_p \left[\frac{A}{d_o/t} - B \right] - C \tag{2.139}$$

Table 2.3: Ranges of d_o/t ratios for various collapse pressure regions when axial stress is zero, i.e., $\sigma_a = 0$. (After API Bul. 5C3, 1989.)

Grade*	|— Yield → Collapse	— Plastic → Collapse	— Transition → Collapse	— Elastic —| Collapse
H-40	16.40	27.01	42.64	
-50	15.24	25.63	38.83	
J, K-55	14.81	25.01	37.21	
-60	14.44	24.42	35.73	
-70	13.85	23.38	33.17	
C-75 and E	13.60	22.91	32.05	
L, N-80	13.38	22.47	31.02	
-90	13.01	21.69	29.18	
C, T-95 and X	12.85	21.33	28.36	
-100	12.70	21.00	27.60	
P-105 and G	12.57	20.70	26.89	
P-110	12.44	20.41	26.22	
-120	12.21	19.88	25.01	
Q-125	12.11	19.63	24.46	
-130	12.02	19.40	23.94	
S-135	11.92	9.18	23.44	
-140	11.84	8.97	22.98	
-150	11.67	8.57	22.11	
-155	11.59	18.37	21.70	
-160	11.52	18.19	21.32	
-170	11.37	17.82	20.60	
-180	11.23	7.47	19.93	

* Grades indicated without letter designation are not API grades but are grades in use or grades being considered for use and are shown for information purposes.

The introduction of the parameter C and the associated generalized decrease of the critical external pressure gives rise to an anomaly: the line corresponding to the plastic collapse, which depends on the respective value of the yield strength, no longer intersects the curve for elastic collapse (Fig. 2.14). Consequently, it is no longer possible to take elastic collapse behavior into consideration.

The discontinuity problem has been mathematically resolved by the creation of an artificial fourth collapse range: the transition collapse. Determination of the collapse strength in this range is accomplished by means of a functional equation. The associated curve begins at the intersection of the curve corresponding to the equation for average plastic collapse strength with the d_o/t coordinate axis, ($p_{p_{av}} = 0$), is tangent to the curve for elastic collapse, and subsequently intersects the curve for plastic collapse:

$$p_t = Y_p \left[\frac{F}{(d_o/t)} - G \right] \tag{2.140}$$

where:

p_t = transition collapse pressure.

The constants F and G are dependent on the respective parameters A and B in Eq. 2.139. In Fig. 2.14, the development and behavior of the collapse strength for the individual collapse ranges for steel grade N-80 are presented. Table 2.1 provides a survey of the individual equations for collapse, as well as the formulas for calculating the individual parameters. Tables 2.2 and 2.3 show the values of empirical parameters used for calculating collapse pressure and the range of d_o/t ratios for various collapse pressure regions, respectively.

EXAMPLE 2-10:

Using data from Table 2.2 and the API formulas from Table 2.1, calculate values of collapse resistance for N-80, $9\frac{5}{8}$ in., 47 lb/ft casing in the, elastic, transition, plastic, and yield ranges. By calculating the d_o/t range determine what value is applicable to this sample casing. Assume zero axial stress.

Solution:

Calculate the d_o/t ratio.

$$d_o/t = \frac{9.625}{0.472} = 20.392$$

From Table 2.2:

$A = 3.071$, $B = 0.0667$, $C = 1955$, $F = 1.998$ and $G = 0.0434$

Substituting these values into the formulas in Table 2.1 gives the results in Table 2.4. Thus, for our sample casing of N-80 with $d_o/t = 20.392$, collapse failure occurs in the plastic range, i.e., $p_c = p_p = 4,760$ psi (API rounds-up figures to the nearest 10 psi).

Assuming a zero axial stress is of a rather limited practical application because it applies only to the neutral point. A more general approach to the calculation of collapse pressure is presented in the section on Biaxial Loading on page 80.

2.3.6 Calculation of Collapse Pressure According to Clinedinst (1977)

Clinedinst (1977) conducted 2,777 collapse pressure tests on casing lengths between 14 in. (355 mm) and 33 in. (850 mm) from six manufacturers and found the following: 49 test results indicated that the use of Barlow's formula (Eq. 2.118) to calculate the collapse pressure for yield range provided better agreement with the experimental results than did the use of the Lamé formula (Eq.

Table 2.4: EXAMPLE 2-10: Failure Model and the d_o/t range for which it is valid.

Failure model			Applicable d_o/t range
1. Elastic			
	p_e	$= \dfrac{46.95 \times 10^6}{20.392\,(20.392-1)^2}$	$d_o/t \geq 31.03$
		$=$ 6,123 psi	
2. Transition			
	p_t	$= \left(\dfrac{1.998}{20.392} - 0.0434\right) 80.000$	$22.48 \leq d_o/t \leq 31.03$
		$=$ 4,366 psi	
3. Plastic			
	p_p	$= 80,000\,(0.0839) - 1,955$	$13.39 \leq d_o/t \leq 22.48$
		$=$ 4,754 psi	
4. Yield			
	p_y	$= 2 \times 80,000 \dfrac{(20.392)\text{-}1}{(20.392)^2}$	$d_o/t \leq 13.39$
		$=$ 7,461 psi	

2.117). He, therefore, recommended the use of the Barlow's formula in which the critical external pressure is limited by the state of stress for which the average tangential stress in the casing wall corresponds to the yield point of the material:

$$p_y = \frac{2\,Y_p}{d_o/t} \tag{2.141}$$

In the elastic range, a formula similar to Eq. 2.136 has been employed. The constant in the numerator has been set equal to a higher value on the basis of the results of 147 tests. The minimum for the collapse resistance includes 99.5 % of the measured data and amounts to 75.6 % of the average test results, or 72.7 % of the theoretical values:

$$p_e = \frac{47.94 \times 10^6}{(d_o/t)\,[\{(d_o/t) - 1\}^2]} \tag{2.142}$$

For the investigation of plastic transition range, 1,594 test specimens from four casing manufacturers have been employed. The error in the experimental results due to the short length of the test specimen was corrected using a multiplier. The corrected value, $p_{(L/d_o)}$, is obtained using the following relationship:

$$p_{(L/d_o)} = p_{(L/d_o=8)}\ (8d_o/L)^{0.0708} \tag{2.143}$$

As is the case with the corresponding API equations, the effect of the out-of-roundness is implicitly contained in the empirical formula. Introducing the effect of length on the test results, Clinedinst found the following solution for determining the average collapse strength in the plastic range:

$$p_{p_{av}} = 1.672 \times 10^6 \, (t/d_o)^{(2.096 - 3.432 \times 10^{-6} \, Y_p)} \, (d_o/L)^{0.0708} \tag{2.144}$$

where:

L = length of the test specimen, in.

The minimum for the collapse strength has been specified at 77.8 % of the average collapse strength provided that no more than 0.5 % of the test results are less than this limit. Hence,

$$p_{p_{min}} = 1.301 \times 10^6 \, (t/d_o)^{(2.096 - 3.432 \times 10^{-6} \, Y_p)} \, (d_o/L)^{0.0708} \tag{2.145}$$

For test specimens having $L/d_o = 8$, the collapse resistance in the plastic range is given by:

$$p_p = \frac{1.123 \times 10^6}{(d_o/t)^{(2.096 - 3.432 \times 10^{-6} \, Y_p)}} \tag{2.146}$$

The results obtained using the equations for calculating the critical collapse pressure for the four collapse ranges are presented in Fig. 2.15. The solid line indicates the methods used by the API, whereas the dashed line indicates the method used by Clinedinst.

2.3.7 Collapse Pressure Calculations According to Krug and Marx (1980)

Krug and Marx (1980), and Krug (1982) conducted 160 collapse pressure tests on casings with d_o/t ratios between 10 and 40 and L/d_o ratios between 2 and 12. In the evaluation they took only the collapse strength in the elasto-plastic transition range into account and made the following observations:

1. Calculated values of average collapse strength in accordance with API procedures are too high. In part this can be attributed to the use of short specimens. Overall, the results exhibit favorable and uniform scattering in which dependence on steel grade is always reflected.

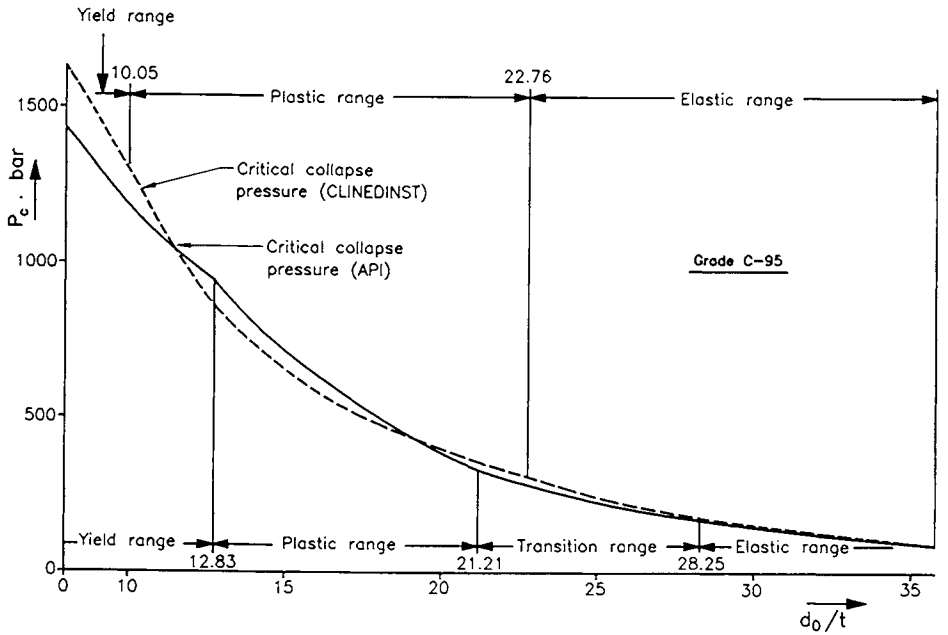

Fig. 2.15: Collapse strength of grade C-95 steel. Comparison between API and Clinedinst formulas. (After Krug, 1982; courtesy of ITE-TU Clausthal.)

2. At low values of collapse pressure (up to about 15.000 psi), the average collapse strength according to Clinedinst (1977) exhibits good agreement with the test results. At high values of collapse pressure, the calculation for high-strength steel once again yields values which are too high – irrespective of d_o/t ratio.

3. For calculation of average collapse values, the API method clearly provides better results. In comparison to the API method, however, the analytical method of Clinedinst (1977) offers the advantage that the calculated value of collapse strength is dependent only on yield strength besides d_o/t ratio: this requires less elaborate calculation.

To simplify calculations Krug and Marx (1980) generalized Clinedinst's formula by introducing the parameters a, b and c, the values of which are obtained experimentally from collapse tests:

$$p_p = a\,(d_o/t)^{b-c\sigma_{0,2}} \tag{2.147}$$

They then applied a statistical approach to obtain the equation for average collapse pressure for the elastoplastic range which provides the optimum agreement with the test results.

$$p_{p_{av}} = \frac{10.697 \times 10^5}{(d_o/t)^{1.929-3.823\times10^{-4}\,\sigma_{0,2}}} \tag{2.148}$$

where the units of $\sigma_{0.2}$ are N/mm^2.

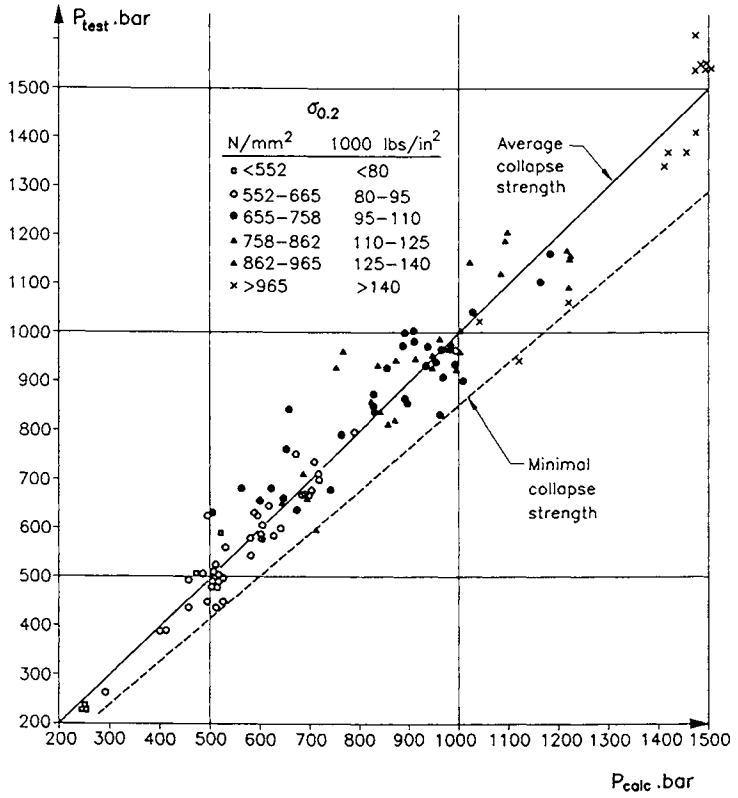

Fig. 2.16: Comparison between measured collapse pressure and average collapse strength according to $p_{p_{av}}$. (After Krug and Marx, 1980; courtesy of ITE-TU Clausthal.)

A comparison between the measured values of the collapse pressure and those calculated for the collapse strength using Eq. 2.148 is presented in Fig. 2.16. For the purpose of specifying a minimum pressure for collapse strength, $p_{p_{min}}$, defined as 85 % of the average collapse strength, $p_{p_{av}}$, in psi, is introduced:

$$p_{p_{min}} = \frac{9.0924 \times 10^5}{(d_o/t)^{1.929-3.823\times10^{-4}\,\sigma_{0.2}}} \tag{2.149}$$

where the units of $\sigma_{0.2}$ are N/mm^2.

In Figs. 2.17 and 2.18, a comparison is made between the collapse strength $p_{p_{av}}$ or $p_{p_{min}}$ and the values calculated using the API and Clinedinst (1977) methods for steel grade C-95.

Chapter 3

PRINCIPLES OF CASING DESIGN

The design of a casing program involves the selection of setting depths, casing sizes and grades of steel that will allow for the safe drilling and completion of a well to the desired producing configuration. Very often the selection of these design parameters is controlled by a number of factors, such as geological conditions, hole problems, number and sizes of production tubing, types of artificial lift equipment that may eventually be placed in the well, company policy, and in many cases, government regulations.

Of the many approaches to casing design that have been developed over the years, most are based on the concept of maximum load. In this method, a casing string is designed to withstand the parting of casing, burst, collapse, corrosion and other problems associated with the drilling conditions. To obtain the most economical design, casing strings often consist of multiple sections of different steel grades, wall thicknesses, and coupling types. Such a casing string is called a combination string. Cost savings can sometimes be achieved with the use of liner tie–back combination strings instead of full strings running from the surface to the bottom.

In this chapter, procedures for selecting setting depths, sizes, grades of steel and coupling types of different casing strings are presented.

3.1 SETTING DEPTH

Selection of the number of casing strings and their respective setting depths is based on geological conditions and the protection of fresh-water aquifers. For example, in some areas, a casing seat is selected to cover severe lost circulation zones whereas in others, it may be determined by differential pipe sticking prob-

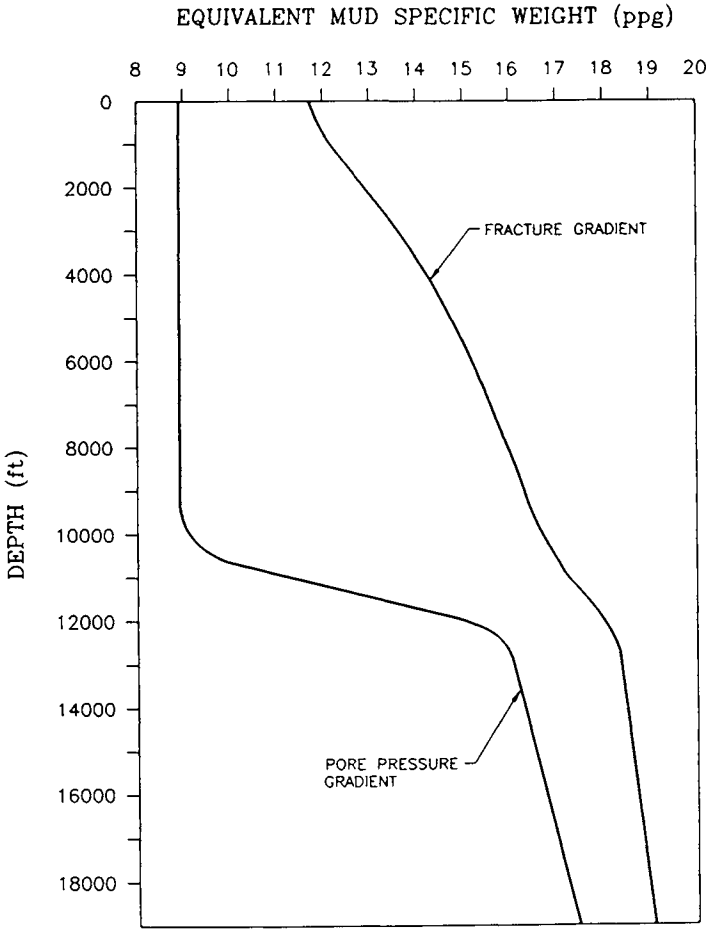

Fig. 3.1: Typical pore pressure and fracture gradient data for different depths.

lems or perhaps a decrease in formation pore pressure. In deep wells, primary consideration is either given to the control of abnormal pressure and its isolation from weak shallow zones or to the control of salt beds which will tend to flow plastically.

Selection of casing seats for the purpose of pressure control requires a knowledge of pore pressure and fracture gradient of the formation to be penetrated. Once this information is available, casing setting depth should be determined for the deepest string to be run in the well. Design of successive setting depths can be followed from the bottom string to the surface. A typical example is presented in Fig. 3.1 to illustrate the relationship between the pressure gradient, fracture gradient and depth.

3.1.1 Casing for Intermediate Section of the Well

The principle behind the selection of the intermediate casing seat is to first control the formation pressure with drilling fluid hydrostatic pressure without fracturing the shallow formations. Then, once these depths have been established, the differential pressure along the length of the pipe section is checked in order to prevent the pipe from sticking while drilling or running casing.

From Fig. 3.2 the formation pressure gradient at 19,000 ft is 0.907 psi/ft (equivalent mud specific weight = 17.45 lb/gal). To control this pressure, the wellbore pressure gradient must be greater than 0.907 psi/ft. When determining the actual wellbore pressure gradient consideration is given to: trip margins for controlling swab pressure, the equivalent increase in drilling fluid specific weight due to the surge pressure associated with the running of the casing and a safety margin. Generally a factor between 0.025 and 0.045 psi/ft (0.48 to 0.9 lb/gal of equivalent drilling mud specific weight) can be used to take into account the effects of swab and surge and provide a safety factor (Adams, 1985). Thus, the pressure gradient required to control the formation pressure at the bottom of the hole would be 0.907 + 0.025 = 0.932 psi/ft (17.95 lb/gal). At the same time, formations having fracture gradients less than 0.932 psi/ft must also be protected. Introducing a safety factor of 0.025 psi/ft, the new fracture gradient becomes 0.932 + 0.025 = 0.957 psi/ft (18.5 lb/gal). The depth at which this fracture gradient is encountered is 14,050 ft. Hence, as a starting point the intermediate casing seat should be placed at this depth.

The next step is to check for the likelihood of pipe-sticking. When running casing, pipe sticking is most likely to occur in transition zones between normal pressure and abnormal pressure. The maximum differential pressures at which the casing can be run without severe pipe sticking problems are: 2,000 - 2,300 psi for a normally pressured zone and 3,000 - 3,300 psi for an abnormally pressured zone (Adams, 1985). Thus, if the differential pressure in the minimal pore pressure zone is greater than the arbitrary (2,000 - 2,300 psi) limit, the intermediate casing setting depth needs to be changed.

From Fig. 3.2, it is clear that a drilling mud specific weight of 16.85 lb/gal (16.35 + 0.5) would be necessary to drill to a depth of 14,050 ft. The normal pressure zone, 8.9 lb/gal, ends at 9,150 ft where the differential pressure is:

$$9,150\,(16.85 - 8.9) \times 0.052 \;=\; 3,783 \text{ psi}$$

This value exceeds the earlier limit. The maximum depth to which the formation can be drilled and cased without encountering pipe sticking problems can be computed as follows:

$$\Delta p = D_n(\gamma_m - \gamma_f) \;\times\; 0.052 \tag{3.1}$$

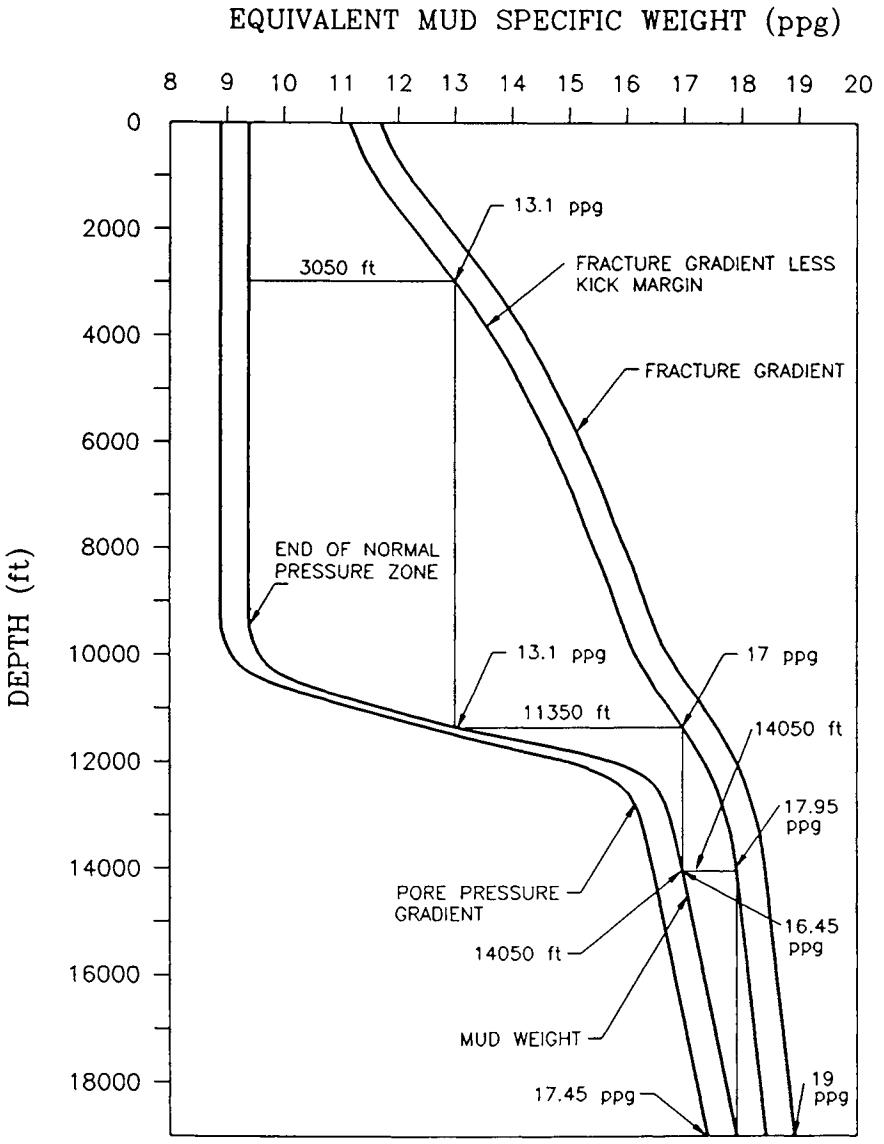

Fig. 3.2: Selection of casing seats based on the pore pressure and fracture gradient.

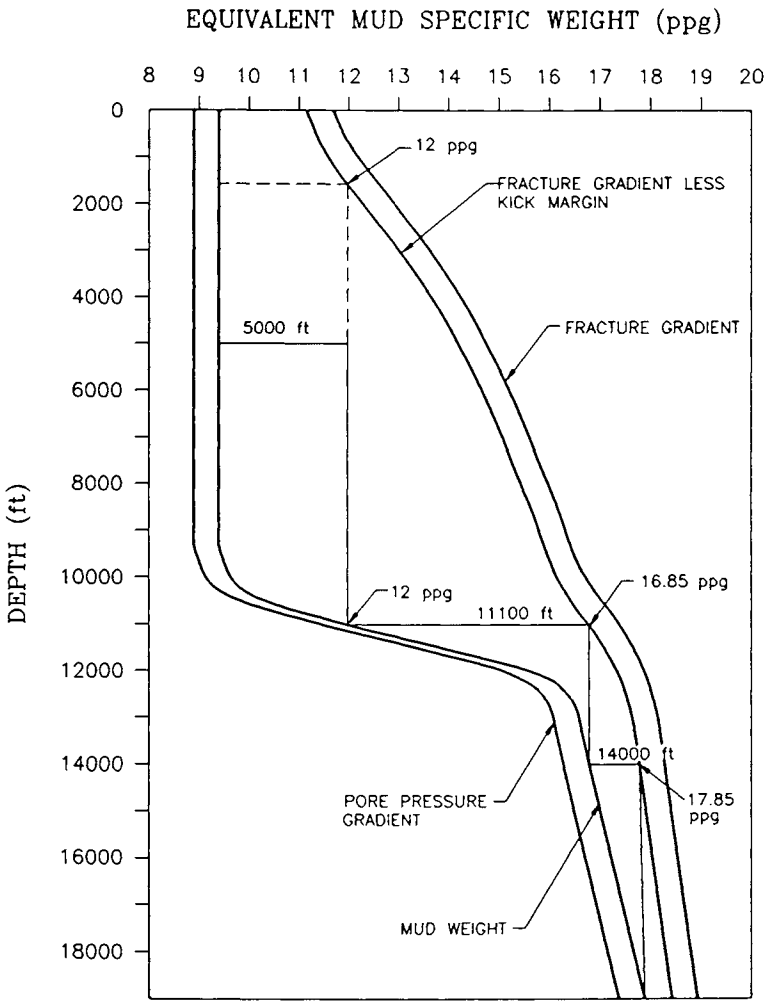

Fig. 3.3: Selection of setting depths for different casings in a 19.000-ft well.

where:

Δp = arbitrary limit of differential pressure, psi.
γ_m = specific weight of new drilling fluid, lb/gal.
γ_f = specific weight of formation fluid, lb/gal.
D_n = depth where normal pressure zone ends, ft.
0.052 = conversion factor from lb/gal to psi/ft.

Given a differential pressure limit of 2.000 psi, the value for the new mud specific weight becomes 13.1 lb/gal (0.681 psi/ft gradient). Now the depth at which the new drilling fluid gradient becomes the same as the formation fluid gradient, is 11,350 ft. For an additional safety margin in the drilling operation, 11,100 ft is selected as the setting depth for this pipe.

The setting depth for casing below the intermediate casing is selected on the basis of the fracture gradient at 11,100 ft. Hence, the maximal drilling fluid pressure gradient that can be used to control formation pressure safely, without creating fractures at a depth of 11,100 ft, must be determined.

From Fig. 3.3, the fracture gradient at 11,100 ft is 0.902 psi/ft (or 17.35 lb/gal equivalent drilling mud weight). Once again, a safety margin of 0.025 psi/ft which takes into account the swab and surge pressures and provides a safety factor is used. This yields a final value for the fracture gradient of 0.877 psi/ft and a mud specific weight of 16.85 lb/gal, respectively. The maximal depth that can be drilled safely with the 16.85 lb/gal drilling fluid is 14,050 ft. Thus, 14,000 ft (or 350 joints) is chosen as the setting depth for the next casing string. Inasofar as this string does not reach the final target depth, the possibility of setting a liner between 11,100 ft and 14,000 ft should be considered.

The final selection of the liner setting depth should satisfy the following criteria:

1. Avoid fracturing below the liner setting depth.
2. Avoid differential pipe sticking problems for both the liner and the section below the liner.
3. Minimize the large hole section in which the liner is to be set and thereby reduce the pipe costs.

As was shown in Fig. 3.2, the mud weight that can be used to drill safely to the final depth is 17.95 lb/gal (gradient of 0.93 psi/ft). This value is lower than the fracture gradient at the liner setting depth.

Differential pressures between 11,100 ft and 14,000 ft and between 14,000 ft and 19,000 ft are 821 psi and 451 psi, respectively. These values are within the prescribed limits.

Thus, the final setting depths for intermediate casing string, drilling liner and production casing string of 11,100 ft, 14,000 ft, and 19,000 ft, respectively, are presented in Fig. 3.3. These setting depths also minimize the length of the large hole sections.

3.1.2 Surface Casing String

The surface casing string is often subjected to abnormal pressures due to a kick arising from the deepest section of the hole. If a kick occurs and the shut–in casing pressure plus the drilling fluid hydrostatic pressure exceeds the fracture resistance pressure of the formation at the casing shoe, fracturing or an underground blowout

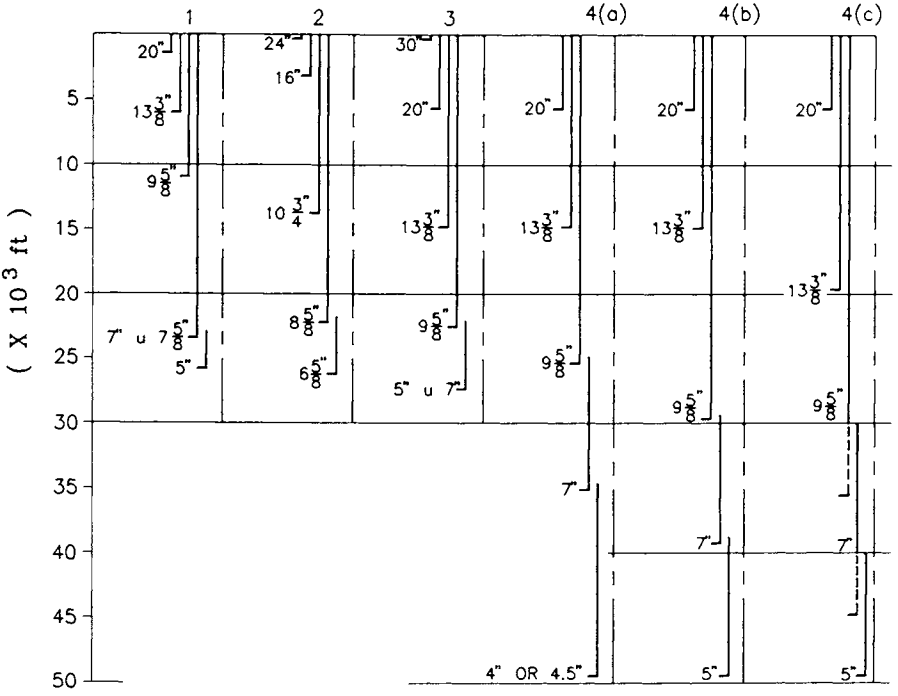

Fig. 3.4: Typical casing program for different depths.

can occur. The setting depth for surface casing should, therefore, be selected so as to contain a kick-imposed pressure.

Another factor that may influence the selection of surface casing setting depth is the protection of fresh-water aquifers. Drilling fluids can contaminate fresh-water aquifers and to prevent this from occurring the casing seat must be below the aquifer. Aquifers usually occur in the range of 2,000 - 5,000 ft.

The relationship between the kick-imposed pressure and depth can be obtained using the data in Fig. 3.1. Consider an arbitrary casing seat at depth D_s; the maximal kick-imposed pressure at this point can be calculated using the following relationship:

$$p_k = G_{p_f} D_i - G_{p_f}(D_i - D_s) \tag{3.2}$$

where:

p_k = kick-imposed pressure at depth D_s, psi.
D_s = setting depth for surface casing, ft.
D_i = setting depth for intermediate casing, ft.
G_{p_f} = formation fluid gradient at depth D_i, psi/ft.

Assume also that formation fluid enters the hole from the next casing setting

depth, D_i. Expressing the kick-imposed pressure of the drilling fluid in terms of formation fluid gradient and a safety margin, SM, Eq. 3.2 becomes:

$$p_k = (G_{p_f} + SM)D_i - G_{p_f}(D_i - D_s) \tag{3.3}$$

or

$$\frac{p_k}{D_s} = SM\left(\frac{D_i}{D_s}\right) + G_{p_f} \tag{3.4}$$

Where p_k/D_s is the kick-imposed pressure gradient at the seat of the surface casing and must be lower than the fracture resistance pressure at this depth to contain the kick.

Now, assume that the surface casing is set to a depth of 1,500 ft and SM, in terms of equivalent mud specific weight, is 0.5 lb/gal. The kick-imposed pressure gradient can be calculated as follows:

$$\begin{aligned} \frac{p_k}{1,500} &= \left(0.052 \times 0.5\left(\frac{11,100}{1,500}\right) + 8.9 \times 0.052\right) \\ &= 0.6552 \text{ psi/ft} \end{aligned}$$

The fracture gradient at 1,500 ft is 0.65 psi/ft (12.49 lb/gal). Clearly, the kick-imposed pressure is greater than the strength of the rock and, therefore, a deeper depth must be chosen. This trial-and-error process continues until the fracture gradient exceeds the kick-imposed pressure gradient. Values for different setting depths and their corresponding kick-imposed fracture and pressure gradients are presented below:

Table 3.1: Fracture and kick-imposed pressure gradients vs depth.

Depth (ft)	Kick-imposed pressure gradient (psi/ft)	Fracture pressure gradient (psi/ft)
1,500	0.6552	0.65
2,000	0.61	0.66

At a depth of 2,000 ft the fracture resistance pressure exceeds the kick-imposed pressure and so 2,000 ft could be selected as a surface casing setting depth. However, as most fresh-water aquifers occur between 2,000 and 5,000 ft the setting depth for surface casing should be within this range to satisfy the dual requirements of prevention of underground blowouts and the protection of fresh-water aquifers.

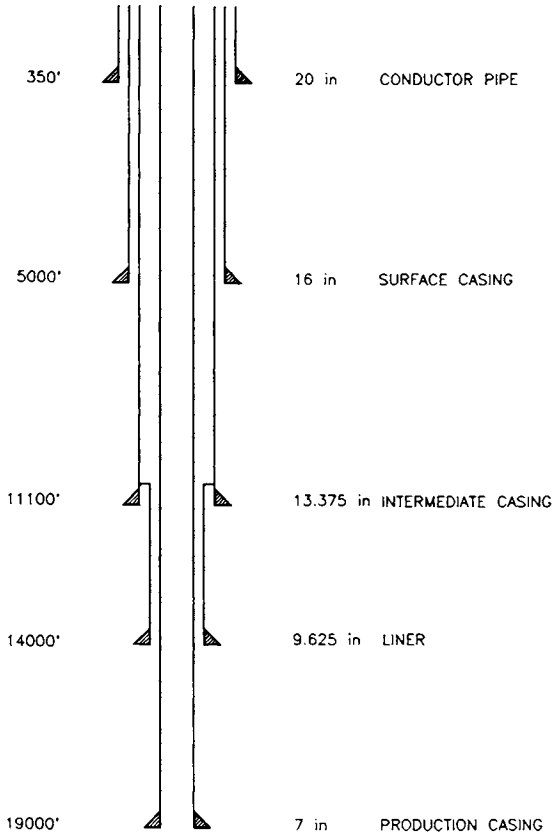

Fig. 3.5: Casing program for a typical 19,000-ft deep well.

3.1.3 Conductor Pipe

The selection of casing setting depth above surface casing is usually determined by drilling problems and the protection of water aquifers at shallow depths. Severe lost circulation zones are often encountered in the interval between 100 and 1,000 ft and are overcome by covering the weak formations with conductor pipes. Other factors that may affect the setting depth of the conductor pipe are the presence of unconsolidated formations and gas traps at shallow depths.

3.2 CASING STRING SIZES

Selection of casing string sizes is generally controlled by three major factors: (1) size of production tubing string, (2) number of casing strings required to reach the final depth, and (3) drilling conditions.

3.2.1 Production Tubing String

The size of the production tubing string plays a vital role in conducting oil and gas to the surface at an economic rate. Small-diameter tubing and subsurface control equipment always restrict the flow rate due to the high frictional pressure losses. Completion and workover operations can be even more complicated with small-diameter production tubing and casing strings because the reduced inside diameter of the tubing and the annular space between the casing and tubing make tool placement and operation very difficult. For these reasons, large-diameter production tubing and casing strings are always preferable.

3.2.2 Number of Casing Strings

The number of casing strings required to reach the producing formation mainly depends on the setting depth and geological conditions as discussed previously. Past experience in the petroleum industry has led to the development of fairly standard casing programs for different depths and geological conditions. Figure 3.4 presents six of these standard casing programs.

3.2.3 Drilling Conditions

Drilling conditions that affect the selection of casing sizes are: bit size required to drill the next depth, borehole hydraulics and the requirements for cementing the casing.

Drift diameter of casing is used to select the bit size for the hole to be drilled below the casing shoe. Thus, the drift diameter or the bit size determines the maximal outside diameter of the successive casing strings to be run in the drilled hole. Bits from different manufacturers are available in certain standard sizes according to the IADC (International Association of Drilling Contractors). Almost all API casing can be placed safely without pipe sticking in holes drilled with these standard bits. Non-API casing, such as thick-wall casing is often required for completing deep holes. The drift diameter of thick-wall pipe may restrict the use of standard bit sizes though additional bit sizes are available from different manufacturers for use in such special circumstances.

The size of the annulus between the drillpipe and the drilled hole plays an important role in cleaning the hole and maintaining a gauge hole. Hole cleaning is the ability of the drilling fluid to remove the cuttings from the annulus and depends mainly on the drilling fluid viscosity, annular fluid velocity, and cutting sizes and shapes. Annular velocity is reduced if the annulus is too large and as a consequence, hole cleaning becomes inadequate. Large hole sections occur in the

Table 3.2: Typical drilling and mud programs for a 19,000-ft well.

Drilling program:

0 – 350 ft	→	26-in. hole
350 – 5,000 ft	→	20-in. hole
5,000 – 11,100 ft	→	17.5-in.hole
11,100 – 14,000 ft	→	12.5-in. hole
14,000 – 19,000 ft	→	8.5-in. hole

Casing program

0 – 350 ft	→	20-in.	conductor pipe
0 – 5,000 ft	→	16-in.	surface casing
0 – 11,100 ft	→	13.375-in.	intermediate casing
11,100 – 14,000 ft	→	9.625-in.	liner
0 – 19,000 ft	→	7-in.	production casing

Formation fluid gradient

0 – 350 ft	→	0.465	psi/ft
350 – 5,000 ft	→	0.465	psi/ft
5,000 – 11,100 ft	→	0.597	psi/ft
11,100 – 14,000 ft	→	0.849	psi/ft
14,000 – 19,000 ft	→	0.906	psi/ft

Mud program

0 – 350 ft	→	9.5	ppg (70.7 lb/ft^3)
0 – 5,000 ft	→	9.5	ppg (70.7 lb/ft^3)
0 – 11,100 ft	→	12.0	ppg (89.8 lb/ft^3)
0 – 14,000 ft	→	16.8	ppg (125.7 lb/ft^3)
0 – 19,000 ft	→	17.9	ppg (133.9 lb/ft^3)

shallow portion of the well and obviously it is here that the rig pumps must deliver the maximum flow rate. Most rig pumps are rated to 3,000 psi though they generally reach maximum flow rate before rated pressure even when operating two pumps together. Should the pumps be unable to clean the surface portion of the hole because they lack adequate capacity then a more viscous drilling fluid will need to be used to support the cuttings.

With increasing depth, the number of casing strings in the hole increases and the hole narrows as does the annular gap between the hole and the casing. Fluid flow in such narrow annular spaces is turbulent and tends to enlarge the hole sections which are sensitive to erosion. In an enlarged hole section. hole cleaning is very poor and a good cementing job becomes very difficult.

Annular space between the casing string and the drilled hole should be large

enough to accommodate casing appliances such as centralizers and scratchers, and to avoid premature hydration of cement. An annular clearance of 0.75 in. is sufficient for a cement slurry to hydrate and develop adequate strength. Similarly, a minimum clearance of 0.375 in. (0.750 in. is preferable) is required to reach the recommended strength of bonded cement (Adams, 1985).

In summary, the selection of casing sizes is a critical part of casing design and must begin with consideration of the production casing string. The pay zone can be analyzed with respect to the flow potential and the drilling problems which are expected to be encountered in reaching it. Assuming a production casing string of 7 in outside diameter, which satisfies both production and drilling requirements, a casing program for a typical 19,000-ft deep well is presented in Fig. 3.5. Table 3.2 presents the drilling fluid program, pore pressures, and fracture gradients encountered at the different setting depths.

3.3 SELECTION OF CASING WEIGHT, GRADE AND COUPLINGS

After establishing the number of casing strings required to complete a hole, their respective setting depths and the outside diameters, one must select the nominal weight, steel grade, and couplings of each of these strings. In practice, each casing string is designed to withstand the maximal load that is anticipated during casing landing, drilling, and production operations (Prentice, 1970).

Often, it is not possible to predict the tensile, collapse, and burst loads during the life of the casing. For example, drilling fluid left in the annulus between the casing and the drilled hole deteriorates with time. Consequently, the pressure gradient may be reduced to that of salt water which can lead to a significant increase in burst pressure. The casing design, therefore, proceeds on the basis of the worst anticipated loading conditions throughout the life of the well.

Performance properties of the casing deteriorate with time due to wear and corrosion. A safety factor is used, therefore, to allow for such uncertainties and to ensure that the rated performance of the casing is always greater than the expected loading. Safety factors vary according to the operator and have been developed over many years of drilling and production experience. According to Rabia (1987), common safety factors for the three principal loads are: 0.85—1.125 for collapse, 1—1.1 for burst and 1.6—1.8 for tension.

Maximal load concept tends to make the casing design very expensive. Minimal cost can be achieved by using a combination casing string—a casing string with different nominal weights, grades and couplings. By choosing the string with the lowest possible weight per foot of steel and the lowest coupling grades that meet

the design load conditions, minimal cost is achieved.

Design load conditions vary from one casing string to another because each casing string is designed to serve a specific purpose. In the following sections general methods for designing each of these casing strings (conductor pipe, surface casing, intermediate casing, production casing and liner) are presented.

Casing-head housing is generally installed on the conductor pipe. Thus, conductor pipe is subjected to a compressional load resulting from the weight of subsequent casing strings. Hence, the design of the conductor pipe is made once the total weight of the successive casing strings is known.

It is customary to use a graphical technique to select the steel grade that will satisfy the different design loads. This method was first introduced by Goins et al. (1965, 1966) and later modified by Prentice (1970) and Rabia (1987). In this approach, a graph of loads (collapse or burst) versus depth is first constructed, then the strength values of available steel grades are plotted as vertical lines. Steel grades which satisfy the maximal existing load requirements of collapse and burst pressures are selected.

Design load for collapse and burst should be considered first. Once the weight, grade, and sectional lengths which satisfy burst and collapse loads have been determined, the tension load can be evaluated and the pipe section can be upgraded if it is necessary. The final step is to check the biaxial effect on collapse and burst loads, respectively. If the strength in any part of the section is lower than the potential load, the section should be upgraded and the calculation repeated.

In the following sections, a systematic procedure for selecting steel grade, weight, coupling, and sectional length is presented. Table 3.3 presents the available steel grades and couplings and related performance properties for expected pressures as listed in Table 3.2.

Table 3.3: Available steel grades, weights and coupling types and their minimum performance properties available for the expected pressures.

Size, outside diameter (in.)	Nominal weight, threads and coupling (lb/ft)	Grade	Pipe		Pipe collapse resistance (psi)	Body yield strength (1000 lbf)	Coupling type	Internal pressure resistance (psi)	Joint strength (1000 lbf)
			Wall thickness (in.)	Inside diameter (in.)					
20	94	K-55	0.438	19.124	520	1,480	LTC	2,110	955
	133	K-55	0.635	18.730	1,500	2,125	BTC	3,036	2,123
16	65	K-55	0.375	15.250	630	1,012	STC	2,260	625
	75	K-55	0.438	15.124	1,020	1,178	STC	2,630	752
	84	L-80	0.495	15.010	1,480	1,929	BTC	4,330	1,861
	109	K-55	0.656	14.688	2,560	1,739	BTC	3,950	1,895
$13\frac{3}{8}$	98	L-80	0.719	11.937	5,910	2,800	BTC	7,530	2,286
	85	P-110	0.608	12.159	4,690	2,682	PTC	8,750	2,290
	98	P-110	0.719	11.937	7,280	3,145	PTC	10,350	2,800
$9\frac{5}{8}$	58.4	L-80	0.595	8.435	7,890	1,350	BTC	8,650	1,396
	47	P-110	0.472	8.681	5,310	1,493	LTC	9,440	1213
7	38	V-150	0.540	5.920	19,240	1,644	Extreme-line	18,900	1,430
	41	V-150	0.590	5.820	22,810	1,782	PTC	20,200	1,052
	46	V-150	0.670	5.660	25,970	1,999	PTC	25,070	1,344
	38	MW-155	0.540	5.920	19,700	1,697	Extreme-line	20,930	1,592
	46	SOO-140	0.670	5.660	24,230	865	PTC	23,400	1,222
	46	SOO-155	0.670	5.660	26,830	2,065	PTC	25,910	1,344

LTC = long thread coupling, STC = short thread coupling, BTC = buttress thread coupling, and PTC = proprietary coupling.

3.3.1 Surface Casing (16-in.)

Surface casing is set to a depth of 5,000 ft and cemented back to the surface. Principal loads to be considered in the design of surface casing are: collapse, burst, tension and biaxial effects. Inasmuch as the casing is cemented back to the surface, the effect of buckling is ignored.

Collapse

Collapse pressure arises from the differential pressure between the hydrostatic heads of fluid in the annulus and the casing, it is a maximum at the casing shoe and zero at the surface. The most severe collapse pressures occur if the casing is run empty or if a lost circulation zone is encountered during the drilling of the next interval.

At shallow depths, lost circulation zones are quite common. If a severe lost-circulation zone is encountered near the bottom of the next interval and no other permeable formations are present above the lost-circulation zone, it is likely that the fluid level could fall below the casing shoe, in which case the internal pressure at the casing shoe falls to zero (complete evacuation). Similarly, if the pipe is run empty, the internal pressure at the casing shoe will also be zero.

At greater depths, complete evacuation of the casing due to lost-circulation is never achieved. Fluid level usually drops to a point where the hydrostatic pressure of the drilling fluid inside the casing is balanced by the pore pressure of the lost circulation zone.

Surface casing is usually cemented to the surface for several reasons, the most important of which is to support weak formations located at shallow depths. The presence of a cement sheath behind the casing improves the collapse resistance by up to 23% (Evans and Herriman, 1972) though no improvement is observed if the cement sheath has voids. In practice it is almost impossible to obtain a void-free cement-sheath behind the casing and, therefore, a saturated salt-water gradient is assumed to exist behind the cemented casing to compensate for the effect of voids on collapse strength. Some designers ignore the beneficial effect of cement and instead assume that drilling fluid is present in the annulus in order to provide a built-in safety factor in the design. In summary, the following assumptions are made in the design of collapse load for surface casing (see Fig. 3.6(a)):

1. The pressure gradient equivalent to the specific weight of the fluid outside the pipe is that of the drilling fluid in the well when the pipe was run.

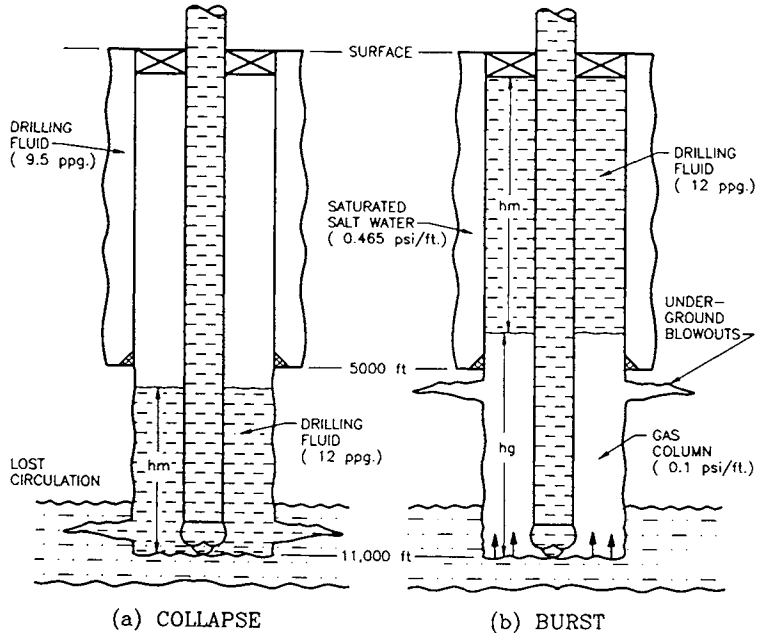

Fig. 3.6: Collapse and burst load on surface casing.

2. Casing is completely empty.

3. Safety factor for collapse is 0.85.

Collapse pressure at the surface = 0 psi

Collapse pressure at the casing shoe:

$$\begin{aligned} \text{Collapse pressure} &= \text{external pressure - internal pressure} \\ &= G_{pm} \times 5{,}000 - 0 \\ &= 9.5 \times 0.052 \times 5{,}000 - 0 \\ &= 2{,}470 \text{ psi} \end{aligned}$$

In Fig. 3.7, the collapse line is drawn between 0 psi at the surface and 2,470 psi at 5,000 ft. The collapse resistances of suitable grades from Table 3.3 are presented below.

Collapse resistances for the above grades are plotted as vertical lines in Fig. 3.7. The points at which these lines intersect the collapse load line are the maximal depths for which the individual casing grade would be suitable. Hence, based on collapse load, the grades of steel that are suitable for surface casing are given in Table 3.5.

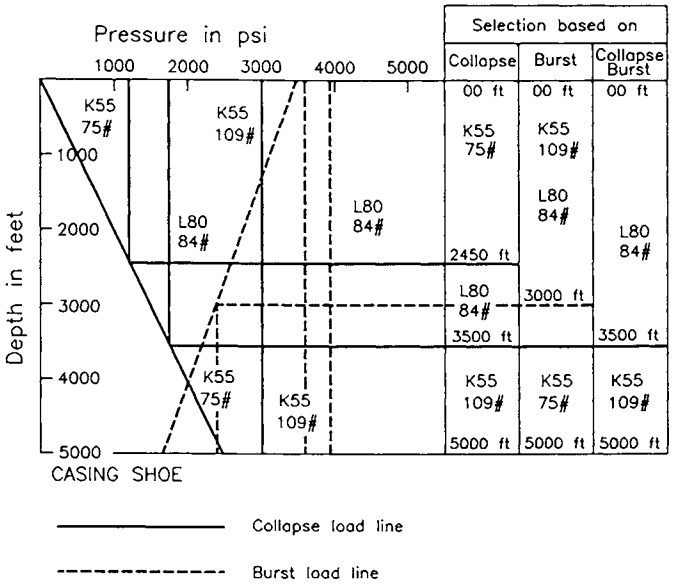

Fig. 3.7: Selection of steel grade and weight based on the collapse and burst load for 16-in. surface casing.

Burst

The design for burst load assumes a maximal formation pressure results from a kick during the drilling of the next hole section. A gas-kick is usually considered to simulate the worst possible burst load. At shallow depths it is assumed that the influx of gas displaces the entire column of drilling fluid and thereby subjects the casing to the kick-imposed pressure. At the surface, the annular pressure is zero and consequently burst pressure is a maximum at the surface and a minimum at the shoe.

For a long section, it is most unlikely that the inflowing gas will displace the entire

Table 3.4: Collapse resistance of grades suitable for surface casing.

Grade	Weight (lb/ft)	Coupling	Collapse resistance (psi)	
			$SF = 1$	$SF = 0.85$
K-55	75	STC	1,020	1,200
L-80	84	STC/BTC	1,480	1,741
K-55	109	BTC	2,560	3,012

Table 3.5: Intervals for surface casing based on collapse loading.

Section	Interval (ft)	Grade and Weight (lb/ft)	Length (ft)
1	0 - 2,450	K-55, 75	2,450
2	2,450 - 3,550	L-80, 84	1,100
3	3,550 - 5,000	K-55, 109	1,450

column of drilling fluid. According to Bourgoyne et al. (1985), burst design for a long section of casing should be such as to ensure that the kick-imposed pressure exceeds the formation fracture pressure at the casing seat before the burst rating of the casing is reached. In this approach, formation fracture pressure is used as a safety pressure release mechanism so that casing rupture and consequent loss of human lives and property are prevented. The design pressure at the casing seat is assumed to be equal to the fracture pressure plus a safety margin to allow for an injection pressure: the pressure required to inject the influx fluid into the fracture.

Burst pressure inside the casing is calculated assuming that all the drilling fluid inside the casing is lost to the fracture below the casing seat leaving the influx-fluid in the casing. The external pressure on the casing due to the annular drilling fluid helps to resist the burst pressure; however, with time, drilling fluid deteriorates and its specific weight drops to that of saturated salt-water. Thus, the beneficial effects of drilling fluid and the cement sheath behind the casing are ignored and a normal formation pressure gradient is assumed when calculating the external pressure or back-up pressure outside the casing.

The following assumptions are made in the design of strings to resist burst loading (see Fig. 3.6(b)):

1. Burst pressure at the casing seat is equal to the injection pressure.
2. Casing is filled with influx gas.
3. Saturated salt water is present outside the casing.
4. Safety factor for burst is 1.1.

Burst pressure at the casing seat = injection pressure - external pressure, p_o, at 5,000 ft.

Injection pressure = (fracture pressure + safety factor) $\times$ 5,000

Again, it is customary to assume a safety factor of 0.026 psi/ft (or equivalent drilling fluid specific weight of 0.5 ppg).

Injection pressure = (14.76 + 0.5) 0.052 × 5,000
= 3,976.6 psi

External pressure at 5,000 ft = saturated salt water gradient × 5,000
= 0.465 × 5,000
= 2,325 psi

Burst pressure at 5,000 ft = 3,976.6 - 2,325
= 1,651.6 psi

Burst pressure at the surface = internal pressure - external pressure

Internal pressure = injection pressure - G_{p_g} × 5,000
= 3,976.6 - 500
= 3,476.6 psi

where:

G_{p_g} = 0.1psi/ft

Burst pressure at the surface = 3,476.6 - 0
= 3,476.6 psi

In Fig. 3.7, the burst load line is drawn between 3,476.6 psi at the surface and 1,651.6 psi at a depth of 5,000 ft. The burst resistances of suitable grades are presented in Table 3.6.

Table 3.6: Burst resistance of grades suitable for surface casing.

Grade	Weight (lb/ft)	Coupling	Burst resistance (psi)	
			$SF = 1$	$SF = 1.1$
K-55	75	STC	2,630	2,391
L-80	84	STC/BTC	4,330	3,936
K-55	109	BTC	3,950	3,591

The burst resistances of the above grades are also plotted as vertical lines in Fig. 3.7. The point of intersection of the load line and the resistance line represents the maximal depth for which the individual grades would be most suitable. According to their burst resistances, the steel grades that can be selected for surface casing are shown in Table 3.7.

Table 3.7: Intervals for surface casing grades based on burst loading.

Section	Depth (ft)	Grade and Weight (lb/ft)	Length (ft)
1	3,000 - 5,000	K-55, 75	2,000
2	0 - 3,000	L-80, 84	3,000
3	0 - 3,000	K-55, 109	3,000

Selection Based on Both Collapse and Burst Pressures

When the selection of casing is based on both collapse and burst pressures (see Fig. 3.7), one observes that:

1. Grade K-55 (75 lb/ft) satisfies the collapse requirement to a depth of 2,450 ft, but does not satisfy the burst requirement.

2. Grade L-80 (84 lb/ft) satisfies burst requirements from 0 to 5,000 ft but only satisfies the collapse requirement from 0 to 3,550 ft.

3. Grade K-55 (109 lb/ft) satisfies both collapse and burst requirements from 0 to 5,000 ft.

4. Steel grade K-55 (75 lb/ft) can be rejected because it does not simultaneously satisfy collapse and burst resistance criteria across any section of the hole.

For economic reasons, it is customary to initially select the lightest steel grade because weight constitutes a major part of the cost of casing. Thus, the selection of casing grades based on the triple requirements of collapse, burst, and cost is summarised in Table 3.8.

Table 3.8: Most economical surface casing based on collapse and burst loading.

Section	Interval (ft)	Grade and Weight (lb/ft)	Coupling	Length (ft)
1	0 - 3,550	L-80, 84	BTC	3,550
2	3,550 - 5,000	K-55, 109	BTC	1,450

Tension

As discussed in Chapter 2, the principal tensile forces originate from pipe weight, bending load, shock loads and pressure testing. For surface casing, tension due to bending of the pipe is usually ignored.

In calculating the buoyant weight of the casing, the beneficial effects of the buoyancy force acting at the bottom of the string have been ignored. Thus, the neutral point is effectively considered to be at the shoe until buckling effects are considered.

The tensile loads to which the two sections of the surface casing are subjected are presented in Table 3.9. The value of $Y_p = 1.861 \times 10^3$ lbf (Column (7)) is the joint yield strength which is lower than the pipe body yield strength of 1.929×10^3 lbf.

Table 3.9: Total tensile loads on surface casing string.

(1) Depth interval (ft)	(2) Grade and Weight (lb/ft)	(3) Buoyant weight of section joint (1,000 lbf) (1) $\times W_n \times BF$ (=0.856)	(4) Cumulative buoyant weight carried by the top joint (1,000 lbf)	(5) Shock load carried by each section (1,000 lbf) $3,200W_n$	(6) Total tension (1,000 lbf) (4) + (5)	(7) $SF = \frac{Y_p}{\text{Total tension}}$
5,000 - 3,550	K-55, 109	135.222	135.222	348.8	484.022	1,738/484.022 = 3.59
3,550 - 0	L-80, 84	255.130	390.352	268.8	659.152	1,861/659.152 = 2.82

It is evident from the above that both sections satisfy the design requirements for tensional load arising from cumulative buoyant weight and shock load.

Pressure Testing and Shock Loading

During pressure testing, extra tensional load is exerted on each section. Thus, sections with marginal safety factors should be checked for pressure testing conditions.

Tensional load due to pressure testing

= burst resistance of weakest grade (L-80, 84) $\times$ 0.6 $\times$ A_s
= 4,330 $\times$ 0.6 $\times$ 24.1 = 62,611.8 lbf

Total tensional load during pressure testing

= cumulative buoyant load + load due to pressure testing

Shock loading occurs during the running of casing, whereas pressure testing occurs after the casing is in place; thus, the affects of these additional tensional forces are considered separately. The larger of the two forces is added to the buoyant and bending forces which remain the same irrespective of whether the pipe is in motion or static.

Hence,

$$SF = \frac{Y_p}{\text{Total tension load}} = \frac{1,861,000}{62,611.8 + 390,352} = 4.11$$

This indicates that the top joint also satisfies the requirement for pressure testing.

Biaxial Effects

It was shown previously that the tensional load has a beneficial effect on burst pressure and a detrimental effect on collapse pressure. It is, therefore, important to check the collapse resistance of the top joint of the weakest grade of the selected casing and compare it to the existing collapse pressure. In this case, L-80 (84 lb/ft) is the weakest grade. Reduced collapse resistance of this grade can be calculated as follows:

Buoyant weight carried by L-80 (84 lb/ft) = 135,222 lbf.

(1) Axial stress due to the buoyant weight is equal to:

$$\sigma_a = \frac{135,222}{\pi(d_o^2 - d_i^2)/4} = \frac{135,222}{\pi(16^2 - 15^2)/4} = 5,608 \text{ psi}$$

(2) Yield stress is equal to:

$$\sigma_y = \frac{1,929,000}{\pi(16^2 - 15^2)/4} = 80,000 \text{ psi}$$

(3) From Eq. 2.163, the effective yield stress is given by:

$$\begin{aligned}\sigma_e &= \sigma_y \left\{ \left[1 - 0.75 \left(\frac{\sigma_a}{\sigma_y} \right)^2 \right]^{0.5} - 0.5 \left(\frac{\sigma_a}{\sigma_y} \right) \right\} \\ &= 80,000 \left\{ \left[1 - 0.75 \left(\frac{5,608}{80,000} \right)^2 \right]^{0.5} - 0.5 \left(\frac{5,608}{80,000} \right) \right\} \\ &= 77,048 \text{ psi}\end{aligned}$$

(4) $d_o/t = 16/0.495 = 32.32$

(5) The values of A, B, C, F and G are calculated using equations in Table 2.1 and the value of σ_e (as determined above, i.e., 77,048 psi) as:

$$\begin{aligned}A &= 3.061 \\ B &= 0.065 \\ C &= 1,867 \\ F &= 1.993 \\ G &= 0.0425\end{aligned}$$

(6) Collapse failure mode ranges can be calculated as follows (Table 2.1):

$$\begin{aligned}\frac{[(A-2)^2 + 8(B + C/\sigma_e)]^{0.5} + (A-2)}{2(B + C/\sigma_e)} &= 13.510 \\ \frac{\sigma_e(A-F)}{C + \sigma_e(B-G)} &= 22.724 \\ \frac{2 + B/A}{3B/A} &= 31.615\end{aligned}$$

Inasmuch as the value of d_o/t is greater than 31.615, the failure mode of collapse is in the elastic region. For elastic collapse, collapse resistance is not a function of yield strength and, therefore, the collapse resistance remains unchanged in the presence of imposed axial load.

Final Selection

Both Section 1 and Section 2 satisfy the requirements for the collapse, burst and tensional load. Thus, the final selection is shown in Table 3.10.

3.3.2 Intermediate Casing ($13\frac{3}{8}$-in. pipe)

Intermediate casing is set to depth of 11,100 ft and partially cemented at the casing seat. Design of this string is similar to the surface-string except that

Table 3.10: Final casing selection for surface string.

Section	Depth (ft)	Grade and Weight (lb/ft)	Length (ft)
1	0 - 3,550	L-80, 84	3,550
2	3,550 - 5,000	K-55, 109	1,450

some of the design loading conditions are extremely severe. Problems of lost circulation, abnormal formation pressure, or differential pipe sticking determine the loading conditions and hence the design requirements. Similarly, with only partial cementing of the string it is now important to include the effect of buckling in the design calculations. Meeting all these requirements makes implementing the intermediate casing design very expensive.

Below the intermediate casing, a liner is set to a depth of 14,000 ft and as a result, the intermediate casing is also exposed to the drilling conditions below the liner. In determining the collapse and burst loads for this pipe, the liner is considered to be the integral part of the intermediate casing as shown in Fig. 3.8.

Collapse

As in the case of surface casing, the collapse load for intermediate casing is imposed by the fluid in the annular space, which is assumed to be the heaviest drilling fluid encountered by the pipe when it is run in the hole. As discussed previously, maximal collapse load occurs if lost circulation is anticipated in the next drilling interval of the hole and the fluid level falls below the casing seat. This assumption can only be satisfied for pipes set at shallow depths.

In deeper sections of the well, lost circulation causes the drilling fluid level to drop to a point where the hydrostatic pressure of the drilling fluid column is balanced by the pore pressure of the lost circulation zone, which is assumed to be a saturated salt water gradient of 0.465 psi/ft. Lost circulation is most likely to occur below the casing seat because the fracture resistance pressure at this depth is a minimum.

For collapse load design, the following assumptions are made (Fig. 3.8):

1. A lost circulation zone is encountered below the liner seat (14,000 ft).
2. Drilling fluid level falls by h_a, to a depth of h_{m_2}.
3. Pore pressure gradient in the lost circulation zone is 0.465 psi/ft (equivalent mud weight = 8.94 ppg).

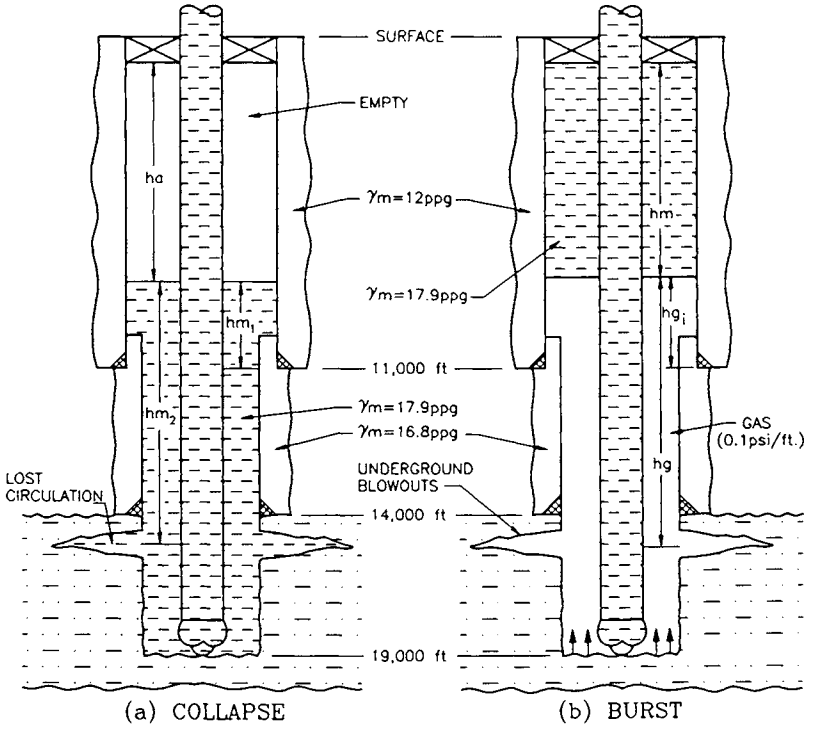

Fig. 3.8: Collapse and burst loads on intermediate casing and liner.

Thus, the design load for collapse can be calculated as follows:

Collapse pressure at surface = 0 psi
Collapse pressure at casing seat = external pressure - internal pressure

$$\begin{aligned} \text{External pressure} &= G_{p_m} \times 11{,}100 \\ &= 12 \times 0.052 \times 11{,}100 \\ &= 6{,}926.4 \text{ psi} \end{aligned}$$

where:

h_{m_1} = the height of the drilling fluid level above the casing seat.

The top of the fluid column from the liner seat can be calculated as follows:

$$\begin{aligned} h_{m_2} &= \frac{G_{p_f} \times 14{,}000}{\gamma_m \times 0.052} = \frac{0.465 \times 14{,}000}{17.9 \times 0.052} \\ &= 6{,}994 \text{ ft} \end{aligned}$$

The distance between the top of the fluid column and the surface, h_a, is equal to:

$$\begin{aligned} h_a &= 14,000 - 6,994 \\ &= 7,006\,\text{ft} \end{aligned}$$

Height of the drilling fluid column above the casing seat, h_{m_1}, is equal to:

$$\begin{aligned} h_{m_1} &= 11,100 - 7,006 \\ &= 4,094\,\text{ft} \end{aligned}$$

Hence, the internal pressure at the casing seat is:

$$\begin{aligned} \text{Internal pressure} &= G_{pm} \times h_{m_1} \\ &= 17.9 \times 0.052 \times 4,094 \\ &= 3,810.7\ \text{psi} \end{aligned}$$

$$\begin{aligned} \text{Collapse pressure at 11,100 ft} &= 6,926.4 - 3,810.7 \\ &= 3,115.7\ \text{psi} \end{aligned}$$

$$\begin{aligned} \text{Collapse pressure at 7,006 ft} &= \text{external pressure} - \text{internal pressure} \\ &= 12 \times 0.052 \times 7,006 - 0 \\ &= 4,371.74\ \text{psi} \end{aligned}$$

In Fig. 3.9, the collapse line is constructed between 0 psi at the surface, 4,371.74 psi at a depth of 7,006 ft and 3,115.7 psi at 11,100 ft. The collapse resistances of suitable steel grades from Table 3.2 are given in Table 3.11 and it is evident that all the steel grades satisfy the requirement for the conditions of maximal design load (4,371.74 psi at 7,006 ft).

Burst

The design load for intermediate casing is based on loading assumed to occur during a gas–kick. The maximal acceptable loss of drilling fluid from the casing is limited to an amount which will cause the internal pressure of the casing to rise to the operating condition of the surface equipment (blowout preventers, choke manifolds, etc.). One should not design a string which has a higher working pressure than the surface equipment, because the surface equipment must be able to withstand any potential blowout. Thus, the surface burst pressure is generally set

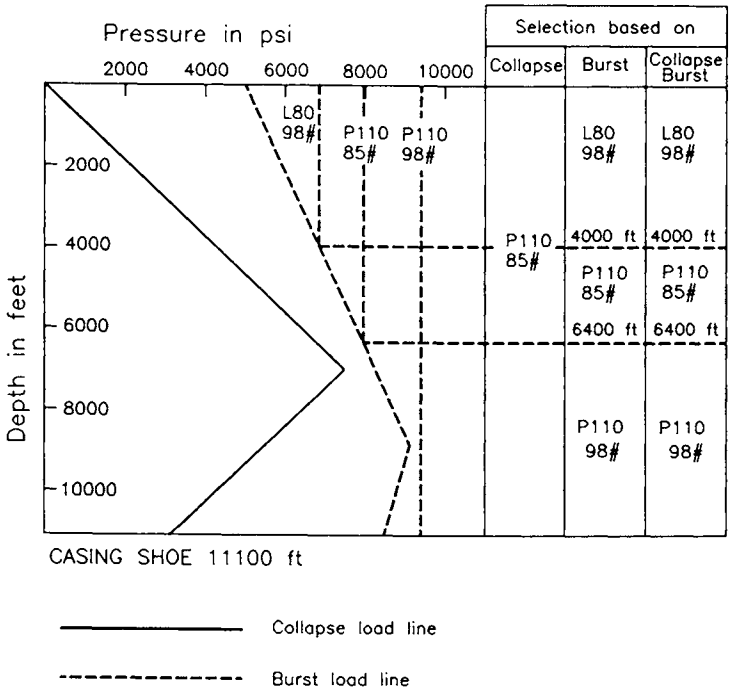

Fig. 3.9: Selection of casing grades and weights based on collapse and burst loads for intermediate casing.

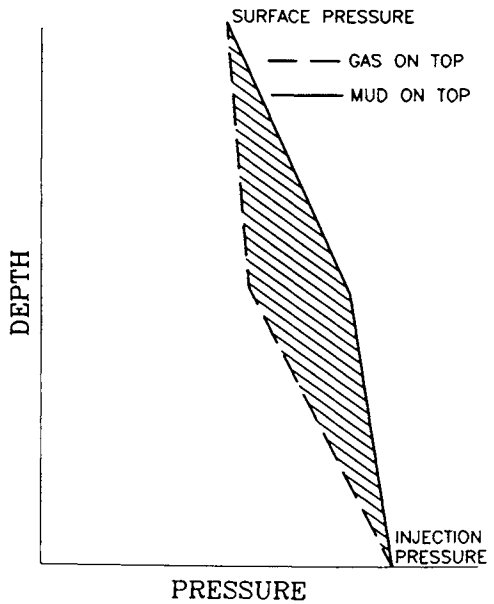

Fig. 3.10: Burst load with respect to the relative position of the drilling fluid and the influx gas.

Table 3.11: Collapse resistance of grades suitable for intermediate casing.

Grade	Weight (lb/ft)	Coupling	Collapse resistance (psi)	
			$SF = 1$	$SF = 0.85$
L-80	98	BTC	5,910	6,953
P-110	85	PTC	4,690	5,517
P-110	98	PTC	7,280	8,564

to the working pressure rating of the surface equipment used. Typical operating pressures of surface equipment are 5,000, 10,000, 15,000 and 20,000 psi.

The relative positions of the influx gas and the drilling fluid in the casing are also important (Fig. 3.10). If the influx gas is on the top of the drilling fluid, the load line is represented by a dashed line. If instead the mud is on the top, the load line is represented by the solid line. From the plot, it is evident that the assumption of mud on top of gas yields a greater burst load than for gas on top of mud.

The following assumptions are made in calculating the burst load:

1. Casing is partially filled with gas.
2. During a gas-kick, the gas occupies the bottom part of the hole and the remaining drilling fluid the top.
3. Operating pressure of the surface equipment is 5,000 psi.

Thus, the burst pressure at the surface is 5,000 psi.

Burst pressure at the casing seat = internal pressure − external pressure.

The internal pressure is equal to the injection pressure at the casing seat. The intermediate casing, however, will also be subjected to the kick-imposed pressure assumed to occur during the drilling of the final section of the hole. Thus, determination of the internal pressure at the seat of the intermediate casing should be based on the injection pressure at the liner seat.

Injection pressure at the liner seat (14,000 ft)

= fracture gradient × depth
= (18.4 + 0.5) × 0.052 × 14,000
= 13,762 psi.

The relative positions of the gas and the fluid can be determined as follows (Fig.

3.8):

$$14,000 = h_g + h_m \tag{3.5}$$

Surface pressure = injection pressure − $(G_{p_g} h_g + G_{p_m} h_m)$

$$5,000 = 13,762 - (0.1 \times h_g + 17.9 \times 0.052 \times h_m) \tag{3.6}$$

Solving Eqs. 3.5 and 3.6 simultaneously, one obtains h_g and h_m:

h_g = 5,141 ft
h_m = 8,859 ft

The length of the gas column from the intermediate casing seat, h_{gi}, is:

h_{gi} = 11,100 − 8,859 = 2,241 ft

Burst pressure at the bottom of the drilling fluid column

= internal pressure − external pressure

Internal pressure at 8,859 ft = 5.000 + 17.9 × 0.052 × 8.859
= 13,246 psi

External pressure at 8859 ft = 0.465 × 8.859
= 4.119 psi

Burst pressure at 8,859 ft = 13,246 − 4,119
= 9,127 psi

Burst pressure at casing seat = internal pressure − external pressure

Internal pressure at 11,100 ft = pressure at 8.859 ft + $(Gp_g \times h_{gi})$
= 13,246 + 224.1
= 13,470 psi

Burst pressure at 11,100 ft = 13,470 − 11,100 × 0.45
= 8,475 psi

In Fig. 3.9, the burst pressure line is constructed between 5,000 psi at the surface, 9,127 psi at 8,859 ft and 8,475 psi at 11,100 ft. The burst resistances of the suitable grades from Table 3.2 are given in Table 3.12.

The grades that satisfy both burst and collapse requirements and the intervals for which they are valid are listed in Table 3.13.

Table 3.12: Burst resistances of grades suitable for intermediate casing.

Grade	Weight (lb/ft)	Coupling	Burst resistance (psi)	
			$SF = 1$	$SF = 1.1$
L-80	98	BTC	7,530	6,845
P-110	85	PTC	8,750	7,954
P-110	98	PTC	10,350	9,409

Table 3.13: Most economical intermediate casing based on collapse and burst loading.

Section	Depth (ft)	Grade and Weight (lb/ft)	Length (ft)
1	0 - 4,000	L-80, 98	4,000
2	4,000 - 6,400	P-110, 85	2,400
3	6,400 - 11,100	P-110, 98	4,700

Tension

The suitability of the selected grades for tension are checked by considering cumulative buoyant weight, buckling force, shock load and pressure testing. A maximal dogleg of 3°/100 ft is considered when calculating the tension load due to bending. Hence, starting from the bottom, Table 3.14 is produced.

It is evident from Table 3.14 that grade L-80 (98 lb/ft) is not suitable for the top section. Before changing the top section of the string the effect of pressure testing can be considered.

Pressure Testing and Shock Loading

Axial tension due to pressure testing:

$$\begin{aligned} &= \text{Grade L-80 burst pressure resistance} \times 0.6 \times A_s \\ &= 7,530 \times 0.6 \times 28.56 = 129,034 \text{ lbf} \end{aligned}$$

$$\begin{aligned} \text{Top joint tension} &= (4) + (6) + 129,034 \\ &= 1,240,007 \text{ lbf} \end{aligned}$$

Table 3.14: Total tensile loads on intermediate casing string.

(1) Depth interval (ft)	(2) Grade and Weight (lb/ft)	(3) Buoyant weight of section joint (1,000 lbf) (1) × W_n × BF $BF = 0.817$	(4) Cumulative buoyant weight carried by the top joint (1,000 lbf)
11,100 - 6,400	P-110, 98	376.310	376.310
6,400 - 4,000	P-110, 85	166.668	542.978
4,000 - 0	L-80, 98	320.264	863.242

(5) Shock load carried by each joint (1,000 lbf) ($3,200W_n$)	(6) Bending load in each section (1,000 lbf) ($63\ d_o W_n \Theta$)	(7) Total tension (1,000 lbf) (4) + (5) + (6)	(8) $SF = \frac{Y_p}{\text{Total tension}}$
313.60	247.731	937.641	2,800/937.64 = 2.98
272.00	214.869	1,029.847	2,290/1,029 = 2.22
313.60	247.731	1,424.573	2,286/1,424 = 1.61

$$SF = \frac{Y_p}{\text{Total tension}} = \frac{2,286,000}{1,240,007} = 1.84$$

The pressure testing calculations indicate that the upper section is suitable. However, it is the worst case that one is designing for and in this case, as Column (5) in Table 3.14 attests, it is the shock load.

Tension load is calculated by considering the cumulative buoyant weight at the top joint (4), shock load (5), and bending load (6). The length of Section 1, x, that satisfies the requirement for tensional load can be calculated as follows:

$$\text{Minimum safety factor } (= 1.8) = \frac{Y_p}{\text{Total tension}}$$

$$\begin{aligned}\text{Total tension load} &= (98x + 2,400 \times 85 + 4,700 \times 98) \times 0.817 + 313,600 \\ &\quad + 24,7731 \\ &= 80.07x + 1,104,309.2 \text{ lbf}\end{aligned}$$

Hence,

$$1.8 = \frac{2,286,000}{80.07x + 1,104,309.2}$$

$$x = \frac{298,243.44}{144.118} = 2{,}069 \text{ ft or } 52 \text{ joints.}$$

Thus, the part of Section 1 to be replaced by a higher grade casing is (4,000 - 2,000) 2,000 ft or 50 joints. If this length is replaced by P-110 (98 lb/ft), the safety factor for tension will be:

$$SF = \frac{2,800,000}{1,424,573} = 1.97$$

In summary, the selection based on collapse, burst, and tension is given in Table 3.15. Table 3.16 shows the reworked tension results based on the revised string.

Table 3.15: Intermediate casing selection based on collapse, burst and tensile loads.

Section	Depth (ft)	Grade and Weight (lb/ft)	Length (ft)
1	0 - 2,000	P-110, 98	2,000
2	2,000 - 4,000	L-80, 98	2,000
3	4,000 - 6,400	P-110, 85	2,400
4	6,400 - 11,100	P-110, 98	4,700

Biaxial Effect

The weakest grade among the four sections is P-110 (85 lb/ft). It is, therefore, important to check for the collapse resistance of this grade under axial tension.

(1) Axial stress, σ_a, carried by P-110 (85 lb/ft) is:

$$\sigma_a = \frac{376,310}{24.39} = 15,431 \text{ psi.}$$

(2) Pipe yield stress:

$$\sigma_y = \frac{2,682,000}{24.39} = 109,981 \text{ psi.}$$

Table 3.16: Total tensile loads on revised intermediate casing string.

(1) Depth interval (ft)	(2) Grade and Weight (lb/ft)	(3) Buoyant weight of section joint (1,000 lbf) (1) × W_n × BF (= 0.817)	(4) Cumulative buoyant weight carried by the top joint (1,000 lbf)
11,100 – 6,400	P-110, 98	376.310	376.310
6,400 – 4,000	P-110, 85	166.668	542.978
4,000 – 2,000	L-80, 98	160.132	703.110
2,000 – 0	P-110, 98	160.132	863.242

(5) Shock load carried by each joint (1000 lbf) ($3,200W_n$)	(6) Bending load in each section (1,000 lbf) ($63\ d_o W_n \Theta$)	(7) Total tension (1,000 lbf) (4) + (5) + (6)	(8) $SF = \frac{Y_p}{\text{Total tension}}$
313.60	247.731	937.641	2,800/937.64 = 2.98
272.00	214.869	1,029.847	2,290/1,029 = 2.22
313.60	247.731	1,264.441	2,286/1,264.44 = 1.81
313.60	247.731	1,424.573	2,800/1,424.57 = 1.97

(3) From Eq. 2.163, the effective yield stress is given by:

$$\begin{aligned}
\sigma_e &= \sigma_y \left\{ \left[1 - 0.75 \left(\frac{\sigma_a}{\sigma_y} \right)^2 \right]^{0.5} - 0.5 \left(\frac{\sigma_a}{\sigma_y} \right) \right\} \\
&= 109,981 \left\{ \left[1 - 0.75 \left(\frac{15,431}{109,981} \right)^2 \right]^{0.5} - 0.5 \left(\frac{15,831}{109,981} \right) \right\} \\
&= 101,450 \text{ psi}
\end{aligned}$$

(4) $d_o/t = 13.375/0.608 = 21.998$.
(5) The values of A to G are calculated using the equations in Table 2.1 and the value of σ_e above:

$A = 3.1483$
$B = 0.0776$
$C = 2,596.26$
$F = 2.0441$
$G = 0.0504$

(6) Collapse failure mode ranges are:

$$\frac{[(A-2)^2+8(B+C/\sigma_e)]^{0.5}+(A-2)}{2(B+C/\sigma_e)} = 12.661$$

$$\frac{\sigma_e(A-F)}{C+\sigma_e(B-G)} = 20.913$$

$$\frac{2+B/A}{3B/A} = 27.389$$

(7) Inasmuch as $d_o/t = 21.99$, the failure mode is in the elasto-plastic region.

(8) Hence, the reduced collapse resistance of P-110 (85 lb/ft) is 4,317 psi.

(9) Thus, the safety factor for collapse at 6,400 ft is:

$$SF_c = \frac{\text{Reduced collapse resistance}}{\text{Collapse load at 6,400 ft}}$$

$$= \frac{4,317}{4,023} = 1.07$$

which satisfies the design criterion $SF_c \geq 0.85$

Table 3.17: Intermediate casing properties and mud weights during landing operation.

Depth (ft)	Grade and Weight (lb/ft)	A_i (in.^{2})	A_o (in.^{2})	A_s (in.^{2})	γ_i (lb/gal)	γ_o (lb/gal)
0 - 2,000	P-110, 98	111.91	140.5	28.59	12	12
2,000 - 4,000	L-80, 98	111.91	140.5	28.59	12	12
4,000 - 6,400	P-110, 85	116.11	140.5	24.39	12	12
6,400 - 10,000	P-110, 98	111.91	140.5	28.59	12	12
10,000 - 11,100	P-110, 98	111.91	140.5	28.59	12	14 (cement)

Buckling

As discussed in Chapter 2, casing buckling will occur when the axial stress is less than the average of the radial and tangential stresses. Thus, the buckling condition for the above casing grades can be found by determining the neutral point along the casing length. Casing sections above this point are stable and those below are liable to buckle.

It is assumed that the pipe is cemented to 10,000 ft from the surface and the specific weight of the slurry is 14 ppg. Thus, the pipe will be subjected to buckling

due to the change in the specific weight of the fluid between the outside and the inside of the casing and the change in the average temperature during the drilling of the next interval. Lengths and properties of the different pipe sections and the mud weight during the landing operation are shown in Table 3.17.

For the conditions summarized in Table 3-17, the values of axial stresses are given in Table 3.18. Note that the two top strings of L-80, 98 lb/ft and P-110, 98 lb/ft have been grouped together in one 4,000-ft string as their ID's, OD's and casing weights are the same.

Table 3.18: Axial stresses on intermediate casing string during landing operation.

Depth (ft)	Grade and Weight (lb/ft)	(1) $W_n(D-x)$ (lbf)	(2) $(A_o p_o - A_i p_i)$ (lbf)	(3) $\sigma_{aw_1} = \frac{(1)-(2)}{A_s}$ (psi)	(4) $\sigma_{ap_1} = \frac{p_i(A_{up_1} - A_{low_1})}{A_s}$ (psi)
11,100	P-110, 98	0	214,099	-7,489	0
10,000	P-110, 98	107,800	214,099	-3,718	0
6,400	P-110, 98	460,600	214,099	8,622	0
6,400	P-110, 85	460,600	214,099	10,107	688
4,000	P-110, 85	664,600	214,099	18,471	688
4,000	L-80, 98	664,600	214,099	15,757	321
0	P-110, 98	1,056,600	214,099	29,468	321

Examples of Calculations in Preparing Table 3.18:

Axial stress, σ_{aw_1} (item 3), due to pipe weight and pressure differences at 6,400 and 4,000 ft, can be calculated as follows:

σ_{aw} at 6,400 ft on pipe section P-110 (98 lb/ft)

$$= \frac{W_n(D-x) - (A_o p_o - A_i p_i)}{A_s}$$

$$= \frac{98\,(11,100 - 6,400) - [140.5 \times 0.052\,(12 \times 10,000 + 14 \times 1,100)}{28.59} \rightarrow$$

$$\rightarrow \frac{-(111.91 \times 12 \times 0.052 \times 11,100)]}{28.59}$$

$$= \frac{460,600 - 214,099}{28.59} = 8,622\,\text{psi}$$

σ_{aw} at 6,400 ft on pipe section P-110 (85 lb/ft):

$$= \frac{460,600 - 214,099}{24.39} = 10,107\,\text{psi}$$

σ_{aw} at 4,000 ft on pipe section L-80 (98 lb/ft)

$$= \frac{[98\,(11,100 - 6,400) + 85\,(6,400 - 4,000)\,] - 214,099}{28.59}$$

$$= \frac{664,600 - 214,099}{28.59} = 15,757\,\text{psi}$$

σ_{ap} (item 4) at 4,600 ft on pipe section P-110 (85 lb/ft)

$$= \frac{p_i\,(A_{up_1} - A_{low_1})}{A_s}$$

$$= \frac{12 \times 0.052 \times 6,400\,(116.11 - 111.91)}{24.39}$$

$$= 688\,\text{psi}$$

σ_{ap} at 4,000 ft on pipe section L-80 (98 lb/ft)

$$= \frac{0.624 \times 6,400\,(116.11 - 111.91) + 0.624 \times 4,000\,(111.91 - 116.11)}{28.59}$$

$$= 321\,\text{psi}$$

The effective axial stresses and the average of the radial and tangential stresses are presented in Table 3.19.

Table 3.19: Effective axial and the average of radial and tangential stresses in the intermediate casing during landing operations.

Depth (ft)	Grade and Weight (lb/ft)	(5) Total axial stress, σ_a (3) + (4) (psi)	(6) $(\sigma_r + \sigma_t)/2 = (A_i G_{p_i} - A_o G_{p_o})\,x/A_{sx}$ (psi)
0	P-110, 98	29,789	0
4,000	L-80, 98	16,078	- 2,496
4,000	P-110, 85	19,158	- 2,496
6,400	P-110, 85	10,794	- 3,994
6,400	P-110, 98	8,622	- 3,994
10,000	P-110, 98	- 3,718	- 6,240
11,100	P-110, 98	- 7,489	- 7,489

An Example of Calculations in Preparing Table 3.19:

Average of radial and tangential stresses (item 6) at any depth x is given by:

$$\left(\frac{\sigma_r + \sigma_t}{2}\right)_x = \frac{A_i\,G_{p_i}\,x - A_o\,G_{p_o}\,x}{A_{sx}}$$

$$\left(\frac{\sigma_r + \sigma_t}{2}\right)_{4,000} = \frac{(111.91 \times 12 - 140.5 \times 12) \times 0.052 \times 4,000}{28.59}$$
$$= -2,496 \text{ psi}$$

The values of axial and average of radial and tangential stresses are plotted in Fig. 3.11 (page 159). From the plot it is evident that the line of axial stress and the average of radial and tangential stresses intersect at the casing shoe, indicating that the casing is not liable to buckle during landing and cementing operations.

Equally important is to check whether the pipe is liable to buckle during the drilling of the next interval. The specific weight of the fluid used to drill the next interval is 17.9 ppg and the annular fluid is again assumed to be saturated salt water (8.94 ppg). Consider also that the pipe is subjected to an average increase in temperature of 90°F and that in calculating the values of axial stress due to the change in fluid densities, the effect of surface pressure is ignored. Table 3.20 summarises the results.

Table 3.20: Stresses in the intermediate casing during the drilling of the next section of borehole.

Depth (ft)	Grade and Weight (lb/ft)	(1) $\Delta\sigma_{aw}$ (psi)	(2) $\Delta\sigma_{ap}$ (psi)	(3) $\sigma_{aw_2} = \sigma_{aw_1} + \Delta\sigma_{aw}$ (psi)	(4) $\sigma_{ap_2} = \sigma_{ap_1} + \Delta\sigma_{ap}$ (psi)
10,000	P-110, 98	5,552	0	1,834	0
6,400	P-110, 98	3,553	0	12,175	0
6,400	P-110, 85	4,260	338	14,398	1,026
4,000	P-110, 85	2,663	338	21,165	1,026
4,000	L-80, 98	2,221	158	17,992	479
0	P-110, 98	0	158	29,483	479

Examples of Calculations in Preparing Table 3.20:

Change in pipe weight (item 1), $\Delta\sigma_{aw}$, due to the change in fluid densities, at 6,400 ft (P-110, 85) is as follows:

$$\Delta\sigma_{aw} = \frac{\nu\, x\, (A_i \Delta G_{p_i} - A_o \Delta G_{p_o})}{A_{sx}}$$
$$= \frac{0.28 \times 6,400 \times 0.052\,[116.11 \times 5.9 - (-3.05) \times 140.5]}{24.39}$$
$$= 4,260 \text{ psi}$$

Change in piston effect (item 2), $\Delta\sigma_{ap}$, due to the change in fluid densities, at 6,400 ft (P-110, 85) is:

$$\begin{aligned}\Delta\sigma_{ap} &= \frac{x\Delta G_{p_i}\left(A_{up_1} - A_{low_1}\right)}{A_s} \\ &= \frac{6,400 \times 0.052 \times 5.9 \times 4.2}{24.37} \\ &= 338\,\text{psi}\end{aligned}$$

In Table 3.21, the values of the total axial stress and the average of radial and tangential stresses are presented.

Table 3.21: Stresses in intermediate casing during drilling of next section of borehole.

Depth (ft)	Grade and Weight (lb/ft)	(5) σ_{aT} (psi)	(6) σ_{aw_2} (psi)	(7) σ_{ap_2} (psi)	(8) σ_a (5) + (6) + (7) (psi)	(9) $(\sigma_r + \sigma_t)/2$ (psi)
0	P-110, 98	- 18,630	29,483	479	11,332	0
4,000	L-80, 98	- 18,630	17,992	479	- 159	5,436
4,000	P-110, 85	- 18,630	21,165	1,026	3,562	7,014
6,400	P-110, 85	- 18,630	14,398	1,026	- 3,206	11,222
6,400	P-110, 98	- 18,630	12,117	0	- 6,453	8,698
10,000	P-110, 98	- 18,630	1,835	0	- 16,795	13,590

Examples of Calculations in Preparing Table 3.21:

Change in axial stress (item 5), σ_{aT}, due to the increase in average temperature (90°F), is given by:

$$\begin{aligned}\sigma_{aT} &= -E\Upsilon\Delta T \\ &= -30 \times 10^6 \times 6.9 \times 10^{-6} \times 90 \\ &= -18,630\,\text{psi}\end{aligned}$$

Average of radial and tangential stresses (item 9), at 10,000 ft (P-110, 98) is:

$$\begin{aligned}\left(\frac{\sigma_r + \sigma_t}{2}\right) &= \frac{\left(A_i G_{p_i} - A_o G_{p_o}\right) x}{A_{sx}} \\ &= \frac{(111.91 \times 17.9 - 140.5 \times 8.94) \times 0.052 \times 10,000}{28.59} \\ &= 13,590\ \text{psi}\end{aligned}$$

Values of axial, radial, and tangential stresses are plotted in Fig. 3.11. From the plot it is evident that the lines of axial stress and the average of radial and tangential stresses intersect at a depth of 2,650 ft. This means that below this

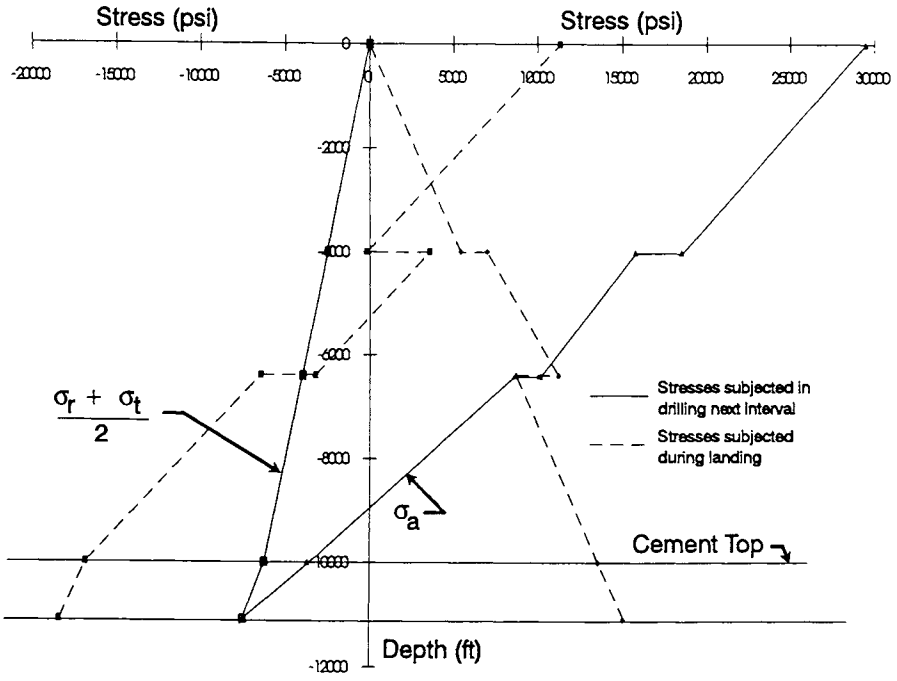

Fig. 3.11: Axial and average of radial and tangential stresses along the length of the pipe.

depth the pipe is liable to buckle and it should, therefore, be cemented up to a depth of 2,650 ft from the surface.

The presence of buckling force does not necessarily mean that the casing will buckle. For buckling to occur, the existing buckling force must exceed the critical buckling force for the casing string. The existing buckling force is:

$$\begin{aligned} F_{buc} &= A_s \left[\left(\frac{\sigma_r + \sigma_t}{2} \right) - \sigma_a \right] \\ &= 28.59\,[13,590 - (-16,795)] \\ &= 868,637 \text{ lbf} \end{aligned}$$

According to Lubinski (1951), the critical buckling force on the intermediate casing can be determined as follows:

$$F_{buc_{cr}} = 3.5\,[EI(W_n BF)^2\,]^{1/3}$$

where:

$$I = \frac{1}{64}\,\pi\,(d_2^4 - d_1^4)$$

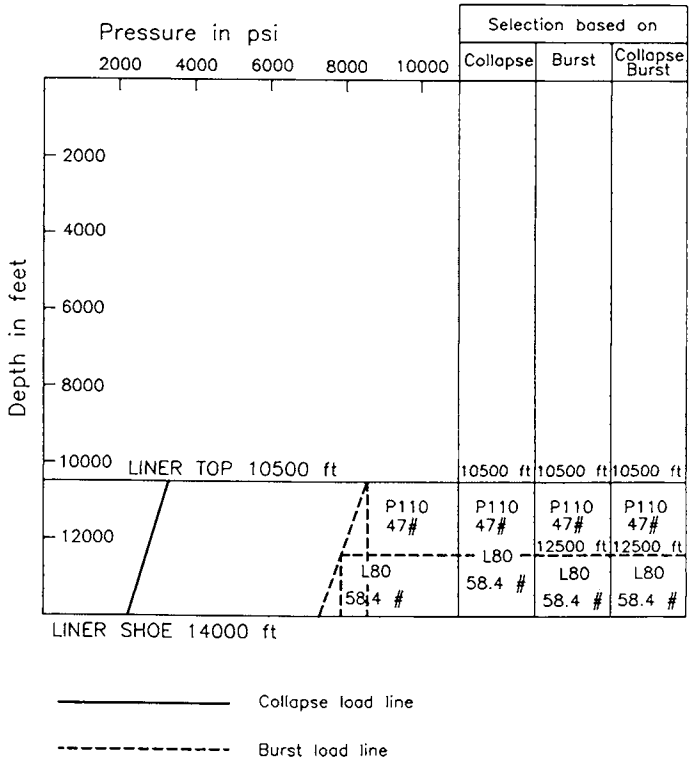

Fig. 3.12: Selection of casing grades and weight based on the collapse and burst loads for liner.

$$= \frac{1}{64}\pi\,(13.375^4 - 11.937^4)$$
$$= 573.97 \text{ in.}^4$$

W_nBF is the buoyant weight/ft and can be calculated as follows:

$$W_nBF = \frac{W_a - (p_oA_o - p_iA_i)\,x}{x}$$
$$= \frac{94,880 - 10,000 \times 0.052\,(140.5 \times 8.94 - 111.91 \times 17.9)}{10.000}$$
$$= 134.7\,\text{lb/ft}$$

Hence,

$$F_{buc_{cr}} = 3.5\,[30 \times 10^6 \times 573.97 \times (134.7)^2\,]^{1/3}$$
$$= 237,482 \text{ lbf}$$

or,

$$\sigma_{buc_{cr}} = \frac{237,482}{28.59} = 8,307 \text{ psi}$$

Thus, the pipe experiences a buckling force which is 3.7 times greater than its critical value.

Figure 3.11 shows that the critical buckling force occurs at about 5,000 ft from the surface and, therefore, the pipe should be cemented to this depth to prevent any permanent deformation that may result due to the buckling.

3.3.3 Drilling Liner ($9\frac{5}{8}$-in. pipe)

Drilling liner is set between 10,500 ft and 14,000 ft with an overlap of 600 ft between $13\frac{3}{8}$ in casing and $9\frac{5}{8}$ in liner. The liner is cemented from the bottom to the top. Design loads for collapse and burst are calculated using the same assumptions as for the intermediate casing (refer to Fig. 3.8). The effect of biaxial load on collapse and design requirement for buckling are ignored.

Collapse

Collapse pressure at 10,500 ft = external pressure – internal pressure

External pressure at 10,500 ft = $Gp_{m_2} \times 10,500$ ft
= $12 \times 0.052 \times 10,500 = 6,552$ ft

Internal pressure at 10,500 ft = $Gp_{m_1} \times$ fluid column height (Fig. 3.8)
= $17.9 \times 0.052 \times (10,500 - 7,006)$
= 3,252 psi

Collapse pressure at 10,500 ft = 6,552 – 3,252
= 3,300 psi

Collapse pressure at 14,000 ft = external pressure – internal pressure

External pressure at 14,000 ft = $12 \times 0.052 \times 14,000$
= 8,736 psi

Internal pressure at 14,000 ft = $17.9 \times 0.052 \times 6,994$
= 6,510 psi

Collapse pressure at 14,000 ft = 8,736 – 6,510
= 2,226 psi

Table 3.22: Collapse resistance of grades suitable for drilling liner.

Grade	Weight (lb/ft)	Coupling	Collapse resistance (psi)	
			$SF = 1$	$SF = 0.85$
P-110	47	LTC	5,310	6,247
L-80	58.4	LTC	7,890	9,282

In Fig. 3.12 the collapse line is constructed between 3,300 psi at 10,500 ft and 2,226 psi at 14,000 ft. The collapse resistances of suitable steel grades from Table 3.3 are given in Table 3.22. Notice that both P-110 (47 lb/ft) and L-80 (58.4 lb/ft) grades satisfy the requirement for collapse load design.

Burst

Burst pressure at 10,500 ft (Fig. 3.8)

$$= \text{internal pressure - external pressure}$$

Internal pressure at 10,500 ft $=$ surface pressure + hydrostatic pressure of drilling fluid column + hydrostatic pressure of the gas column

$$= 5{,}000 + 8{,}901.6 \times 17.9 \times 0.052 + (10{,}500 - 8{,}901.6) \times 0.1$$
$$= 13{,}445 \text{ psi}$$

External pressure at 10,500 ft $=$ hydrostatic head of the salt water column
$$= 0.465 \times 10{,}500$$
$$= 4{,}882.5 \text{ psi}$$

Burst pressure at 10,500 ft $= 13{,}445.44 - 4{,}882.5$
$$= 8{,}563 \text{ psi}$$

Burst pressure at 14,000 ft $=$ injection pressure at 14.000 ft - saturated salt water column
$$= 13{,}788.32 - 0.465 \times 14{,}000$$
$$= 7{,}278 \text{ psi}$$

In Fig. 3.12, the burst pressure line is constructed between 8,563 psi at 10,500 ft and 7,278 psi at 14,000 ft. The burst resistances of the suitable grades from Table 3.3 are shown in Table 3.23. The burst resistances of these grades are also plotted in Fig. 3-12 as vertical lines and those grades that satisfy both burst and

Table 3.23: Burst resistances of grades suitable for drilling liner.

Grade	Weight (lb/ft)	Coupling	Burst resistance (psi)	
			$SF = 1$	$SF = 1.1$
L-80	54.4	LTC	8,650	7,864
P-110	47	LTC	9,440	8,581

collapse design requirements are given in Table 3.24.

Tension

Suitability of the selected grade for tension is checked by considering cumulative buoyant weight, shock load, and pressure testing. The results are summarized in Table 3.25.

Final Selection

From Table 3.25 it follows that L-80 (58.4 lb/ft) and P-110 (47 lb/ft) satisfy the requirement for tension due to buoyant weight and shock load. Inasmuch as the safety factor is double the required margin, it is not necessary to check for pressure testing.

3.3.4 Production Casing (7-in. pipe)

Production casing is set to a depth of 19,000 ft and partially cemented at the casing seat. The design load calculations for collapse and burst are presented in Fig. 3.13.

Collapse

The collapse design is based on the premise that the well is in its last phase of production and the reservoir has been depleted to a very low abandonment

Table 3.24: Most economical drilling liner based on collapse and burst loads.

Section	Depth (ft)	Grade and Weight (lb/ft)	Length (ft)
1	10,500 - 12,500	P-110, 47	2,000
2	12,500 - 14,000	L-80, 58	1,500

Table 3.25: Total tensile loads on drilling liner.

(1) Depth (ft)	(2) Grade and Weight (lb/ft)	(3) Buoyant weight of section joint (1,000 lbf) (1) × W_n × BF $BF = 0.743$	(4) Cumulative buoyant weight carried by the top joint (1,000 lbf)
14,000 – 12,500	L-80, 58.4	65.105	65.105
12,500 – 10,500	P-110, 47	69.861	134.966

(5) Shock load carried by each section (1,000 lbf) (3,200 W_n)	(6) Total tension (1,000 lbf) (4) + (5)	(7) $SF = \frac{Y_p}{\text{Total tension}}$
186.88	251.985	1,151/251.985 = 4.57
150.40	285.366	1,213/285.366 = 4.25

pressure (Bourgoyne et al., 1985). During this phase of production, any leak in the tubing may lead to a partial or complete loss of packer fluid from the annulus between the tubing and the casing. Thus, for the purpose of collapse design the following assumptions are made:

1. Casing is considered empty.

2. Fluid specific weight outside the pipe is the specific weight of the drilling fluid inside the well when the pipe was run.

3. Beneficial effect of cement is ignored.

Based on the above assumptions, the design load for collapse can be calculated as follows:

Collapse pressure at surface = 0 psi

Collapse pressure at casing seat

= external pressure – internal pressure

= 17.9 × 0.052 × 14,000 – 0

= 13,031 psi

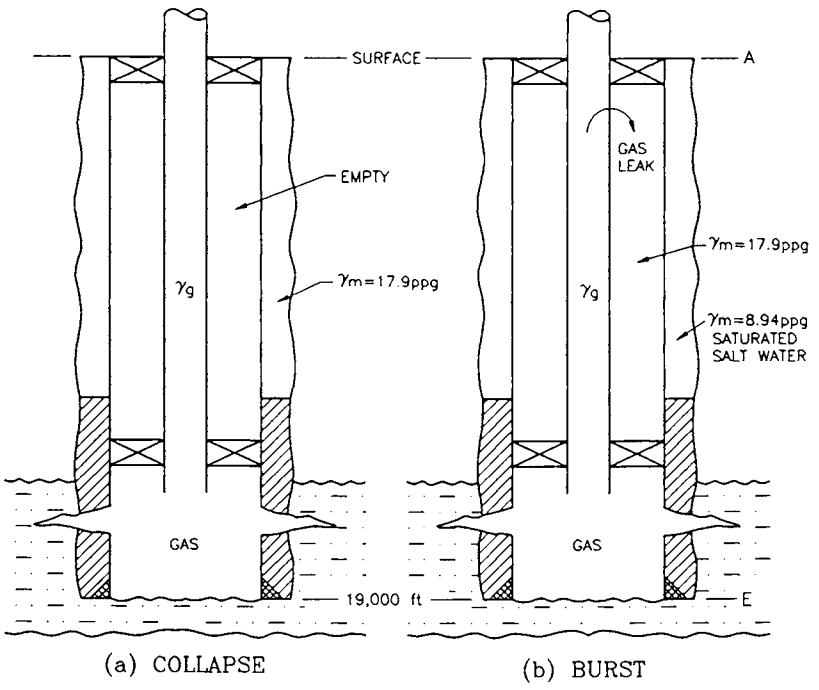

Fig. 3.13: Collapse and burst loads on the production casing.

In Fig. 3.13, the collapse line is constructed between 0 psi at the surface and 13,031 psi at 19,000 ft. Collapse resistance of the suitable grades from Table 3.3 are presented in Table 3.26 and all these grades satisfy the requirement for maximum collapse design load.

Table 3.26: Collapse resistance of grades suitable for production casing.

Grade	Weight (lb/ft)	Coupling	Collapse resistance (psi)	
			$SF = 1$	$SF = 0.85$
V-150	38	PTC	19,240	22,635
V-150	41	PTC	22,810	26,835
V-150	46	PTC	25,970	30,552
SOO-155	46	PTC	26,830	31,564

Burst

In most cases, production of hydrocarbons is via tubing sealed by a packer, as shown in Fig. 3.13. Under ideal conditions, only the casing section above the shoe will be subjected to burst pressure. The production casing, however, must

be able to withstand the burst pressure if the production tubing fails. Thus, the design load for burst should be based on the worst possible scenario.

For the purpose of the design of burst load the following assumptions are made:

1. Producing well has a bottomhole pressure equal to the formation pore pressure and the producing fluid is gas.

2. Production tubing leaks gas.

3. Specific weight of the fluid inside the annulus between the tubing and casing is that of the drilling fluid inside the well when the pipe was run.

4. Specific weight of the fluid outside the casing is that of the deteriorated drilling fluid, i.e., the specific weight of saturated salt water.

Based on the above assumptions, the design for burst load proceeds as follows:

Burst load at surface = internal pressure − external pressure

Internal pressure at surface = shut-in bottomhole pressure − hydrostatic head of the gas column
= 17.45 × 0.052 × 19,000 − 0.1 × 19,000
= 15,340.6 psi

Burst pressure at surface = 15,340.6 − 0
= 15,340.6 psi

Burst pressure at casing shoe = internal pressure − external pressure

Internal pressure at casing shoe = hydrostatic pressure of the fluid column + surface pressure due to gas leak at top of tubing
= 17.9 × 0.052 × 19,000 + 15,340.6
= 33,025.8 psi

External pressure at shoe = 0.465 × 19,000
= 8,835 psi

Burst pressure at casing shoe = 33,025.8 − 8,835
= 24,190.8 psi

In Fig. 3.13, the burst line is drawn between 15,350.6 psi at the surface and 24,190.8 psi at 19,000 ft. The burst resistances of the suitable grades from Table 3.3 are shown in Table 3.27 and are plotted as vertical lines in Fig 3.14.

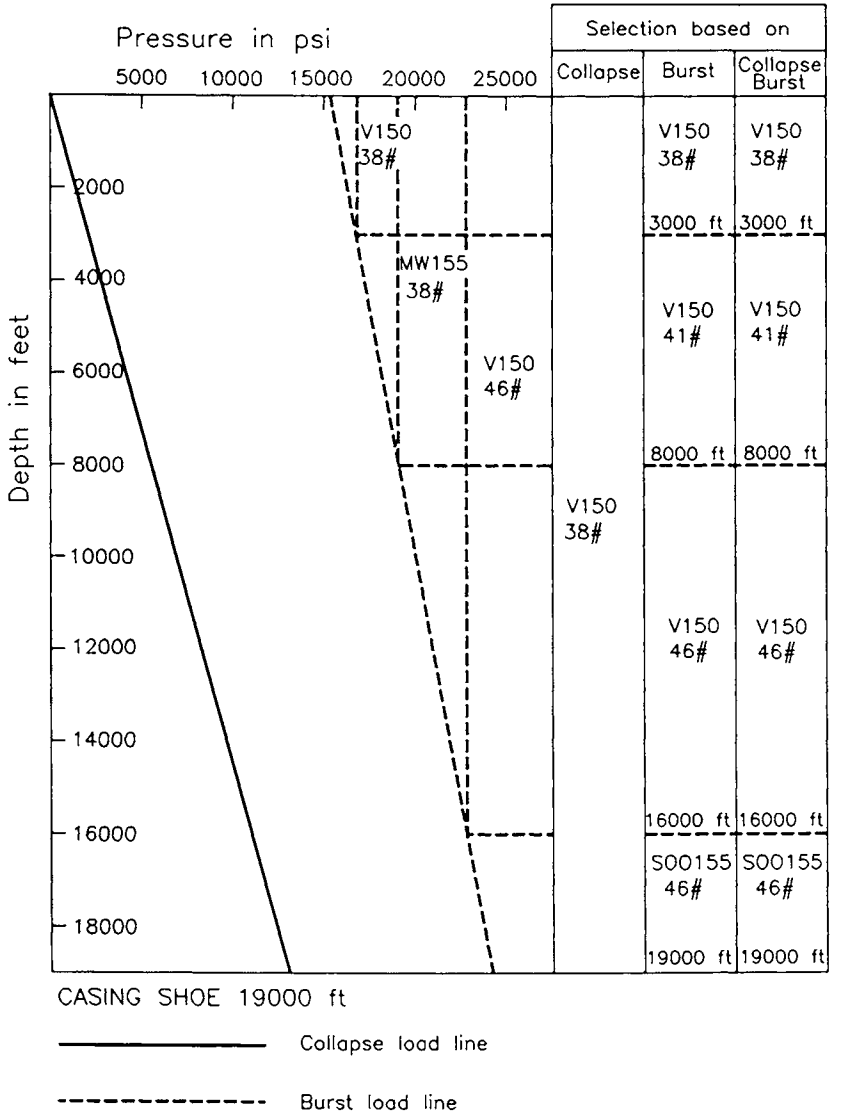

Fig. 3.14: Selection of casing grades and weights based on the collapse and burst loads for the production casing.

Table 3.27: Burst resistance of grades suitable for production casing.

Grade	Weight (lb/ft)	Coupling	Burst resistance (psi)	
			$SF = 1$	$SF = 1.1$
V-150	38	PTC	18,900	17,182
MW-155	38	Extreme-line	20,930	19,028
V-150	46	PTC	25,070	22,790
SOO-155	46	PTC	25,910	23,550

Selection based on collapse and burst

From Fig. 3.14, it is evident that grade SOO-155, which has the highest burst resistance properties, satisfies the design requirement up to 17,200 ft. It will also satisfy the design requirement up to 16,000 ft if the safety factor is ignored. Thus, grade SOO-155 can be safely used only if it satisfies the other design requirements. The top of cement must also reach a depth of 17,200 ft to provide additional strength to this pipe section. Hence, the selection based on collapse and burst is shown in Table 3.28.

Table 3.28: Most economical production casing based on collapse and burst loads.

Section	Depth (ft)	Grade and Weight (lb/ft)	Coupling	Length (ft)
1	0 - 3,000	V-150, 38	PTC	3,000
2	3,000 - 8,000	MW-155, 38	Extreme-line	5,000
3	8,000 - 16,000	V-150, 46	PTC	8,000
4	16,000 - 19,000	SOO-155, 46	PTC	3,000

Tension

The suitability of the selected grades under tension is checked by considering cumulative buoyant weight, shock load, and pressure testing. Thus, starting from the bottom, Table 3.29 is produced which shows that all the sections satisfy the requirement for tensional load based on buoyant weight and shock load.

Pressure Testing

Grade V-150 (38 lb/ft) has the lowest safety factor and should, therefore, be checked for pressure testing. Tensional load carried by this section due to the

Table 3.29: Total tensile loads on production casing.

(1) Depth (ft)	(2) Grade and Weight (lb/ft)	(3) Buoyant weight of each section joint (1.000 lbf) (1) $\times W_n \times BF$ $BF = 0.726$	(4) Cumulative buoyant weight carried by the top joint (1,000 lbf)
19,000 – 16,000	SOO-155, 46	100.25	100.25
16,000 – 8,000	V-150, 46	267.34	367.59
8,000 – 3,000	MW-155, 38	138.03	505.62
3,000 – 0	V-150, 38	82.82	588.43

(5) Shock load carried by each joint (1,000 lbf) $3{,}200 \times W_n$	(6) Total load carried by the top joint (1,000 lbf)	(7) $SF = \frac{Y_p}{\text{Total load}}$
147.20	247.51	1,344/247.51 = 5.43
147.20	514.79	1,344/514.79 = 2.61
121.60	627.21	1,592/627.21 = 2.56
121.60	710.03	1,430/710.03 = 2.01

pressure testing is equal to:

$$\begin{aligned} F_t &= 18{,}900 \times 0.6 \times A_s \, (A_s = 10.95) \\ &= 124{,}173 \text{ lbf} \end{aligned}$$

Total tension load carried by V-150 (38 lb/ft)

$$\begin{aligned} &= \text{buoyant weight carried by the top joint} \\ &= + \text{ tensional load due to the pressure testing} \\ &= 588{,}430 + 124{,}173 \\ &= 712{,}603 \text{ lbf} \end{aligned}$$

$$SF = \left(\frac{Y_p}{\text{Total load}}\right) = \frac{1{,}430{,}000}{712{,}603} = 2.01$$

Inasmuch as this value is greater than the design safety factor of 1.8, grade V-150 (38 lb/ft) satisfies tensional load requirements.

Biaxial Effect

Axial tension reduces the collapse resistance and is most critical at the joint of the weakest grade. All the grades selected for production casing have significantly higher collapse resistance than required. Casing sections from the intermediate position, however, can be checked for reduced collapse resistance (V-150, 46 lb/ft) at 8,000 ft.

As illustrated previously, the modified collapse resistance of grade V-150 (46 lb/ft) under an axial load of 367,356 lbf can be calculated to be 23,250 psi. Hence,

$$\begin{aligned} SF \text{ for collapse} &= \frac{\text{Reduced collapse resistance}}{\text{Collapse pressure at 8,000 ft}} \\ &= \frac{23,250}{5,600} \\ &= 4.15 \end{aligned}$$

Final Selection

The final selection is summarized in Table 3.30.

Table 3.30: Final casing selection for production casing string.

Depth (ft)	Grade and Weight (lb/ft)	Coupling
0 - 3,000	V-150, 38	PTC
3,000 - 8,000	MW-155, 38	Extreme-line
8,000 - 16,000	V-150, 46	PTC
16,000 - 19,000	SOO-155, 46	PTC

Buckling

Usually, buckling is prevented by cementing up to the neutral point where no potential buckling exists. As discussed previously (p.116), the depth of the neutral point, x, can be determined by using the following equation:

$$x = \frac{D(W_n - A_o G_{p_{cm}} + A_i G_{p_i}) + (1-2\nu)(A_o \Delta p_{s_o} - A_i \Delta p_{s_i})}{W_n - (A_o G_{p_o} - A_i G_{p_i})} \quad \text{continue} \rightarrow$$

$$\rightarrow \quad \frac{+ (A_{up_1} - A_{low_1}) \times [\, D_{\Delta A_s}(G_{p_i} + \Delta G_{p_i}) + \Delta p_{s_1}] - A_s E \Upsilon T + F_{as}}{-(1-\nu)(A_o \Delta G_{p_o} - A_i \Delta G_{p_i}) + A_o(G_{p_o} - G_{p_{cm}})}$$

where:

$$
\begin{aligned}
W_n &= \text{average weight} \\
&= \frac{(W_{n_1} \times l_1) + (W_{n_2} \times l_2)}{D} \\
&= \frac{38 \times 8,000 + 46 \times 11,000}{19,000} \\
&= 42.63 \text{ lb/ft}
\end{aligned}
$$

$$
\begin{aligned}
A_i &= \text{average internal area of the pipe} \\
&= \frac{(A_i)_1 \times l_1 + (A_i)_2 \times l_2}{D} \\
&= \frac{27.51 \times 8,000 + 25.14 \times 11,000}{19,000} \\
&= 26.16 \text{ in.}^2
\end{aligned}
$$

$$
\begin{aligned}
A_s &= \text{average cross-sectional area of the steel} \\
&= \frac{A_{s_1} \times l_1 + A_{s_2} \times l_2}{D} \\
&= \frac{10.95 \times 8,000 + 13.32 \times 11,000}{19,000} \\
&= 12.33 \text{ in.}^2 \\
\gamma_i &= \gamma_o = 17.9 \text{ ppg} \\
\Delta\gamma_i &= \Delta\gamma_o = 0 \text{ ppg} \\
\Delta G_{p_i} &= \Delta G_{p_o} = 0 \text{ psi/ft} \\
\Delta p_{si} &= \Delta p_{so} = 0 \text{ psi}
\end{aligned}
$$

$$
\begin{aligned}
(A_{up_1} - A_{low_1}) &= \text{average change in internal diameter} \\
&= 27.53 - 26.16 \\
&= 2.37 \text{ in.}^2
\end{aligned}
$$

It is also assumed that γ_{cm}[a] = 18.5 ppg, $\Delta T = 45°\text{F}$ and $F_{as} = 0$. Hence (see Eq. 2.212):

$$
\begin{aligned}
D_{TOC} &= \frac{19,000\,(42.63 - 38.46 \times 18.5 \times 0.052 + 26.14 \times 0.931) + 0}{42.63 - (38.46 \times 17.9 \times 0.052)} \rightarrow \text{continue} \\
&\rightarrow \frac{+2.37 \times 8,000 \times 0.931 - 12.32 \times 6.9 \times 10^{-6} \times 30 \times 10^{6} \times 45 + 0}{+26.14 \times 17.9 \times 0.052 - 0 + 38.46(0.931 - 0.962)}
\end{aligned}
$$

[a] γ_{cm} is the specific weight of the cement slurry, lb/gal.

$$= \frac{472,280}{29.42}$$
$$= 16,053 \text{ ft.}$$

Thus, the casing between 16,053 ft and 19,000 ft is under compressive load and is liable to buckle. To prevent buckling of the pipe it must be cemented to 16,053 ft from the surface.

Alternatively, an overpull, F_{as}, equal in magnitude to the difference between the axial stress and the average of radial and tangential stresses can be applied at the surface after landing of the pipe. If, for example, the maximal depth of the cement top is set at 18,000 ft, the magnitude of the over-pull required to prevent buckling of the pipe can be obtained as follows:

$$18,000 = \frac{472,280 + F_{as}}{29.42}$$

and solving for F_{as}:

$$F_{as} = 57,280 \text{ lbf}$$

3.3.5 Conductor Pipe (26-in. pipe)

Conductor pipe is set to a depth of 350 ft and cemented back to the surface. In addition to the principal loads of collapse, burst, and tension, it is also subjected to a compression load, because it carries the weight of the other pipes. Thus, the conductor pipe must be checked for compression load as well.

Collapse

In the design of collapse load, the following assumptions are made (refer to Fig. 3.15):

1. Complete loss of fluid inside the pipe.
2. Specific weight of the fluid outside the pipe is that of the drilling fluid in the well when the pipe was run.

Collapse pressure at the surface = 0

Collapse pressure at the casing shoe = $9.5 \times 0.052 \times 320 - 0$
= 158 psi

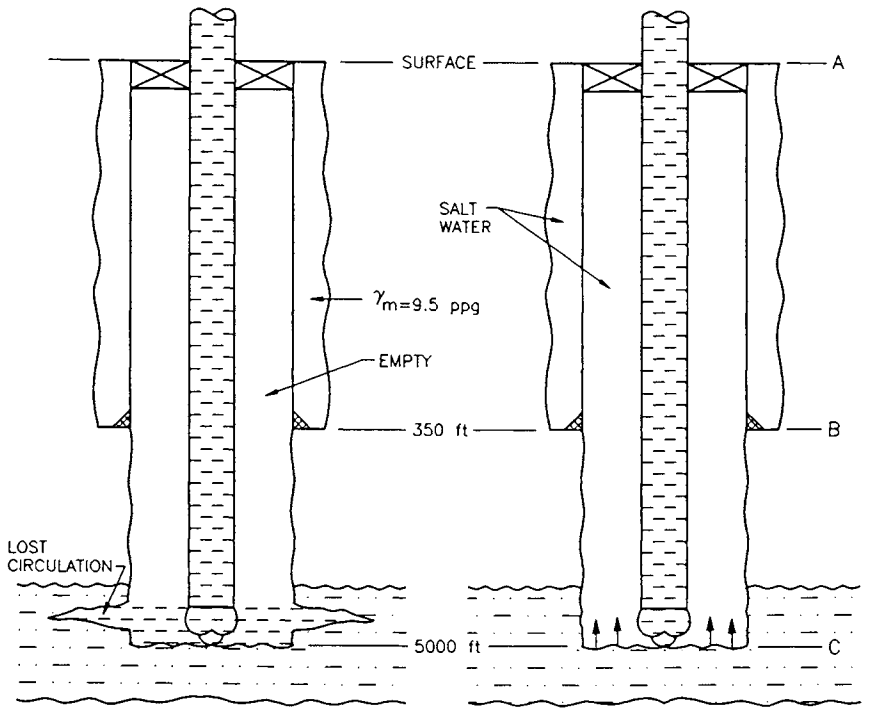

Fig. 3.15: Collapse and burst loads on conductor.

Burst

In calculating the burst load, it is assumed that no gas exists at shallow depths and a saturated salt water kick is encountered in drilling the next interval. Hence, in calculating the burst pressure, the following assumptions are made (refer to Fig. 3.13):

1. Casing is filled with saturated salt water.

2. Saturated salt water is present outside the casing.

Burst pressure at casing shoe = internal pressure − external pressure

Internal pressure at casing shoe = formation pressure at 5,000 ft
− hydrostatic pressure due to the salt water between 350 and 5,000 ft
= $0.465 \times 5{,}000 - [(5{,}000 - 350) \times 0.465]$
= 162.75 psi

$$\begin{aligned}\text{Burst pressure at casing shoe} &= 162.75 - 0.465 \times 350\\ &= 0 \text{ psi}\end{aligned}$$

$$\begin{aligned}\text{Burst pressure at surface} &= \text{formation pressure at 5,000 ft}\\ &\quad - \text{hydrostatic pressure at the}\\ &\quad \text{fluid column} - \text{external pressure}\\ &= 5.000\ (0.465 - 0.465) - 0\\ &= 0 \text{ psi}\end{aligned}$$

Selection based on collapse and burst

As shown in Table 3.3, both available grades have collapse and burst resistance values well in excess of those calculated above. Conductor pipe will, however, be subjected to a compression load resulting from the weight of casing-head housing and subsequent casing strings. Taking this factor into consideration, grade K-55 (133 lb/ft) with regular buttress coupling can be selected.

Compression

In checking for compression load, it is assumed that the tensile strength is equal to the compressive strength of casing. A safety factor of greater than 1.1 is desired.

Compressive load carried by the conductor pipe is equal to the total buoyant weight, W_{bu}, of the subsequent casing strings.

$$\begin{aligned}\text{Compressive load} &= W_{bu} \text{ of surface pipe}\\ &\quad + W_{bu} \text{ of intermediate pipe} + W_{bu} \text{ of liner}\\ &\quad + W_{bu} \text{ of production pipe}\\ &= 390.093 + 863.242 + 134.928 + 588,430\\ &= 1,976,990 \text{ lbf}\end{aligned}$$

$$\begin{aligned}\text{Safety Factor, } SF &= \frac{Y_p \text{ of K-55 (133 lb/ft)}}{\text{Total buoyant weight}}\\ &= \frac{2,125,000}{1,976,990} = 1.08\end{aligned}$$

This suggests that the steel grade K-55, 133 satisfies the requirement for compression load.

3.4 SUPPLEMENTARY EXERCISES

(1) A $13\frac{3}{8}$-in. surface casing to be set to a depth of 6,000 ft. The mud weight is 9.2 ppg, the expected formation pore pressure is 0.465 psi/ft and a bottomhole pressure of 4,600 psi is expected when drilling the next hole section. The design factors to be satisfied are: 1 for collapse, 1.2 for internal yield and 1.8 for tensile strength. Assume that all API J, K, L and P grades are available. Design this pipe for the worst possible loading conditions.

(2) Design a $9\frac{5}{8}$-in. intermediate casing to be set to a depth of 10,500 ft. The mud weight and expected formation pressure are respectively: 9.8 ppg and 0.48 psi/ft. A bottomhole pressure of 7,570 psi is expected when drilling the next hole section (production pipe). Assume that all API K, L, N, C and P grades are available. Satisfy the same design factors used in Problem 1.

(3) Design a 7-in. production casing to be set to a depth of 13,500 ft. The expected mud weight and pore pressure are respectively: 11.5 ppg and 0.57 psi/ft. Assume a gas leak at the tubing hanger and satisfy the same design factors as in Problems 1 and 2. All API J,C,L,P and N grades are available.

(4) A 20-in. conductor pipe is to be set to a depth of 500 ft. Check the compressional load on this pipe if it is to support the strings designed in Problems 1, 2 and 3.

(5) The pore pressure and fracture gradient data shown in Table 3.31 is for a typical well. Develop a mud and casing program for this well and design individual casings based, in each case, on the assumption of worst possible loading conditions. Design factors for collapse, burst and tension are: 1.1, 1.2 and 1.8. All API casing grades are available.

Table 3.31: Data for Question (5).

Depth (ft)	Pore Pressure (ppg)	Fracture Pressure (ppg)	Depth (ft)	Pore Pressure (ppg)	Fracture Pressure (ppg)
0 - 1,000	8.9	12.0	6,000 - 8,000	9.3	15.5
1,000 - 2,000	8.9	12.5	8,000 - 10,000	11.4	16.3
2,000 - 4,000	8.9	13.8	10,000 - 12,000	13.5	17.0
4,000 - 6,000	8.9	14.5	12,000 - 14,000	14.3	17.5

3.5 REFERENCES

Adams, N.J., 1985. *Drilling Engineering - A Complete Well Planning Approach.* Penn Well Books, Tulsa, OK, USA, pp. 117–149.

Bourgoyne, A.T., Jr., Chenevert, M.E., Millheim, K.K. and Young F.S., Jr., 1985. *Applied Drilling Engineering.* SPE Textbook Series, 2: 330–350.

Evans, G.W. and Harriman, D.W., 1972. *Laboratory Tests on Collapse Resistance of Cemented Casing.* 47th Annual Meeting SPE of AIME, San Antonio, TX, Oct. 8–11, SPE Paper No. 4088, 6 pp.

Goins, W.C., Jr., 1965,1966. A new approach to tubular string design. *World Oil*, 161(6, 7)[a]: 135–140, 83–88; 162(1.2): 79–84, 51–56.

Lubinski, A., 1951. Influence of tension and compression on straightness and buckling of tubular goods in oil wells. *Trans. ASME*, 31(4): 31–56.

Prentice, C.M., 1970. Maximum load casing design. *J. Petrol. Tech.*, 22(7): 805–810.

Rabia, H., 1987. *Fundamentals of Casing Design.* Graham and Trotman Ltd., London, UK, pp. 48–58, 75–99.

[a]Volume 161, no. 6, pp. 135–140; vol 161, no. 7, pp. 83–88 etc.

Chapter 4

CASING DESIGN FOR SPECIAL APPLICATIONS

Today, the wells drilled by the petroleum and other energy development industries cover a wide range of drilling conditions. Highly deviated and even horizontal wells are being drilled to complete reservoirs which otherwise could not be produced economically. Wells are being drilled and completed in widely disparate environments from below freezing conditions in the permafrost zones of Alaska and Canada, to thermal energy recovery projects up to 500 °F: and steam injection projects between 300 °F and 400 °F, to the extremely high collapse pressure conditions arising from massive salt domes in various parts of the world.

Severe drilling and borehole conditions place additional requirements on casing design. As a result, it is often difficult to meet API requirements for principal design loads such as collapse, burst, and tension. In the following sections the current practices used in designing casing for highly deviated wells and the severe collapse loads that arise from the swelling of salt formations in very deep wells and thermal wells, are reviewed.

4.1 CASING DESIGN IN DEVIATED AND HORIZONTAL WELLS

Calculation of the axial loads is the most challenging part of directional-well casing design. Using the maximum load principle, the concept of the maximum pulling load is applied. This concept is derived from the observation that the greatest value of tensile stress in directional-well casing occurs during the casing running operation. Working the string up generates the highest tensile loading because the friction (drag) generated by the normal force between the casing and the borehole and the friction factor (this last parameter is discussed later in this

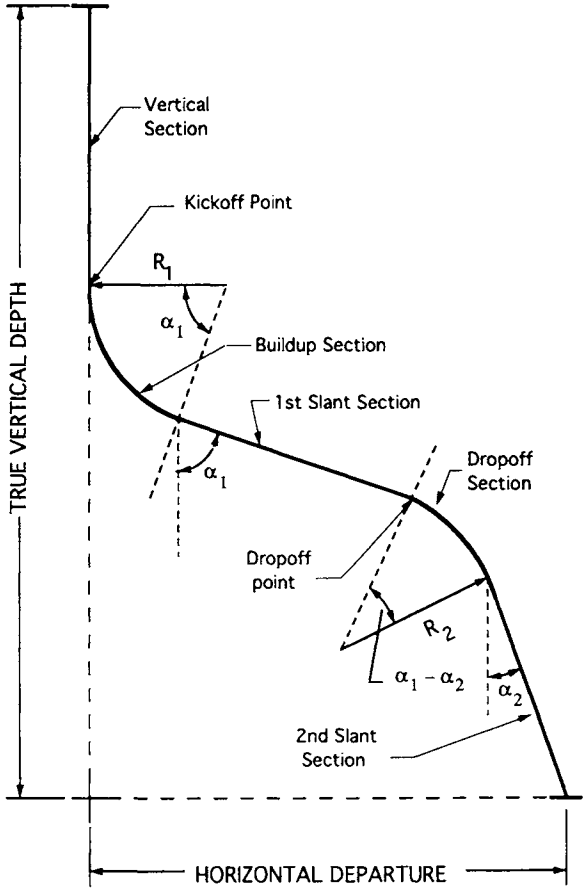

Fig. 4.1: Typical deviated well profile.

chapter) oppose the direction of motion of the string.

The magnitude of the drag force depends on the friction factor and the normal force exerted by the casing. Maximal drag force is usually experienced either when the casing is pulled on after it is stuck in a tight spot or on the upstroke when reciprocating the pipe during cementing operations. In order to determine the drag-associated axial force, one requires an accurate knowledge of well profile, hole geometry and borehole friction factor.

4.1.1 Frictional Drag Force

Drag-associated tensional load can best be determined by calculating drag force on unit sections and summing them up over the entire length of the casing. Inasmuch as the maximal load is experienced while pulling out of the hole, the

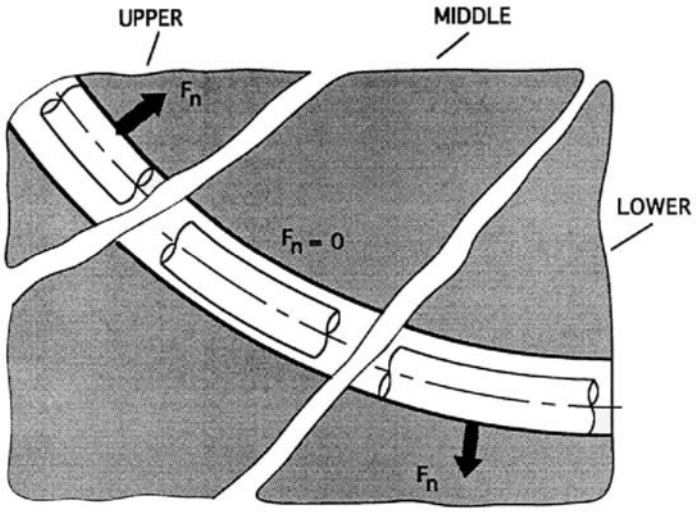

Fig. 4.2: Possible directions of the normal forces in a buildup section. (After Maidla, 1987.)

calculation should proceed from the bottom of the casing in a series of steps. Each step represents the borehole sections of two consecutive stations of the directional survey.

The well profile of a typical deviated hole can be divided into three major sections (Fig. 4.1), namely :

1. Buildup. Inclination increases with increasing depth.
2. Drop-off. Inclination decreases with increasing depth.
3. Slant hole. Inclination remains constant with increasing depth.

4.1.2 Buildup Section

Besides the frictional factor, borehole frictional drag is also controlled by the direction and the normal force. In a buildup section, the three positions of the casing as shown in Fig. 4.2 are possible: uppermost, middle and the lowermost position (Maidla, 1987). The normal and axial forces acting on each unit section are presented in Figs. 4.3 and 4.4. From the free-body diagram, the normal force F_n can be expressed as:

$$F_n = 2 F_a \cos\left(90 - \frac{|\Delta\alpha|}{2}\right)$$

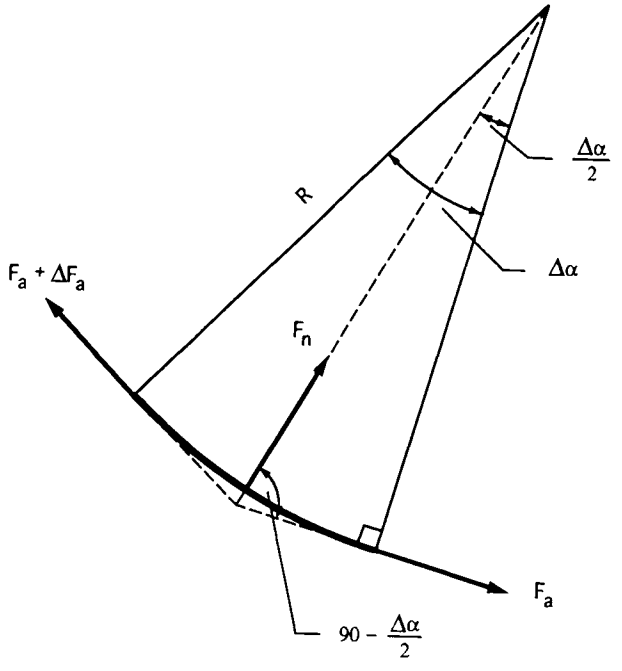

Fig. 4.3: Determination of normal force in buildup section.

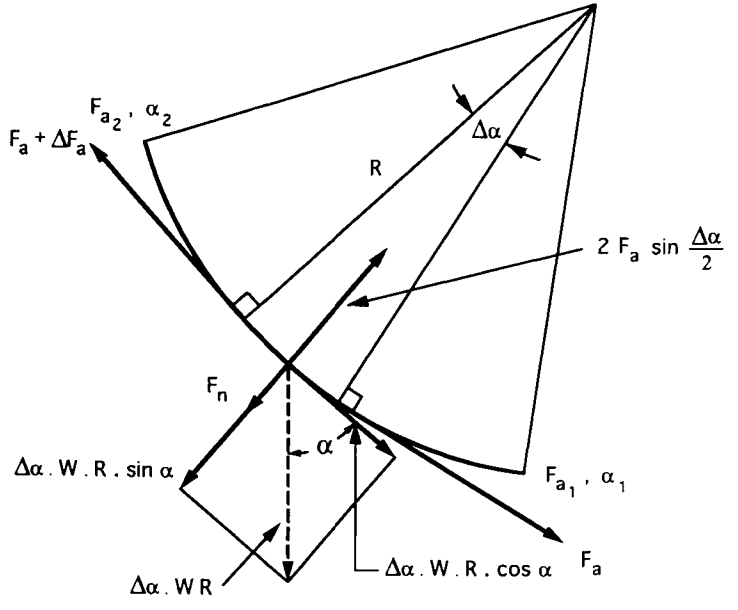

Fig. 4.4: Forces acting on a small element within the buildup section.

$$= 2 \sin\left(\frac{|\Delta\alpha|}{2}\right) \tag{4.1}$$

where:

F_a = axial force on the unit section, lbf.
$\Delta\alpha$ = angle subtended by unit section at radius R.

Inasmuch as $\Delta\alpha/2$ is very small compared to R, $\sin(\Delta\alpha/2) \approx \Delta\alpha/2$. Hence, the Eq. 4.1 yields:

$$F_n = 2 F_a \frac{|\Delta\alpha|}{2} = F_a |\Delta\alpha| \tag{4.2}$$

Considering the buildup section in general, the resultant normal force while pulling out of the hole is the vector sum of the normal components of the weight and the axial force of the unit section (Fig. 4.4). Therefore:

$$\begin{aligned} F_n &= \Delta\alpha W R \sin\alpha - F_a \Delta\alpha \\ &= \Delta\alpha(W R \sin\alpha - F_a) \end{aligned} \tag{4.3}$$

where:

W = weight of the unit section, lb/ft.
= $W_n BF$
R = radius of curvature, ft.

The magnitude of the drag force, F_d, which acts in a direction opposite to pipe movement is given by:

$$F_d = -f_b |F_n| \tag{4.4}$$

or

$$F_d = -f_b |\Delta\alpha W R \sin\alpha - F_a \Delta\alpha| \tag{4.5}$$

where:

f_b = borehole friction factor.
$|F_n|$ = absolute value of the normal force, lbf.

The incremental axial force, ΔF_a ($F_{a_2} - F_{a_1} = \Delta F_a > 0$), over the incremental arc length ($\alpha_2 - \alpha_1 = \Delta\alpha < 0$) when the casing is being pulled (indicated by negative $\Delta\alpha W R \cos\alpha$), is given by:

$$\Delta F_a = |F_d| - \Delta\alpha W R \cos\alpha \tag{4.6}$$

or,

$$\Delta F_a = +f_b \left| \Delta\alpha\, WR \sin\alpha - F_a\, \Delta\alpha \right| - \overbrace{\Delta\alpha}^{<0}\, WR\cos\alpha \tag{4.7}$$

Hence, at equilibrium, the following differential equation is obtained:

$$\frac{dF_a}{d\alpha} = -f_b \left| WR\sin\alpha - F_a \right| - WR\cos\alpha \tag{4.8}$$

If the casing is in contact with the upper side of the hole, $(WR\sin\alpha - F_a) < 0$ and, therefore, Eq. 4.8 can be rewritten as:

$$\frac{dF_a}{d\alpha} = -f_b \left(F_a - WR\sin\alpha \right) - WR\cos\alpha \tag{4.9}$$

Rearranging Eq. 4.9, yields:

$$\frac{dF_a}{d\alpha} + f_b\, F_a = WR\left(f_b\, \sin\alpha - \cos\alpha \right) \tag{4.10}$$

The value of F_a in Eq. 4.10 can be found by first considering the homogeneous solution and then the particular solution as follows:

$$F_a = F_{a_{homo}} + F_{a_{part}} \tag{4.11}$$

Considering first the homogeneous solution:

$$\begin{aligned} \frac{dF_a}{d\alpha} &+ f_b\, F_a = 0 \\ \frac{dF_a}{d\alpha} &= -f_b\, F_a \\ \frac{dF_a}{F_a} &= -f_b\, d\alpha \end{aligned} \tag{4.12}$$

Integrating Eq. 4.12, yields:

$$\begin{aligned} \ln F_a &= -f_b\, \Delta\alpha + C \\ F_{a_{homo}} &= C e^{-f_b \alpha} \end{aligned} \tag{4.13}$$

where:

C = constant of integration.

Now, consider the particular solution of the form:

$$F_{a_{part}} = A\cos\alpha + B\sin\alpha \tag{4.14}$$

$$\frac{dF_{a_{part}}}{d\alpha} = -A\sin\alpha + B\cos\alpha \tag{4.15}$$

Substituting Eqs. 4.14 and 4.15 into Eq. 4.10, yields:

$$\begin{aligned} &-A\sin\alpha + B\cos\alpha + f_b A\cos\alpha + f_b B\sin\alpha \\ &\quad = +f_b WR\sin\alpha - WR\cos\alpha \end{aligned} \tag{4.16}$$

Equating for the coefficients, yields:

$$\begin{aligned} -A\sin\alpha + f_b B\sin\alpha &= +f_b WR\sin\alpha \\ -A + f_b B &= +f_b WR \end{aligned} \tag{4.17}$$

$$\begin{aligned} +f_b A\cos\alpha + B\cos\alpha &= -WR\cos\alpha \\ +f_b A + B &= -WR \end{aligned} \tag{4.18}$$

Now solving for A and B using a matrix solution yields:

$$\Delta_1 = \begin{vmatrix} -1 & +f_b \\ +f_b & 1 \end{vmatrix} = -(1 + f_b^2) \tag{4.19}$$

$$\Delta_2 = \begin{vmatrix} f_b WR & f_b \\ -WR & 1 \end{vmatrix} = 2f_b WR \tag{4.20}$$

$$\Delta_3 = \begin{vmatrix} -1 & f_b WR \\ f_b & -WR \end{vmatrix} = WR(1 - f_b^2) \tag{4.21}$$

Hence

$$A = \frac{\Delta_2}{\Delta_1} = -\left[\frac{2f_b WR}{1 + f_b^2}\right] \tag{4.22}$$

$$B = \frac{\Delta_3}{\Delta_1} = -\left[\frac{WR(1 - f_b^2)}{1 + f_b^2}\right] \tag{4.23}$$

Thus, the particular solution for F_a is obtained by substituting Eq. 4.22 and Eq. 4.23 into Eq. 4.14:

$$F_{a_{part}} = -\frac{2 f_b WR}{1 + f_b^2} \cos\alpha - \frac{WR(1 - f_b^2)}{1 + f_b^2} \sin\alpha \tag{4.24}$$

Inasmuch as $F_a = F_{a_{homo}} + F_{a_{part}}$, the expression for F_a is obtained by combining Eqs. 4.13 and 4.24:

$$F_a(\alpha) = C\, e^{-f_b \alpha} - \frac{WR}{1 + f_b^2}\left[2 f_b \cos\alpha + \sin\alpha\,(1 - f_b^2)\right] \tag{4.25}$$

Applying the first boundary condition, $F_a(\alpha_1) = F_{a_1} = \text{constant}$, one obtains:

$$F_{a_1} = C\, e^{-f_b \alpha_1} - \frac{WR}{1 + f_b^2}\left[2 f_b \cos\alpha_1 + \sin\alpha_1\,(1 - f_b^2)\right] \tag{4.26}$$

Solving for C:

$$C = e^{f_b \alpha_1} F_{a_1} + \frac{WR\, e^{f_b \alpha_1}}{1 + f_b^2}\left[2 f_b \cos\alpha_1 + \sin\alpha_1\,(1 - f_b^2)\right] \tag{4.27}$$

Substituting the expression for C into Eq. 4.25:

$$\begin{aligned} F(\alpha) \;=\; & e^{-f_b(\alpha - \alpha_1)} F_{a_1} + \frac{WR\, e^{-f_b(\alpha - \alpha_1)}}{1 + f_b^2}\left[2 f_b \cos\alpha_1 + \sin\alpha_1\,(1 - f_b^2)\right] \\ & - \frac{WR}{1 + f_b^2}\left[2 f_b \cos\alpha + \sin\alpha\,(1 - f_b^2)\right] \end{aligned} \tag{4.28}$$

The second boundary condition is:

$$F_a(\alpha_2) = F_{a_2} = \text{constant}$$

Substituting the second boundary condition into Eq. 4.28, the tensile force at the point of interest (position 2), where $\alpha = \alpha_2$, is obtained:

$$F_{a_2} = e^{-f_b(\alpha_2-\alpha_1)}F_{a_1} + \frac{W\,R\,e^{-f_b(\alpha_2-\alpha_1)}}{1+f_b^2}\left[2f_b\cos\alpha_1 + \sin\alpha_1\,(1-f_b^2)\right] - \frac{WR}{1+f_b^2}\left[2\,f_b\cos\alpha_2 + \sin\alpha_2\,(1-f_b^2)\right] \tag{4.29}$$

Representing $e^{-f_b(\alpha_2-\alpha_1)} = K_B$ for buildup, one obtains the following expression for F_{a_2} in the uppermost section:

$$F_{a_2} = K_B\,F_{a_1} + \frac{WR}{1+f_b^2}\left[(1-f_b^2)\,(K_B\sin\alpha_1 - \sin\alpha_2) + 2\,f_b\,(K_B\cos\alpha_1 - \cos\alpha_2)\right] \tag{4.30}$$

where:

$$R = \frac{l_1 - l_2}{\alpha_1 - \alpha_2} \tag{4.31}$$

l_1 and l_2 are the lengths of pipe in feet and the units of α_1 and α_2 are radians.

Note that the angles α_1 and α_2 are obtained from surveys taken during the drilling of the well and, therefore, it is not true to say that:

$$R = \frac{l_1 - l_2}{\alpha_1 - \alpha_2} = \frac{180}{\pi}\,\frac{1}{\dot{\alpha}}\,\frac{100}{1}$$

Whereas $\dot{\alpha}$ and, therefore, R are constants in the planned well, R is not constant in an actual well.

The additional tension due to frictional drag for both the intermediate and upper sections can be obtained following the same procedure as illustrated for the upper section.

For the intermediate section:

$$F_{a_2} = F_{a_1} + WR\,(\sin\alpha_1 - \sin\alpha_2) \tag{4.32}$$

For the lower section:

$$F_{a_2} = K_B\,F_{a_1} + \frac{WR}{1+f_b^2}\left[(1-f_b^2)\,(K_B\sin\alpha_1 - \sin\alpha_2) - 2\,f_b\,(K_B\cos\alpha_1 - \cos\alpha_2)\right] \tag{4.33}$$

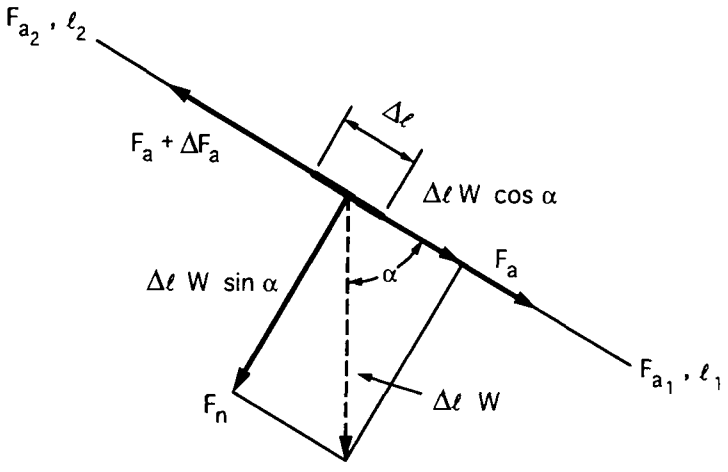

Fig. 4.5: Forces acting on a small element within the slant section.

4.1.3 Slant Section

For the slant portion of the borehole, the forces acting on a unit section of the casing are presented in Fig. 4.5. The tensional load is controlled only by the type of operation, that is, pulling out or running in. At equilibrium, the differential equation is:

$$\frac{dF_a}{d\ell} = W(f_b \sin\alpha + \cos\alpha) \tag{4.34}$$

Solving Eq. 4.34 for tensional load while pulling out of the hole, yields:

$$F_{a_2} = F_{a_1} + W(l_1 - l_2)(f_b \sin\alpha_1 + \cos\alpha_1) \tag{4.35}$$

and while running in the hole:

$$F_{a_2} = F_{a_1} + W(l_1 - l_2)(\cos\alpha_1 - f_b \sin\alpha_1) \tag{4.36}$$

4.1.4 Drop-off Section

For the drop-off portion of the hole, the forces acting on the unit section of the pipe are presented in Figs. 4.6 and 4.7. At equilibrium, the differential equation is:

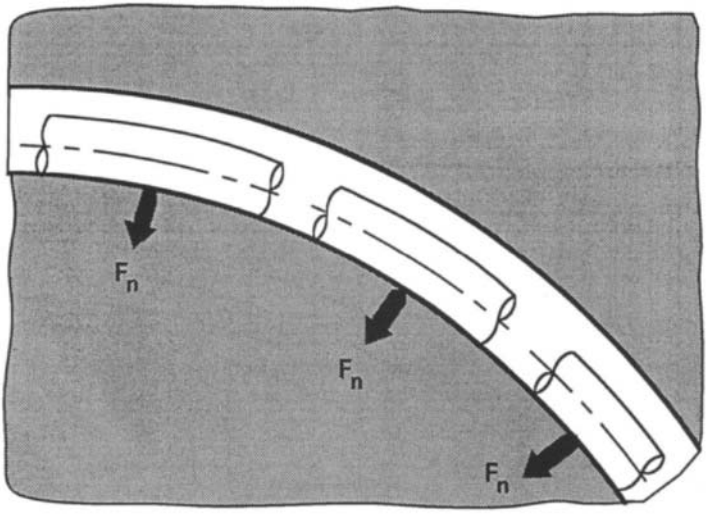

Fig. 4.6: Direction of the normal force, F_n, in a dropoff section. (After Maidla, 1987).

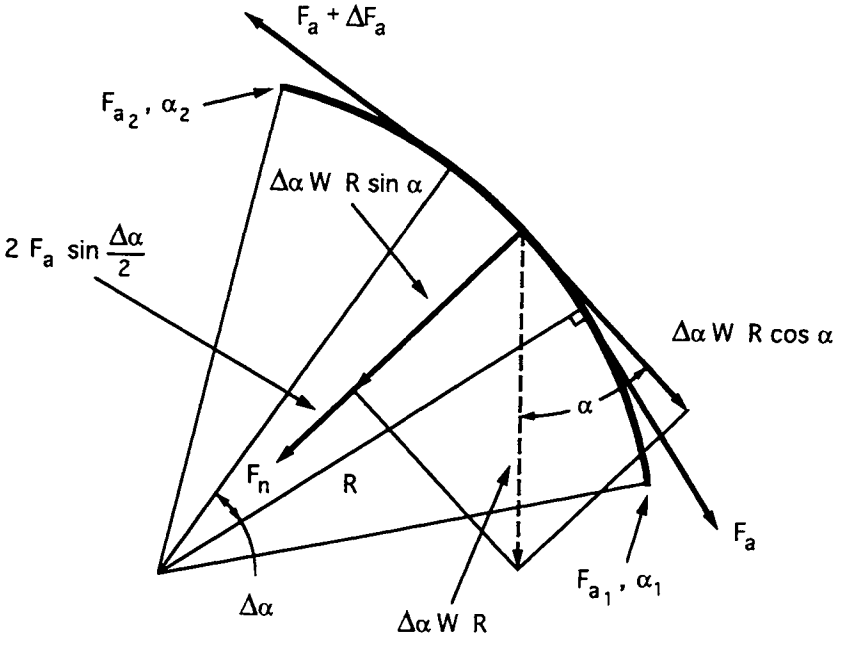

Fig. 4.7: Forces acting on a small casing element within the dropoff section.

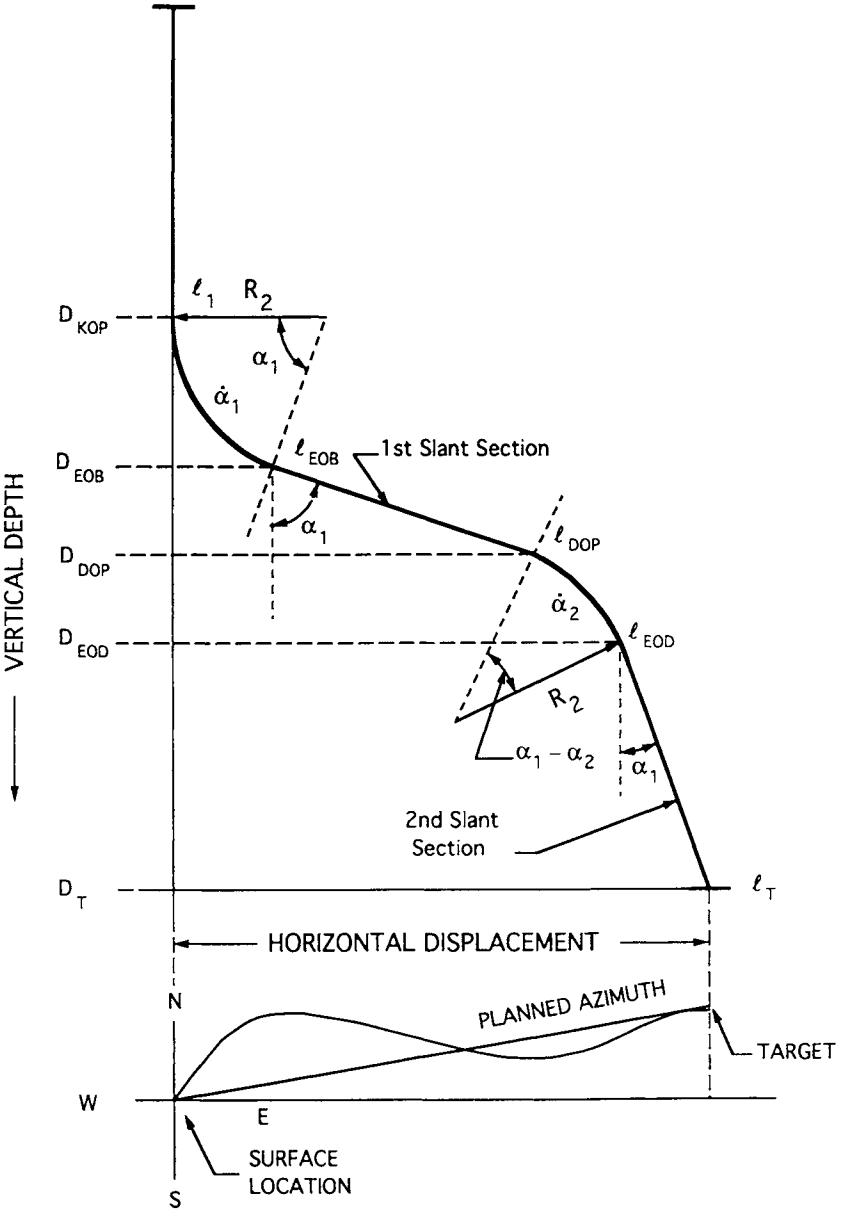

Fig. 4.8: Vertical and plan view of a typical deviated well.

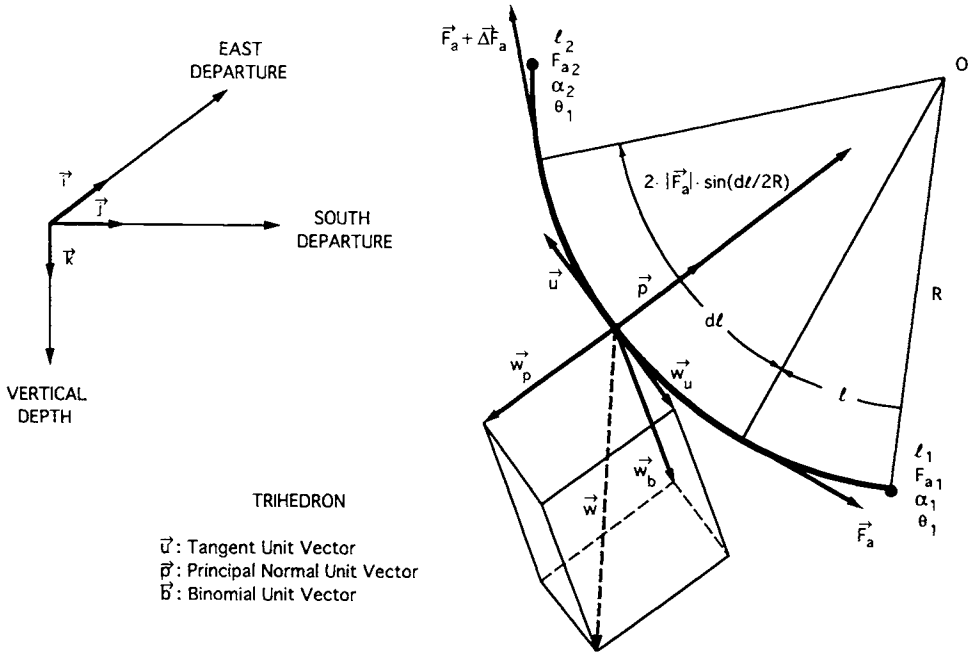

Fig. 4.9: Force acting on a small element within the buildup section. (After Maidla, 1987.)

$$\frac{dF_a}{d\alpha} = f_b\,(WR\sin\alpha + F_a) + WR\cos\alpha \tag{4.37}$$

When Eq. 4.37 is solved for the pulling out operation, the tensional load is given by:

$$\begin{aligned} F_{a_2} &= K_D\,F_{a_1} - \frac{WR}{1+f_b^2}\left[(f_b^2-1)(\sin\alpha_2 - K_D\sin\alpha_1)\right. \\ &\quad \left. + 2\,f_b\,(\cos\alpha_2 - K_D\cos\alpha_1)\right] \end{aligned} \tag{4.38}$$

and similarly for the running in operation:

$$\begin{aligned} F_{a_2} &= K_D\,F_{a_1} - \frac{WR}{1+f_b^2}\left[(f_b^2-1)(\sin\alpha_2 - K_D\sin\alpha_1)\right. \\ &\quad \left. - 2\,f_b\,(\cos\alpha_2 - K_D\cos\alpha_1)\right] \end{aligned} \tag{4.39}$$

where:

$$K_D = e^{f_b(\alpha_2-\alpha_1)} \tag{4.40}$$

4.1.5 2–D versus 3–D Approach to Drag Force Analysis

The method of calculating drag force presented in the previous section is based on the analysis of a two-dimensional well profile which consists of vertical and horizontal sections only. In practice, however, the spatial factors, such as bit walk, bearing angle, dogleg, etc., will cause the hole to deviate from the normal course and result in a three-dimensional well profile (vertical, horizontal and azimuth) as shown in Fig. 4.8. These effects are particularly noticeable in the buildup portion of the hole.

The forces acting on a unit section of the casing in the buildup section of the hole are presented in Fig. 4.9. From the state of equilibrium, the differential equation for drag-associated axial force, F_a, can be expressed as follows (Maidla, 1987):

$$\frac{dF_a}{dl} = W_u(l) \pm f_b C_s(l) W_N(l) \tag{4.41}$$

where:

$$\begin{aligned}
C_s(l) &= \text{correction factor for the effect of the surface contact area between the pipe and borehole.} \\
W_N(l) &= \text{buoyant weight projection on the principal normal direction} \\
&= \left\{ W_b(l)^2 + \left[W_p(l) + \frac{F_a(l)}{R(l)} \right]^2 \right\}^{0.5} \qquad (4.42) \\
R(l) &= \text{Hole-curvature after drilling. The results, which are a function of depth, are obtained from hole surveys.} \\
W_u(l) &= \text{unit buoyant weight projection on the tangent direction} \\
&= \vec{w}\,\vec{u}(l) \\
&= |\, dl \cdot W_{bu} (AZ \sin\lambda + VZ \cos\lambda) \,| \qquad (4.43)
\end{aligned}$$

$$\begin{aligned}
W_b(l) &= \text{unit buoyant weight projection on the binormal direction} \\
&= \vec{w}.\vec{b}(l) \;=\; dl\, W_{bu}\,(\mathrm{AX} \cdot \mathrm{VY} - \mathrm{VX} \cdot \mathrm{AY}) \qquad (4.44) \\
W_p(l) &= \text{unit buoyant weight projection on the principal normal direction} \\
&= \vec{w}.\vec{p}(l) \\
&= W_{bu} (AZ \cos\lambda - VZ \sin\lambda) \qquad (4.45) \\
W_{bu} &= \text{buoyant weight} \\
&= W_n \cdot BF
\end{aligned}$$

$$\lambda = \frac{(l_1 - l_2 - l)\,\beta}{l_1 - l_2} \tag{4.46}$$

$$VX = \sin\alpha_2 \cos\theta_2 \tag{4.47}$$

$$VY = \sin\alpha_2 \sin\theta_2 \tag{4.48}$$

$$VZ = \cos\alpha_2 \tag{4.49}$$

$$UX = \sin\alpha_1 \sin\theta_1 \tag{4.50}$$

$$UZ = \cos\alpha_1 \tag{4.51}$$

$$\beta = \arccos(UX \times VX + UY \times VY + UZ \times VZ) \tag{4.52}$$

$$AX = \frac{UX - VX\cos\beta}{\sin\beta} \tag{4.53}$$

$$AY = \frac{UY - VY\cos\beta}{\sin\beta} \tag{4.54}$$

$$AZ = \frac{UZ - VZ\cos\beta}{\sin\beta} \tag{4.55}$$

$$\theta = \text{bearing angle in radians.} \tag{4.56}$$

$$\beta = \text{overall angle change in radians.} \tag{4.57}$$

$$\lambda = \text{contact angle in radians (axial).} \tag{4.58}$$

$$R(l) = \left[\frac{l_1 - l_2}{\arccos\left[\cos(\theta_1 - \theta_2)\,\sin\alpha_1\,\sin\alpha_2 + \cos\alpha_1\,\cos\alpha_2\right]}\right] \tag{4.59}$$

In Eq. 4.41, the positive sign implies an upward pipe movement, whereas the negative sign denotes a downward movement. Equations 4.42 to 4.45 describe projections of the distributed pipe weight on the trihedron axis (Kreyszig, 1983) associated with any given point of the well trajectory.

In Eq. 4.41, a correction factor, C_s, is introduced to take into account the effect of contact surface between the pipe and the borehole. As reported by Maidla (1987), C_s is a function of the contact surface angle, ϕ, and is expressed as:

$$C_s(l) = \frac{2}{\pi}\phi(l)\left[\left(\frac{4}{\pi}\right) - 1\right] + 1 \tag{4.60}$$

C_s varies between 1 ($\phi(l) = 0$) and $4/\pi$ ($\phi(l) = \pi/2$) as shown in Fig. 4.10.

Initially, the circles of Fig. 4.10 are internally tangent. However, as the pipe is deformed the internal circle shifts laterally by Δd as illustrated by the dashed arc. The approximate pipe deformation in the direction of the distributed normal

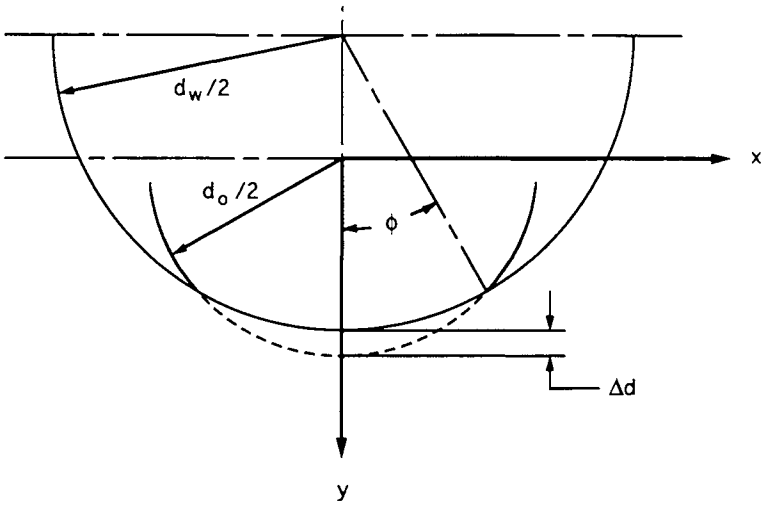

Fig. 4.10: Surface of the contact between borehole and the casing. (After Maidla, 1987.)

force, $W_N(l)$, is:

$$\Delta d = \frac{\pi}{24\,E}\, W_N(l)\, \frac{d_o}{t} \tag{4.61}$$

The pipe to borehole contact surface area, $\phi(l)$, is given by:

$$\phi(l) = \left[\arctan\left(\frac{2\,X}{2\,Y - d_w + d_o}\right)\right] \tag{4.62}$$

where X and Y are the coordinates of the point of intersection of the two circles. The cartesian plane x-y is assumed to be normal to the pipe at point l and its origin (0,0) to lie at the borehole centreline. X and Y are given by:

$$Y = 0.25\left[\frac{d_o^2 - d_w^2 + (d_w - d_o + 2\,\Delta d)^2}{d_w - d_o + 2\,\Delta d}\right] \tag{4.63}$$

$$X = 0.5\,(d_o^2 - 4\,Y^2)^{0.5} \tag{4.64}$$

where:

d_o	=	external diameter of the casing, in.
d_w	=	diameter of the well, in.
Δd	=	the approximate pipe deformation in the direction of the applied normal force, in.
t	=	thickness of the casing, in.
E	=	modulus of elasticity.
$W_N(l)$	=	distributed normal force from Eq. 4.42, lb/ft.

In Eq. 4.60, the following assumptions are made:

1. Pipe deformation is elastic.
2. Contact surface has the same geometry as the borehole.
3. There is a linear relationship between the contact surface correction factor, C_s and the contact angle, λ.
4. Contact surface as shown in Fig. 4.10, is controlled by an arc between the intersection points of two circles.

After multiple simulation runs, Maidla (1987) found that $C_s(l)$ was close to unity in all cases. He, therefore, concluded that the effect could be ignored in most calculations.

Generally, it is not possible to solve Eq. 4.41 analytically and instead numerical integration must be used. Equation 4.41 does not consider torsional effects which might also contribute to the normal force.

4.1.6 Borehole Friction Factor

The borehole friction factor results from a complex interaction between the tubular string and the borehole. Its value depends primarily upon lithology, borehole surface configuration (washouts, keyseats, ledges, etc.), pipe surface configuration (centralizers, coating, etc.), casing, coupling size relative to the borehole size, and lubricity of drilling fluid and mud cake. Inasmuch as these parameters vary from well to well, it is not possible to determine any specific value of friction factor for a given well.

In a recent study, Maidla (1987) proposed the following mathematical model to estimate the borehole friction factor, f_b:

$$f_b = \frac{|\, F_h - F_{bu_v} \pm F_{vd} \,|}{\int_0^{\ell} W_d(l, f_b)\, dl} \tag{4.65}$$

where:

F_h = hook load, lbf.
F_{bu_v} = vertical projected buoyant weight of pipe, lbf.
F_{vd} = hydrodynamic viscous drag, lbf.
$W_d(l, f_b)$ = unit drag or rate of drag change, lb/ft.
l = length of pipe, ft.
ℓ = measured depth, ft.

The unit drag force, $W_d(l, f_b)$, is implicit in both depth, l, and friction factor, f_b, and, therefore, Eq. 4.65 cannot be solved explicitly.

The plus and minus signs in Eq. 4.65 relate to running in and pulling out situations, respectively. The term 'hydrodynamic viscous drag' represents the effect of surge and swab pressures associated with drilling fluid flow resulting from pipe movement in the borehole. Viscous drag can be quantified using the well known theory of viscous drag for Power-Law fluids in borehole (Fontenot and Clark, 1974; Burkhardt, 1961; and Bourgoyne et al., 1985), which assumes the pipe is closed end and that the inertial forces and transient effects are negligible. Hence, the hydrodynamic viscous drag can be expressed in terms of viscous pressure gradient as:

$$\text{For laminar flow: } \frac{dp}{dl} = \frac{K\, v_{av}^{n}}{14.4 \times 10^{4}\,(d_w - d_o)^{1+n}} \left(\frac{2 + 1/n}{0.0208}\right)^{n} \tag{4.66}$$

$$\text{For turbulent flow: } \frac{dp}{dl} = \frac{f\, v_{av}^{2}\, \gamma_m}{21.1(d_w - d_o)} \tag{4.67}$$

where:

K and n = Power-Law parameters.
γ_m = drilling fluid specific weight, lb/gal.
f = flow frictional factor.
v_{av} = equivalent displacement velocity, ft/s.

The value for flow friction factor can be calculated by solving the Dodge and Metzner (1959) equation:

$$\left(\frac{1}{f}\right)^{0.5} = \frac{4}{n^{0.75}} \log\left(N_{Re}\, f^{(1-0.5n)}\right) - \frac{0.395}{n^{1.2}} \tag{4.68}$$

where N_{Re}, the Reynolds number, is given by:

$$N_{Re} = 10.9 \times 10^{4}\, \frac{\gamma_m\, v_{av}^{(2-n)}}{K} \left(\frac{0.0208\,(d_w - d_o)}{2 + 1/n}\right)^{n} \tag{4.69}$$

Equivalent displacement velocity can be calculated as follows:

$$v_{av} = v_p \left[\frac{(d_o/d_w)^2}{1 - d_o/d_w} + C_c\right] \tag{4.70}$$

where:

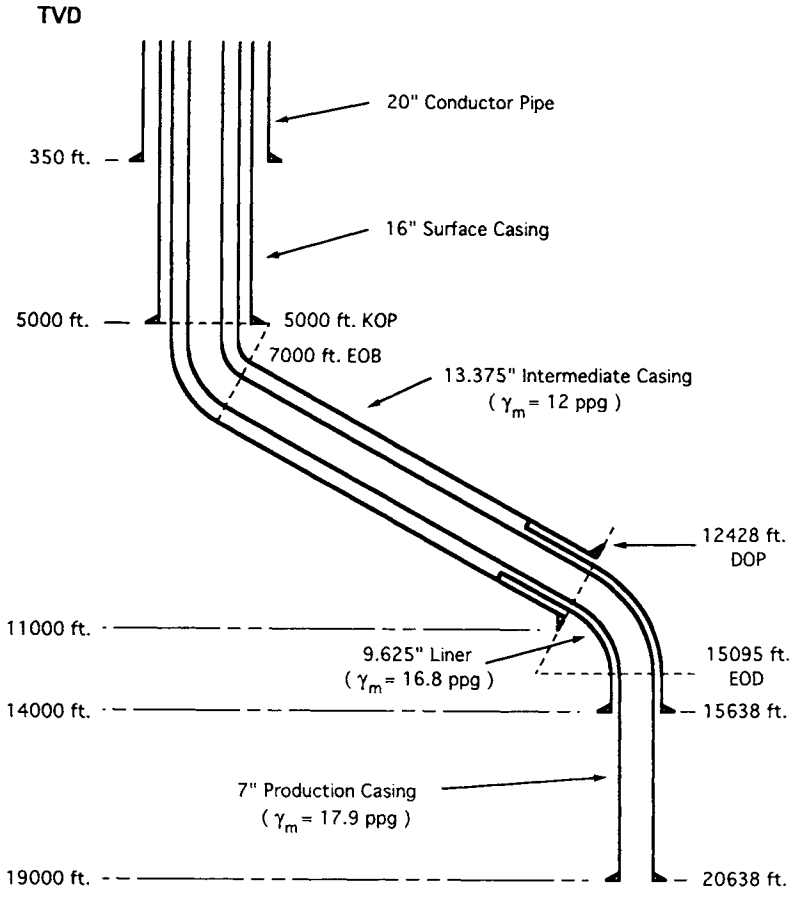

Fig. 4.11: Example of casing program for a deviated well.

v_p = velocity of the pipe, ft/s.
C_c = clinging constant.

Clinging constant, C_c, which depends on the type of fluid flow and the ratio of pipe diameter to borehole diameter, can be expressed empirically as (Maidla, 1987):

For laminar flow:

$$C_c = \frac{(d_o/d_w)^2 - 2\,(d_o/d_w)^2 \ln d_o/d_w - 1}{2\,(1 - (d_o/d_w)^2)\ln d_o/d_w} \tag{4.71}$$

For turbulent flow:

$$C_c = \left(\frac{(d_o/d_w)^4 + d_o/d_w}{(1 + d_o/d_w)\,(1 - (d_o/d_w)^2)^2}\right)^{0.5} - \left(\frac{(d_o/d_w)^2}{1 - (d_o/d_w)^2}\right) \tag{4.72}$$

Table 4.1: Planned trajectory of the deviated well.

Kickoff point	5.000 ft
Buildup rate ($\dot{\alpha}_1$)	2 °/100 ft
End of buildup	7.000 ft
Inclination angle (α_1)	40.0 degrees
Dropoff point	12.428 ft
Dropoff rate ($\dot{\alpha}_2$)	1.5 °/100 ft
End of drop	15.095 ft
Inclination angle (α_2)	0.0 degrees
Total measured depth	20.638 ft

Thus, from Eq. 4.65 it is evident that the borehole friction factor depends on drilling fluid properties, casing string composition, well profile, borehole geometry, hook loads (measured while running or pulling the casing), casing string velocity and the measured depth of the casing shoe. To determine the value of the borehole friction factor (BFF) one begins by assuming some initial value of the BFF and recurrently calculates the axial load from the casing shoe upward until the calculated hook load is determined. If the calculated hook load does not match the measured value, a new value of BFF is calculated and the procedure is repeated until the measured hook load is obtained.

4.1.7 Evaluation of Axial Tension in Deviated Wells

The BFF obtained by the above method is not a measured value but rather is calculated from the hook load measurement. A major error can, therefore, arise if the axial load predicted from the mathematical model is incorrect; consequently, it is important to include all the factors in Eq. 4.65. Maidla (1987) has made a series of field investigations and reported that most values of borehole friction factor fall within the range of 0.25 to 0.45.

A deviated well with buildup, slant and dropoff sections will be considered here to study the effect of hole deviation on casing design. The well is kicked at 5.000 ft with a maximal inclination of 40° at an average buildup rate of 2°/100 ft. The well is then held at this inclination to 12.428 ft measured depth and finally dropped off to a maximal inclination of 40° to the vertical axis at an average dropoff rate of 1.5°/100 ft. The drilling conditions, casing program and the well profile are presented in Table 4.1 and Fig. 4.11. The true vertical depth of the casing shoes, pore pressure gradient and drilling fluid program as shown in Table 4.1 remain the same in all the examples and, consequently, the collapse and burst load on each casing string will remain the same in all the examples.

In this section, the suitability of the selected steel grades in tension will be investigated by considering the total tensile force resulting from casing buoyant weight, bending force, shock load, and frictional drag force. It is important to

note that although shock and drag forces occur when the pipe is in motion, it is unlikely that both can exist simultaneously, because the effect of drag force vanishes before the shock load is generated. Thus, the tension due to drag and shock load are calculated separately and only the maximal value is considered in the design of casing for tension (maximal design load concept).

Depth conversion will be made by projecting the actual well profile (measured depth) onto the vertical axis (true vertical depth). Vertical depth and inclination angle are calculated for all casing unit sections. The following formulas are used to calculate the depths and inclinations (refer to Fig. 4.11) :

1. For the vertical portion, $0 \leq \ell_1 \leq \ell_{KOP}$:

$$D_1 = \ell_1 \tag{4.73}$$

2. For the buildup portion, $\ell_{KOP} < \ell_2 \leq \ell_{EOB}$:

Let the buildup rate equal $\dot{\alpha}_1$ degrees per 100 ft, and the radius of curvature equal R ft. Thus:

$$\begin{aligned} \frac{\dot{\alpha}_1}{360} &= \frac{100}{2\pi R} \\ \rightarrow \quad R &= \frac{18{,}000}{\pi \dot{\alpha}_1} \end{aligned}$$

The vertical projection of the measured depth $(\ell_2 - \ell_{KOP})$ in the buildup section is:

$$D = R \sin\theta$$

where:

$$\begin{aligned} \theta &= (\ell_2 - \ell_{KOP}) \\ &\qquad \text{in the buildup section} \\ &= \dot{\alpha}_1 (\ell_2 - \ell_{KOP}) \times 10^{-2} \end{aligned}$$

Thus

$$\begin{aligned} D &= \frac{18\,000}{\pi \dot{\alpha}_1} \sin\left(\dot{\alpha}_1 (\ell_2 - \ell_{KOP}) \times 10^{-2}\right) \\ &= R_1 \sin\left(\dot{\alpha}_1 (\ell_2 - \ell_{KOP}) \times 10^{-2}\right) \end{aligned}$$

True vertical depth for $\ell_{KOP} < \ell_2 \leq \ell_{EOB}$:

$$\begin{aligned} D_2 &= D_{KOP} + \frac{18{,}000}{\pi \dot{\alpha}_1} \sin\left(\dot{\alpha}_1 (\ell_2 - \ell_{KOP}) \times 10^{-2}\right) \\ &= D_{KOP} + R_1 \sin\left(\dot{\alpha}_1 (\ell_2 - \ell_{KOP}) \times 10^{-2}\right) \end{aligned} \tag{4.74}$$

3. For the first slant portion, $\ell_{EOB} < \ell_3 \leq \ell_{DOP}$, the vertical projection of the measured depth, $(\ell_3 - \ell_{EOB})$, is:

$$\begin{aligned} D &= (\ell_3 - \ell_{EOB}) \sin(90 - \alpha_1) \\ &= (\ell_3 - \ell_{EOB}) \cos \alpha_1 \end{aligned}$$

True vertical depth for $\ell_{EOB} < \ell_3 \leq \ell_{DOP}$:

$$\begin{aligned} D_3 &= D_{KOP} + \frac{18,000}{\pi \dot{\alpha}_1} \sin\left(\dot{\alpha}_1 (\ell_{EOB} - \ell_{KOP}) \times 10^{-2}\right) \\ &\quad + (\ell_3 - \ell_{EOB}) \cos \alpha_1 \\ &= D_{KOP} + R_1 \sin \alpha_1 + (\ell_3 - \ell_{EOB}) \cos \alpha_1 \\ &= D_{EOB} + (\ell_3 - \ell_{EOB}) \cos \alpha_1 \end{aligned} \tag{4.75}$$

Thus, for a measured depth of 12,428 ft the TVD is:

$$\begin{aligned} D_3 &= 5,000 + \frac{18,000}{\pi 2} \sin 40 + (12,428 - 7,000) \cos 40 \\ &= 11,000 \text{ ft} \end{aligned}$$

4. For the drop-off portion, $\ell_{DOP} < \ell_4 \leq \ell_{EOD}$, the vertical projection of the measured depth, $(\ell_4 - \ell_{DOP})$, is:

$$\begin{aligned} D &= \frac{18,000}{\pi \dot{\alpha}_2} \sin\left(\dot{\alpha}_2 (\ell_4 - \ell_{DOP}) \times 10^{-2}\right) \\ &= R_2 \sin(\dot{\alpha}_2 (\ell_4 - \ell_{DOP}) \times 10^{-2}) \end{aligned}$$

True vertical depth for $\ell_{DOP} < \ell_4 \leq \ell_{EOD}$:

$$\begin{aligned} D_4 &= D_{KOP} + \frac{18,000}{\pi \dot{\alpha}_1} \sin\left(\dot{\alpha}_1 (\ell_{EOB} - \ell_{KOP}) \times 10^{-2}\right) \\ &\quad + (\ell_{DOP} - \ell_{EOB}) \cos \alpha_1 \\ &\quad + \frac{18,000}{\pi \dot{\alpha}_2} \sin(\dot{\alpha}_2 (\ell_4 - \ell_{DOP}) \times 10^{-2}) \end{aligned} \tag{4.76}$$

$$\begin{aligned} &= D_{KOP} + R_1 \sin \alpha_1 + (D_{DOP} - D_{EOB}) \\ &\quad + R_2 \sin(\dot{\alpha}_2 (\ell_4 - \ell_{DOP}) \times 10^{-2}) \end{aligned} \tag{4.77}$$

$$\begin{aligned} &= D_{KOP} + (D_{EOB} - D_{KOP}) + (D_{DOP} - D_{EOB}) \\ &\quad + R_2 \sin(\dot{\alpha}_2 (\ell_4 - \ell_{DOP}) \times 10^{-2}) \\ &= D_{DOP} + R_2 \sin(\dot{\alpha}_2 (\ell_4 - \ell_{DOP}) \times 10^{-2}) \end{aligned} \tag{4.78}$$

5. For the second slant portion, $\ell_{EOD} < \ell_5 \leq \ell_T$, the vertical projection of the measured depth, $(\ell_5 - \ell_{EOD})$, is:

$$D = (\ell_5 - \ell_{EOD}) \cos \alpha_2$$

True vertical depth for $\ell_{EOD} < \ell_5 \leq \ell_T$:

$$\begin{aligned} D_5 &= D_{KOP} + \frac{18,000}{\pi \dot{\alpha}_1} \sin(\dot{\alpha}_1 (\ell_{EOB} - \ell_{KOP}) \times 10^{-2}) \\ &\quad + (\ell_{DOP} - \ell_{EOB}) \cos \alpha_1 \\ &\quad + \frac{18,000}{\pi \dot{\alpha}_2} \sin(\dot{\alpha}_2 (\ell_{EOD} - \ell_{DOP}) \times 10^{-2}) + (\ell_5 - \ell_{EOD}) \cos \alpha_2 \\ &= D_{DOP} + R_2 \sin(\alpha_1 - \alpha 2) + (\ell_5 - \ell_{EOD}) \cos \alpha_2 \\ &= D_{EOD} + (\ell_5 - \ell_{EOD}) \cos \alpha_2 \end{aligned} \tag{4.79}$$

(4.80)

Thus, for a measured depth of 15,095 ft the TVD is:

$$\begin{aligned} D_5 &= 5,000 + \frac{18,000}{\pi 2} \sin 40 + (12,428 - 7,000) \cos 40 \\ &\quad + \frac{18,000}{\pi 1.5} \sin(40 - 0) \\ &= 13,455 \text{ ft} \end{aligned}$$

Similarly, for a measured depth of 20,638 ft the TVD is:

$$\begin{aligned} D_5 &= 13,455 + (20,638 - 15,095) \\ &= 18,998 \text{ ft} \end{aligned}$$

where:

D	=	true vertical depth.
ℓ	=	measured depth.
Subscripts:		
DOP	=	dropoff point.
EOB	=	end of build.
EOD	=	end of dropoff.
KOP	=	kickoff point.

A friction factor of 0.35 will be used to calculate the drag associated tension on the casing. The effect of friction on axial load during downward movement is ignored.

For the buildup section, the tension load will be calculated by arbitrarily dividing this section into three equal parts: top, middle, and bottom. For the slant and dropoff sections, the tension load will be calculated by considering each of them as one section.

The approach to the buildup section is very arbitrary and not at all ideal, but this is an example of a hand calculation of a problem which can accurately be solved with a computer (Chapter 5 shows how).

In practice, the pipe will lie on the lower side, $WR\sin\alpha > F_a$, for most of the interval. At some point, probably quite near to the kick-off point, $WR\sin\alpha = F_a$ and the pipe, like the 'Grand Old Duke of York's 10,000 Men', is 'neither up nor down'. Finally, near the top of the interval, $WR\sin\alpha < F_a$ and the pipe will touch the top of the hole. Quite obviously, in the drop-off section of the hole, $WR\sin\alpha > F_a$ across the entire interval.

A two-dimensional model will be used to determine the drag-associated axial tension, because a numerical solution to the three-dimensional model is outside the scope of this section (refer to Chapter 5). For the purpose of casing design, a two-dimensional model has a strong practical appeal: it is simple to use.

The buoyant weight of the casing will be calculated using the true vertical depth of the well, because the horizontal component of the pipe is fully supported by the wall of the hole.

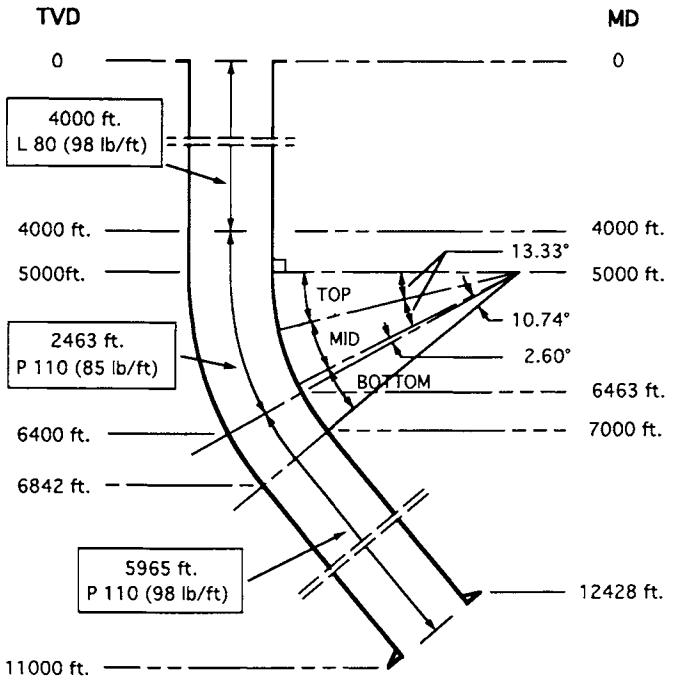

Fig. 4.12: Example of well profile showing steel grade and weight for intermediate casing.

Intermediate Casing

The well profile with the steel grades and weights (based on collapse and burst loads) is presented in Fig. 4.12. Starting from the bottom, the tensional load due

to buoyant weight and frictional drag can be calculated as shown in the Example Calculations.

Table 4.2: Total tensile load in intermediate casing string.

(1) True vertical depth (ft)	(2) Grade and Weight (lb/ft)	(3) Measured depth (ft)	(4) Angle of inclination (degrees)	(5) Tensional load carried by the top joint, lbf: $F_a = F_{bu} + F_d$
11,100 - 6,400	P-110, 98	12,428 - 6,463	40 - 29.26	502,782
6,400 - 4,000	P-110, 85	6,463 - 4,000	29.26 - 0	723,218
4,000 - 0	L-80, 98	4,000 - 0	0	1,043,257

(6) Bending force ($63\ d_o W_n \theta$) $\theta = 3°/100$ ft (lbf)	(7) Total tensional load = buoyant weight + frictional drag + bending force (lbf)	(8) Total tensional load = buoyant weight + bending force + shock load (lbf)
247,732	750,514	855,064
214,869	938,087	958,224
247,732	1,290,989	1,341,996

Example Calculation:

Tensional load due to the buoyant weight and frictional drag on pipe section P-110 (98 lb/ft) can be calculated as follows:

1. For the slant section, from 12,428 to 7,000 ft:

$$\begin{aligned} F_a &= F_{a1} + W\,(l_1 - l_2)\,(f_b \sin\alpha_1 + \cos\alpha_1) \\ &= 430,395 \text{ lbf} \end{aligned}$$

where:

$$\begin{aligned} F_{a1} &= \text{tensional load at } 12,428 \text{ ft} = 0 \text{ lbf} \\ W &= BF \times 98 \text{ lb/ft} \\ &= 0.816 \times 98 = 80 \text{ lb/ft} \\ l_1 - l_2 &= 12,428 - 7,000 = 5,428 \text{ ft} \\ f_b &= 0.35 \text{ (assumed)} \\ \alpha_1 &= 40° \end{aligned}$$

2. For the buildup section, from 7,000 ft to 6,463 ft (bottom part of buildup section):

$$F_a = K_B F_{a1} + \frac{WR}{1 + f_b^2}\left[(1 - f_b^2)\,(K_B \sin\alpha_1 - \sin\alpha_2)\right.$$

$$
\begin{aligned}
& -2 f_b (K_B \cos \alpha_1 - \cos \alpha_2)] \\
&= 459,578 + 43,204 \\
&= 502,782 \text{ lbf}
\end{aligned}
$$

where:

F_{a1} = 430,395 lbf
α_2 = 29.26° at 6,463 ft measured depth.
α_1 = 40° at 7,000 ft measured depth.
K_B = $e^{-f_b(\alpha_2 - \alpha_1)}$ = 1.0678
R = 2,866 ft

The tensional load on the pipe section P-110 (85 lb/ft) from 6,463 ft to 5,000 ft can be calculated as follows:

3. For the bottom part of buildup section, from 29.26° to 26.66° inclination angle:

$$
\begin{aligned}
F_a &= K_B F_{a1} + \frac{WR}{1 + f_b^2} \left[(1 - f_b^2)(K_B \sin \alpha_1 - \sin \alpha_2) \right. \\
&\quad \left. -2 f_b (K_B \cos \alpha_1 - \cos \alpha_2) \right] \\
&= 509,803 + 7,299 \\
&= 517,101 \text{ lbf}
\end{aligned}
$$

where:

F_{a1} = 502,782 lbf
W = 0.816 × 85 = 69.4 lb/ft
α_2 = 26.99°
α_1 = 29.26°
K_B = $e^{-f_b(\alpha_2 - \alpha_1)}$ = 1.014
R = 2,866 ft

4. For the middle part of the buildup section, from 26.66° to 13.33° inclination angle:

$$
\begin{aligned}
F_a &= F_{a1} + WR(\sin \alpha_1 - \sin \alpha_2) \\
&= 517,101 + 43,386 \\
&= 560,487 \text{ lbf}
\end{aligned}
$$

where:

F_{a1} = 517,101 lbf
W = 69.4 lb/ft
α_2 = 13.33°
α_1 = 26.66°
R = 2,866 ft

5. For upper part of the buildup section, from 13.33° to 0° inclination angle, for P-110 (85 lb/ft) :

$$\begin{aligned} F_a &= K_B F_{a1} + \frac{WR}{1+f_b^2}\left[(1-f_b^2)(K_B \sin\alpha_1 - \sin\alpha_2)\right. \\ &\quad \left. +2f_b(K_B\cos\alpha_1 - \cos\alpha_2)\right] \\ &= 608,036 + 45,786 \\ &= 653,821 \text{ lbf} \end{aligned}$$

where:

$F_{a1} = 560{,}487$ lbf
$W = 69.4$ lb/ft
$\alpha_2 = 0°$
$\alpha_1 = 13.33°$
$K_B = e^{-f_b(\alpha_2-\alpha_1)} = 1.0848$
$R = 2{,}866$ ft

6. For vertical section, from 5,000 ft to 4,000 ft, for P-110 (85 lb/ft):

$$\begin{aligned} F_a &= F_{a1} + W(5,000 - 4.000) \\ &= 732,217 \text{ lbf} \end{aligned}$$

where:

$F_{a1} = 653{,}821$ lbf
$W = 69.4$ lb/ft

7. Tension load at the top of the casing section L-80 (98 lb/ft) is given by:

$$\begin{aligned} F_a &= F_{a1} + W(4,000) \\ &= 1,043,257 \text{ lbf} \end{aligned}$$

where:

$F_{a1} = 732{,}217$ lbf
$W = 98 \times 0.816 = 80$ lb/ft.

Drilling Liner

Figure 4.13 presents the well profile and steel grades and weight selected based on the collapse and burst loads. Starting from the bottom, the tensional loads due to the buoyant weight are shown in Table 4.3.

Example Calculation:

Pipe section, L-50 (58.4 lb/ft), 14,128 ft to 15,638 ft.

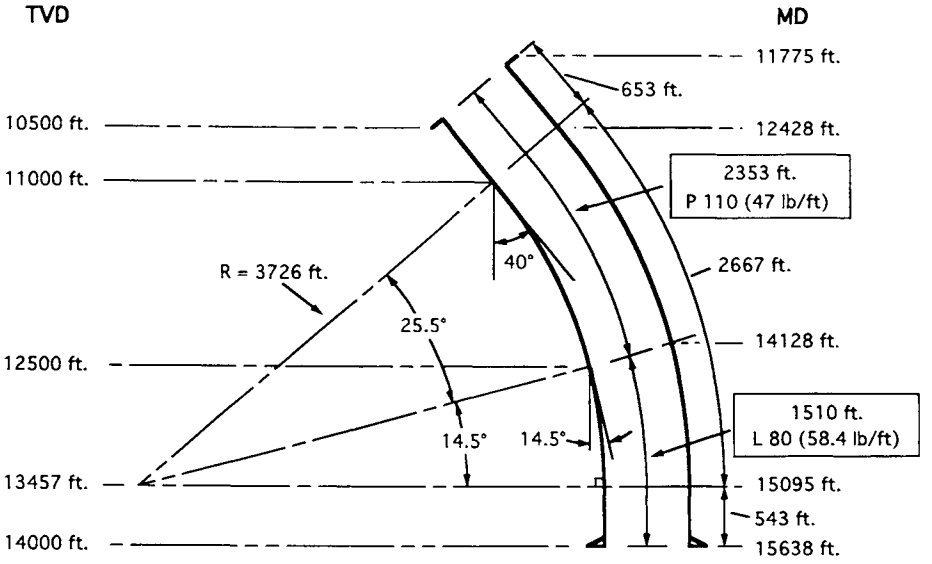

Fig. 4.13: Example of well profile showing steel grade and weight for a liner.

1. For the vertical section from 15,638 ft to 15,095 ft:

$$\begin{aligned} F_a &= W_n \times BF \times (15,638 - 15,095) \\ &= 58.4 \times 0.743 \times 543 \\ &= 23,561 \text{ lbf} \end{aligned}$$

2. For the dropoff section from 15,095 ft to 14,128 ft, with inclination angle of 0° to 14.5°:

$$\begin{aligned} F_a &= K_D F_{a1} - \frac{WR}{1+f_b^2}\left[(f_b^2-1)(\sin\alpha_2 - K_D \sin\alpha_1)\right. \\ &\quad \left. +2f_b(\cos\alpha_2 - K_D\cos\alpha_1)\right] \\ &= 69,938 \text{ lbf} \end{aligned}$$

where:

$$\begin{aligned} F_{a1} &= 23{,}561 \text{ lbf} \\ W &= 58.4 \times 0.743 = 43.39 \text{ lb/ft} \\ R &= 3{,}726 \text{ ft} \\ f_b &= 0.35 \\ \alpha_1 &= 0° \\ \alpha_2 &= 14.5° \\ K_D &= e^{f_b(\alpha_2-\alpha_1)} = 1.0926 \end{aligned}$$

Pipe section P-110, (47 lb/ft), from 14,128 ft to 11,775 ft.

Table 4.3: Total tensile load for drilling liner.

(1) True vertical depth (ft)	(2) Grade, and Weight (lb/ft)	(3) Measured depth (ft)	(4) Angle of inclination (degrees)
14,000 - 12,500	L-80, 58.4	15,638 - 14,128	0 - 14.5
12,500 - 10,500	P-110, 47	14,128 - 11,775	14.5 - 40

(5) Tensional load carried by the top joint, $F_a = F_{bu} + F_d$ (lbf)	(6) Bending force $= 63\, d_o W_n \theta$ $\theta = 3°/100$ft (lbf)	(7) Total tensional load = buoyant weight + frictional drag + bending force (lbf)	(8) Total tensional load = buoyant weight + bending force + shock load (lbf)
69,938	106,237	176,175	358,222
169,587	85,499	255,086	370,865

3. For the dropoff section from 14,128 ft to 12,428 ft:

$$\begin{aligned} F_a &= K_D F_{a1} - \frac{WR}{1+f_b^2}\left[(f_b^2-1)(\sin\alpha_2 - K_D \sin\alpha_1)\right. \\ &\quad \left. +2 f_b (\cos\alpha_2 - K_D \cos\alpha_1)\right] \\ &= 146,988 \text{ lbf} \end{aligned}$$

where:

$$\begin{aligned} F_{a1} &= 69{,}938 \text{ lbf} \\ W &= 47 \times 0.743 = 34.92 \text{ lb/ft} \\ R &= 3{,}726 \text{ ft} \\ f_b &= 0.35 \\ \alpha_1 &= 14.5° \\ \alpha_2 &= 40° \\ K_D &= e^{f_b(\alpha_2-\alpha_1)} = 1.1686 \end{aligned}$$

4. For the slant section from 11,775 to 12,428 ft

$$\begin{aligned} F_a &= F_{a1} + W(l_1 - l_2)(f_b \sin\alpha_1 + \cos\alpha_1) \\ &= 169,587 \text{ lbf} \end{aligned}$$

where:

$$\begin{aligned} F_{a1} &= 146{,}988 \text{ lbf} \\ W &= 34.92 \text{ lb/ft} \\ l_1 &= 12{,}428 \text{ ft} \\ l_2 &= 11{,}775 \text{ ft} \\ \alpha_1 &= 40° \end{aligned}$$

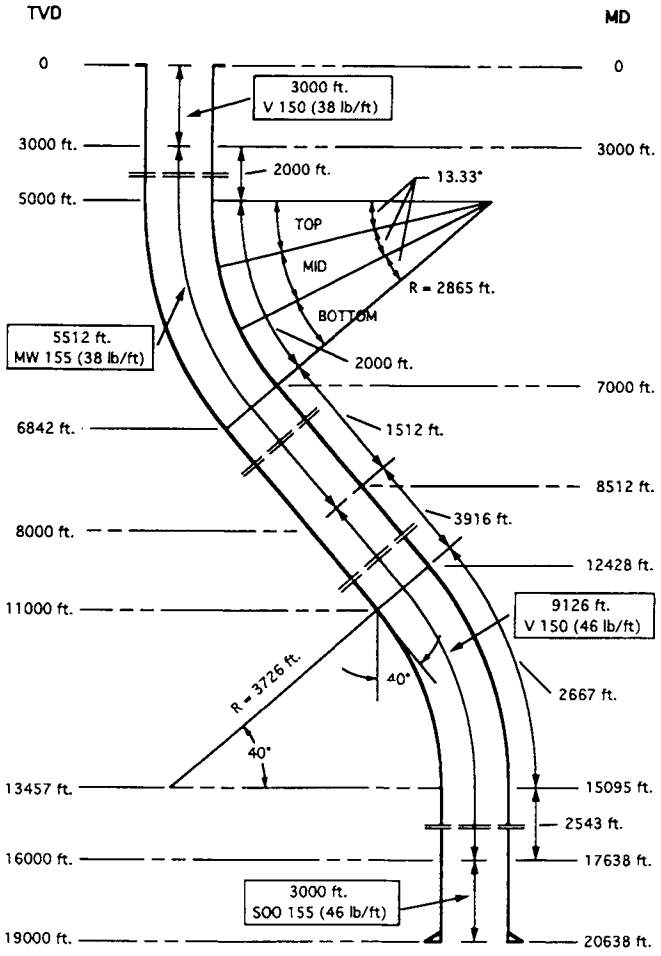

Fig. 4.14: Example of well profile showing steel grade and weight for production casing.

Production Casing

The well profile, the steel grades and weight, selected on the basis of collapse and burst loads are presented in Fig. 4.14. Starting from the bottom, the tensional load based on the concept of frictional drag and shock load are shown in Table 4.4.

The values of drag-associated tensional load for intermediate, liner and production casings are found almost the same way as those of the tension due to the shock load. This suggests that for a well profile presented in Fig. 4.11 and an assumed value for friction factor of 0.35, shock load can be substituted for drag force for ease of calculation of the design load for tension.

Equations 4.30, 4.32, 4.33, 4.35 and 4.38 are extremely useful to estimate the

drag force for casing in complicated well profiles, if the hole trajectory and other parameters such as bit walk, dog legs and bearing angles are known. It is equally important to know the exact value of the friction factor, because it is a major contributor to the frictional drag.

Table 4.4: Total tensile load in production casing.

(1) True vertical depth (ft)	(2) Grade and Weight (lb/ft)	(3) Measured depth (ft)
19,000 - 16,000	SOO-155, 46	20,638 - 17,638
16,000 - 8,000	V-150, 46	17,638 - 8,512
8,000 - 3,000	MW-155, 38	8,512 - 3,000
3,000 - 0	V-150, 38	3,000 - 0

(4) Angle of inclination (degrees)	(5) Tensional load carried by the top joint $F_a = F_{bu} + F_d$ (lbf)	(6) Bending force $= 63\ d_o W_n \theta$ $\theta = 3°/100$ft (lbf)
0	100,212	60,858
0 - 40	468,226	360,858
40 - 0	711,846	50,274
0	794,630	50,274

(7) Total tension = buoyant weight + frictional drag + bending force (lbf)	(8) Total tension = buoyant weight + shock load + bending force (lbf)
161,070	308,308
529,084	575,648
762,120	677,494
844,904	760,304

Further Examples

Using the planned trajectory data in Table 4.5, three production casing strings for a typical deviated well (Fig. 4.1), a single-build horizontal well (Fig. 4.15) and a double-build horizontal well (Fig. 4.15) were generated using the program introduced in Chapter 5.

To calculate the tensional load in the top joint of the strings, Eqs. 4.30, 4.32,

Table 4.5: Planned trajectories of (a) typical deviated well, (b) single-build horizontal well and, (c) double-build horizontal well.

	Typical Deviated	Single Build	Double Build
Kickoff point (ft)	5,000	3,000	5,000
Buildup rate ($\dot{\alpha}_1$) (°/100 ft)	2	2	2
End of buildup (ft)	7,000	7,500	7,000
Inclination angle (α_1) (deg.)	40	90	40
Dropoff point (ft)	12,480	12,500	-
Second build (ft)	-	-	12,480
Dropoff rate ($\dot{\alpha}_2$) (°/100 ft)	2	2	-
Buildup rate ($\dot{\alpha}_2$) (°/100 ft)	-	-	2
End of dropoff (ft)	14,480	12,500	-
End of build (ft)	-	-	13,480
Inclination angle (α_2) (deg.)	0	90	90
Total measured depth (ft)	16,720	12,500	16,720
Total vertical depth (ft)	15,120	5,865	11,449
Additional information common to all three examples:			
Minimum casing interval = 2,000 ft			
Design = minimum cost (see Chapter 5)			
Pseudo friction factor = 0.35			
Design factor burst = 1.1			
Design factor collapse = 1.125			
Design factor yield = 1.8			
Specific weight of mud = 16.8 lb/gal			
Design string = 7-in. production			

4.33, 4.35 and 4.38 were used. In all three cases, for the top buildup section it was assumed that the casing rested on the upper-middle-bottom part of the hole for an equal third of the interval as in the previous example. In the case of the double build, like the dropoff, the casing was assumed to rest on the bottom of the hole for the entire section of the second build.

At this point it is worthwhile to reiterate what was said earlier about the validity of these assumptions and in particular the one concerning the buildup section. Namely, that they need bear little relation to what actually occurs in practice. Just how close they are to the computer generated solution is illustrated in Table 4.6, which summarizes the results for each case and records the error between the value calculated using this approach and that produced using the computer program. Even the 'errors' must be taken with a grain of salt because by changing the buildup assumption from upper-middle-bottom (each 1/3 of interval) to upper-bottom (each 1/2 of interval) the errors change to -7%, -0.3% and -12% for the typical, single-build and double-build wells, respectively.

Table 4.6: Production combination strings for: (a) typical deviated well, (b) single-build horizontal well, (c) double-build horizontal well.

Typical Deviated Well (see Table 5.21 on page 307).		
Casing interval, measured depth (ft)	Grade and Weight (lb/ft)	Tensional load on top joint (lbf)
16,720 - 14,200	P-110, 38	73,612
14,200 - 11,520	P-110, 35	167,449
11,520 - 0	P-110, 32	490,333
Computed value = 484,623 lbf (Error = -1.2%)		
Single Build Horizontal Well (see Table 5.22 on page 308).		
Casing interval, measured depth (ft)	Grade and Weight (lb/ft)	Tensional load on top joint (lbf)
12,500 - 0	S-95, 23	152,930
Computed value = 169,839 lbf (Error = 10%)		
Double Build Horizontal Well (see Table 5.23 on page 309).		
Casing interval, measured depth (ft)	Grade and Weight (lb/ft)	Tensional load on top joint (lbf)
16,720 - 12,280	S-105, 32	69,537
12,280 - 9,760	P-110, 32	128,915
9,760 - 7,240	S-95, 29	182,726
7,240 - 0	S-95, 26	356,893
Computed value = 336,018 lbf (Error = -6.2%)		

"Computed value" is that generated in Examples 5.11 and 5.12

4.1.8 Application of 2–D Model in Horizontal Wells

In a horizontal well or horizontal drainhole, the inclination angle reaches 90° through the reservoir section. Two common profiles of a horizontal well are shown in Fig. 4.15.

In a typical horizontal well as shown in Fig. 4.15(a), two buildup sections, a slant section and a horizontal section are used to achieve the inclination of 90°. In the second type (see Fig. 4.15(b)), the well profile consists of a rapid buildup section and a horizontal section. Typical buildup rates used are presented in Fig. 4.16.

Equations 4.30, 4.32 and 4.33 can be used to calculate the drag-associated tensional load for both upper and lower buildup sections of type one and the buildup

section of type two well profile. Equation 4.35 can be used for the slant part of the buildup section of the type one well profile and it can also be used to determine the tensional load on the casing in the horizontal section ($\alpha_1 = 90°$) of both well profiles.

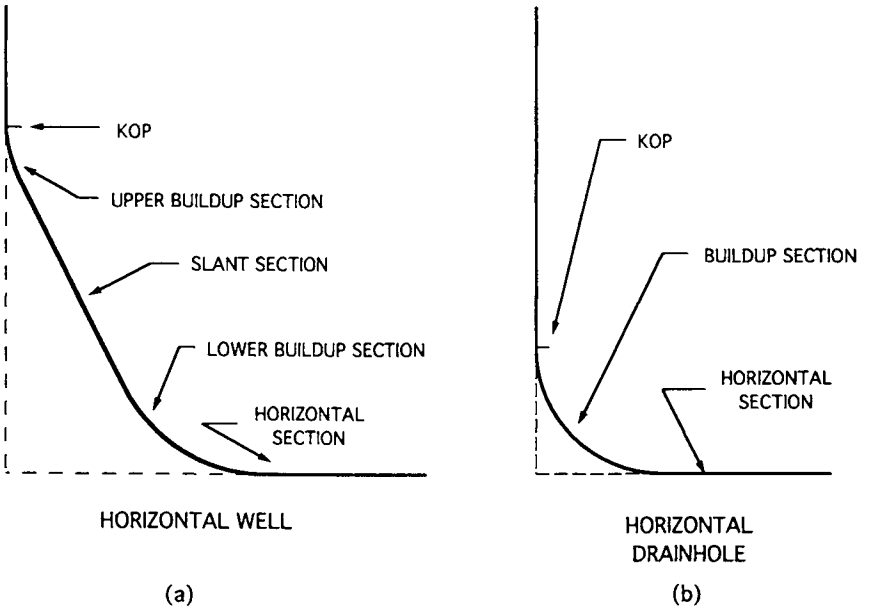

Fig. 4.15: Typical profiles of horizontal well and horizontal drainhole.

4.2 PROBLEMS WITH WELLS DRILLED THROUGH MASSIVE SALT-SECTIONS

Long sections of salt deposits present difficult problems in well completions because they create excessive loads on casing. It is generally accepted that salt creep can generate very high wellbore pressures and that in an unsupported wellbore it takes place in three stages. Primary creep starts with a relatively high rate of deformation just after the salt formation is drilled. After a certain time, this rate falls and a period of essentially low rate of deformation persists which is known as secondary creep. It is in the final stage, however, that salt creep reaches its maximal value and if the pressure and temperature exceed 3,000 psi and 278 °F, respectively, salt creep can generate very high wellbore pressures. Typically, an abnormal pressure gradient ranging from 1.0 psi/ft to 1.48 psi/ft can be applied to the casing leading to its collapse (Marx and El-Sayed, 1985; El-Sayed and Khalaf, 1987). Severe salt creep-related casing problems have been reported in

the Gulf of Suez (Pattillo and Rankin, 1981) and West Germany (Burkowsky et al., 1981).

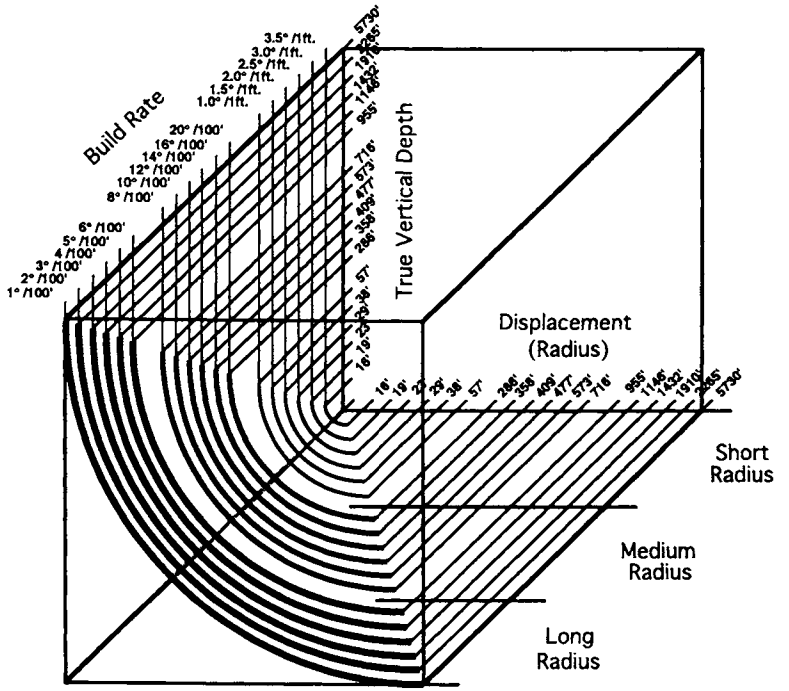

Fig. 4.16: Typical buildup rates for horizontal drainholes. (After Fincher, 1989.)

Two principal methods have been adopted to overcome the problem of casing collapse: thick-wall ($\geq$ 1 in.) casing (Ott and Schillinger, 1982) and cemented casing string (Marx and El-Sayed, 1984). The most effective solution seems to be to use cemented pipe-in-pipe casing (composite casing).

4.2.1 Collapse Resistance for Composite Casing

Although the improvement of collapse resistance in composite casing has been recognized by several investigators (Evans and Harriman, 1972; Pattillo and Rankin, 1981; and Burkowsky et al., 1981), it was Marx and El-Sayed (1984) who first provided theoretical and experimental results. The authors showed that for a composite pipe (Fig. 4.17), the contact pressure at the interface and the resulting tangential stresses could be expressed in terms of internal and external pressures, modulus of elasticity of the individual pipes and the cement, and the physical dimensions of the casing. Collapse behavior of the composite pipe can be distinguished in two principal ranges: elastic collapse and yield collapse.

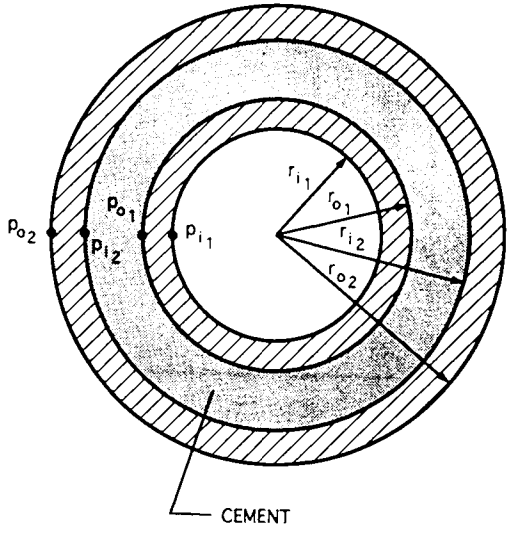

Fig. 4.17: Cross-sectional view of composite casing.

4.2.2 Elastic Range

Using Lamé's equation for thick-walled pipe and Eqs. 2.114 and 2.115, pressures and resulting stresses for homogeneous and isotropic composite pipe can be expressed as follows:

For the interface between the outer pipe and the cement sheath, ($r = r_{i_2}$):

$$\text{Tangential stress, } \sigma_t = \frac{p_{i_2}\,(r_{o_2}^2 + r_{i_2}^2) - 2\,p_{o_2}\,r_{o_2}^2}{(r_{o_2}^2 - r_{i_2}^2)} \tag{4.81}$$

$$\text{Radial stress, } \sigma_r = -p_{i_2} \tag{4.82}$$

Radial deformation;

$$\Delta r_{i_2} = \frac{r_{i_2}}{E}\left[(1-\nu^2)\,\frac{p_{i_2}\,(r_{o_2}^2 + r_{i_2}^2) - 2\,p_{o_2}\,r_{o_2}^2}{(r_{o_2}^2 - r_{i_2}^2)} + (\nu + \nu^2)\,p_{i_2}\right] \tag{4.83}$$

For the cylindrical cement sheath ($r = r_{i_2}$):

$$\sigma_t = \frac{2\,p_{o_1}\,r_{o_1}^2 - p_{i_2}\,(r_{i_2}^2 - r_{o_1}^2)}{(r_{i_2}^2 - r_{o_1}^2)} \tag{4.84}$$

$$\sigma_r = -p_{i_2} \tag{4.85}$$

$$\Delta r'_{i_2} = \frac{r_{i_2}}{E_{cm}} \left[(1 - \nu_{cm}^2) \frac{2\, p_{o_1}\, r_{o_1}^2 - p_{i_2} (r_{i_2}^2 - r_{o_1}^2)}{(r_{i_2}^2 - r_{o_1}^2)} + (\nu_{cm} + \nu_{cm}^2)\, p_{i_2} \right] \tag{4.86}$$

For the interface between the cement sheath and the inner pipe ($r = r_{o_1}$):

$$\sigma_t = \frac{p_{o_1} (r_{i_2}^2 + r_{o_1}^2) - 2 p_{i_2} r_{i_2}^2}{(r_{i_2}^2 - r_{o_1})^2} \tag{4.87}$$

$$\sigma_r = -p_{o_1} \tag{4.88}$$

$$\Delta r'_{o_1} = \frac{r_{o_1}}{E_{cm}} \left[(1 - \nu_{cm}^2) \frac{p_{o_1} (r_{i_2}^2 + r_{o_1}^2) - 2 p_{i_2} r_{i_2}^2}{(r_{i_2}^2 - r_{o_1}^2)} + (\nu_{cm} + \nu_{cm}^2)\, p_{o_1} \right] \tag{4.89}$$

For the inner pipe ($r = r_{o_1}$):

$$\sigma_t = \frac{2 p_{i_1} r_{i_1}^2 - p_{o_1} (r_{o_1}^2 - r_{i_1}^2)}{(r_{o_1}^2 - r_{i_1}^2)} \tag{4.90}$$

$$\sigma_r = -p_{o_1} \tag{4.91}$$

$$\Delta r_{o_1} = \frac{r_{o_1}}{E} \left[(1 - \nu^2) \frac{2\, p_{i_1} r_{i_1}^2 - p_{o_1} (r_{o_1}^2 - r_{i_1}^2)}{(r_{o_1}^2 - r_{i_1}^2)} + (\nu + \nu^2)\, p_{o_1} \right] \tag{4.92}$$

where:

E_{cm} = Modulus of elasticity for the cement sheath.
ν_{cm} = Poisson's ratio for cement sheath.

From the continuity of radial deformation at the interface one obtains:

$$\Delta r_{i_2} = \Delta r'_{i_2}$$
$$\Delta r_{o_1} = \Delta r'_{o_1}$$

Finally, substituting Eq. 4.83 into Eq. 4.86 and Eq. 4.89 into Eq. 4.92, one obtains the following expressions for collapse resistance of the composite pipe:

$$\begin{aligned} & p_{i_2} \left[\left(\frac{1 - \nu^2}{E} \right) \left(\frac{r_{o_2}^2 + r_{i_2}^2}{r_{o_2}^2 - r_{i_2}^2} \right) - \left(\frac{\nu_{cm} + \nu_{cm}^2}{E_{cm}} \right) \right. \\ & \quad \left. + \left(\frac{1 - \nu_{cm}^2}{E_{cm}} \right) \left(\frac{r_{i_2}^2 - r_{o_1}^2}{r_{i_2}^2 - r_{o_1}^2} \right) + \left(\frac{\nu + \nu^2}{E} \right) \right] \\ & = p_{o_1} \left[\left(\frac{1 - \nu_{cm}^2}{E_{cm}} \right) \left(\frac{2 r_{o_1}^2}{r_{i_2}^2 - r_{o_1}^2} \right) \right] + p_{o_2} \left[\left(\frac{1 - \nu^2}{E} \right) \left(\frac{2\, r_{o_2}^2}{r_{o_2}^2 - r_{i_2}^2} \right) \right] \end{aligned} \tag{4.93}$$

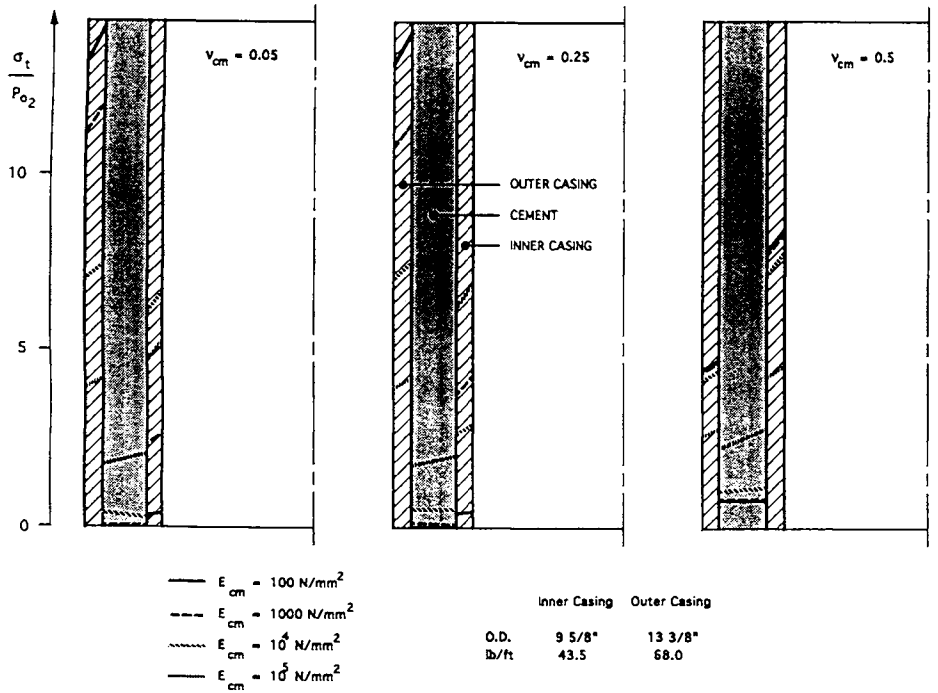

Fig. 4.18: Tangential stress in $13\frac{3}{8}$ - $9\frac{5}{8}$-in. composite casing as a function of modulus of elasticity and Poisson's ratio of cement sheath. (After El-Sayed, 1985; courtesy of ITE-TU Clausthal.)

and

$$p_{o_1}\left[\left(\frac{1-\nu^2}{E}\right)\left(\frac{r_{o_1}^2+r_{i_1}^2}{r_{o_1}^2-r_{i_1}^2}\right)-\left(\frac{\nu+\nu^2}{E}\right)+\left(\frac{1-\nu_{cm}^2}{E_{cm}}\right)\left(\frac{r_{i_2}^2-r_{o_1}^2}{r_{i_2}^2-r_{o_1}^2}\right)+\left(\frac{\nu_{cm}+\nu_{cm}^2}{E_{cm}}\right)\right]$$
$$= p_{i_1}\left[\left(\frac{1-\nu^2}{E}\right)\left(\frac{2r_{i_1}^2}{r_{o_1}^2-r_{i_1}^2}\right)\right]+p_{i_2}\left[\left(\frac{1-\nu_{cm}^2}{E_{cm}}\right)\left(\frac{2r_{i_2}^2}{r_{i_2}^2-r_{o_1}^2}\right)\right] \qquad (4.94)$$

From the above equations, values of p_{i_2}, p_{o_1} and σ_t can be determined from the physical dimensions of the pipes, internal and external pressures, and the modulus of elasticity of steel and cement.

4.2.3 Yield Range

Collapse strength of the composite pipe is defined with reference to a state in which the tangential stress of the inner or outer pipe attains the value of its yield

strength. According to the theory of distortional energy, the yield strength of the inner or outer pipe can be expressed as follows:

$$2\sigma_{y_1} = \sqrt{(\sigma_{r_1} - \sigma_{t_1})^2 + (\sigma_{t_1} - \sigma_{z_1})^2 + (\sigma_{z_1} - \sigma_{r_1})^2} \tag{4.95}$$

or

$$2\sigma_{y_2} = \sqrt{(\sigma_{r_2} - \sigma_{t_2})^2 + (\sigma_{t_2} - \sigma_{z_2})^2 + (\sigma_{z_2} - \sigma_{r_2})^2} \tag{4.96}$$

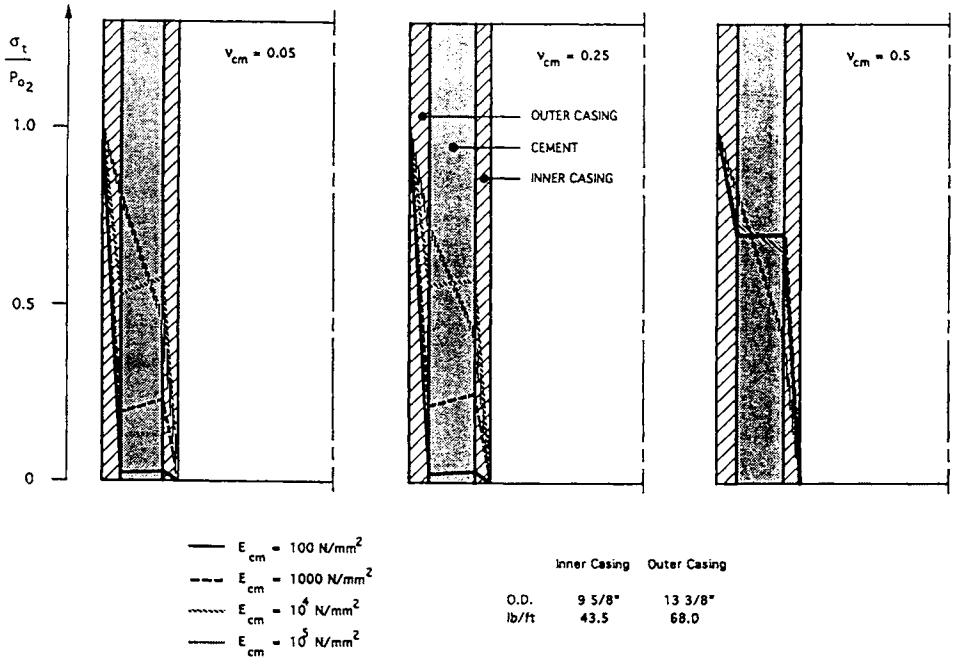

Fig. 4.19: Radial stress in $13\frac{3}{8}$ - $9\frac{5}{8}$-in. composite casing as a function of modulus of elasticity and Poisson's ratio of cement sheath. (After El-Sayed, 1985; courtesy of ITE-TU Clausthal.)

Defining σ_{y_1} and σ_{y_2} as the yield strengths of the inner and outer pipes with a permanent deformation of 0.2 %, and substituting the values of σ_t, σ_r, $E_{cm} = 5,691 + 376\,\sigma_{cm} - 1.19\,\sigma_{cm}^2$ and $E = 2.1 \times 10^5$ N/mm^2, the yield strength of the individual pipe can be obtained in metric units as follows (El- Sayed, 1985):

$$\sigma_{y_1} = 3\left[\frac{(p_{o_1} - p_{i_1})\,r_{o_1}^2}{(r_{o_1}^2 - r_{i_1}^2)}\right]^2 + \left[\sigma_z - \frac{p_{i_1} r_{i_1}^2}{r_{o_1}^2 - r_{i_1}^2} + \frac{p_{o_1} r_{o_1}^2}{r_{o_1}^2 - r_{i_1}^2}\right] \tag{4.97}$$

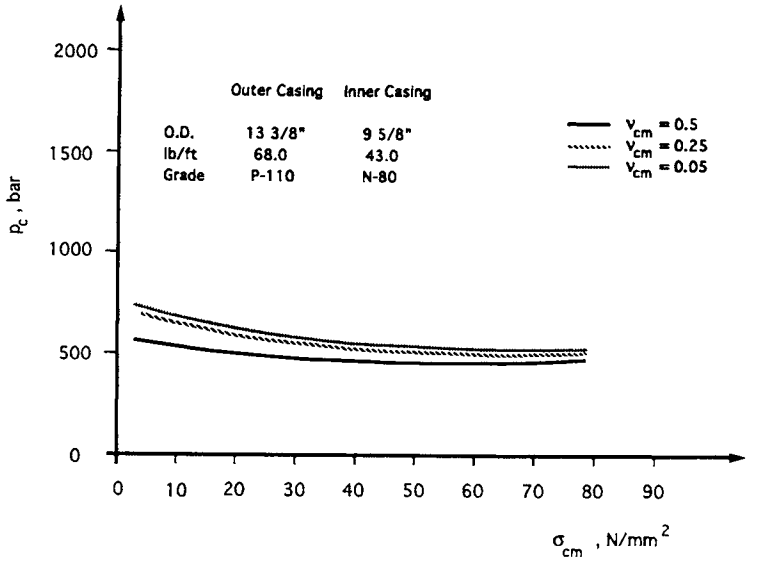

Fig. 4.20: Collapse resistance of the composite pipe as a function of compressive strength and Poisson's ratio of cement. (After El-Sayed, 1985; courtesy of ITE-TU Clausthal.)

and

$$\sigma_{y_2} = 3\left[\frac{(p_{o_2} - p_{i_2})\, r_{o_2}^2}{(r_{o_2}^2 - r_{i_2}^2)}\right]^2 + \left[\sigma_z - \frac{p_{i_2} r_{i_2}^2}{r_{o_2}^2 - r_{i_2}^2} + \frac{p_{o_2} r_{i_2}^2}{r_{o_2}^2 - r_{i_2}^2}\right] \tag{4.98}$$

where:

σ_{cm} = compressive strength of cement, N/mm^2.

Using Eqs. 4.93, 4.94, 4.97 and 4.98, the stress distribution in the composite pipe and its collapse resistance were computed by El-Sayed (1985) (see Figs. 4.18 through 4.20). From the figures the following observations can be made:

1. Maximum stress occurs in the outer pipe.

2. Minimum stress occurs in the cement sheath.

3. Stress on the outer pipe increases with increasing E_{cm}, i.e., the collapse resistance increases.

4. Stress on the inner pipe decreases with increasing E_{cm}, i.e., the collapse resistance decreases.

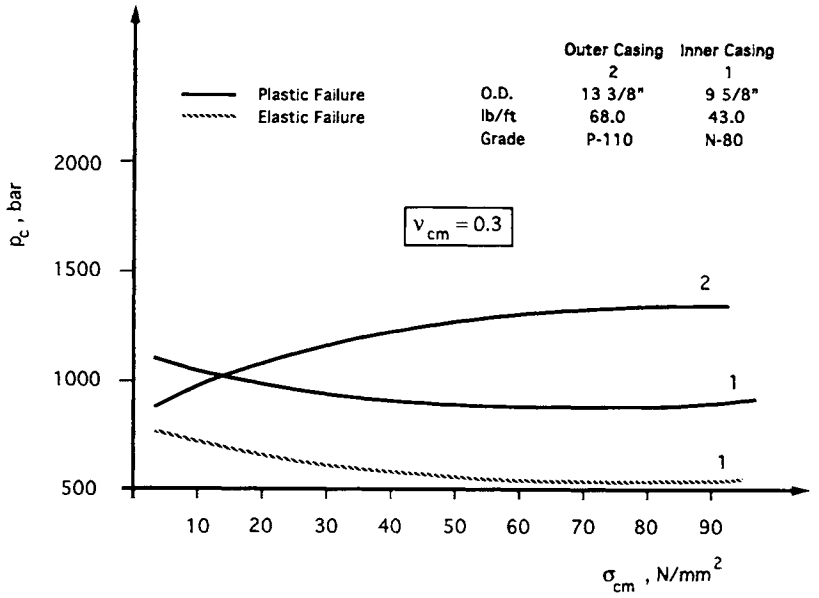

Fig. 4.21: Collapse resistance of the composite pipe as a function of compressive strength of cement. (After El-Sayed, 1985; courtesy of ITE-TU Clausthal.)

This behavior is explained by the fact that at low values of E_{cm}, the tangential stress in the outer pipe exceeds its yield strength and results in collapse. At high values of E_{cm} the composite pipe starts to collapse at the inner pipe. This suggests that cement with a high modulus of elasticity does not necessarily increase the collapse resistance of the composite pipe. Collapse resistance in the yield range (Fig. 4.21) displays similar behavior to that observed in the elastic range.

Test results obtained on two sets of composite pipes ($13\frac{3}{8}$ - $9\frac{5}{8}$-in. and 7 - 5-in.) by Marx and El-Sayed (1984) show behavior (Fig. 4.22) similar to that predicted by their theoretical model. The pipe failure observed for all specimens was, however, in the plastic range (Fig. 4.23). Collapse failure in the plastic range can be explained as follows. As the external and internal pressures increase, the cement sheath experiences a confining pressure, which results both in an increase in compressive strength and the modulus of elasticity of cement and a corresponding decrease in Poisson's ratio. With further increases in the external pressure, the modulus of elasticity of the cement decreases and Poisson's ratio increases. As the changes in the modulus of elasticity, Poisson's ratio and external pressure (increasing) continue, the composite pipe reaches a stage where the tangential stress exceeds the value of the yield strength of any one of the pipes. Consequently, the composite pipe starts to yield and finally collapses. The effect of the combined loads improves the collapse resistance (Fig. 4.22), thereby improving the behavior of the cement sheath.

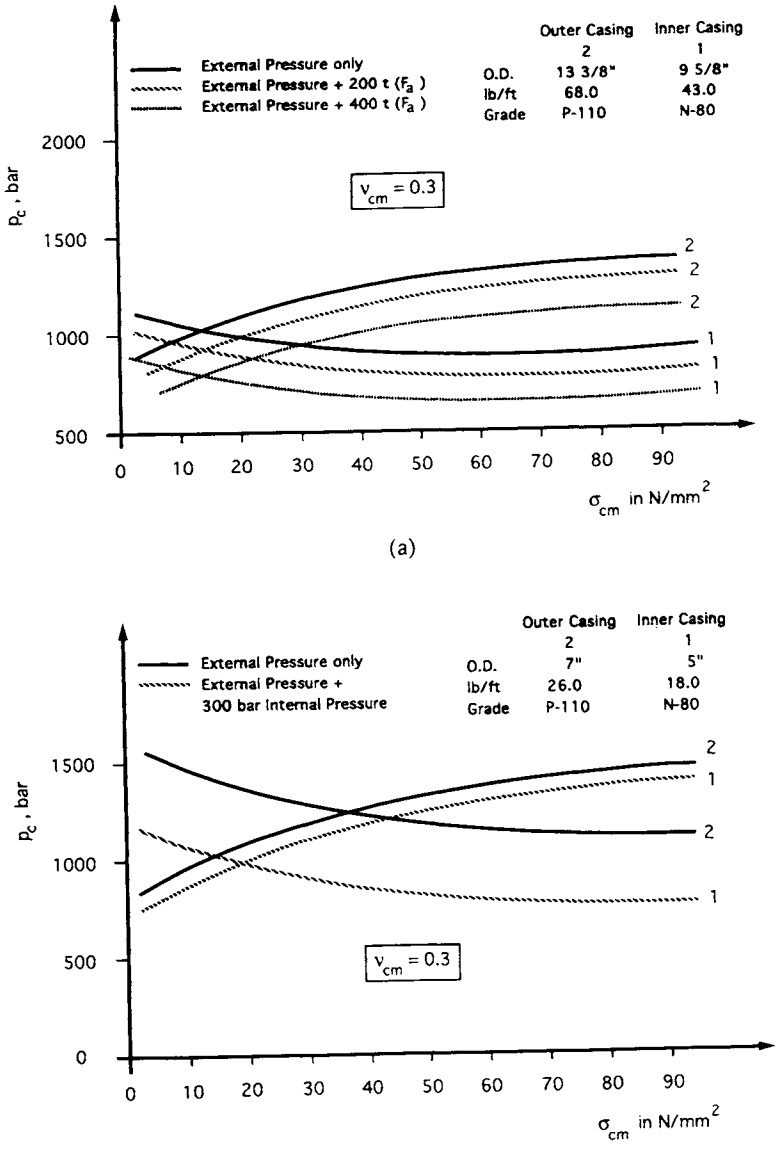

Fig. 4.22: Collapse resistance of the outer and inner pipe as a function of compressive strength of cement; (a) $13\frac{3}{8}$ - $9\frac{5}{8}$-in. and (b) 7 - 5-in. (After El-Sayed, 1985; courtesy of ITE-TU Clausthal.)

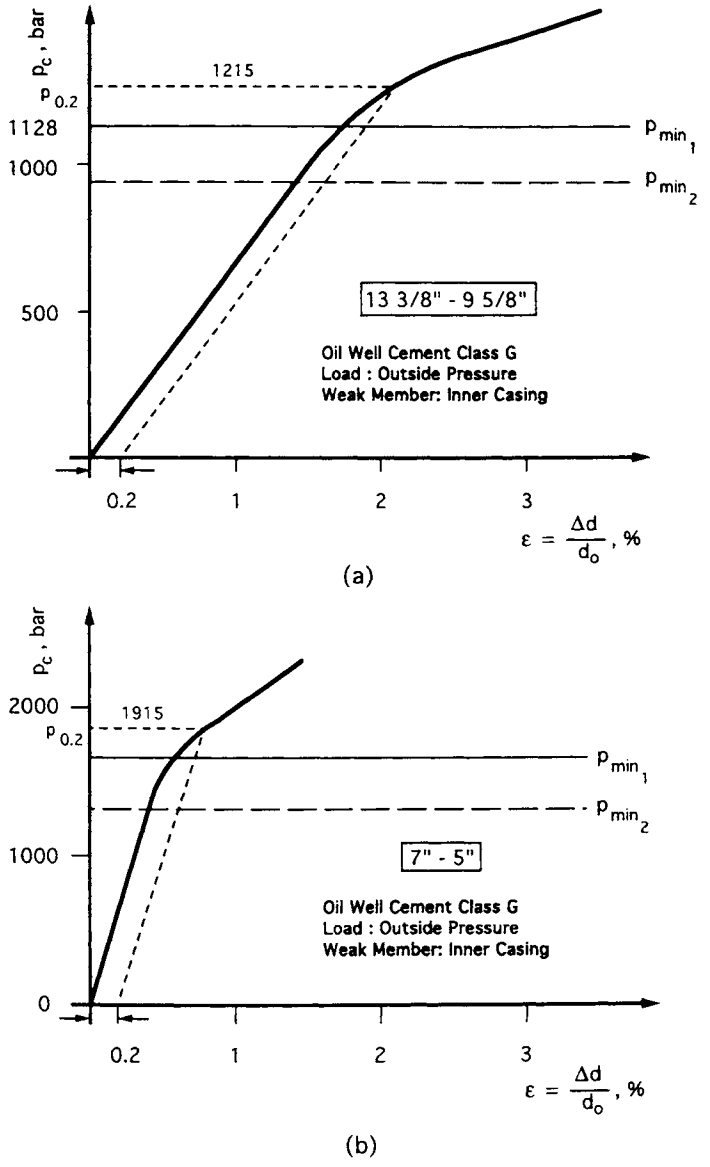

Fig. 4.23: Collapse failure of the composite pipe as a function of external pressure; (a) $13\frac{3}{8}$ - $9\frac{5}{8}$-in. and (b) 7 - 5-in. (After El-Sayed, 1985; courtesy of ITE-TU Clausthal.)

On the basis of the results obtained from the theoretical model and the laboratory experiments, Marx and El-Sayed (1985) suggested the following formula for calculating the collapse resistance of composite casing:

$$p_{c_{cp}} = p_{c_1} + p_{c_2} + \sigma_{cs_{p_{c_1}}} \left[\frac{2.05}{(d_o/t)_{cs}} - 0.028 \right] \tag{4.99}$$

where:

$(d_o/t)_{cs}$ = ratio of outside diameter of the cement sheath to its thickness.
$p_{c_{cp}}$ = overall collapse resistance of the composite (pipe) body, psi.
p_{c_1} = collapse resistance of the inside pipe, psi.
p_{c_2} = collapse resistance of the outside pipe, psi.
$\sigma_{cs_{p_{c_1}}}$ = collapse stress of the cement sheath under the external pressure p_{c_1}, psi.
= $\sigma_{cm} + 2p_{c_1} \left(\frac{\sin\varphi}{1 - \sin\varphi} \right)$.
σ_{cm} = compressive strength of the cement.
φ = angle of internal friction calculated from Mohr's circle.

The compressive strength of cement and the angle of internal friction for the collapse resistance of the composite pipe can be computed from Eq. 4.99. The equation also shows that the collapse resistance of the composite pipe is the sum of the collapse resistance of the individual pipes. Inasmuch as the collapse resistance of the cement sheath cannot be predicted as a single pipe, Marx and El-Sayed (1985) suggested the following simplified equation:

$$p_{c_{cp}} = K_r (p_{c_1} + p_{c_2}) \tag{4.100}$$

where:

K_r = reinforcement factor.

The value of K_r lies between 1.17 and 2.03.

4.2.4 Effect of Non-uniform Loading

When the formation flows under the action of overburden pressure, it is more likely that the casing will be subjected to non-uniform loading as shown in Fig. 4.24. Nonuniform loading is generally caused by inadequate filling of the annulus with cement, which leaves the casing partially exposed to the flowing formation. Generally, two effects of nonuniform loading of casing are recognized: curvature and point-load effects (Nester et al., 1955).

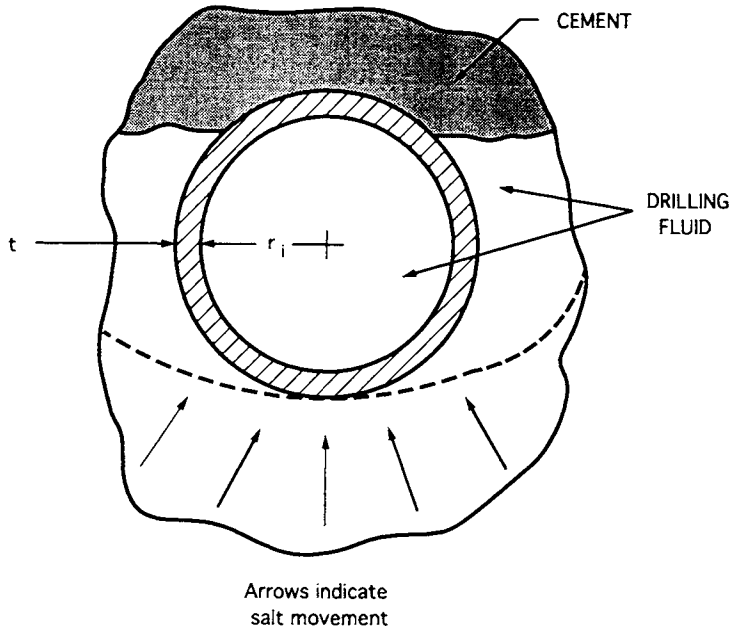

Fig. 4.24: Point loading effect due to the flow of salt. (After Cheatham and McEver, 1964.)

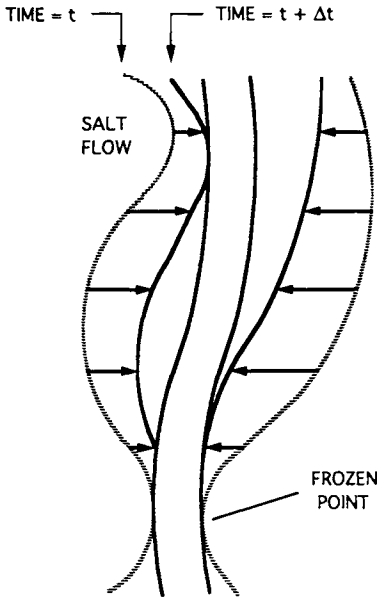

Fig. 4.25: Curvature effect due to the salt flow. (After Cheatham and McEver, 1964.)

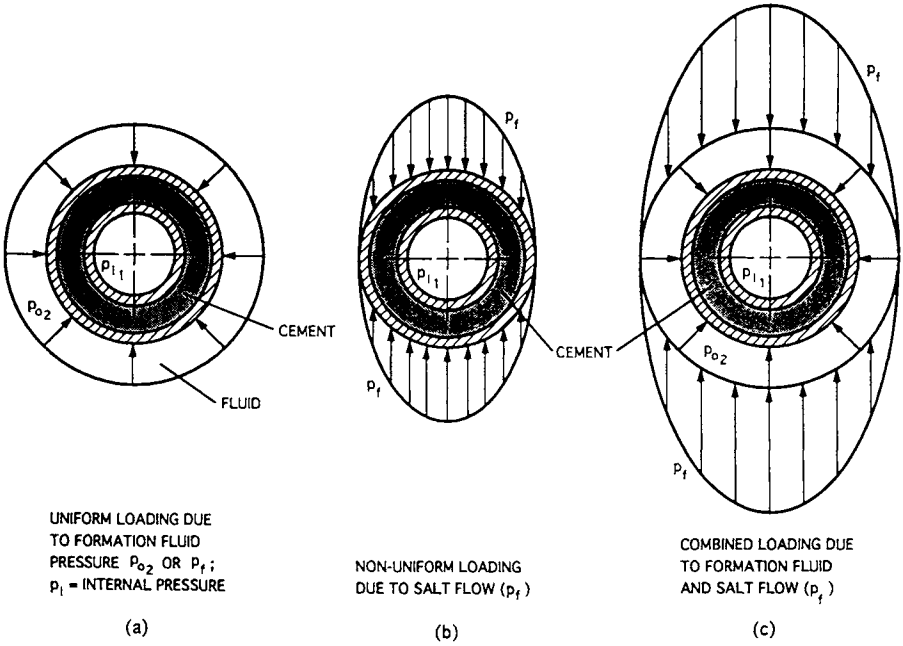

Fig. 4.26: Different modes of loading on composite casing. (After El-Sayed et al., 1989.)

The curvature effect is shown in Fig. 4.25. The accentuated irregular shape of the borehole axis is a result of washouts by the drilling fluid. At the in-gauge section of the hole, the flowing (salt) formation comes in contact with the pipe and restricts its movement. In the out-of-gauge section, particularly in sections where drilling fluid instead of cement surrounds the pipe, the formation continues to flow and closes the borehole. The flow of formation above or below the frozen point (gauge section of the hole or where there is an adequate filling of the annulus with cement) can cause severe bending loads.

Point loading generally occurs when the annulus is partially filled with cement; the remaining volume is occupied by drilling fluid. When salt flows, the unsupported part of the casing is subjected to point loading (Fig. 4.25). As depicted in Fig. 4.26, p_{i_1} and p_{o_2} are the hydrostatic heads due to the presence of drilling fluid in the annulus and borehole. The concentrated force represents the point loading by the formation and the resulting reaction forces on the opposite side of the casing (see Fig. 4.26(b)). Figure 4.26(c) represents the combined effects of uniform load due to drilling fluid (p_{o_2} and p_{i_1}) and nonuniform load due to formation flow (p_f). This imbalance can lead to radial deformation of the outer pipe and a severe loading situation.

In a theoretical study, El-Sayed and Khalaf (1989) showed that the radial deformation caused by nonuniform external loading is transmitted to the cement and the inner casing. This results in additional internal stresses in the cement and the inner pipe, and additional contact pressures on the surfaces between the outer pipe and cement, and the cement and inner pipe. The authors found that the non-uniform external loading could reduce the collapse resistance of the composite pipe by as much as 20 %.

4.2.5 Design of Composite Casing

As discussed previously, the generalized casing string for use in any situation is one designed to withstand the maximum conceivable load to which it might be subjected during the life of the well. In view of this, for the design of casing adjacent to a salt section, the following loading conditions are assumed:

1. Casing is expected to be evacuated at some point in the drilling operation.
2. Placement of cement opposite the salt section is often difficult and, therefore, any beneficial effect of cement is ignored.
3. Uniform external pressure exerted by the salt is considered to be equal to the vertical depth, i.e., at 1,000 ft pressure is 1,000 psi. A typical abnormal pressure gradient is 1.48 psi/ft.
4. The effect of non-uniform loading is taken into consideration by increasing the usual safety factor by at least 20 %.

The intermediate casing string described in Chapter 3 is again considered; however, in this example, a salt section is assumed to extend from 6,400 to 11,100 ft. and the collapse design for P-110 (98 lb/ft) casing is rechecked.

$$\begin{aligned} \text{Collapse pressure at } 6,400 \text{ ft} &= 12 \times 0.052 \times 6,400 \\ &= 3,993.6 \text{ psi.} \end{aligned}$$

$$\begin{aligned} \text{Collapse pressure at } 11,100 \text{ ft} &= 1.48 \times 11,100 \\ &= 16,428 \text{ psi.} \end{aligned}$$

Collapse resistance of the current casing grade P-110 (98 lb/ft) = 7,280 psi.

$$SF \text{ for collapse} = \frac{7,280}{16,428} = 0.433$$

Alternatively, a liner may be run adjacent to the salt section and the annulus between the two casing cemented. The physical properties of the composite pipe are given in Table 4.7.

Table 4.7: Physical properties of composite pipe.

Property	Outer pipe	Inner pipe
Grade:	P-110	N-80
OD, in.	$13\frac{3}{8}$	$9\frac{5}{8}$
W_n, lb/ft	92	58.4
p_c, psi	7,282	7,890

Assuming a K_r (reinforcement factor) of 1.6, the collapse resistance is calculated as:

$$p_{co} = K\,(p_{c_1} + p_{c_2}) = 1.6\,(7,890 + 7,282) = 24,275.2 \text{ psi}$$

Thus,

$$SF \text{ for collapse } = \frac{24,275.2}{16,428} = 1.47$$

Generally, it is not possible to obtain a 100% effective cement job in the long annular section of two concentric pipes. A safety factor of 1.5 should, therefore, be used to allow for any uncertainties in the quality of the cement and to ensure that the rated performance is greater than the expected load.

4.3 STEAM STIMULATION WELLS

Steam or hot water is often used as the heat transfer medium for the application of heat to a reservoir containing highly viscous crude oil. As a consequence, tubing and casing are placed into an environment of extreme temperatures where typically the upper temperature range varies between 400°F and 600°F. The upper temperature limit is expected to rise to 700°F in the near future.

When steam is injected into a well, the casing is gradually heated up and tends to elongate in direct proportion to the change in temperature. Inasmuch as most casing is cemented, the tendency to elongate is replaced by a compressive stress in the casing. Casing failure occurs initially when the temperature-induced compressive stresses exceed the yield strength of the casing. Subsequent cooling

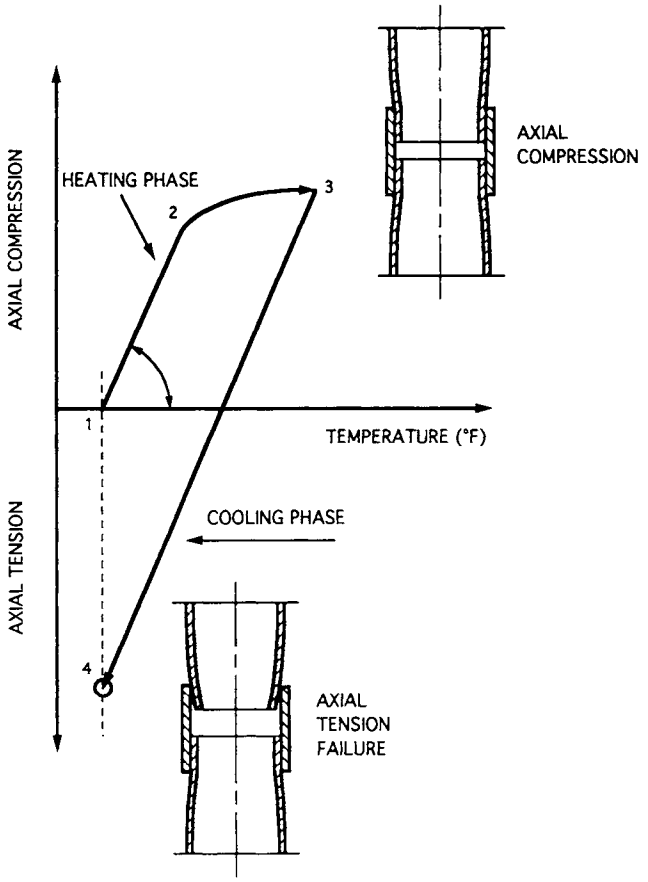

Fig. 4.27: Thermal cyclic loading diagram for elastic perfect plastic material and the failure of casing coupling.

of the casing while the well is shut-in or producing, relieves the compressive stress although the deformation produced during the steam injection phase creates a tensile stress as the casing temperature returns to the normal levels that existed prior to steam injection. Often, this tensile force buildup results in either joint failure at the last engaged pipe thread, or tensile failure by pin-end jumpout.

Willhite and Dietrich (1966) were the first to present a comprehensive method for assessing pipe failure under cyclic thermal loading. Holliday (1969) and Goetzen (1985) extended this work and presented a complete analytical treatment for the design of casing strings for use in steam stimulation wells.

In the following sections, the mechanism of casing failure is discussed in detail to provide a basis for selecting safe operating temperatures and related material properties. Next, a systematic method for estimating casing temperature during steam injection is presented. Finally, different techniques used to protect casing

Chapter 5

COMPUTER-AIDED CASING DESIGN

E.E. Maidla and **A.K. Wojtanowicz.**

5.1 OPTIMIZING THE COST OF THE CASING DESIGN

This chapter addresses the optimization theory that results in assuring the selection of the cheapest combination casing string (Fig. 5.1).

After calculating the loads that the casing will be subjected to, the engineer is faced with the decision of selecting an appropriate casing grade, weight and thread, such that these properties meet or exceed the calculated load conditions. This is not an easy task because many casings qualify and, therefore, the question arises: which casing is the best choice? The answer is: the one that can withstand all loads at the absolute (or ultimate) minimal cost possible. Finding this casing string is not straight-forward because the type of casing selected affects the calculated loads, which are a result of the wall thickness, and leads to an implicit solution. Sometimes simple cases may be solved by trial and error.

In the case of directional wells, the problem is further complicated because the loads and the trajectory length for a fixed surface location and target are a function of factors including drilling costs, risk assessment and casing program costs. Therefore, different spatial configurations will alter the final casing cost. Considering all well costs, might not be the critical issue but it is the specific topic addressed in this book.

The following questions must be answered here:

1. What is the absolute minimal cost of a combination casing string, given external loads, design factors, and casing supply?

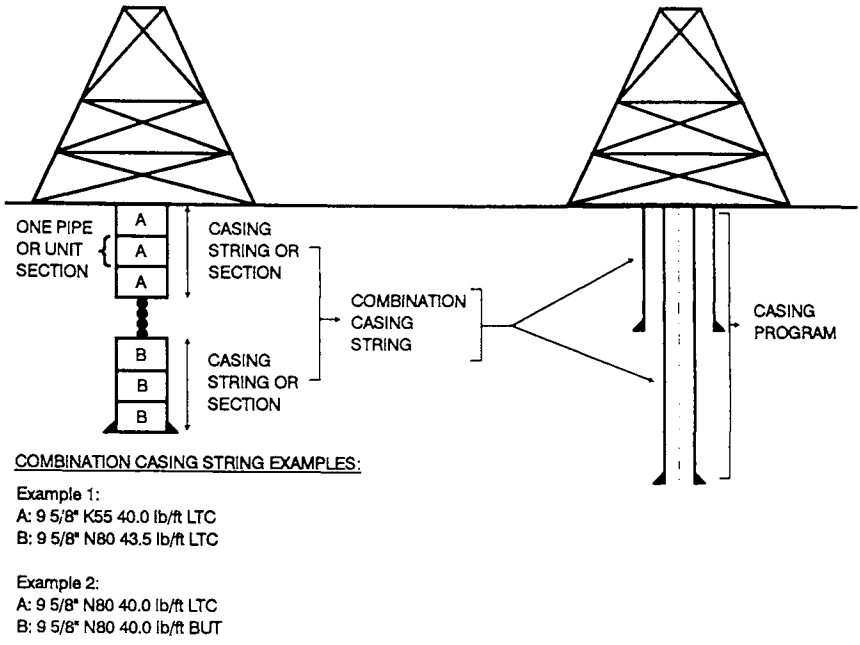

Fig. 5.1: Casing nomenclature.

2. What is the quantitative effect of certain decisions made by the casing designer (value of the design factors or number of sections) on the cost of casing?

3. How significant, given specific loads, is the conflict between the minimum weight and the minimum price criteria for selecting casing?

4. How do the external casing loads in directional wells affect casing cost?

5. What is the correlation between the directional well profile and its minimum cost?

6. What is the effect of the borehole friction factor (also referred to here as friction factor, and pseudo friction factor) on casing design in directional wells?

5.1.1 Concept of the Minimum Cost Combination Casing String

The casing program of most oil wells represents the greatest single item of expense in well cost. It can be as much as 18% of the completed well cost. Therefore,

even a small reduction in casing cost can save a considerable amount of money. This objective has traditionally been achieved by initially minimizing the number and length of strings and then by designing a combination casing string.

In vertical wells, optimumizing a combination casing string has been a challenge for casing designers. The optimization principle is based on considering the possibility of several combinations of grade, weight, thread and smallest allowable section length that satisfy some predetermined external load condition. Eventually, a combination casing string is selected that allows the minimum total cost. Insofar as there are a very large number of combinations, several stepwise procedures have been developed for casing grade, weight, and thread selection without explicit cost expressions. Generally it is observed, when following these procedures, that the casing price increases with increasing casing grade, weight, and strength (burst, collapse, pipe body yield, and connection). Thus, the lowest grade and weight casing, with the lowest possible values of mechanical strength, should give the lowest cost. Unfortunately, this procedure does not always yield the minimum cost simply because the casing grade, weight and cost cannot be simultaneously minimized.

5.1.2 Graphical Approach to Casing Design: Quick Design Charts

The Quick Design Charts allow for fast design of an entire combination casing string. An example is shown in Fig. 5.2. To obtain the string for a $9\frac{5}{8}$-in. hole drilled with 12-ppg mud, the casing length is entered on the abscissa and the individual casing string depths are displayed on the ordinate. For each depth section, the chart also provides the casing weight, grade and thread type.

A number of factors can limit the use of these charts. However, depending upon the way in which the charts were originally developed, the following limitations may apply:

- Load calculation criteria are not mentioned. The entire design may not meet the design demands or, on the contrary, may exceed the loading requirements and result in expensive, over-designed, combination casing strings.
- Limited in use to a given casing diameter.
- Limited in use to a given mud weight.
- Limited to vertical wells.
- If many manufacturers are considered, problems will arise when non-API casing is selected.

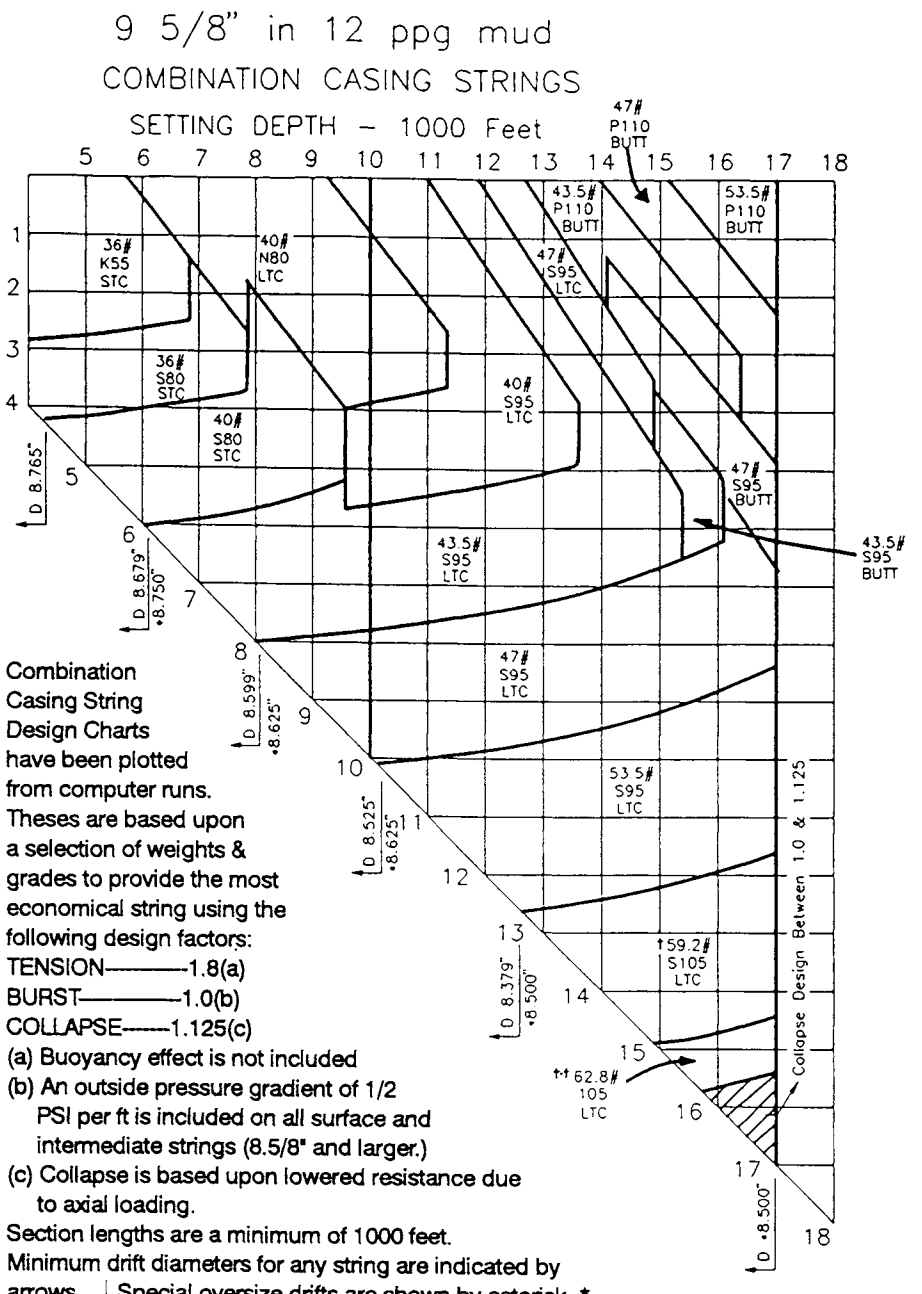

Fig. 5.2: Quick design chart. (Courtesy of Lone Star Steel Co.)

- Axial loads are not used to correct for collapse resistance.
- Buoyancy is not considered.
- The cost design criteria are not mentioned.
- The charts are restricted to a very particular load scenario.

EXAMPLE 5-1: The Use of Quick Design Charts.

Using Fig. 5.2 and Table B.1 (see Appendix B), design an intermediate combination string for a well that will be drilled in a well-known field. Examine all the possibilities and in particular, aim for the most economical design.

The following data for Example 5-1 was carefully chosen to illustrate the strength of the Quick Design Chart:

$9\frac{5}{8}$-in. intermediate casing set at 10,000 ft
Smallest casing section allowed: 1,000 ft
Design factor for burst: 1.0
Design factor for collapse: 1.125
Design factor for pipe body yield: 1.8
Production casing depth (next casing): 15,000 ft
Mud specific weight while running casing: 12 lb/gal
Equivalent circulating specific weight to fracture the casing shoe: 15 lb/gal
Heaviest mud specific weight to drill to the production depth: 15 lb/gal
blowout preventer working pressure: 5,000 psi

Although this data works well for Example 5-1, real data cannot always be slotted so readily into a Quick Design Chart as will be demonstrated in Exercises 6, 7, 8 and 9.

Solution:

The combination casing string obtained directly from Fig. 5.2 is shown in Table 5.1. The prices for the casings come from Table B.1, which is a printout of the file

Table 5.1: Quick Design Chart Solution to Example 5-1.

Depth, ft	Description	Price, US$/100 ft
10,000 - 7,757	47.0 lb/ft S-95 LTC	3,421.44
7,757 - 5,607	43.5 lb/ft S-95 LTC	3,007.88
5,607 - 3,850	40.0 lb/ft S-95 LTC	2,783.29
3,850 - 1,000	40.0 lb/ft N-80 LTC	2,565.56
1,000 - 0	40.0 lb/ft S-95 LTC	2,783.29

PRICE958.CPR. From Table 5.1, the total cost, US$ 291,266 and total buoyant weight, 345,570 lbf can be deduced easily.

A five-section string design is more complicated than it needs to be. Further analysis can be performed to check the cost of reducing this number. This particular design chart considers the decrease in collapse resistance due to axial loading. However,the chart is not based on API Bul. 5C3 (1989), which is much more restrictive for non-API casing grades (e.g. S-95). The chart uses a higher table ratings for collapse than those that would be obtained using the API's formulas. For API casing grades, a casing of equal weight can always be substituted for one of higher grade because the replacement will have a higher collapse resistance; this is not necessarily true for non-API casing grades. In this example, substituting N-80 with S-95 in the interval 3,850 to 1,000 ft results in the combination casing string shown in Table 5.2.

Table 5.2: Modified Quick Design Chart Solution to Example 5-1.

Depth, ft	Description	Price, $/100 ft
10,000 - 7,757	47.0 lb/ft S-95 LTC	3,421.44
7,757 - 5,607	43.5 lb/ft S-95 LTC	3,007.88
5,607 - 0	40.0 lb/ft S-95 LTC	2,783.29
Note 1: S-95 is not an API grade.		
Note 2: Collapse **was not** corrected in accordance with API Bul. 5C3, 1989.		

As in the earlier case, the total cost, $297,471 and total buoyant weight, 345,570 lbf are easily calculated from Table 5.2.

With this design, the engineer is challenged by the decision either to spend an extra $6,205 (an increase of 2.13% in cost) and limit the number of sections to three, or to retain the original chart-derived five-section string. A simplified string may mean cost savings elsewhere when field operations are considered together with minimum quantities to be purchased, logistics, etc.

5.1.3 Casing Design Optimization in Vertical Wells

Cost Optimization Criteria for Casing Design

The development of the model was based on both the casing design theory presented in the previous chapters and the theory of optimization (Roberts, 1964; and Phillips, 1976). The following design elements were used in the development of the computer model:

1. For casing loading patterns, the Maximum Load Method (Prentice, 1971) for surface, intermediate, and production casing is considered. An example detailing all of the calculations is provided in this chapter. At each depth, the maximum external and internal pressure values can be predetermined on the basis of the casing run, the specific weight of the drilling fluid (subsequently referred to as mud weight), the maximum anticipated mud weight that will be in contact with the casing, the fracture gradient at the casing seat, and the pore pressure at the bottom of the next casing depth.

2. For tension calculations the maximum surface running loads are considered. This is because the compression force acting at the lower end of the casing is at a minimum and, therefore, axial tension load is at a maximum. As depth increases, the hydrostatic pressure increases, as does the compressional force acting on the lower end of the casing.

3. Buoyancy and bending (see Lubinski's Eq. 2.39) are considered.

4. Shock and pressure test loadings are not considered.

The calculations for string design in directional wells have already been covered in Chapter 4 but will be addressed again later in this chapter because the computer program allows for some formula simplifications.

As mentioned above, the program in its present form does not consider the effects of shock or pressure test loading. However, the program code is provided to allow for further modification, if required.

Bending effects are considered using Lubinski's formula which considers the pipe to be supported at two points rather than in continuous contact with the borehole. This somewhat more complex approach to bending is easily implemented in a computer program, though not in manual calculations.

Finally, buckling effects have to be considered separately, as demonstrated in the examples in Chapter 3.

Casing Design Optimization Theory

The optimization model for the absolute minimum cost is first formulated in a general way and is then simplified.

The casing string is arbitrarily divided into N unit sections of equal length, Δl. In the computer program, this is done by dividing the measured depth by the casing length (a necessary input to the program). The casing design procedure starts at the bottom of the casing string and proceeds, in a stepwise manner, to

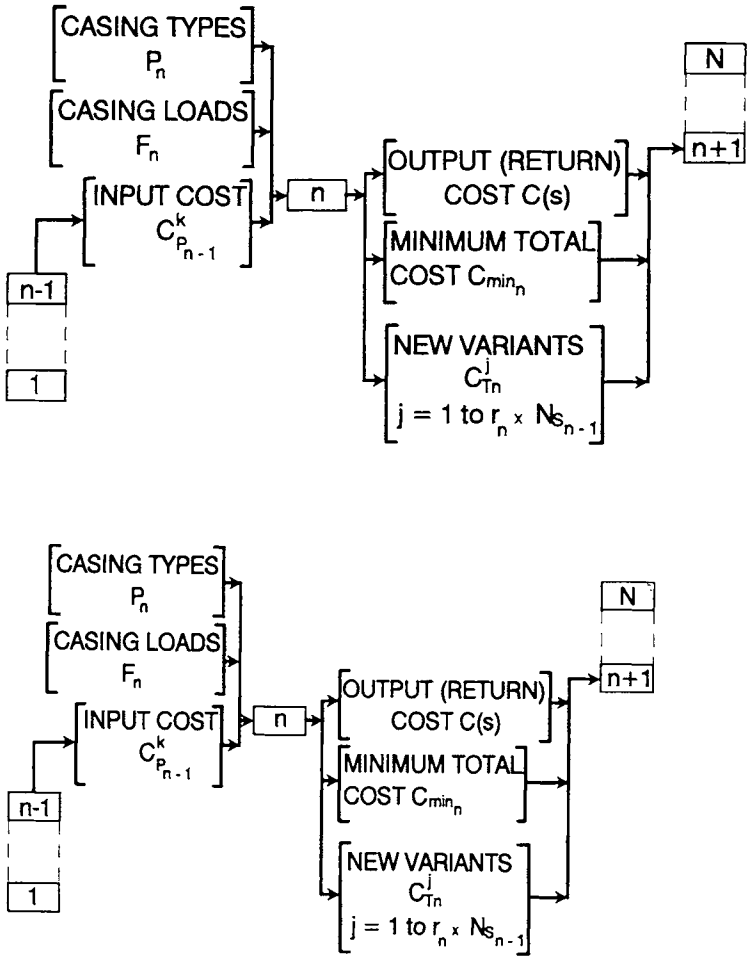

Fig. 5.3: Recurrent calculation procedure for optimum casing design.

the top (Fig. 5.3). The absolute minimum cost problem is formulated as follows:

$$C_T = \min_{s \in (1, N_{co})} C(s) \tag{5.1}$$

where:

C	=	cost of a particular combination casing string, US$.
C_T	=	minimum cost of combination casing string, US$.
N_{co}	=	total number of combination casing strings possible.
s	=	index of casing string combinations ($1 \leq s \leq N_{co}$)

Equation 5.1 must satisfy collapse pressure. burst pressure and axial load require-

ments (constraints):

$$(p_{cc})_n \geq R_c\,(\Delta p_c)_n \tag{5.2}$$
$$(p_{cb})_n \geq R_b\,(\Delta p_b)_n \tag{5.3}$$
$$(F_t)_n \geq R_t\,F_{A_n} \tag{5.4}$$

where:

Δp_c = differential collapse load, psi.
Δp_b = differential burst load, psi.
F_{A_n} = axial load at the top of the casing considered, lbf.
R_c, R_b, R_t = design factor[a] for collapse, burst and tension, respectively, d-less[b].
p_{cc} = collapse pressure rating corrected for biaxial stress (API Bul. 5C3, 1989), psi.
p_{cb} = either burst pressure rating corrected for biaxial or triaxial stress[c], psi
F_t = casing axial load rating (either pipe body yield or joint strength, whichever is smaller), lbf.

and

$$F_{A_n} = F_{A_{n-1}} + \Delta\ell\,W_n\,\cos(\alpha_n) + \sum_{j=1}^{N_a} F_j \tag{5.5}$$

where:

n = $1, 2 \cdots N$
N_a = number of axial forces considered

Note that only the nomenclature for the variables introduced in this chapter will be provided. Refer to Appendix 1 at the end of the book for the others.

The summation term in Eq. 5.5 represents all axial forces other than casing weight. These axial forces include, but are not limited to, buoyant force, linear belt friction (axial friction force generated to pull and move a belt around a curved surface), bending force, viscous drag (a result of the fluid viscosity effect), and stabbing effect (stabbing the casing into the formation while running it into the well). In vertical wells, the axial load is:

$$F_{A_n} = F_{A_{n-1}} + \Delta\ell\,W_n - 0.052\,\gamma_m\,l_n\,(A_{sn} - A_{sn-1}) \tag{5.6}$$

[a]The design factor (R) is selected by the engineer, whereas the safety factor (SF) is the value obtained after selecting the casing; this way $SF \geq R$.

[b]Dimensionless

[c]Normally triaxial stress is not corrected for. Triaxial stress correction, which is appropriate for designing casing for deep wells is left up to the engineer to introduce into the program.

where:

A_s = pipe cross-sectional area, in^2.
γ_m = specific weight of the well fluid, lb/gal.

For the force calculation, n varies from 0 to N because its effect is considered at both ends of the casing; therefore, for N pipes in a combination casing string, the program calculates $N + 1$ forces.

Thus for vertical wells, where externally generated forces are not significant (friction forces), the initial conditions are:

F_{A_0} = $0.052\,\gamma_m\,D_T\,A_{S_0}$, the hydrostatic forces acting on the first pipe.
A_{S_0} = A_{S_1}, the initial condition for the cross-sectional area.

Referring again to Eq. 5.6, it can be seen that F_{A_1} refers to the force acting on the top of the first casing. For directional wells, the conditions are changed because the hydraulic force acting on the casing end does not induce normal forces that would, in turn, generate friction forces.

At each unit section n, the set of the best casing is selected from the available casing supply. The best casing includes the cheapest and the lightest ones. The best casing choice for any unit section depends on all previous decisions, i.e., $n-1, n-2, \cdots, 1$ due to the additive nature of axial loads. Such a problem, from the standpoint of the optimization theory, is classified as the multistage decision process and is solved using a computer and the recurrent technique of dynamic programming. The definitions and recurrent formulas are covered in General Theory of Casing Optimization.

The general solution described above is impractical. It requires a relatively large amount of computer memory and time-consuming calculations. Also, large number of variants may be generated as the recursions progress. Therefore, the only practical solution to this problem is to reduce the number of casing variants.

Major Conflict in Casing Design: Weight vs Price

The analysis of the iterative procedure for casing design shows that the only source of the multitude of casing variants is the dilemma between casing weight and casing price. This dilemma has been observed by many casing designers, and is known as the "Weight/Price Conflict". The conflict arises from the observation that the decision made in favor of the cheapest casing for any bottom section of casing string may eventually yield a more expensive combination casing string. On the other hand, the combination casing string with a lighter (yet more expensive) lower part may be cheaper overall due to the reduction in axial load supported by the upper casing strings. The concept of the weight/price conflict is illustrated in Fig. 5.4. Insofar as the conflict cannot be resolved before the casing

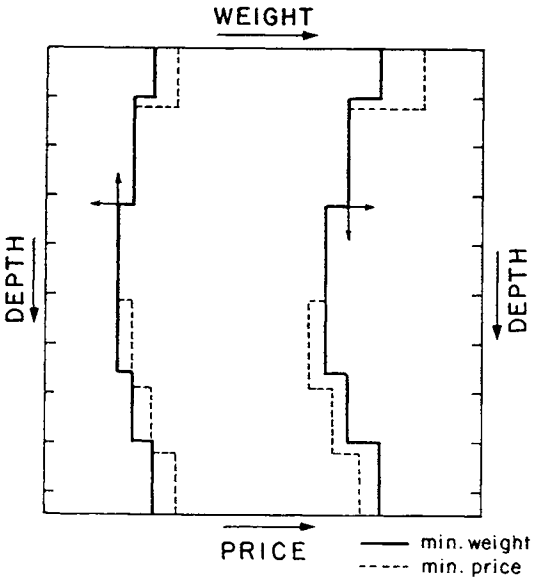

Fig. 5.4: Hypothetical conflict between minimum weight and minimum price design methods. (After Wojtanowicz and Maidla, 1987; courtesy of the SPE.)

design is completed, every casing that is lighter than the cheapest one has to be memorized at each step of the casing design, thereby generating new variants.

Over the course of a large number of calculations, however, it was noticed that the weight/price conflict depends on the price structure of each steel mill. Two examples will be solved to illustrate this observation. The first will be solved for a particular case where the conflict was present when using API grades only. Another will be solved for a case which shows no conflict of design methods when API grades were considered together with commercial grades from a particular steel mill.

Theory for the Minimum Weight Casing Design Method

The minimum weight casing design method is based on selecting the cheapest casing from among the lightest available. Priority is given to the weight over the price. Mathematically, this can be written as:

$$C_T = \Delta\ell \sum_{n=1}^{N} P_n \tag{5.7}$$

$$P_n = \min_{r\in(a,b)} P_n^r \tag{5.8}$$

$$P_n^r = \min_{m\in(c,d)} W_n^m \tag{5.9}$$

where:

a = the lowest value of r within a given weight m.

b = the highest value of r within a given weight m.
c = the lowest value of m that satisfies load requirements.
C = cost, US$.
d = the highest value of m that satisfies load requirements.
m = index of casing weight that satisfies load requirements.
n = number of the casing section being designed.
$n = 3$ means the third pipe from lower end.
P = distributed price, US$/100ft.
r = index of casing that satisfies load requirements.
W = distributed weight, lb/ft.

EXAMPLE 5-2: Understanding the Notation

For a particular well, the design factors for burst, collapse, and pipe body yield are 1.1, 1.125 and 1.5, respectively. The loads at the point of interest are 5,020 psi for burst, 6,000 psi for collapse and 881,333 lbf for tension. The casings available are listed in Table B.1 (Appendix B) (For this example only, the table values do not need to be corrected for axial loads.). The measured depth of the well is 10,000 ft, and the individual pipe length is 40 ft. Using this information, answer the following:

1. Define N_p, N_W and N, and determine their values.

2. What are the possible values for r and for m?

3. What are the values of r when $m = 3, 5, 7$ and 9 ?

4. Why are the values of $r = 53$ and 79 not considered to be viable alternatives?

Solution:

1. N_p is the number of all casings to be considered in the design. From Table B.1 this number is 98. N_W is the number of casing weights within the casing file. The following weights are in the file: 36, 40, 43.5, 47, 53.5, 58.4, 61.0 lb/ft; thus, $N = 7$. N is the number of pipes of casing (or unit sections) in the combination casing string; therefore, $N \approx 10{,}000 \div 40 = 250$. ($N$ is only approximately equal to 250 because casing lengths are not always 40 ft even for the common case of API length range 3 (see page 12), and certainly this is not the case for API ranges 1 and 2. Throughout this chapter the casing length is assumed to be 40 ft.

2. The design loads are:

(a) For burst, $5,020 \times 1.1 = 5,522$ psi.

(b) For collapse, $6,000 \times 1.125 = 6,750$ psi.

(c) For tension, $881,333 \times 1.5 = 1,322,000$ lbf.

Selecting from Table B.1 (Appendix B), the values for r and m that exceed these requirements are found:

(a) $r = 61, 62, 63, 64, 70, 71, 72, 73, 74, 75, 76, 77, 78, 80, 81, 82, 83, 84, 85, 86, 87, 88, 89, 90, 91, 92, 93, 94, 95, 96, 97, 98.$

(b) $m = 4, 5, 6, 7.$

In the case of m, the lightest casing weight that meets load requirements is 47 lb/ft; the 3 weights below this 36, 40 and 43.5 lb/ft, do not.

3. From the previous answer, $m = 3$ is not a viable option because it fails to meet the load constraints and, therefore, no r's within this weight range will either. For $m = 5$, the corresponding r values are 61, 62, 63, 64, 70, 71, 72, 73, 76, 77, and 78 . Finally, for $m = 7$, the r values are 80, 82, 87, 89, 90, 92, 94, 95, 97, and 98.

4. Neither $r = 53$ nor $r = 9$ meets the design requirements. Specifically, $r = 53$ does not meet the collapse constraint and $r = 79$ does not meet the pipe body yield constraint due to the thread strength limitations.

Program Description and Procedure for Minimum Weight Design

Within a given set of load constraints, the lightest casing is chosen. In the computer program provided, this is achieved through a routine that sorts the casing PRICE.DAT table first by weight, and then within the same weight category by price.

This particular computer program was developed and written in FORTRAN 77 and can be run on any personal computer. The source code is provided with the disk so that it can be modified if required; however, it is suggested that rather than using the master disk, a backup should be used.

EXAMPLE 5-3: Minimum Weight Design Method

Using the computer program, rework Example 5-1 to design a casing string based on the minimum weight design method.

Solution:

The program CSG3DAPI.EXE uses the API criteria for collapse correction calculations (API Bul. 5C3, 1989). First, create an ASCII file named CSGLOAD.DAT

Table 5.3: Combination casing string – minimum weight design method (Example 5-3).

```
                    INTERMEDIATE CASING DESIGN
THE WELL DATA USED IN THIS PROGRAM WAS:
     .EQUIVALENT FRACTURE GRADIENT AT CASING SEAT=15.0 PPG
     .BLOW OUT PREVENTER RESISTANCE= 5000. PSI
     .DENSITY OF THE MUD THE CASING IS SET IN=12.0 PPG
     .DENSITY OF HEAVIEST MUD IN CONTACT WITH THIS CASING=15.0 PPG
     .TRUE VERTICAL DEPTH OF THE NEXT CASING SEAT=15000. FT
     .PORE PRES. AT NEXT CASING SEAT DEPTH= 9.0 PPG
     .MINIMUM CASING STRING LENGTH= 1000. FT
     .DESIGN FACTOR: BUR=1.000; COL=1.125; YIELD=1.800
     .TRUE VERTICAL DEPTH OF THE CASING SEAT=10000. FT
     .DESIGN METHOD: MINIMUM WEIGHT

9 5/8" CASING PRICE LIST. FILE REF.:PRICE958.CPR
MAIN PROGRAM: CSG3DAPI

TOTAL PRICE=299031. U.S.DOLLARS
TOTAL STRING BUOYANT WEIGHT=344841. LB
DI=10000- 8520   L= 1480 NN= 6   W=43.5 M=3 MB=1.73 MC=1.13 MY=19.1   P=2983.77
DI= 8520- 7080   L= 1440 NN=13   W=43.5 M=3 MB=1.80 MC=1.13 MY=11.5   P=3216.91
DI= 7080- 5640   L= 1440 NN=18   W=43.5 M=3 MB=1.86 MC=1.15 MY= 8.9   P=3488.41
DI= 5640- 4640   L= 1000 NN=13   W=43.5 M=3 MB=1.49 MC=1.13 MY= 6.3   P=3216.91
DI= 4640- 3640   L= 1000 NN= 6   W=43.5 M=2 MB=1.18 MC=1.14 MY= 3.7   P=2879.99
DI= 3640- 2640   L= 1000 NN= 6   W=40.0 M=3 MB=1.00 MC=1.25 MY= 3.5   P=2743.75
DI= 2640- 1640   L= 1000 NN=13   W=40.0 M=2 MB=1.18 MC=1.62 MY= 2.9   P=2783.29
DI= 1640- 0      L= 1640 NN= 6   W=40.0 M=2 MB=1.04 MC=2.37 MY= 2.1   P=2565.56

THE MEANING OF SYMBOLS:
     .DI, DEPTH INTERVAL, (FT)
     .L, LENGTH, (FT)
     .NN, TYPE OF GRADE (SEE THE GRADE CODE BELOW)
     .W, UNIT WEIGHT, (LB/FT)
     .M IS THE TYPE OF THREAD: 1...SHORT; 2...LONG; 3...BUTTRESS
     .MB, MC, MY, MINIMUM SAFETY FACTORS FOR BURST, COLLAPSE, AND YIELD
     .P, UNIT CASING PRICE.....$/100FT
GRADE CODE:
NN 1= ...H40     NN 2= ...J55     NN 3= ...K55     NN 4= ...C75     NN 5= ...L80
NN 6= ...N80     NN 7= ...C95     NN 8= ..P110     NN 9= ..V150     NN13= ...S95
NN14= .CYS95     NN15= ..S105     NN16= ...S80     NN17= ..SS95     NN18= .LS110
NN19= .LS125
```

that contains the data for the design. The instructions for how to do this are shown in the program listing itself under CSG3DAPI.FOR. However, the CSGAPI.BAT file is a batch file formulated to help edit the necessary data and then to run the program. For this example only, a step-by-step walk through the program will be made.

Again, following the instructions in CSGAPI.BAT, a price file named PRICE.DAT must be created. The price file used in this example is shown in Table B.1 (Appendix B). In addition to the price, the file PRICE.DAT contains the casing properties necessary to undertake the design.

To proceed to this point:

1. Insert the program disk.
2. Type "CSGAPI". A screen will appear titled "PROGRAM PRICE."
3. Choose [1] to read a file. Hit enter.

Table 5.4: Combination casing string - minimum weight design method: 3 Sections (Example 5-3).

```
                    INTERMEDIATE CASING DESIGN
THE WELL DATA USED IN THIS PROGRAM WAS:
     .EQUIVALENT FRACTURE GRADIENT AT CASING SEAT=15.0 PPG
     .BLOW OUT PREVENTER RESISTANCE= 5000. PSI
     .DENSITY OF THE MUD THE CASING IS SET IN=12.0 PPG
     .DENSITY OF HEAVIEST MUD IN CONTACT WITH THIS CASING=15.0 PPG
     .TRUE VERTICAL DEPTH OF THE NEXT CASING SEAT=15000. FT
     .PORE PRES. AT NEXT CASING SEAT DEPTH= 9.0 PPG
     .MINIMUM CASING STRING LENGTH= 2500. FT
     .DESIGN FACTOR: BUR=1.000; COL=1.125; YIELD=1.800
     .TRUE VERTICAL DEPTH OF THE CASING SEAT=10000. FT
     .DESIGN METHOD: MINIMUM WEIGHT

9 5/8" CASING PRICE LIST. FILE REF.:PRICE958.CPR
MAIN PROGRAM: CSG3DAPI

TOTAL PRICE=313169. U.S.DOLLARS
TOTAL STRING BUOYANT WEIGHT=355246. LB
DI=10000- 7080   L= 2920 NN=13   W=43.5 M=3 MB=1.80 MC=1.13 MY=11.5   P=3216.91
DI= 7080- 4560   L= 2520 NN=18   W=43.5 M=3 MB=1.72 MC=1.15 MY= 7.1   P=3488.41
DI= 4560- 0      L= 4560 NN= 6   W=43.5 M=2 MB=1.09 MC=1.16 MY= 2.3   P=2879.99

THE MEANING OF SYMBOLS:
     .DI, DEPTH INTERVAL, (FT)
     .L, LENGTH, (FT)
     .NN, TYPE OF GRADE (SEE THE GRADE CODE BELOW)
     .W, UNIT WEIGHT, (LB/FT)
     .M IS THE TYPE OF THREAD: 1...SHORT; 2...LONG; 3...BUTTRESS
     .MB, MC, MY, MINIMUM SAFETY FACTORS FOR BURST, COLLAPSE, AND YIELD
     .P, UNIT CASING PRICE.....$/100FT

GRADE CODE:
NN 1= ...H40     NN 2= ...J55     NN 3= ...K55     NN 4= ...C75     NN 5= ...L80
NN 6= ...N80     NN 7= ...C95     NN 8= ..P110     NN 9= ..V150     NN13= ...S95
NN14= .CYS95     NN15= ..S105     NN16= ...S80     NN17= ..SS95     NN18= .LS110
NN19= .LS125
```

4. Choose PRICE958.CPR. Hit enter.

5. Choose [4] to Exit. Hit enter.

6. A screen will appear titled "PROGRAM CSGLOAD."

7. Choose [3] to initialize the data. Input the requested information. Note that even if the well is vertical, the current version of the program will ask for deviated hole data; just answer with a zero. If unsure of the data to enter for this example, check with Table 5.4.

8. When the data input is complete, an input file will be created and the "PROGRAM CSGLOAD" screen will reappear. When creating the data files, try to develop a logical system of naming them.

9. Choose [4]. Hit enter.

10. The program will run provided the input data is correct.

11. The result will be outputted to the screen and to a file DESIGN.OUT. If there are likely to be multiple runs, this file needs to be renamed after each run to avoid overwriting it in the subsequent run.

As a result of running the program CSG3DAPI, (using the CSGAPI.BAT file) a file named DESIGN.OUT, as shown in Table 5.3, is generated. This file contains the following information:

- The casing string being designed. In this case, an intermediate casing string.
- A summary of the inputted well data used to run the program.
- The design criteria. Here, it is the minimum weight criteria.
- The name of the price file used and the main program name. In this example, PRICE958.DAT and CSG3DAPI were used, respectively.
- The casing string's total price of $299,031 and buoyant weight of 344,841 lbf, are also listed.
- At this point, the sectional breakdown of the string is given. The first section for depth interval (DI), 10,000 ft to 8,520 ft with a length of 1,480 ft, is an N-80 43.5 lb/ft Buttress thread that costs $2,983.77/100 ft. In this interval, the lowest actual safety factors for burst (thread or body, whichever is the smallest), collapse and yield (thread or body, whichever is the smallest) are 1.73, 1.13 and 19.1, respectively.
- The remainder of the output is an explanation of the nomenclature used in the file.

For the lower part of the casing string, the limiting constraint is collapse. The lowest of the three safety factors, the value for collapse, equals the collapse design factor given earlier, whereas both the burst and yield constraint values are higher than their design safety factors. Near the surface, however, the limiting constraint is now burst loading.

Another point to observe is that the design suggests a tapered string (combination casing string) with eight main sections, all of which have lengths above the required minimum of 1,000 ft. As in the previous example using the Quick Design Charts, it is reasonable to try to keep the number of sections down to three. In this particular program, the desired number of sections is obtained by altering the minimum length and observing the output. Of course, this requirement can be built into the main program to avoid the trial and error procedure suggested above. However, the decision of whether or not to do so is left up to the engineer, as the source code is included on the disk package. In this example, by altering the minimum length requirement to 2,500 ft, the desired result is achieved as shown in Table 5.4.

Prior to comparing the above results to the Quick Design Chart method, several program refinements will be illustrated with further examples. Finally, comparison and cost analysis of all the methods are made.

Theory on the Minimum Cost Casing Design Method

The minimum cost casing design method always selects the cheapest casing that meets the load requirements. Mathematically, this can be written as:

$$C_T = \Delta\ell \sum_{n=1}^{N} P_n \tag{5.10}$$

$$P_n = \min_{r\in(a,b)} P_n^r \tag{5.11}$$

where:

a = the lowest value of r that satisfies load requirements.
b = the highest value of r that satisfies load requirements.

Program Description and Procedure for the Minimum Cost Design

Within a given set of load constraints, the selection is made such that the cheapest pipe is chosen. In the computer program, this is achieved by sorting the casing PRICE.DAT table by price.

EXAMPLE 5-4: Minimum Price Design Method

Again using the computer program, this time rework Example 5-1 to design a casing string based on the minimum price design method.

Solution:

The program CSG3DAPI uses the API approved method for collapse correction calculations (API Bul. 5C3, 1989). First create an ASCII file named CSGLOAD. DAT, which contains the required design data. The batch file created to help edit the necessary data and then run the program is called CSGAPI.BAT, but the method is the same as detailed in Example 5-3.

After running the program CSG3DAPI, a file named DESIGN.OUT, as shown in Table 5.5, is generated.

The format of the output (Table 5.5) is the same as previously described in Example 5-3, except that this time the design is different from the earlier minimum weight design. The reason for this is that the design criteria was changed to include minimum cost.

In this example, seven intervals of grades N-80 (NN6) and S-95 (NN13) are suggested. Consider the design output for the depth interval from 8,520 to 5,440 ft; the only difference between the two casing sections is thread type: long thread and buttress, respectively. To analyze why the change in thread type occurred, refer to Table B.1 (Appendix B). First identify the line that contains casing N-80.

Table 5.5: Combination casing string - minimum price design method (Example 5-4).

```
                    INTERMEDIATE CASING DESIGN
THE WELL DATA USED IN THIS PROGRAM WAS:
      .EQUIVALENT FRACTURE GRADIENT AT CASING SEAT=15.0 PPG
      .BLOW OUT PREVENTER RESISTANCE= 5000. PSI
      .DENSITY OF THE MUD THE CASING IS SET IN=12.0 PPG
      .DENSITY OF HEAVIEST MUD IN CONTACT WITH THIS CASING=15.0 PPG
      .TRUE VERTICAL DEPTH OF THE NEXT CASING SEAT=15000. FT
      .PORE PRES. AT NEXT CASING SEAT DEPTH= 9.0 PPG
      .MINIMUM CASING STRING LENGTH= 1000. FT
      .DESIGN FACTOR: BUR=1.000; COL=1.125; YIELD=1.800
      .TRUE VERTICAL DEPTH OF THE CASING SEAT=10000. FT
      .DESIGN METHOD: MINIMUM COST

9 5/8" CASING PRICE LIST. FILE REF.:PRICE958.CPR
MAIN PROGRAM: CSG3DAPI

TOTAL PRICE=288651. U.S.DOLLARS
TOTAL STRING BUOYANT WEIGHT=357075. LB
DI=10000- 8520   L= 1480 NN= 6   W=43.5 M=3 MB=1.73 MC=1.13 MY=19.1   P=2983.77
DI= 8520- 6440   L= 2080 NN= 6   W=47.0 M=2 MB=1.56 MC=1.13 MY= 6.8   P=3014.47
DI= 6440- 5440   L= 1000 NN= 6   W=47.0 M=3 MB=1.45 MC=1.22 MY= 6.4   P=3223.84
DI= 5440- 4440   L= 1000 NN= 6   W=47.0 M=2 MB=1.35 MC=1.20 MY= 4.3   P=3014.47
DI= 4440- 3440   L= 1000 NN= 6   W=43.5 M=2 MB=1.16 MC=1.18 MY= 3.4   P=2879.99
DI= 3440- 2360   L= 1080 NN=13   W=40.0 M=2 MB=1.18 MC=1.25 MY= 3.1   P=2783.29
DI= 2360- 0      L= 2360 NN= 6   W=40.0 M=2 MB=1.00 MC=1.66 MY= 2.1   P=2565.56

THE MEANING OF SYMBOLS:
      .DI, DEPTH INTERVAL (FT)
      .L, LENGTH (FT)
      .NN, TYPE OF GRADE (SEE THE GRADE CODE BELOW)
      .W, UNIT WEIGHT (LB/FT)
      .M IS THE TYPE OF THREAD: 1...SHORT; 2...LONG; 3...BUTTRESS
      .MB, MC, MY, MINIMUM SAFETY FACTORS FOR BURST, COLLAPSE, AND YIELD
      .P, UNIT CASING PRICE.....$/100FT

GRADE CODE:
NN 1= ...H40     NN 2= ...J55     NN 3= ...K55     NN 4= ...C75     NN 5= ...L80
NN 6= ...N80     NN 7= ...C95     NN 8= ..P110     NN 9= ..V150     NN13= ...S95
NN14= .CYS95     NN15= ..S105     NN16= ...S80     NN17= ..SS95     NN18= .LS110
NN19= .LS125
```

47.00 lb/ft long thread (M=2), at a cost of \$3,014.47/100 ft; then identify the line containing casing N-80, 47.00 lb/ft Buttress (M=3), at a cost of \$3,223.84/100 ft. Notice that both casings have the same collapse and burst resistances. Returning to the computer output again (Table 5.5), it is apparent that the collapse rating is the limiting restriction that determined the change from long threads to buttress threads. Given that the collapse ratings for both casings is the same, why is there a change from long thread to more expensive Buttress thread?

The answer lies in the program's use of API Bul. 5C3 (1989) formulas to calculate the collapse resistance. Instead of using the tabular value for collapse resistance shown in manufacturer's specifications, API Bul. 5C3 (1989) calculates the collapse resistance based on the yield strength value. The algorithm used in the program will be explained later; suffice to say that, in this example, the pipe body yield in Table B.1 (Appendix B) was chosen as the smaller of the pipe body and the joint strength.

As in the previous examples, the solutions for a three-section string were inves-

Table 5.6: Combination casing string - minimum price design method: Three sections (Example 5-4).

```
                    INTERMEDIATE CASING DESIGN
THE WELL DATA USED IN THIS PROGRAM WAS:
     .EQUIVALENT FRACTURE GRADIENT AT CASING SEAT=15.0 PPG
     .BLOW OUT PREVENTER RESISTANCE= 5000. PSI
     .DENSITY OF THE MUD THE CASING IS SET IN=12.0 PPG
     .DENSITY OF HEAVIEST MUD IN CONTACT WITH THIS CASING=15.0 PPG
     .TRUE VERTICAL DEPTH OF THE NEXT CASING SEAT=15000. FT
     .PORE PRES. AT NEXT CASING SEAT DEPTH= 9.0 PPG
     .MINIMUM CASING STRING LENGTH= 2500. FT
     .DESIGN FACTOR: BUR=1.000; COL=1.125; YIELD=1.800
     .TRUE VERTICAL DEPTH OF THE CASING SEAT=10000. FT
     .DESIGN METHOD: MINIMUM COST

9 5/8" CASING PRICE LIST. FILE REF.:PRICE958.CPR
MAIN PROGRAM: CSG3DAPI

TOTAL PRICE=301398. U.S.DOLLARS
TOTAL STRING BUOYANT WEIGHT=372510. LB
DI=10000- 6480   L= 3520 NN= 6   W=47.0 M=2 MB=1.57 MC=1.13 MY= 6.7   P=3014.47
DI= 6480- 3960   L= 2520 NN= 6   W=47.0 M=3 MB=1.31 MC=1.22 MY= 4.7   P=3223.84
DI= 3960- 0      L= 3960 NN= 6   W=43.5 M=2 MB=1.09 MC=1.31 MY= 2.2   P=2879.99


THE MEANING OF SYMBOLS:
     .DI, DEPTH INTERVAL (FT)
     .L, LENGTH (FT)
     .NN, TYPE OF GRADE (SEE THE GRADE CODE BELOW)
     .W, UNIT WEIGHT (LB/FT)
     .M IS THE TYPE OF THREAD: 1...SHORT; 2...LONG; 3...BUTTRESS
     .MB, MC, MY, MINIMUM SAFETY FACTORS FOR BURST, COLLAPSE, AND YIELD
     .P, UNIT CASING PRICE.....$/100FT

GRADE CODE:
NN 1= ...H40    NN 2= ...J55    NN 3= ...K55    NN 4= ...C75    NN 5= ...L80
NN 6= ...N80    NN 7= ...C95    NN 8= ..P110    NN 9= ..V150    NN13= ...S95
NN14= .CYS95    NN15= ..S105    NN16= ...S80    NN17= ..SS95    NN18= .LS110
NN19= .LS125
```

tigated; the results are shown in Table 5.6. The only difference between the two bottom sections is in the thread type. The change of the thread type indicates that the yield strength rather than body yield was considered in the calculations. Thus, the limiting constraint is again the collapse resistance. Whether or not to consider the joint strength in the collapse calculations is debatable because it will depend on the manner in which the joint fails. Insofar as this information is not available in the tables, the result is somewhat conservative.

Comparison of the Results

The results of the three-section combination string calculated in the last three examples will be compared and explained. In this particular example only, the casing load plots for collapse and burst are calculated to aid in the analysis. The results are shown in Figs. 5.5 and 5.6.

Casing Loads for Collapse

The load line is given by connecting points A, B, and C with a straight line.

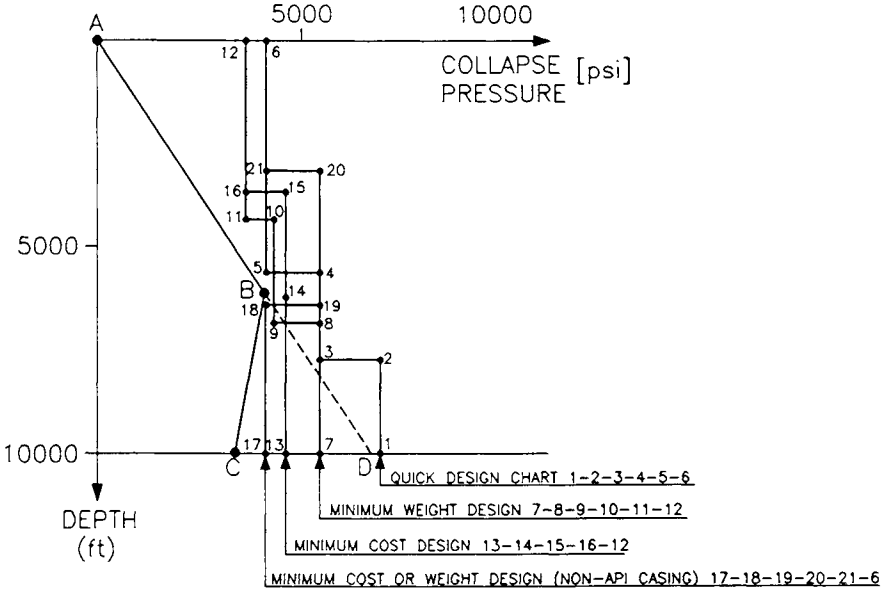

Fig. 5.5: Casing load study for collapse.

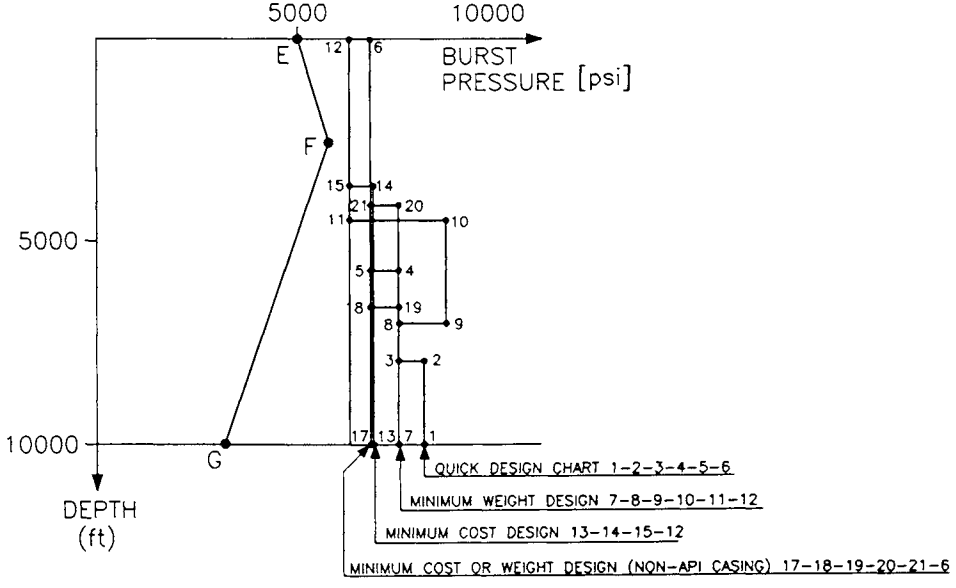

Fig. 5.6: Casing load study for burst.

1. Depth (D) and pressure (p) at point A:

   $D_A = 0 \qquad p_A = 0.$

2. Depth and pressure at point B:

   (a) To determine the depth at B, calculate the height (H) of the hydrostatic column of the heaviest mud used to drill to the next casing setting depth that equals the formation pore pressure at that depth:

   $0.052 \times 15 \times H = 0.052 \times 9.0 \times 15{,}000$

   $H = 9{,}000$ ft

   $D_B = 15{,}000 - 9{,}000 = 6{,}000$ ft

   (b) Pressure: $p_B = 0.052 \times 6{,}000 \times 12 \times 1.125 = 4{,}212$ psi.

3. Depth and pressure at point C:

   $D_C = 10{,}000$ ft

   $p_C = (0.052 \times 10{,}000 \times 12 - 0.052 \times 4{,}000 \times 15) \times 1.125 = 3{,}510$ psi.

4. Point D lies at the intersection of the straight line that passes through points A and B and the straight line that passes through point C, parallel to the collapse pressure axis.

Casing Loads for Burst

The load line is determined by using a straight line to connect the points E, F, and G in Fig. 5.6.

1. Depth and pressure at point E:

   $D_E = 0$

   The surface burst pressure is either the lowest value of the BOP working pressure or the surface pressure of gas column inside the casing with fracturing pressure at the casing seat.

   (a) Pressure at the casing seat (p_{E1})

   $p_{E1} = 0.052 \times 15 \times 10{,}000 = 7{,}800$ psi.

   (b) Pressure at the surface (p_{E2})

   Consider a static column of methane gas (M=16) at the surface, a bottomhole temperature calculated by assuming an average surface temperature of 70°F, and a temperature gradient of 1.2°F/100 ft. Using the equation of state for ideal gas behavior, the following formula can be derived:

$$p_{E2} = (p_{E1} + 14.7) \times e^{\left(\frac{-D}{51{,}182 + 1.159 \times D}\right)} - 14.7 \text{ psi}$$

where the pressures are in psig and the depth is in feet. Therefore:

$$p_{E2} = (7,800 + 14.7) \times e^{\left(\frac{-10,000}{51.182 + 1.159 \times 10,000}\right)} - 14.7 = 6,649 \text{ psi}$$

The BOP working pressure is given as (p_{E3}):

$p_{E3} = 5,000$ psi.

The smallest value, corrected by the design factor, is selected:

$p_E = 5,000 \times DFB = 5,000 \times 1.0 = 5,000$ psi.

where DFB is the design factor for burst.

2. Depth and pressure at point F:

   At point F, pressure equilibrium is achieved with the gas column, the BOP maximum working pressure and the heaviest mud gradient in contact with the internal casing wall.

   Using a stright line to approximate the pressure curve between p_{E1} and p_{E2} gives:

$$D_F = \frac{p_{E3} - p_{E2}}{\frac{p_{E1} - p_{E2}}{D_G} - 0.052 \times \gamma_2}$$

   where γ_2 (ppg) is the specific weight ("density") of the heaviest mud in contact with the internal casing wall and D_G is the total depth. In the following example, D_G is 10,000 ft. Thus:

$$D_F = \frac{5,000 - 6,649}{\left(\frac{7,800 - 6,649}{10,000}\right) - 0.052 \times 15.0} = 2,480 \text{ ft.}$$

   Assuming that a backup pressure gradient of 0.465 psi/ft is acting on the external casing wall, the pressure at point F is equal to

$$p_F = (5,000 + 0.052 \times 15 \times 2,480 - 0.465 \times 2,480) \times 1.0 = 5,781 \text{ psi.}$$

3. Depth and pressure at point G:

   $D_G = 10,000$ ft

   $p_G = (p_{E1} - 0.465 \times D_G) \times DFB$

   $p_G = (7,800 - 0.465 \times 10,000) \times 1.0 = 3,150$ psi.

These values and the casing properties (Table B.1, Appendix B) are plotted in Figs. 5.5 and 5.6.

The results of the different design methods are shown in Table 5.7[a]. Notice that in none of the designs has the load constraints been violated (In doing this analysis.

[a]The data above was purposely chosen to emphasize the strength of the Quick Design Chart. Exercises 6, 7, 8, and 9, are formulated more realistically for cases in which the data does not readily fit the Quick Design Chart scenario.

Table 5.7: Design comparison of different methods.

Length, ft Bottom to Top	Description	Burst (psi)	Collapse (psi)
Quick Design Charts - $ 297,471			
2,243	S-95, 47.0 lb/ft LTC	8,150	7,100
2,150	S-95, 43.5 lb/ft LTC	7,510	5,600
5,607	S-95, 40.0 lb/ft LTC	6,820	4,230
Note: Collapse **was not** corrected according to API Bul. 5C3 (1989).			
Minimum Weight Design - API - $ 313,169			
2,920	S-95, 43.5 lb/ft BUT	7,510	5,600
2,520	LS-110, 43.5 lb/ft BUT	8,700	4,420
4,560	N-80, 43.5 lb/ft LTC	6,330	3,810
Note: Collapse according to API Bul. 5C3 (1989).			
Minimum Cost Design - API - $ 301,398			
3,520	N-80, 47.0 lb/ft LTC	6,870	4,750
2,520	N-80, 47.0 lb/ft BUT	6,870	4,750
3,960	N-80, 43.5 lb/ft LTC	6,330	3,810
Note: Collapse according to API Bul. 5C3 (1989).			
Cheapest Solution			
Min. Cost and Min. Weight Design - $ 283,989			
3,200	S-95, 40.0 lb/ft LTC	6,820	4,230
2,520	S-95, 43.5 lb/ft LTC	7,510	5,600
4,280	S-95, 40.0 lb/ft LTC	6,820	4,230
Note: Collapse based on a modification to API Bul. 5C3 (1989).			

care must be taken to account for collapse reduction due to the axial loading.). This being the case, why is the quick design chart design less expensive than the two computer designs? Furthermore, not only is it less expensive, but the mechanical properties for burst and collapse are, in most instances, superior to the computer-generated designs.

The reason for this difference is that until now the API Bul. 5C3 (1989) has been used to calculate the corrected collapse properties of casing that were developed according to API tubular specifications. In these calculations, the corrected collapse rating (considering axial loads) was found by using the yield stress of the pipe and by disregarding manufacturing processes or other factors that might increase the total collapse rating. For example, compare the API casing collapse rating for C-95, 40 lb/ft of 3,330 psi against a non-API casing collapse rating for

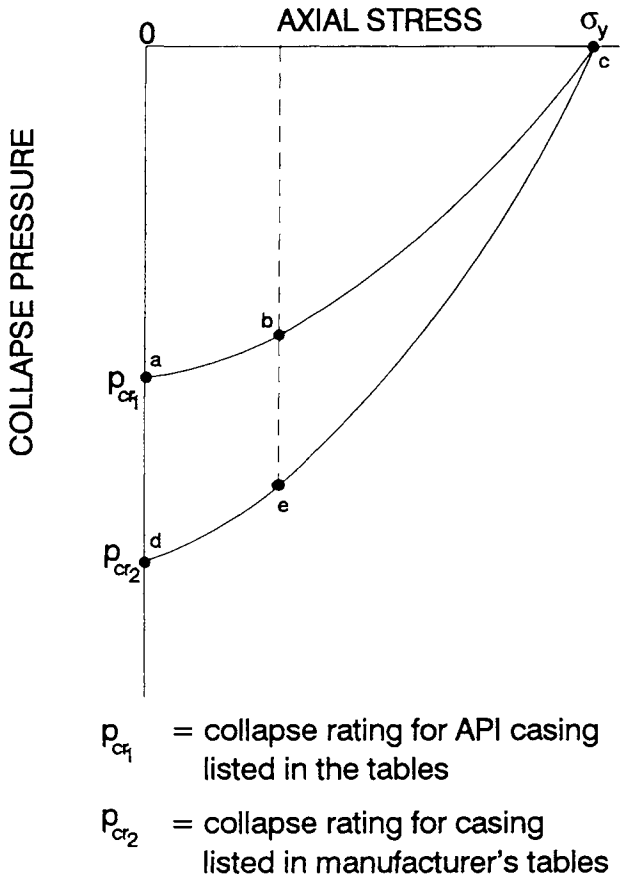

Fig. 5.7: Diagram of non-API casing collapse pressure correction.

S-95, 40 lb/ft of 4,230 psi. The difference is significant and, moreover, the cost of the S-95 is less than that of the C-95. Thus, by following the API Bul. 5C3 (1989) method for calculating collapse resistance, the design results will be as demonstrated in the above examples.

For a non-API casing, an alternative to this procedure is to consider a reduction of the manufacturer's collapse rating proportional to that which occurs in the API procedure. According to the API formulas for corrected collapse rating due to axial loading, the collapse pressure predictions follow path *abc* in Fig. 5.7. Non-API casings have better collapse resistance and, therefore, higher values are reported for these casings in the tables for zero axial stress (p_{cr2} or point *d*). Assuming p_{cr2} is correct, it is unlikely that the actual casing pressure failure behavior would follow path *dabc*. As an alternative to this practice, path *dec* is suggested for these cases. The question now becomes how to find point e?

The only point known so far is p_{cr2}, which is obtained directly from the man-

Table 5.8: Minimum cost design for non-API casing using the modified API collapse calculations.

```
                    INTERMEDIATE CASING DESIGN
THE WELL DATA USED IN THIS PROGRAM WAS:
     .EQUIVALENT FRACTURE GRADIENT AT CASING SEAT=15.0 PPG
     .BLOW OUT PREVENTER RESISTANCE= 5000. PSI
     .DENSITY OF THE MUD THE CASING IS SET IN=12.0 PPG
     .DENSITY OF HEAVIEST MUD IN CONTACT WITH THIS CASING=15.0 PPG
     .TRUE VERTICAL DEPTH OF THE NEXT CASING SEAT=15000. FT
     .PORE PRES. AT NEXT CASING SEAT DEPTH= 9.0 PPG
     .MINIMUM CASING STRING LENGTH= 2500. FT
     .DESIGN FACTOR: BUR=1.000; COL=1.125; YIELD=1.800
     .TRUE VERTICAL DEPTH OF THE CASING SEAT=10000. FT
     .DESIGN METHOD: MINIMUM COST

9 5/8" CASING PRICE LIST. FILE REF.:PRICE958.CPR
MAIN PROGRAM: CASING3D

TOTAL PRICE=283989. U.S.DOLLARS
TOTAL STRING BUOYANT WEIGHT=333864. LB
DI=10000- 6800   L= 3200 NN=13   W=40.0 M=2 MB=1.60 MC=1.13 MY= 8.2   P=2783.29
DI= 6800- 4280   L= 2520 NN=13   W=43.5 M=2 MB=1.46 MC=1.45 MY= 4.9   P=3007.88
DI= 4280- 0      L= 4280 NN=13   W=40.0 M=2 MB=1.18 MC=1.47 MY= 2.6   P=2783.29

THE MEANING OF SYMBOLS:
     .DI, DEPTH INTERVAL (FT)
     .L, LENGTH (FT)
     .NN, TYPE OF GRADE (SEE THE GRADE CODE BELOW)
     .W, UNIT WEIGHT (LB/FT)
     .M IS THE TYPE OF THREAD: 1...SHORT; 2...LONG; 3...BUTTRESS
     .MB, MC, MY, MINIMUM SAFETY FACTORS FOR BURST, COLLAPSE, AND YIELD
     .P, UNIT CASING PRICE.....$/100FT

GRADE CODE:
NN 1= ...H40     NN 2= ...J55     NN 3= ...K55     NN 4= ...C75     NN 5= ...L80
NN 6= ...N80     NN 7= ...C95     NN 8= ..P110     NN 9= ..V150     NN13= ...S95
NN14= .CYS95     NN15= ..S105     NN16= ...S80     NN17= ..SS95     NN18= .LS110
NN19= .LS125
```

ufacturer's pipe specification tables. The pressure at point a can be calculated using the API collapse formula for axial loads (flowchart shown in Table 2.1) for zero axial stress. Similarly, the pressure at point b can be calculated using the API formula for the appropriate value of axial stress. (This would be the value of corrected collapse pressure only if the API correction criteria is used.)

The collapse pressure, p_e, can be obtained by assuming the following relationship between these pressures:

$$\frac{p_d}{p_a} = \frac{p_e}{p_b} \tag{5.12}$$

Rearranging Eq. 5.12 results in:

$$p_e = \frac{p_d}{p_a} \times p_b \tag{5.13}$$

The computer program for minimum price design with a minimum section length of 2,500 ft, was rerun after modifying the manufacturer's collapse ratings in the manner shown in Fig. 5.7 and Eq. 5.13.

Table 5.9: Minimum weight design for non-API casing using the modified API collapse calculations.

```
                    INTERMEDIATE CASING DESIGN
THE WELL DATA USED IN THIS PROGRAM WAS:
      .EQUIVALENT FRACTURE GRADIENT AT CASING SEAT=15.0 PPG
      .BLOW OUT PREVENTER RESISTANCE= 5000. PSI
      .DENSITY OF THE MUD THE CASING IS SET IN=12.0 PPG
      .DENSITY OF HEAVIEST MUD IN CONTACT WITH THIS CASING=15.0 PPG
      .TRUE VERTICAL DEPTH OF THE NEXT CASING SEAT=15000. FT
      .PORE PRES. AT NEXT CASING SEAT DEPTH= 9.0 PPG
      .MINIMUM CASING STRING LENGTH= 2500. FT
      .DESIGN FACTOR: BUR=1.000; COL=1.125; YIELD=1.800
      .TRUE VERTICAL DEPTH OF THE CASING SEAT=10000. FT
      .DESIGN METHOD: MINIMUM WEIGHT

9 5/8" CASING PRICE LIST. FILE REF.:PRICE958.CPR
MAIN PROGRAM: CASING3D

TOTAL PRICE=283989. U.S.DOLLARS
TOTAL STRING BUOYANT WEIGHT=333864. LB
DI=10000- 6800   L= 3200 NN=13   W=40.0 M=2 MB=1.60 MC=1.13 MY= 8.2   P=2783.29
DI= 6800- 4280   L= 2520 NN=13   W=43.5 M=2 MB=1.46 MC=1.45 MY= 4.9   P=3007.88
DI= 4280- 0      L= 4280 NN=13   W=40.0 M=2 MB=1.18 MC=1.47 MY= 2.6   P=2783.29

THE MEANING OF SYMBOLS:
      .DI, DEPTH INTERVAL (FT)
      .L, LENGTH (FT)
      .NN, TYPE OF GRADE (SEE THE GRADE CODE BELOW)
      .W, UNIT WEIGHT (LB/FT)
      .M IS THE TYPE OF THREAD: 1...SHORT; 2...LONG; 3...BUTTRESS
      .MB, MC, MY, MINIMUM SAFETY FACTORS FOR BURST, COLLAPSE, AND YIELD
      .P, UNIT CASING PRICE.....$/100FT

GRADE CODE:
NN 1= ...H40    NN 2= ...J55    NN 3= ...K55    NN 4= ...C75    NN 5= ...L80
NN 6= ...N80    NN 7= ...C95    NN 8= ..P110    NN 9= ..V150    NN13= ...S95
NN14= .CYS95    NN15= ..S105    NN16= ...S80    NN17= ..SS95    NN18= .LS110
NN19= .LS125
```

As an exercise, the engineer should make the suggested program modifications as detailed in the following steps:

1. The subroutine to be modified in CSG3DAPI.FOR is SUBROUTINE PCOR.

2. Delete line 68, IF(CFNAPI.GT.1.)THEN.

3. Delete line 69, CFNAPI=1.0.

4. Delete line 70, ENDIF.

5. Recompile to produce an updated .EXE file.

After recompiling and rerunning the program, the output should appear as it is in Table 5.8. If it does not, compare the modified file with CASING3D.FOR on the disk. The revised string shows a significant decrease in price, $13,482, from the earlier cheapest alternative, the Quick Design Chart. These casing loads were added to Figs. 5.5 and 5.6 for comparison with the earlier results.

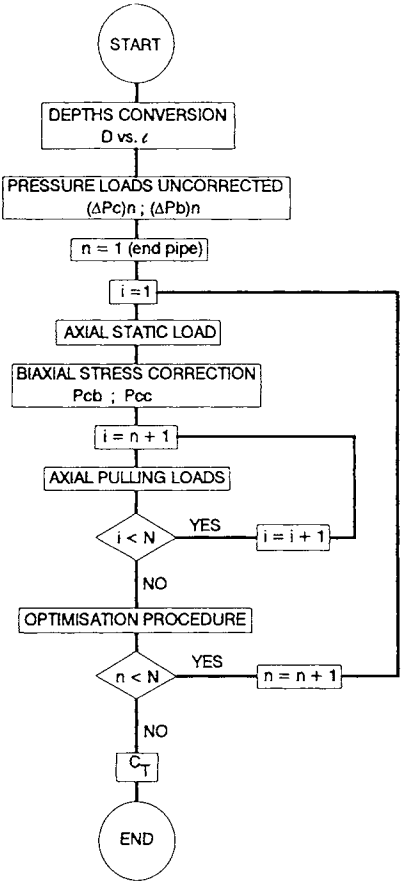

Fig. 5.8: Flow diagram of the minimum-cost casing design program for directional wells. (After Wojtanowicz and Maidla, 1987; courtesy of SPE.)

All subsequent examples are based on this modification. The modified program is named CASING3D.EXE and the batch file provided to help run it is named CASING.BAT.

Comparison between the minimum cost and minimum weight methods using the API collapse calculations shown in Tables 5.4 and 5.6 show a $11,771 cost increase when a lighter string of casing was selected. However, if the same example is rerun after implementing the changes in the program for the use of non-API casing in designs, the results using the minimum weight and the minimum price criteria are the same as shown in Tables 5.8 and 5.9. Provided the design criteria for non-API casing is agreed upon, this design represents the most economical alternative in Table 5.5.

5.1.4 General Theory of Casing Optimization

The combination casing string design is considered a multistage decision-making procedure in which the next step decision depends upon the previous decisions. The general concept of the discrete version of dynamic programming is applied (Roberts, 1964; Phillips et al., 1976). Dynamic programming terminology is defined by the following five attributes.

1. A stage is a unit section of casing string (length $\Delta\ell$) or a step in the recurrent design procedure. At each stage, the set of the optimal casing variants is selected (Fig. 5.3).

2. Stage variables, F_n, are loads supported by the nth casing unit section:

$$F_n = F_n\left(\Delta p_b, \Delta p_c, F_{A_n}\right) \tag{5.14}$$

In general, there are $\left(N_{S_{n-1}} \times N_W\right)$ combinations of the loads at stage n, where:

$N_{S_{n-1}}$ = number of possible different variants of casing string below section n.
N_W = number of different casing unit weights.

The axial loads, F_{A_n}, for the nth unit section are calculated using Eq. 5.5. These loads can also be computed using Eq. 5.6 for vertical wells and Eqs. 5.39 — 5.45 for directional wells.

3. Decision variables, P_n, involve the type of casing. In the computer program, each type of casing is represented by one number, i.e., the unit price of casing. For the nth unit section, the number of casing variants available is $r_n \times N_{S_{n-1}}$.

The conversion from casing price to grade, weight, and type of casing joint is made before the results are printed out. The total number of casings available for unit section n is selected considering the constraints given by Eqs. 5.2, 5.3, and 5.4.

4. Return function, C_{T_n}, is the total cost of n unit sections of casing:

$$C^j_{T_n} = C_{T_n}\left(F_n, P_n\right) \tag{5.15}$$
$$C^j_{T_n} = \Delta\ell \times P_n + \Delta\ell \times \left(P_{n-1} + P_{n-2} + \cdots + 1\right) \tag{5.16}$$
$$C^j_{T_n} = \Delta\ell \times P_n + C^k_{T_{n-1}} \tag{5.17}$$

where:

j = varies from 1 to $r_n \times N_{S_{n-1}}$.
k = varies from 1 to $N_{S_{n-1}}$.

5. Accumulated total return, C_{p_n}, is the minimal cost of n sections of casing for each load, F_n. As the load is dependent only on the unit length's weight, each of which is represented here by m, cost optimization is carried out at each stage by selecting the cheapest casing within each of the possible casing weights and by identifying the casings that are lighter than the cheapest one. The procedure is described as follows.

$$W_{m_n} = \min_{s\in(a,b)} (W_n(s)) \tag{5.18}$$

$$P_{W_n} = P_{W_n}(W_{m_n}) \tag{5.19}$$

$$W_{ref_n} = \min_{u\in(c,d)} W_{m_n}(u) \tag{5.20}$$

$$W_{p_n} \leq W_{ref_n} \tag{5.21}$$

$$P_{p_n} = P_{p_n}(W_{p_n}) \tag{5.22}$$

$$C^i_{p_n} = \Delta\ell \times P_{p_n}(v) + C^k_{p_{n-1}} \tag{5.23}$$

where:

a = the smallest value of P_n within m, US$/100 ft.
b = the largest value of P_n within m, US$/100 ft.
c = the smallest value of P_{W_n}, US$/100 ft.
d = the largest value of P_{W_n}, US$/100 ft.
k = varies from 1 to $N_{S_{n-1}}$.
i = varies from 1 to $(r_{p_n} \times k)$.
P_{p_n} = distributed price of the W_{ref_n} of casing, US$/100 ft.
P_{W_n} = distributed price of the cheapest casing within m, US$/100 ft.
r_{p_n} = number of W_{p_n} weights.
W_{m_n} = distributed weight of the cheapest casing within m, lb/ft.
W_{p_n} = distributed weight of casing lighter or equal to W_{ref_n}, lb/ft.
W_{ref_n} = distributed weight of the cheapest casing at stage n, lb/ft.

6. Absolute minimal cost, C_{min_n}, at stage n is given by:

$$C_{min_n} = \min_{v\in(e,f)} \left(\Delta\ell \times P_{p_n}(v) + C^k_{p_{n-1}}\right) \tag{5.24}$$

where:

e = the smallest value of P_{p_n}, US$/100 ft.
f = the largest value of P_{p_n}, US$/100 ft.

Inasmuch as the transition of the cost and transition of the axial load from step $n-1$ to step n is achieved by simple addition, the principle of optimality can be

applied and Eq. 5.24 becomes:

$$C_{min_n} = \left[\min_{v \in (e,f)} (\Delta \ell \times P_{p_n}(v)) \right] + C^k_{p_{n-1}}. \tag{5.25}$$

For $n = N$, Eq. 5.25 gives the minimal cost of the combination casing string desired. This cost corresponds to the optimum configuration of the casing string stored in the computer memory.

Simplification of the Theory. In some practical computations, the lack of the price/weight conflict has been observed. Mathematically, this means that $r(W_{p_n})$ has only one value and this is equal to $r\left(W_{ref_n}\right)$. For the particular cases where this happens the optimization procedure can be simplified. Namely, at any unit section of the casing string, there is only one set of loads supported by the $n-1$ casing section, meaning that the above formulation will equal both formulations for the minimum weight method and the minimum cost method presented earlier.

5.1.5 Casing Cost Optimization in Directional Wells

Directional Well Formulation

The minimum-cost casing procedure for vertical wells can be expanded to directional wells because the flexible structure of the model allows for independent calculations of casing loads and cost minimization. For this procedure, the following assumptions are made:

1. The well is planed in a vertical plane; therefore, its trajectory is confined to two dimensions.

2. Only elastic properties of casing are considered in bending calculations.

3. The bending contribution to the axial stress is expressed as an equivalent axial force.

4. The bending contribution to the normal force is neglected because its impact on the final design is very small.

5. The effect of inclination on axial loads is considered by using the axial component of casing weight.

6. The favorable effect of mechanical friction on axial load during downward pipe movement is not considered.

7. The unfavorable effect of mechanical friction on axial load during upward pipe movement is considered.

Chapter 6

AN INTRODUCTION TO CORROSION AND PROTECTION OF CASING

Corrosion is defined as the chemical degradation of metals by reaction with the environment. The destruction of metals by corrosion occurs either by direct chemical attack at elevated temperatures (500+°F) in a dry environment or by electrochemical processes at low temperature in a water-wet or moist environment.

Corrosion attacks casing during drilling and producing operations through electrochemical processes in the presence of electrolytes and corrosive agents in drilling, completion, packer and production fluids.

6.1 CORROSION AGENTS IN DRILLING AND PRODUCTION FLUIDS

The components present in fluids which promote the corrosion of casing in drilling and producing operations are oxygen, carbon dioxide, hydrogen sulfide, salts and organic acids. Destruction of metals is influenced by various physical and chemical factors which localize and increase corrosion damage.

The conditions which promote corrosion include:

- Energy differences in the form of stress gradients or chemical reactivities across the metal surface in contact with a corrosive solution.
- Differences in concentration of salts or other corrodants in electrolytic so-

lutions.

- Differences in the amount of solid or liquid deposits on the metal surface, which are insoluble in the electrolytic solutions.
- Temperature gradients over the surface of the metal in contact with a corrosive solution.
- Compositional differences in the metal surface.

Corrosion of metals continues provided electrically conductive metal and solution circuits are available to bring corrodants to the anodic and cathodic sites. Four conditions must be present to complete the electrochemical reactions and corrosion circuit:

1. Presence of a driving force or electrical potential. The difference in reaction potentials at two sites on the metal surface must be sufficient to drive electrons through the metal, surface films and liquid components of the corrosion circuit.
2. Presence of an electrolyte. Corrosion occurs only when the circuit between anodic and cathodic sites is completed by an electrolyte present in water.
3. Presence of both anodic and cathodic sites. Anodic and cathodic areas must be present to support the simultaneous oxidation and reduction reactions at the metal-liquid interface. Metal at the anode ionizes.
4. Presence of an external conductor. A complete electron electrolytic circuit between anodes and cathodes of the metal through the metal surface films, surrounding environment and fluid-solid interfaces is necessary for the continuance of corrosion.

In the environment surrounding the metal, the presence of water provides conducting paths for both corrodants and corrosion products. The corrodant may be a dissolved gas, liquid or solid. The corrosion products may be ions in solution, which are removed from the metal surface, ions precipitated as various salts on metal surfaces and hydrogen gas.

6.1.1 Electrochemical Corrosion

The conditions needed to promote many types of corrosion can be found in most oil wells. The basic electrochemical reactions, which occur simultaneously at the cathodic and anodic areas of metal and cause many forms of corrosion damage, are as follows:

1. At the cathode, the hydrogen (or acid) ion (H^+) removes electrons from the cathodic surfaces to form hydrogen gas (H_2):

   $$2e^- + 2H^+ \rightarrow 2H^0 \rightarrow H_2 \text{ (in acidic solution).}$$

   If oxygen is present, electrons are removed from the metal by reduction of oxygen:

   $$4e^- + O_2 + 4H^+ \rightarrow 2H_2O \text{ (in acidic solution)}$$
   $$4e^- + 2H_2O + O{-}2 \rightarrow 4OH^- \text{ (in neutral or alkaline solution)}$$

2. At the anode, a metal ion (e.g., Fe^{2+}) is released from its structural position in the metal through the loss of the bonding electrons and passes into solution in the water as soluble iron, or reacts with another component of the environment to form scale. The principal reaction is:

   $$Fe - 2e^- \rightarrow Fe^{2+}$$

Thermodynamic data indicates that the corrosion process in many environments of interest should proceed at very high rates of reaction. Fortunately, experience shows that the corrosion process behaves differently. Studies have shown that as the process proceeds, an increase in concentration of the corrosion products develops rapidly at the cathodic and anodic areas. These products at the metal surfaces serve as barriers that tend to retard the corrosion rate. The reacting components of the environment may be depleted locally, which further tends to reduce the total corrosion rate.

The potential differences between the cathodic and anodic areas decrease as corrosion proceeds. This reduction in potential difference between the electrodes upon current flow is termed polarization. The potential of the anodic reaction approaches that of the cathode and the potential of the cathodic reaction approaches that of the anode.

Electrode polarization by corrosion is caused by: changing the surface concentration of metal ions, adsorption of hydrogen at cathodic areas, discharge of hydroxyl ions at anodes, or increasing the resistance of the electrolyte and films of metal-reaction products on the metal surface. Changes (increase or decrease) in the amount of these resistances by the introduction of materials or electrical energy into the system will change the corrosion currents and corrosion rate.

A practical method to control corrosion is through cathodic protection, whereby polarization of the structure to be protected is accomplished by supplying an

external current to the corroding metal. Polarization of the cathode is forced beyond the corrosion potential. The effect of the external current is to eliminate the potential differences between anodic and cathodic areas on the corroding metal. Removal of the potential differences stops local corrosion action. Cathodic protection operates most efficiently in systems under cathodic control, i.e., where cathodic reactions control the corrosion rate.

Materials may cause an increase in polarization and retard corrosion by absorbing on the surface of the metals and thereby changing the nature of the surface. Such materials act as inhibitors to the corrosion process. On the other hand, some materials may reduce polarization and assist corrosion. These materials, called depolarizers, either assist or replace the original reactions and prevent the buildup of original reaction products.

Oxygen is the principal depolarizer which aids corrosion in the destruction of metal. Oxygen tends to reduce the polarization or resistance, which normally develops at the cathodic areas, with the accumulation of hydrogen at these electrodes. The cathodic reaction with hydrogen ion is replaced by a reaction in which electrons at the cathodic areas are removed by oxygen and water to form hydroxyl ions (OH^-) or water:

$$O_2 + 2\,H_2O + 4\,e^- \rightarrow 4\,OH^- \text{ (in neutral and alkaline solutions)}$$
$$O_2 + 4\,H^+ + 4\,e^- \rightarrow 2\,H_2O \text{ (in acid solutions)}$$

Polarization of an electrode surface reduces the total current and corrosion rate. Though the rate of metal loss is reduced by polarization, casing failures may increase if incomplete polarization occurs at the anodes. For example, inadequate anodic corrosion inhibitor will reduce the effective areas of the anodic surfaces and thus localize the loss of metal at the remaining anodes. This will result in severe pitting and the destruction of metal.

Resistances to the corrosion process generally do not develop to the same degree at the anodic and cathodic areas. These resistances reduce the corrosion rate, which is controlled by the slowest step in the corrosion process. Electrochemical corrosion comprises a series of reactions and material transport to and from the metal surfaces. Complete understanding of corrosion and corrosion control in a particular environment requires knowledge of each reaction which occurs at the anodic and cathodic areas.

Components of Electrochemical Corrosion

The various components which are involved in the process of corrosion of metal are: the metal, the films of hydrogen gas and metal corrosion products, liquid

and gaseous environment, and the several interfaces between these components.

Metal is a composite of atoms which are arranged in a symmetrical lattice structure. These atoms may be considered as particles which are held in an ordered arrangement in a lattice structure by bonding electrons. These electrons, which are in constant movement about the charged particles, move readily throughout the lattice structure of metal when an electric potential is applied to the system. If bonding electrons are removed from their orbit about the particle center, the resulting cation will no longer be held in the metal's crystalline structure and can enter the electrolyte solution.

Electrochemical corrosion is simply the process of freeing these cations from their organized lattice structure by the removal of the bonding electrons. Inasmuch as certain of the lattice electrons move readily within the metal under the influence of electrical potentials, the locations on the surface of the metal from which the cations escape and the locations from which the electrons are removed from the metal need not be and generally are not the same. Corrosion will not occur unless electrons are removed from some portion of the metal structure.

All metals are polycrystalline with each crystal having a random orientation with respect to the next crystal. The metal atoms in each crystal are oriented in a crystal lattice in a consistent pattern. The pattern gives rise to differences in spacing and, therefore, differences in cohesive energy between the particles, which may cause preferred corrosion attack. At the crystal boundaries the lattices are distorted, giving rise to preferred corrosion attack. In the manufacture and processing of metals, in order to gain desirable physical properties, both the composition and shape of the crystals may be made non-uniform, distorted or preferably oriented.

This may increase the susceptibility of the metal to corrosion attack. Undistorted single crystals of metals experience comparatively little or no corrosion under the same conditions which may destroy commercial pieces of the same metal. Compositional changes in metal alloy crystals and crystal boundaries, which are present in steels and alloys, can promote highly localized corrosion.

Chemistry of Corrosion and Electromotive Force Series

Oxidation takes place when a given substance loses electrons or share of its electrons. On the other hand, reduction occurs when there is a gain in electrons by a substance. A substance that yields electrons to something else is called a reducing agent, whereas the substance which gains electrons is termed an oxidizing agent. Thus, electrons are always transferred from the reducing agent to the oxidizing agent. In the example below, two electrons are transferred from metallic iron to cupric ion:

Table 6.1: Electromotive force series

Electrode reaction	Standard electrode potential. E^0 in Volts, 25°C
$Li = Li^+ + e^-$	+3.05
$K = K^+ + e^-$	+2.922
$Ca = Ca^{2+} + 2e^-$	+2.87
$Na = Na^+ + e^-$	+2.712
$Mg = Mg^{2+} + 2e^-$	+2.375
$Be = Be^{2+} + 2e^-$	+1.85
$Al = Al^{3+} + 3e^-$	+1.67
$Mn = Mn^{2+} + 2e^-$	+1.029
$Zn = Zn^{2+} + 2e^-$	+0.762
$Cr = Cr^{3+} + 3e^-$	+0.74
$Ga = Ga^{3+} + 3e^-$	+0.53
$Fe = Fe^{2+} + 2e^-$	+0.440
$Cd = Cd^{2+} + 2e^-$	+0.402
$In = In^{3+} + 3e^-$	+0.340
$Tl = Tl^+ + e^-$	+0.336
$Co = Co^{2+} + 2e^-$	+0.277
$Ni = Ni^{2+} + 2e^-$	+0.250
$Sn = Sn^{2+} + 2e^-$	+0.136
$Pb = Pb^{2+} + 2e^-$	+0.126
$H_2 = 2H^+ + 2e^-$	0.000
$Cu = Cu^{2+} + 2e^-$	- 0.345
$Cu = Cu^+ + e^-$	- 0.522
$2Hg = Hg_2^{2+} + 2e^-$	- 0.789
$Ag = Ag^+ + e^-$	- 0.800
$Pd = Pd^{2+} + 2e^-$	- 0.987
$Hg = Hg^{2+} + 2e^-$	- 0.854
$Pt = Pt^{2+} + 2e^-$	ca. - 1.2
$Au = Au^{3+} + 3e^-$	- 1.50
$Au = Au^+ + e^-$	- 1.68

$$\underset{\text{metallic iron}}{Fe^0} + \underset{\text{cupric ion}}{Cu^{2+}} \rightarrow \underset{\text{ferrous ion}}{Fe^{2+}} + \underset{\text{metallic copper}}{Cu^0}$$

The emf (electromotive force) series is presented in Table 6.1; potentials given are those between the elements in their standard state at 25°C and their ions at unit activity in the solution at 25°C. A plus sign (+) for E° shows that, for the above conditions, the reduced form of the reactant is a better reducing agent than H_2. On the other hand, a negative (–) sign indicates that the oxidized form of the reactant is better oxidizing agent than H^+. Thus, in general, any ion is better oxidizing agent than the ions above it.

Actual Electrode Potentials

In the emf series, each metal will reduce (or displace from solution) the ion of any metal below it in the series, providing all of the materials have unit activities. The activity of a pure metal in contact with a solution does not change with the environment. The activity of an ion, however, changes with concentration and the activity of a gas changes with partial pressure.

An electrode reaction, in which a metal M is oxidized to its ion M^{n+}, liberating n electrons, may be represented by the relation: $M = M^{n+} + ne^-$. The actual electrode potential of this reaction may be calculated from the standard electrode potential by the use of the following expression:

$$E = E^\circ - \frac{RT}{nF} \ln \left(M^{n+}\right)$$

where:

E	=	actual electrode potential at the given concentration (Volts).
E°	=	standard electrode potential (Volts).
R	=	universal gas constant; 8.315 Volt Coulombs/°K.
T	=	absolute temperature (°K).
n	=	number of electrons transferred.
F	=	the Faraday, 96,500 Coulombs.
M^{n+}	=	concentration of metal ions.

At 25 °C (298°K), the formula becomes:

$$E = E^\circ - \frac{0.05915}{n} \log_{10} \left(M^{n+}\right)$$

The actual electrode potential for a given environment may be computed from the above relation. Table 6.2 shows how the actual electrode potentials of iron and cadmium vary with change in concentration of the ions.

Table 6.2: Variation in actual electrode potentials of iron and cadmium with change in concentration of ions.

Reaction	Activity (moles/kg water)			
	1	0.1	0.01	0.001
	Actual electrode potential (Volts)			
$Fe = Fe^{2+} + 2e^-$	+0.440	+0.470	+0.499	+0.529
$Cd = Cd^{2+} + 2e^-$	+0.402	+0.431	+0.461	+0.490

It is apparent from Table 6.2 that iron will reduce cadmium when their ion concentrations are equal, but the reverse holds true when the concentration of cadmium ion becomes sufficiently lower than that of the ferrous ion.

It is well to note that the standard electrode potentials are a part of the more general standard oxidation-reduction potentials. Textbooks on physical chemistry also contain a general expression for calculating the actual oxidation-reduction potential from the standard oxidation-reduction potential.

Galvanic Series

Dissimilar metals exposed to electrolytes exhibit different potentials or tendencies to go into solution or react with the environment. This behavior is recorded in tabulations in which metals and alloys are listed in order of increasing resistance to corrosion in a particular environment. Coupling of dissimilar metals in an electrolyte will cause destruction of the more reactive metal, which acts as an anode and provides protection for the less reactive metal, which acts as a cathode.

6.2 CORROSION OF STEEL

In most corrosion problems, the important differences in reaction potentials are not those between dissimilar metals but those which exist between separate areas interspersed over all the surface of a single metal. These potential differences result from local chemical or physical differences within or on the metal, such as variations in grain structure, stresses and scale, inclusions in the metal, grain boundaries, scratches or other surface conditions. Steel is an alloy of pure iron and small amounts of carbon present as Fe_3C with trace amounts of other elements. Iron carbide (Fe_3C) is cathodic with respect to iron.

Inasmuch as in typical corrosion of steel anodic and cathodic areas lie side by side on the metal surface, in effect it is covered with both positive and negative sites.

During corrosion, the anodes and cathodes of metals may interchange frequently.

6.2.1 Types of Corrosion

Numerous types of steel destruction can result from the corrosion process, which are listed under the following classes of corrosion:

1. Uniform attack. The entire area of the metal corrodes uniformly resulting in thinning of the metal. This often occurs to drillpipe, but usually is the least damaging of different types of corrosive attacks. Uniform rusting of iron and tarnishing of silver are examples of this form of corrosion attack.

2. Crevice corrosion. This is an example of localized attack in the shielded areas of metal assemblies, such as pipes and collars, rod pins and boxes, tubing and drillpipe joints. Crevice corrosion is caused by concentration differences of a corrodant over a metal surface. Electrochemical potential differences result in selective crevice or pitting corrosion attack.

   Oxygen dissolved in drilling fluid promotes crevice and pitting attack of metal in the shielded areas of a drillstring and is the common cause of washouts and destruction under rubber pipe protectors.

3. Pitting corrosion. Pitting is often localized in a crevice but can also occur on clean metal surfaces in a corrosive environment. An example of this type of corrosion attack is the corrosion of steel in high-velocity sea water, low-pH aerated brines, or drilling fluids. Upon formation of a pit, corrosion continues as in a crevice but, usually, at an accelerated rate.

4. Galvanic or two-metal corrosion. Galvanic corrosion may occur when two different metals are in contact in a corrosive environment. The attack is usually localized near the point of contact.

5. Intergranular corrosion. Metal is preferentially attacked along the grain boundaries. Improper heat treatment of alloys or high-temperature exposure may cause precipitation of materials or non-homogeneity of the metal structure at the grain boundaries, which results in preferential attack.

   Weld decay is a form of intergranular attack. The attack occurs in a narrow band on each side of the weld owing to sensitizing or changes in the grain structure due to welding. Appropriate heat treating or metal selection can prevent the weld decay.

   Ring worm corrosion is a selective attack which forms a groove around the pipe near the box or the external upset end. This type of selective attack is avoided by annealing the entire pipe after the upset is formed.

6. Selective leaching. One component of an alloy is removed by the corrosion process. An example of this type of corrosion is the selective corrosion of zinc in brass.

7. Erosion-corrosion. The combination of erosion and corrosion results in severe localized attack of metal. Damage appears as a smooth groove or hole in the metal, such as in a washout of the drillpipe, casing or tubing. The washout is initiated by pitting in a crevice which penetrates the steel. The erosion-corrosion process completes the metal destruction.

   The erosion process removes protective films from the metal and exposes clean metal surface to the corrosive environment. This accelerates the corrosion process.

   Impingement attack is a form of erosion-corrosion process, which occurs after the breakdown of protective films. High velocities and presence of abrasive suspended material and the corrodants in drilling and produced fluids contribute to this destructive process.

   The combination of wear and corrosion may also remove protective surface films and accelerate localized attack by corrosion. This form of corrosion is often overlooked or recognized as being due to wear. The use of inhibitors can often control this form of metal destruction. For example, inhibitors are used extensively for protection of downhole pumping equipment in oil wells.

8. Cavitation corrosion. Cavitation damage results in a sponge-like appearance with deep pits in the metal surface. The destruction may be caused by purely mechanical effects in which pulsating pressures cause vaporization and formation and collapse of the bubbles at the metal surface. The mechanical working of the metal surface causes destruction, which is amplified in a corrosive environment. This type of corrosion attack, examples of which are found in pumps, may be prevented by increasing the suction head on the pumping equipment. A net positive suction head should always be maintained not only to prevent cavitation damage, but also to prevent possible suction of air into the flow stream. The latter can aggravate corrosion in many environments.

9. Corrosion due to variation in fluid flow. Velocity differences and turbulence of fluid flow over the metal surface cause localized corrosion. In addition to the combined effects of erosion and corrosion, variation in fluid flow can cause differences in concentrations of corrodants and depolarizers, which may result in selective attack of metals. For example, selective attack of metal occurs under the areas which are shielded by deposits from corrosion, i.e., scale, wax, bacteria and sediments, in pipeline and vessels.

10. Stress corrosion. The term stress corrosion includes the combined effects of stress and corrosion on the behavior of metals. An example of stress

corrosion is that local action cells are developed due to the residual stresses induced in the metal and adjacent unstressed metal in the pipe. Stressed metal is anodic and unstressed metal is cathodic. The degree to which these stresses are induced in pipes varies with the metallurgical properties and the cold work caused by the weight of the pipe, effects of slips, notch effects at tool joints and the presence of H_2S gas. In the oil fields, H_2S-induced stress corrosion has been instrumental in bringing about sudden failure of pipes.

In the absence of sulphide, hydrogen collects in the presence of the pipe as a film of atomic hydrogen which quickly combines with itself to form molecular hydrogen gas (H_2). The hydrogen gas molecules are too large to enter the steel and, therefore, usually bubble off harmlessly.

In the presence of sulphide, however, hydrogen gradient into the steel is greatly increased. The sulphide and higher concentration of hydrogen atoms work together to maximize the number of hydrogen atoms that enter the steel. Once in the steel, atomic hydrogen tries to accumulate to form molecular hydrogen which results in high stress in the metal. This is known as hydrogen-induced stress. Presence of atomic hydrogen in steel reduces the ductility of the steel and causes it to break in a brittle manner.

The amount of atomic hydrogen required to initiate sulphide stress cracking appears to be small, possibly as low as 1 ppm, but sufficient hydrogen must be available to establish a differential gradient required to initiate and propagate a crack. Laboratory tests suggest that H_2S concentrations as low as 1-3 ppm can produce cracking of highly-stressed and high-strength steels (Wilhelm and Kane, 1987).

Although stress-corrosion cracking can occur in most alloys, the corrodants which promote stress cracking may differ and be few in number for each alloy. Cracking can occur in both acidic and alkaline environments, usually in the presence of chlorides and/or oxygen.

6.2.2 External Casing Corrosion

The external casing corrosion may be caused by one or a combination of the following:

- Corrosive formation water (having high salinity).
- Bacterially-generated H_2S.
- Electrical currents.

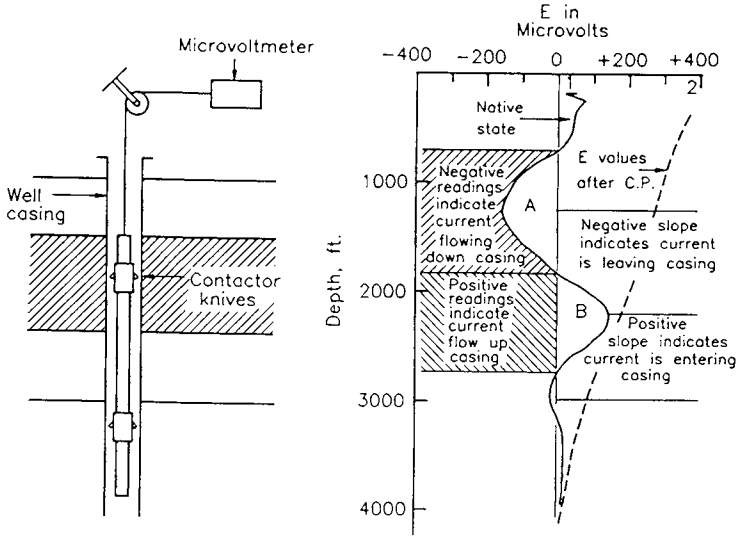

Fig. 6.1: Casing potential profile test equipment and example of plotting data. (After Jones, 1988, p.66, fig 1.8-2; courtesy of OGCI Publications, Tulsa, OK.)

- Corrosive completion fluids.
- Movements along faults which cross the borehole (this gives rise to weak, damaged steel zones susceptible to corrosion).

Electrolytic corrosion is the main source of casing corrosion. The current flow may originate from either potential gradients between the formations traversed by the casing and between the well casing and long flowlines (> 1 V), or it may enter from the electrical grounding systems and connecting flowlines.

The origin of stray currents is not easy to determine. The use of a voltmeter across an open flowline–to–wellhead flange, however, will show whether or not the electrical current is entering the well, i.e., whether or not electrons are leaving the casing.

6.2.3 Corrosion Inspection Tools

A variety of tools and interpretation techniques are employed to monitor corrosion because a large amount of information is required for interpretation from both single and multiple casing. Four types of tools are considered here (Watfa, 1989):

1. Electromagnetic casing corrosion detection.
2. Multifinger caliper tool (mechanical).

3. Acoustic tool.

4. Casing potential profile tool.

The Electromagnetic Corrosion Detection

In essence these tools consist of a number of electromagnetic flux transmitters and receivers that are linked by the casing string(s) in much the same way as the core in a transformer links the primary and secondary coils.

For a qualitative measure of the average circumferential thickness of multiple casings (Watfa, 1989), the phase shift between the transmitted and received signals is measured. The phase shift related to the thickness of the casing is as follows:

$$\phi = 2\pi t\sqrt{\mu\sigma f}$$

where:

t = combined thickness of all casings.
σ = combined conductivity of all casings.
μ = combined magnetic permeability of all casings.
f = tool frequency.

By increasing f, the depth of investigation can be reduced to include only the inner casing and values of σ and μ can be determined. Increasing f still further provides an accurate measure of the ID of the inner casing string. All three measurements can be made simultaneously to provide an overall view of material losses.

For a more detailed analysis of the inner casing string a multi-armed, pad-tool can be used which generates a localized flux in the inner wall of the casing by means of a central, high-frequency, pad-mounted signal coil. Flux distortions measured at the two adjacent receiver or 'measure' coils, are indicative of inner pipe corrosion.

In a second measurement, electromagnets located on the main tool body generate a flux in the inner casing. Again, the presence of corrosion will induce a flux leakage, which is measured by the two measure coils. This measure is a qualitative evaluation of total inner casing corrosion.

Multi-Finger Caliper Tool

The multi-finger caliper tool consists of a cluster of mechanical feelers that are distributed evenly around the tool. Each of these feelers gives an independent

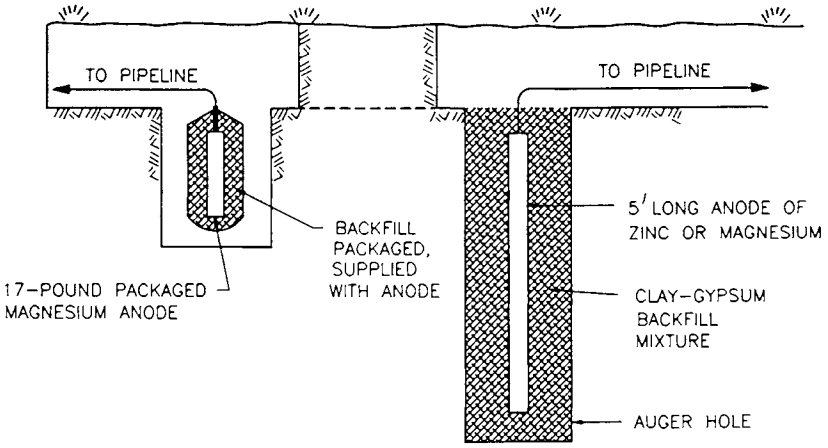

Fig. 6.2: Typical installation of galvanic anodes. (After NACE, Houston, TX, *Control of Pipeline Corrosion*, fig. 8-6.)

measurement of the radius. The small size of feelers allows small anomalies in the inner casing wall to be detected and measured. The multi-finger caliper gives an accurate construction of the changes in the internal diameter of the casings.

Acoustic Tool

The acoustic tool consists of eight high-frequency ultra-sonic transducers. The transducers act as receiver and transmitter, and two measurements are obtained from each transducer. These measurements are: internal diameter, which is measured from the time interval of signal emission to the echo return, and the internal casing thickness.

Casing Potential Profile Curves

Corrosion damage to the casing can be detected easily using the casing potential profile tool. This tool measures the voltage drop (IR drop) across a length of casing (e.g., 25-ft) between two contact knives (see Fig. 6.1).

Logging (from bottom to the top) is done at intervals equal to the spacing of the knife contractors. Voltage (IR) drops are then plotted versus depth (casing potential profile). As shown in Fig. 6.1, readings on the left (−) side of zero indicate that current flows down the pipe, whereas positive values (+) show that flow is upward. Consequently, the curve sloping to the left from bottom indicates corroding zone (anode), where electrons are leaving the casing.

6.3 PROTECTION OF CASING FROM CORROSION

Casing can be protected by one or a combination of the following:

- Using wellhead insulator (electrical insulation of well casing from the flowline).
- Cementation (placement of a uniform cement sheath around casing).
- Placing completion fluids around casing which has not been cemented (these fluids should be oxygen-free, high-pH and thixotropic).
- Cathodic protection.
- Steel grades.

6.3.1 Wellhead Insulation

Use of electrical insulation stops current flow down the casing from the surface and reduces both internal and external casing corrosion. Dielectric insulation materials for both screw and flange joints are commonly used to insulate casing from flowlines. Insulation of wells by connecting them to a single battery is often recommended. It should be noted that when the flowline is at high potential due to cathodic protection, it may induce interference corrosion. In this case, the insulating joints may be partially shunted or wellhead potential is elevated by attaching a sacrificial anode (see Fig. 6.2). Heat resistant material should be selected for hot, high-pressure wells to prevent failure of insulation materials.

6.3.2 Casing Cementing

In addition to wellhead insulation, the best available procedure of reducing casing failure due to external corrosion is the placement of a uniform cement sheath opposite all corrosive formations, e.g., chlorine- and sulphur-rich formation waters. Diffusional supply of chlorine and sulphate ions to the interface of the casing can be inhibited by reducing porosity and permeability of the cement sheath. Most API oilwell cements contain tricalcium alumina, which forms complex salts of calcium chloroaluminate upon contact with chlorine ions, and calcium sulphoalumina hydrates upon contact with sulphate ions. Both of these reaction products lead to the formation of porous and permeable set cement. Upon long exposure (2-5 years) to these environments, the cement matrix begins to deteriorate and ultimately collapses leaving the casing without any protection (Rahman, 1988).

Full-length cementing of surface casing and production casing is recommended for deep wells. Pozzolan blended ASTM type I cement (API Class B or C), which is resistant to chlorine and sulphate attack and at the same time develops strong cement matrix, should be used. Additives such as fuel ash, blast furnace slag or silica flour is added to the cement to improve its properties (porosity, permeability and strength).

6.3.3 Completion Fluids

Casing that is not cemented should be protected by oxygen-free, high-pH and thixotropic completion fluid. Residual dissolved oxygen initiates corrosion pitting and promotes subsequent bacterial growth. Oxygen contained in most completion fluids is best controlled by chemical conversion to a harmless reaction product. Common scavengers used to remove oxygen are zinc-phosphate and zinc-chromate. These inhibitors are used at concentrations of 500-800 mg/l. Low pH values, on the other hand increase hydrogen availability in fluids which initiates hydrogen-induced stress cracking. Completion fluids should be thixotropic in order to suspend solids and maintain the required hydrostatic head of the fluid column. This reduces the stresses on casing due to collapse and buckling loads.

As discussed earlier, both hydrogen and sulphide components of hydrogen sulphide are instrumental in bringing about sudden failures in casings. Hydrogen sulphide may enter the completion fluid from formations that contain H_2S, or originate from bacterial action on sulphur compounds commonly present in completion fluids, from thermal degradation of sulphur-containing fluid additives, from chemical reactions with tool joint thread lubricants that contain sulphur, and from thermal degradation of organic additives.

Scavengers and film-forming organic inhibitors are utilized in the treatment of water-based completion fluids. Common inhibitors used to remove H_2S from completion fluid are iron sponge, zinc oxide and zinc carbonate and sodium or potassium chromate. Iron sponge is a highly porous synthetic oxide of iron and reacts with H_2S to form iron sulphite, whereas zinc oxide and zinc carbonate remove H_2S by forming precipitates of sulphide, whereas chromates remove H_2S by oxidation process.

Film-forming organic inhibitors have been found very effective in protecting casing from contaminants. They are typically oily liquid or wax-like solids with large chains or rings with positively-charged amine nitrogen group on one end. Their structure can be represented as follows:

$R.NH_2$	$R_2.NH$	R_3N	$[R_4N]^+$
Primary	Secondary	Tertiary	Quaternary

where:

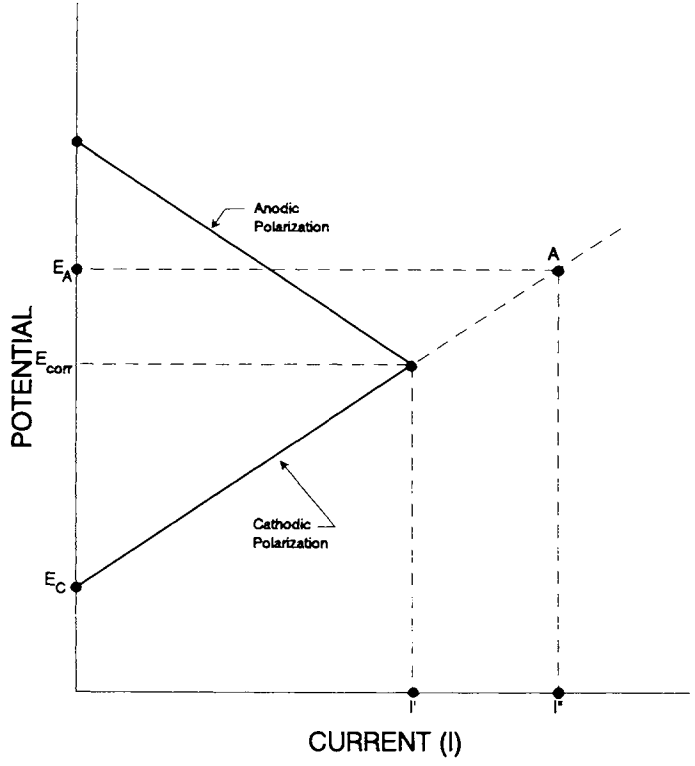

Fig. 6.3: Diagram illustrating the theory of cathodic protection. I'' = current required to produce complete cathodic protection. Current must exceed equilibrium corrosion current, I', to provide any protection. Corrosion will cease when the flow of cathodic current (I'') increases cathodic polarization to the open circuit potential (E_A) of the anode as shown at point A.

R represents the hydrocarbon chain or ring portions of the molecule.

In water, the amine groups take on an additional hydrogen that gives them a net positive-charge. Thus, the polar amine groups are adsorbed to the casing and the hydrocarbon portion forms an oily, water-repellent surface film. The amine inhibitors actually work best where H_2S is present and O_2 is absent, because they can react with H_2S to form a complex compound which helps to build a protective film. (For details see Jones, 1988.)

6.3.4 Cathodic Protection of Casing

Cathodic protection is used in many oilfields to protect the casing against external corrosion. Corrosion occurs at the anode, as electrons leave the anodic areas and move towards the cathodic areas. If electrons are forced into the anodic areas,

corrosion will not occur.

The first step in the control of external casing corrosion is to provide a complete cement sheath and bond between the pipe and the formation over all external areas of the casing strings as discussed previously.

Cathodic protection involves supplying electrons to the metal to make the potential more negative. Complete protection is achieved when all the surface area of the metal acts as a cathode in the particular environment.

The increase in electronegative potential can be achieved by use of sacrificial anodes (magnesium, aluminium and zinc) or by an impressed direct current. The potentials required for protection differ with the environment and the electrochemical reactions which are involved. For example, Blaunt (1970) noted that iron corroding in neutral aerated soil has a reduction potential of 0.579 V. The potential is limited by the activity and solubility of ferrous hydroxide. If iron is exposed to H_2S in oxygen-free environment, the potential is increased to 0.712 V and is controlled by the solubility of ferrous sulfide.

Measurements of potential are made by use of reference half cells. The copper-copper sulfate half cell is widely used for potential measurements of pipe in soils. The criteria for protection of iron with this half cell is -0.85 V in aerated soil and -0.98 V in an H_2S system.

The theory of cathodic protection is illustrated in Fig. 6.3. As shown in Fig. 6.3, the polarization of cathodic areas of steel must be extended until the potential E_c of the cathodic surfaces reaches the potential E_a of the anodic surfaces. The current which is applied in cathodic protection (I'') must exceed the equilibrium corrosion current (I') of the metal in its corrosive environment without cathodic protection.

The two types of cathodic protection most commonly used are: galvanic and impressed-current. When anodes (e.g., aluminium) are electrically coupled to steel (immersed in the same electrolyte), cathodic-protection current is generated. As a result of oxidation of aluminium, electrons are forced into the steel, because electrochemical potential of aluminium is higher than that of steel (see electromotive force series, Table 6.1). Inasmuch as aluminium is consumed in the process, it is called a "sacrificial anode".

In the case of the impressed-current cathodic-protection, rectifiers are used to convert alternating current to direct current. The negative side of the direct current is connected to the casing, whereas the positive side is connected to the buried anodes. The anode material in this case is essentially inert (see Fig. 6.4).

Interference bond on an insulating flange at a cathodically protected casing is shown in Fig. 6.5. In the absence of bond, the interference current on the electrically isolated flowline would leave through the soil at point A, causing

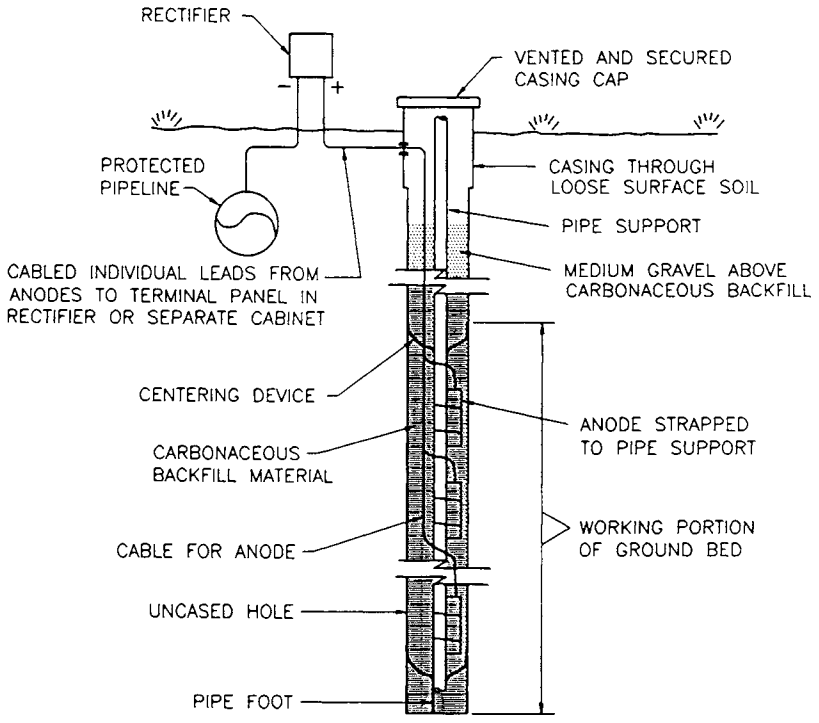

Fig. 6.4: Deep well groundbed design using anode and carbonaceous backfill in open hole. (Courtesy of NACE, Houston, TX, Control of Pipeline Corrosion, fig. 8-12.) Can be used for either a pipeline or casing.

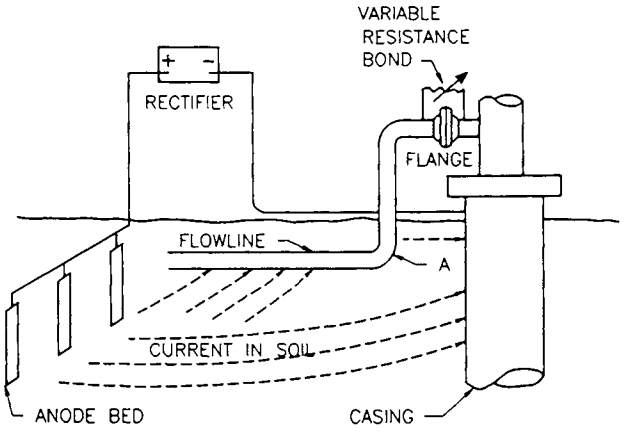

Fig. 6.5: Adjustable interference bond across an insulating (isolating), flange connecting a buried flowline to the cathodically-protected casing. (After Jones, 1988, p. 34, fig. 1.4-6; Courtesy of the OGCI Publications, Tulsa, OK.)

corrosion of the flowline (Jones, 1988).

As shown in Fig. 6.5, the insulating flange electrically isolates the casing from the surface equipment. This confines the cathodic protection current to the casing.

6.3.5 Steel Grades

Past experience suggests that susceptibility to stress corrosion cracking of high strength steel is large. In order to avoid stress corrosion cracking, a variety of materials have been introduced to oil field tubing. They include: martensitic stainless steel, austenitic-ferrite stainless steel, high alloy austenitic stainless steel, nickel base alloys and titanium alloys. Chromium-containing martensitic stainless steel has also been used because of its resistance to corrosion in carbon dioxide environments. A stainless steel with 9%-12% chromium can obtain a high level of corrosion resistance. Recently, these grades of casing and tubing have been offered with an AISI 420 composition (13% chromium) and 80,000 psi minimum yield strength. Experience with these materials have been good (Wilhelm and Kane, 1987).

According to API classification casing grades, which have been found realistically applicable to oil field condition where H_2S is present and ambient temperatures are encountered, are: J-55, C-15, N-80, MOD (modified) N-80, SIO-95, and P - 110 (Kane and Greer, 1977). Susceptibility to stress cracking decreases as the temperature increases. Hence as the temperature increases with increase in depth higher strength steel grade can be utilized, e.g., SOO-140. Field experience also suggests that large concentration of H_2S affects P-110 casings. (For details see Jones, 1988.)

6.3.6 Casing Leaks

In repairing the casing leaks, one can either (1) isolate the leak with a packer (inexpensive) or (2) replace the casing (very expensive). Casing leaks can cause loss of production and, possibly, eventual loss of a well. The log of cumulative leaks is often a linear function of time (Fig. 6.6). The curve is often an approximate one, because in many cases casing leaks can go undetected for long time. In many cases, however, the extrapolation of the leak-frequency versus time curve is surprisingly accurate and can aid in an economic analysis (feasibility of cathodic protection).

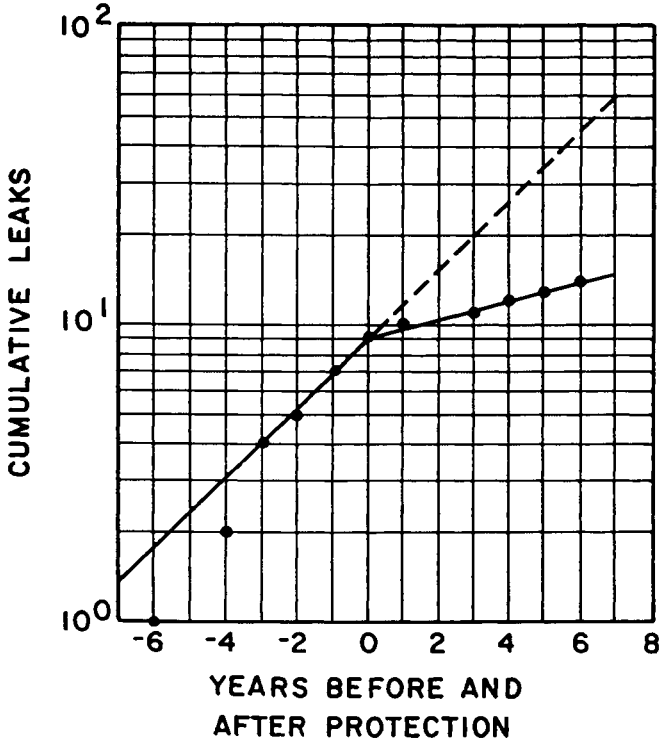

Fig. 6.6: Leak frequency, Clairmont Field, Kent County, TX. (After Kirklen, 1973, fig. 4; courtesy of the SPE.)

6.4 REFERENCES

American Petroleum Institute. 1977. *Design Calculations for Sucker Rod Pumping Systems.* API RP 11L. Dallas. TX. 24 pp.

American Petroleum Institute. 1983. *API Recommended Practice for Care and Use of Subsurface Pumps.* API RP 11AR. Dallas. TX. 41 pp.

Annand, R.R.. 1981. *Corrosion Characteristics and Control in Deep. Hot Gas Wells.* Southwestern Petroleum Short Course.

Battelle Memorial Institute, 1949. *Prevention of the Failure of Metals under Repeated Stress.* Wiley, New York. N.Y.. 295 pp.

Bertness, T.A, 1957. Reduction of failures caused by corrosion in pumping wells. *API Drilling Prod. Pract.*, 37: 129-135.

Bertness, T.A. and Blaunt. F.E. 1969. *Corrosion Control of Platforms in Cook Inlet*, Alaska. Offshore Technology Conference. Paper No. OTC 1049. Soc. Pet. Eng. A.I.M.E., May 18-21. Houston. TX. 8 pp.

Blaunt, F.E., 1970 Fundamentals of cathodic protection. In: *Proc. Corrosion Course*, Univ. Oklahoma. Sept. 14-16.

Chilingar, G.V. and Beeson. C.M., 1969. *Surface Operations in Petroleum Production.* Am. Elservier. New York. N.Y.. 397 pp.

Cron C.J. and Marsh. G.A, 1983. Overview of economic and engineering aspects of corrosion in oil and gas production. *J. Pet. Tech.*, 35(6): 1033-1041.

Davis, J.B.. 1967. *Petroleum Microbiology.* Elsevier. Amsterdam. 604 pp.

Doig, K. and Wachter, A.P., 1951. Bacterial casing corrosion in the Ventura Field. *Corrosion*, 7: 221-224.

Dean, H.J., 1977. Avoiding drilling and completion corrosion. *Pet. Eng.*, 10(9): 23-28.

Fontana, M.G. and Greene, N.D.. 1967. *Corrosion Engineering.* McGraw-Hill, New York, N.Y., 391 pp.

Gatzke, L.K. and Hausler, R.H.. 1983. *Gas Well Corrosion Inhibition with KP 223/KP 250.* NACE Annu. Conf.. April 18-22. Anaheim, CA.

Hackerman, N. and Snavely, E.S.. 1971. Fundamentals of inhibitors. In: *NACE*

Basic Corrosion Course. NACE, Houston, TX, (9): 1-25.

Hilliard, H.M., 1980, *Corrosion Control in Cotton Valley Production*. Soc. Pet. Eng. Cotton Valley Symp., SPE 9062, Tyler, TX, May 21, 4 pp.

Hudgins, C.M., 1969. A review of corrosion problems in the petroleum industry. *Mater. Prot.*, 8(1): 41-47.

Hudgins, C.M., McGlasson, R.L., Mehdizadeh, P. and Rosborough, W.M., 1966. Hydrogen sulfide cracking of carbon and alloy steels. *Corrosion*, 22(8): 238-251.

Ironite Products Co., 1979. *Hydrogen Sulfide Control*. 41 pp.

Jones, L.W., 1988. *Corrosion and Water Technology*. Oil and Gas Consultants International, Inc., Tulsa, OK, 202 pp.

Kane, R.D. and Greer, J.B., 1977. Sulphide stress cracking of high-strength steels in laboratory and oilfield environments. *J. Petrol. Technol.*, 29(11): 1483-1488.

Kirklen, C.A., 1973. *Well Casing Cathodic Protection Effectiveness - An Analysis in Retrospect*. Paper presented at 48th Annu. Fall Meet., Soc. Petrol. Engrs. AIME, Las Vagas, NV, Sept. 30 - Oct. 3: 6 pp.

Kubit, R.W., 1968. *E log I - Relationship to Polarization*. Paper No. 20, Conf. N.A.C.E., Cleveland, OH, 13 pp.

Martin, R.L., 1979. Potentiodynamic polarization studies in the field. *Mater. Perform.*, 18(3): 41-50.

Martin, R.L., 1980. Inhibition of corrosion fatigue of oil well sucker rod strings. *Mater. Perform.*, 19(6): 20-23.

Martin, R.L., 1982. *Use of Electrochemical Methods to Evaluate Corrosion Inhibitors under Laboratory and Field Conditions*. U.M.I.S.T. Conf. on Electrochemical Techniques, Manchester.

Martin, R.L., 1983. Diagnosis and inhibition of corrosion fatigue and oxygen influenced corrosion. *Mater. Perform.*, 32(9): 41-50.

May, P.D., 1978. Hydrogen sulfide control. *Drilling-DCW*, April.

Meyer, F.H., Riggs, O.L., McGlasson, R.L. and Sudbury, J.D., 1958. Corrosion products of mild steel in hydrogen sulfide environments. *Corrosion*, 14(2): 109-115.

N.A.C.E. (National Association of Corrosion Engineers), 1979. *Corrosion Control in Petroleum Production*. N.A.C.E. TPC Publ. No. 5: 101 pp.

N.G.A.A. (National Gasoline Association of America), 1953. *Condensate Well*

Corrosion. N.G.A.A., Tulsa, OK, 203 pp.

Ray, J.D., Randall, B.V. and Parker, J.C., 1978. *Use of Reactive Iron Oxide to Remove H_2S from Drilling Fluid*. 53rd Annu. Fall Tech. Conf. Soc. Pet. Eng. AIME, Oct. 1-3, Houston, TX, 4 pp.

Rhodes, F.H. and Clark, J.M., 1936. Corrosion of metals by water and carbon dioxide under pressure. *Ind. Eng. Chem.*, 28(9): 1078-1079.

Simpson, J.P., 1979. A new approach to oil-base muds for lower-cost drilling. *J. Pet. Tech.*, 31(5): 643-650.

Snavely, E.S., 1971. Chemical removal of oxygen from natural waters. *J. Pet. Tech.*, 23(4): 443-446.

Snavely, E.S. and Blaunt, F.E., 1969. Rates of reaction of dissolved oxygen with scavengers in sweet and sour brines. *Corrosion*, 25(10): 397-404.

Staehle, R.W., 1978. $70 billion plus or minus $21 billion. *Corrosion*, 34(6): 1-3 (editorial).

Starkey, R.L., 1958. The general physiology of the sulfate-reducing bacteria in relation to corrosion. *Prod. Mon.*, 22(8): 397-404.

Uhlig, H.H. (Editor), 1948. *The Corrosion Handbook*. Wiley, New York, N.Y., 1188 pp.

Uhlig, H.H., 1965. *Corrosion and Corrosion Control*. Wiley, New York, N.Y., 3rd ed., 371 pp.

Watkins, J.W. and Wright, J., 1953. Corrosive action on steel by gases dissolved in water. *Pet. Eng.*, 25(12): 50-57.

Watkins, M. and Greer, J.B., 1977. Corrosion Testing of Highly Alloyed Materials For Deep, Sour Gas Well Environments. *J. Petrol. Technol.*, 28(6): 698-704.

Wendt, R.P., 1979a. *The Kinetics of Ironite Sponge H_2S Reactions*. Pet. Div. Am. Soc. Mech. Eng., Energy Technol. Conf., Houston, TX, Nov. 5-9, 1978: 7 pp.

Wendt, R.P., 1979b. Control of hydrogen sulfide by alkalinity may be dangerous to your health. *Pet. Eng. Internat.*, 51(6): 66-74.

Wendt, R.P., 1979c. Alkalinity control of H_2S in muds is not always safe. *World Oil*, 188(2): 60-61.

Whitman, W., Russell, R. and Altieri, V., 1924. *Ind. Eng. Chem.*, 16: 665.

Weeter, R.F., 1965. Desorption of oxygen from water using natural gas for coun-

tercurrent stripping. *J. Pet. Tech.*, 17(5): 515-520.

Zaba, J., 1962. *Modern Oil-Well Pumping*. The Petroleum Publishing Company, Tulsa, OK, 145 pp.

Appendix A

NOMENCLATURE

a_f = thermal diffusivity of formation.
A_i = area corresponding to internal area, in.^{2}
A_{jp} = area under last perfect thread, in.^{2}
A_{low1} = internal area of the lower section of the pipe at depth $D_{\Delta A_s}$, in.^{2}.
A_o = area corresponding to external area, in.^{2}
A_s = pipe cross-sectional area, in.^{2}
A_{sc} = area steel in coupling, in.^{2}
A_{sp} = A_s = area of steel in pipe body, in.^{2}
A_{sx} = cross-sectional area of the pipe at depth x, in.^{2}
A_{up1} = internal area of the upper section of pipe at depth $D_{\Delta A_s}$, in.^{2}
BF = buoyancy factor, lbf.
c = radial clearance, in.
C = cost, US$.
C_c = clinging constant.
C_{P_n} = accumulated total return, minimal cost of n sections of casing for each load, F_n, US$.
$C_s(l)$ = correction factor for contact surface between pipe and borehole.
C_{T_n} = return function, total cost of n unit sections of casing, US$.
d_{box} = internal diameter of the joint under the last perfect thread, in.
d_{root} = diameter at the root of the coupling thread of the pipe in the powertight position for API Round thread casing and tubing, in.
d_{co} = outside diameter of coupling, in.
d_{oc} = outside diameter of the coupling, in.
d_i = internal diameter, in.
d_{j_i} = internal diameter of the joint, in.

d_{jo} = external diameter of the joint, in.
d_o = outside diameter, in.
d_{pin} = external diameter of the pin under the last perfect thread, in.
d_w = diameter of the wellbore, in.
D = vertical depth, ft.
D_n = depth where normal pressure zone ends, ft.
D_i = setting depth of intermediate casing, ft.
D_s = setting depth of surface casing, ft.
D_{DOP} = true vertical depth of dropoff point, ft.
D_{EOB} = true vertical depth of end of build, ft.
D_{EOD} = true vertical depth of end of dropoff, ft.
D_{KOP} = true vertical depth of kickoff point, ft.
D_T = true vertical total depth, ft.
D_{TOC} = depth of the top of cement, ft.
$D_{\Delta A_s}$ = depth of change in pipe cross-section A_s of the pipe, ft.
E = modulus of elasticity, 30×10^6 psi.
E_{cm} = Young's Modulus of cement sheath, psi.
E_r = reduced modulus, psi.
E_t = tangent modulus - localised slope of stress-strain curve in the elastoplastic transition range of material, psi.
f = flow friction factor.
f_b = borehole friction factor.
$f(t)$ = transient heat conduction factor.
F_a = axial force, lbf.
F_{ab} = total tensile failure load with bending Θ, lbf.
$F_{a_{homo}}$ = axial force - homogeneous solution, lbf.
$F_{a_{part}}$ = axial force - particular solution, lbf.
F_{ae} = total effective axial force, lbf.
F_{aj} = tensional force for joint failure, lbf.
F_{air} = weight of string in air, lbf.
F_{ap} = piston force, lbf.
F_{as} = force applied at surface, lbf.
F_{a_u} = total tensile load at fracture, lbf.
F_{a_T} = axial force arising from a change in temperature, lbf.
F_{aw} = weight of casing string carried by the joint above the TOC, lbf.
F_{a_1} = axial force at α_1 - equivalent to $F_{a_{\alpha 1}}$, lbf.
F_{a_2} = axial force at α_2 - equivalent to $F_{a_{\alpha 2}}$, lbf.
F_b = bending force, lbf.
F_{bu} = buoyant force acting at the casing shoe, lbf.
F_{bu_v} = vertical projected buoyant weight of pipe, lbf.
F_{buc} = buckling force, lbf.
$F_{buc_{cr}}$ = critical buckling force, lbf.

F_{b_v} = vertical component of bouyant force, lbf.
F_d = drag force, lbf.
F_h = hook load, lbf.
F_n = normal force, lbf.
F_r = radial force, lbf.
$F_{r,t}$ = radial and tangential force at any depth x, lbf.
F_s = shock load, lbf.
$F_{s_{peak}}$ = peak shock load, lbf.
F_t = tangential force, lbf.
F_{vd} = hydrodynamic viscous drag force, lbf.
F_w = force exerted by the borehole wall at the couplings, lbf.
g = gravity force, ft/s^2.
G = $\frac{r_1}{r_2}$.
$G_{p_{cm}}$ = pressure gradient of cement slurry, psi/ft.
G_{p_f} = formation fluid gradient at depth H_i, psi/ft.
G_{p_g} = pressure gradient of gas, psi/ft.
G_{p_i} = pressure gradient of fluid in the casing, psi/ft.
G_{p_m} = pressure gradient of mud, psi/ft.
G_{p_o} = pressure gradient of fluid in the annulus at r_{o_2}, psi/ft.
h_a = distance between top of fluid and surface (Collapse), ft.
h_g = gas interval between bottom of fluid and formation fracture, ft.
h_{gi} = gas interval between casing seat and top of gas column, ft.
h_{m_1} = distance between shoe and fluid top (Collapse), ft.
h_{m_2} = distance between fluid top and formation fracture (Collapse), ft.
H_{st} = enthalpy of steam, Btu/lbm.
H_w = enthalpy of water, Btu/lbm.
I = moment of inertia, in.^{4}
J = distance between the end of the pipe and center of the coupling in the power tight position, in.
k_c = thermal conductivity of casing, Btu/hr ft °F.
k_e = thermal conductivity of the formation, Btu/hr ft °F.
k_{ins} = thermal conductivity of insulating material, Btu/hr ft °F.
k_j = thermal conductivity of 'j'th completion element, Btu/hr ft °F.
k_{tb} = thermal conductivity of tubing, Btu/hr ft °F.
K = Power Law parameter.
K_B = buildup constant.
K^* = collapse coefficient (Sturm).
K_D = dropoff constant.
K_r = reinforcement factor.

K_1 & K_2 = constants in the Lamé equations.
l = length of pipe, ft.
l_j = length of joint, ft.
l_{jc} = length of casing with coupling, ft.
ℓ = measured depth, ft.
ℓ_{DOP} = measured depth of dropoff point, ft.
ℓ_{EOB} = measured depth of end of build, ft.
ℓ_{EOD} = measured depth of end of dropoff, ft.
ℓ_{KOP} = measured depth of kickoff point, ft.
ℓ_T = measured total depth, ft.
L = length of the test specimen, in.
L_{et} = length of engaged thread, in.
L_c = coupling length, in.
L_l = make-up loss, in.
m = mass of pipe of length $V_s\Omega$, lbm.
$\dot{m}$ = mass flow rate of the fluids (steam & water), lbm/s.
M = bending moment, ft-lbf.
M_{p_o} = bending moment at any section of ring caused by external pressure p_o, ft-lbf.
n = Power Law parameter.
N_{Re} = Reynolds number.
N_W = number of different casings of unit weight.
p_b = burst pressure rating of material (Barlow), psi.
p_{br} = burst pressure rating of material defined by the API, psi.
p_c^* = collapse pressure for stresses above the elastic limit (Sturm), psi.
p_{cb} = burst pressure rating corrected for biaxial or triaxial stress, psi.
p_{cc} = collapse pressure rating for biaxial stress (API Bul. 5C3, 1989), psi.
p_{ce} = collapse pressure in the elastic range (Bresse), psi.
$p_{c_{cp}}$ = collapse resistance of the composite pipe body, psi.
p_{cr} = critical value for external pressure for collapse of ring, psi.
p_{ct_t} = critical external pressure for collapse in the transition range based on E_t, the tangent modulus, psi.
p_{ct_r} = critical external pressure for collapse in the transition range based on E_r, the reduced modulus, psi.
p_{cy_1} = critical collapse pressure for onset of internal yield in ideally plastic material (Lamé), psi.
p_{cy_2} = critical collapse pressure for onset of internal yield in casing (Barlow), psi.
p_{c_1} = collapse resistance of the inside pipe, psi.

p_{c_2} = collapse resistance of the outside pipe, psi.

$p_{D_{\Delta A_s}}$ = internal pressure at depth $D_{\Delta A_s}$, psi.

p_e = collapse pressure in the elastic range for $E = 30 \times 10^6$ psi and $\nu = 0.3$ (API), psi.

$p_{e'}$ = collapse pressure in the upper elastic range (API) from Clinedinst, psi.

p_i = internal pressure, psi.

p_{i_1} = internal pressure at r_{i_1}, psi.

p_{i_2} = internal pressure of 2nd string (composite casing) at r_{i_2}, psi.

p_k = kick-imposed pressure at depth D, psi.

p_o = external pressure, psi .

$p_{o_{eq}}$ = external pressure equivalent, psi.

p_{o_1} = external pressure at r_{o_1}, psi.

p_{o_2} = external pressure of 2nd string (composite casing) at r_{o_2}.

$p_{p_{av}}$ = average collapse strength in plastic range (API), psi.

$p_{p_{min}}$ = minimum plastic collapse strength (API), psi.

p_{s_i} = change in surface pressure inside pipe, psi.

p_{s_o} = change in surface pressure outside pipe, psi.

p_t = transition collapse pressure (API), psi.

p_y = collapse pressure in the yield range (API), psi.

P = distributed price, US$/100ft.

P_E = potential energy.

P_{P_n} = distributed price of the W_{ref_n} of casing, US$/100ft.

P_{W_n} = distributed price of the cheapest casing within m, US$/100 ft.

q_{st} = steam quality.

Q = heat flow, Btu/hr.

Q_{con} = heat transfer coefficient (natural convection and conduction), Btu/hr.

Q_{rad} = heat transfer coefficient (radiation), Btu/hr.

r^* = radius of ring prior to deformation.

r_c = radial clearance between hole and casing, in.

r_i = internal radius of casing, in.

r_{i_1} = internal radius of innermost string, in.

r_{i_2} = internal radius of 2nd or outer string in composite casing = outside radius of cement, in.

r_o = external radius of casing, in.

r_{o_1} = external radius of innermost casing = internal radius of cement in composite casing, in.

r_{o_2} = outside radius of 2nd or outer string of composite casing, in.

r_{tb_i} = inside radius of tubing, in.

r_{tb_o} = outside radius of tubing, in.

R = radius of curvature, ft.

$R(l)$ = hole curvature after drilling, ft.
SF = safety factor.
SM = safety margin.
t = wall thickness, in.
T_b = bottom hole temperature, °F.
T_{c_i} = temperature of inside of casing, °F.
T_{cm_o} = temperature at outer surface of cement sheath, °F
T_e = undisturbed temeprature of the formation, °F.
T_h = temperature at the cement-formation interface, °F.
T_i = temperature at internal surface, °F.
T_o = temeprature at external surface, °F.
T_s = surface temperature, °F.
T_{st} = temperature of flowing fluid (steam) inside tubing, °F.
T_{tb_i} = temperature at the inside surface of the tubing, °F.
T_{tb_o} = temperature at the outside surface of the tubing, °F.
T_1 = initial temperature, °F.
T_2 = final temperature, °F.
U_{tot} = overall heat tranfer coefficient, Btu/hr sq ft °F.
v = velocity of the two-phase mixture, ft/s.
v_{av} = equivalent displacement velocity, ft/s.
V_p = velocity at which pipe is running into hole, ft/s.
V_s = velocity of induced stress wave in casing, ft/s.
W = $W_n BF$
= weight of unit section, lb/ft.
W_a = weight of string in air, lb/ft.
W_b = buoyancy force acting on the pipe, lb/ft.
$W_b(l)$ = unit buoyant weight projection on the binormal direction, lb/ft.
$W_d(l)$ = $W_d(l, f_b)$
= unit drag or rate of drag change, lb/ft.
W_e = effective weight of the pipe, lb/ft.
W_{m_n} = distributed weight of the casing within m, lb/ft.
W_n = nominal weight per unit length, lb/ft.
$W_N(l)$ = buoyant weight projection on the principal normal direction, lb/ft.
$W_p(l)$ = unit buoyant weight projection on the principal normal direction, lb/ft.
W_{pe} = plain end weight per unit length, lb/ft.
W_{p_n} = distributed weight of casing lighter or equal to W_{ref_n}, lb/ft.
W_{ref_n} = distributed weight of the cheapest casing at stage n, lb/ft.
W_{tc} = threaded and coupled weight per unit length, lb/ft.

$W_u(l)$ = unit buoyant weight projection on the tangential direction, lb/ft.
Y_p = yield strength, psi.
Y_{pa} = yield strength of axial stress equivalent grade, psi.
= σ_y for $\sigma_a = 0$
α = angle of inclination to the vertical, deg.
$\dot{\alpha}$ = rate of change of inclination, deg.
α_1 = angle of inclination between the vertical and the slant section, deg.
$\dot{\alpha_1}$ = buildup rate, ° /100 ft.
α_2 = angle of inclination between the vertical and the end of of the dropoff, deg.
$\dot{\alpha_2}$ = dropoff rate, ° /100 ft.
β = overall angle change, radians.
γ_{cm} = specific weight of cement slurry, lb/gal.
γ_f = specific weight of formation fluid, lb/gal.
γ_m = specific weight of drilling fluid, lb/gal.
γ_{m_n} = new specific weight of drilling fluid, lb/gal.
γ_s = specific weight of steel, 489.5 lb/ft^3.
ΔT_{max} = refer to Fig. 4.27 on page 225.
ΔT_x = refer to Fig. 4.27 on page 225.
ΔT_{yp} = temperature at which yield point is reached, °F.
$\Delta\varepsilon_2$ = deformation of outside surface of pipe.
ε_x = deformation in the x-axis.
ε_y = deformation in the y-axis.
ε_a = deformation in the z-axis.
θ = bearing angle change, rad.
Θ = degrees per 100 feet of pipe, 'dogleg severity'.
λ = contact angle, rad.
ν = Poisson's ratio.
ν_{cm} = Poisson's ratio for cement sheath.
ξ = ratio of Young's modulus to the tangent modulus at the yield point, σ_y.
σ_s = stress resulting from slip action, psi.
σ_a = axial stress, psi.
σ_{abu_1} = change in axial stress due to the effect of change in fluid specific weight on buoyant weight, psi.
σ_{abu_2} = change in axial stress due to the effect of change in surface pressure on buoyant weight, psi.
σ_{ap} = axial stress due to piston effect, psi.
σ_{ap_1} = $\sigma_{ap} + \Delta\sigma_{ap}$, psi.
$\Delta\sigma_{ap}$ = change in piston effect due to effect of changing in fluid densities and surface pressures, psi.

σ_{a_T} = additional axial stress due to a change in temperature.
σ_{aw} = axial stress due to pipe weight, psi.
σ_{aw_1} = $\sigma_{aw} + \Delta\sigma_{aw}$, psi.
$\Delta\sigma_{aw}$ = $\sigma_{abu_1} + \sigma_{abu_2}$
$\sigma_{buc_{cr}}$ = critical stress for buckling, psi.
σ_{cm} = compressive strength of cement, psi.
$\sigma_{cs_{p_{c1}}}$ = collapse resistance of the cement sheath under the external pressure p_{c1}, psi.
σ_e = effective yield strength under combined load, psi.
σ_E = limit of elasticity, psi.
σ_{max} = maximum total stress, psi.
$\overline{\sigma}_n$ = average nominal stress, psi.
σ_{res} = residual axial stress present prior to heating body, psi.
σ_{p_o} = tangential stress due to external pressure p_o, psi.
σ_{red} = reduced yield strength due to axial loading, psi.
σ_s = stress resulting from the action of slips, psi.
σ_t = tangential stress due to internal pressure, psi.
σ_u = minimum ultimate yield strength of the material, psi.
σ_{uc} = minimum ultimate yield strength of the coupling, psi.
σ_{up} = minimum ultimate yield strength of the pipe, psi.
$\overline{\sigma}_{t_{Er}}$ = average tangential stress for a particular value of E_r, psi.
$\sigma_{t_{max}}$ = maximum tangential stress, psi.
σ_y = minimum yield strength, psi.
σ_{y_T} = yield stress corrected for temperature (hot yield stress), psi.
σ_{yj} = joint yield stress (cold yield stress).
σ_z = σ_a = axial stress, psi.
$\sigma_{0.2}$ = tensile stress required to produce a total elongation of 0.2 % of the gauge length of the test specimen, psi.
Υ = coefficient of thermal expansion.
ϕ = contact surface angle, rad.
φ = angle of internal friction calculated from Mohr's circle.
ψ^2 = F_a/EI = definition.
Ψ^2 = $1 + ((r^*)^3 p_o)/EI$ = definition.
Ω = time, second.

INDEX

C

E

F

R

T